HUMBOLDT-UNIVERSITÄT ZU BERLIN

Using modern microscopy and image analysis methods to study dosage compensation in *C. elegans*

D I S S E R T A T I O N

zur Erlangung des akademischen Grades

doctor rerum naturalium

(Dr. rer. nat.)

im Fach Biologie

eingereicht an der Lebenswissenschaftlichen Fakultät

der Humboldt Universität zu Berlin

von

Laura Breimann, M. Sc

Präsidentin der Humboldt Universität: Prof. Dr.-Ing. Dr. Sabine Kunst

Dekan der Lebenswissenschaftlichen Fakultät: Prof. Dr. Dr. Christian Ulrichs

Gutachter/innen: 1. Prof. Dr. Ana Pombo

2. Dr. Stephan Preibisch

3. Prof. Dr. Simone Reber

Tag der mündlichen Prüfung: 06.12.2021

Table of Contents

Abstract

Condensins are essential for chromosome compaction and have been implicated in transcription regulation. The mechanistic foundation of their transcription regulatory function is poorly understood. A clear paradigm to address this question is an X-specific condensin (DC for dosage compensation) in *C. elegans*, which specifically binds to and represses X chromosomes in XX hermaphrodites by 2-fold. In my thesis, I studied condensin DC binding dynamics to the X chromosome and how condensin DC affects transcription kinetics in single embryos across development.

Condensins might engage dynamically with chromatin to form loops, compact chromatin, and regulate transcription, as recent studies utilizing new microscopy methods suggest. To study the dynamics of condensin DC binding, I established fluorescence recovery after photobleaching (FRAP) in *C. elegans* adult intestinal cells. With this method, I studied how the ATPase domain and different histone modifiers regulate the dynamic binding of condensin DC. We found that the ATPase domain is critical for binding of the complex and that the noncatalytic activity of a histone demethylase increases the dynamics of condensin DC binding, which is crucial for its role in transcription regulation.

To further study the mechanism of condensin DC in transcription regulation on the X chromosome during embryogenesis, I used an imaging approach based on widefield single-molecule RNA fluorescence in situ hybridization (smFISH). To detect single RNA spots accurately in 3D in large datasets, we developed a new open-source detection tool. To stage vast numbers of embryos to their exact developmental time point, we used advanced machine learning. I obtained thousands of smFISH images for a set of condensin DC-regulated and control genes and extracted mature and nascent RNA counts in 3D, which I used to determine transcription burst characteristics throughout embryonic development. We found that condensin DC regulates the frequency of transcription initiation to down-regulate X-chromosomal genes.

Taken together, I used modern microscopy methods to study the regulation of dosage compensation in *C. elegans*. My results provide new insight into condensin-mediated transcription regulation, which can be used to inform future studies on the mechanism of condensins in transcription regulation in *C. elegans* and other organisms.

Zusammenfassung

Condensine sind essentiell für die Faltung von Chromatin und wurden auch mit der Transkriptionsregulation in Verbindung gebracht. Jedoch ist der genaue Mechanismus für die Transkriptionsregulation ist nicht gut verstanden. Das X Chromosom spezifische Condensin DC, was in der Dosiskompensation in *C. elegans* eine wichtige Rolle spielt, ist ein gutes Beispiel um die Rolle von Condensinen in der Regulation von Transkription zu untersuchen. Condensin DC bindet an die beiden X Chromosome in *C. elegans* Hermaphroditen und reduziert die Transkription um die Hälfte. In meiner Dissertation habe ich die Bindungsdynamik von Condensin DC untersucht und wie Condensin DC die Transkriptionskinetik während der Embryonalentwicklung verändert.

Condensine binden möglicherweise dynamisch an Chromatin um DNA Schlaufen zu bilden, Chromatin zu komprimieren und Transkription zu regulieren. Um das dynamische Binden von Condensin DC zu untersuchen habe ich „fluorescence recovery after photobleaching“ (FRAP) in Adulten Darmzellen von *C. elegans* etabliert. Mit dieser Methode habe ich untersucht, wie die ATPase Domäne und verschiedene Histon-modifizierende Enzyme das dynamische Binden von Condensin DC regulieren. Wir haben herausgefunden, dass die ATPase Domäne entscheidend für das Binden des Komplexes ist und das eine nicht-katalytische Aktivität einer Histon Demethylase die Bindedynamik von Condensin DC erhöht. Die richtige Bindedynamik von Condensin DC war entscheidend für die Funktion in der Transkriptionsregulation.

Um den Mechanismus der Transkriptionsregulation während der Embryonalentwicklung besser zu verstehen, habe ich einen Mikroskopie Ansatz gewählt, der auf dem Nachweis von einzelnen RNA Molekülen beruht (smFISH). Um in vielen Bildern einzelne fluoreszierende Punkte in 3D genau nachzuweisen, haben wir eine neue open-source Anwendung entwickelt. Die aufgenommenen Embryos haben wir mithilfe von maschinellem Lernen in verschiedene Entwicklungsstadien geordnet. Mit dieser Methode habe ich tausende smFISH Bilder aufgenommen um die Transkription von mehreren Condensin DC regulierten Genen zu untersuchen ebenso wie andere Kontroll-Gene. Aus diesen Bildern habe ich Informationen über die Genexpression gesammelt und Transkriptions-Kinetiken bestimmt. Wir haben herausgefunden, dass Condensin DC die Häufigkeit der einzelnen Transkriptionsereignisse reguliert.

Zusammenfassend, in meiner Dissertation habe ich moderne Mikroskopie Methoden verwendet um die Regulation der Dosiskompensation in *C. elegans* zu untersuchen. Meine Ergebnisse geben neue Einblicke in die Transkriptionsregulation von Condensinen und können die Basis sein für neue Untersuchungen um die Rolle von Condensinen in der Transkriptionsregulation in *C. elegans* und auch in anderen Organismen zu erforschen.

Acknowledgments

Firstly, I would like to thank my supervisors Stephan and Sevinç. I am so grateful to have had guidance from two very different mentors, learn from your experience, and be supported in so many ways. Thank you, Stephan, for all your excitement in discovering new things, giving me the freedom and support to look at the things I found interesting, and visit so many places. Thank you, Sevinç, for welcoming me so warmly in your lab, sharing your knowledge, and helping whenever I needed it. I learned a lot from you two, thank you!

I would like to thank Ana Pombo for being part of my thesis committee and gently pushing me in the right direction. I am grateful for your constructive feedback and support on this journey.

Thank you, Andrew Woehler, for teaching me so many things about microscopy and keeping my most used microscope from falling apart! I also thank the different members of the Woehler lab for the fun and great discussions we had over the years.

Thank you to the Preibisch lab members. Especially Dhana, our adopted lab member, without your help, in the beginning, things would have taken me a lot longer! Thank you to Klim for your work on my projects in the early phases and all the silly things we did together. Thank you to Ella for the great collaboration on so many projects and for your patience in teaching Python to me. Thank you, Friedrich, for all your support and ideas during lab meetings. A big thanks to all the students I got the chance to supervise; I loved your ideas and questions, Lennon, Kustrim, and Vic-Fabienne. Thank you, Marwan, for saving me on the last stretch. Thank you, Nikita, for sharing your Thor lab candy. Additional thanks to Leo and Peter. Thank you, Andrea and Mandy, for your hard work to keep the lab running and support my projects.

A big thank you to the Ercan lab. I always loved spending time with you, having great discussions and fun evenings. A special thanks to the monkeys Lena, Ana, and Matt. Thank you to Sarah for inspiring me. Thank you to David and Jun for the fun working together. And thank you to Bhavana, Anna, Avrami, Daniel, Siyu, and Yuya for being great lab colleagues.

Thank you to our lab neighbors the Tursun lab for always supporting me by sharing their materials and knowledge on keeping the worms happy. Especially Sergej, Selman, Andreas, and Ismail. And thank you to Baris for always having an open door so I can drop in and ask random questions.

Thank you to the BIMSB NYU exchange program, and especially the coordinators Grietje and Christian. I'm so grateful I got the opportunities and the support from this great program.

Thank you to Tim and Fouad for bringing joy to work, going beyond to make things happen, and keeping everything working.

Thank you to Jana and Ronny for supporting me so generously and consistently having a helping hand.

Thank you to the Birol lab, especially Melissa, Isabella, and Elisabeth, for the late-night chats and all your support.

Thank you to the graduate office, especially Michaela working so hard to make the PhD experience as easy and fair as it can be.

Thank you to all the terrific BIMSB labs, including the Pombo and Schwarz labs, for making this a special place with many inspiring and fun people.

A big thank you to so many people at MDC, like the members of the anti-harassment task force, working hard to create a great place to work together and make science.

Thank you to the HU graduate office and especially Jana Lahmer for the excellent support.

Thank you to the Joachim-Herz Fellowship for their support and the great community they are building. So happy I got to spend time with wonderful people like Valentin.

Thank you to my mellow yellow family for the love over the years, starting with amazing MDC beer hours and leading to so much more. Particularly Carlos for always being there for me, especially when I didn't know I needed it.

I am incredibly grateful for Gesa and Marta, my never stopping cheerleaders on this long journey. You made it so easy to forget failed experiments and celebrate every little victory.

I am so grateful to my family for supporting me and visiting me wherever my science takes me. Thank you for all the care packages which helped me survive some late time points.

Nothing would be the same without you, Kalle. Thank you for your love and care, and for believing in me.

Publications

2021 A noncatalytic activity of the H4K20 demethylase DPY-21 regulates condensin DC binding, **Laura Breimann***, Ana Karina Morao*, Jun Kim, David Jimenez, Nina Maryn, Krishna Bikkasani, Michael J Carrozza, Sarah Elizabeth Albritton, Maxwell Kramer, Lena Annika Street, Kustrim Cerimi, Vic-Fabienne Schumann, Ella Bahry, Stephan Preibisch, Andrew Woehler, Sevinc Ercan, bioRxiv

2021 RS-FISH: Precise, interactive and scalable smFISH spot detection using Radial Symmetry, Ella Bahry*, **Laura Breimann***, Leo Epstein*, Klim Kolyvanov, Kyle IS Harrington, Timothée Lionnet, Stephan Preibisch, bioRxiv

2019 Light-microscopy methods in C. elegans research, **Laura Breimann***, Friedrich Preusser*, Stephan Preibisch, Current Opinion in Systems Biology 13, 82-92

2018 DamID profiling of dynamic Polycomb-binding sites in Drosophila imaginal disc development and tumorigenesis, Marco La Fortezza, Giovanna Grigolon, Andrea Cosolo, Alexey Pindyurin, **Laura Breimann**, Helmut Blum, Bas van Steensel, Anne-Kathrin Classen, Epigenetics & chromatin 11 (1), 1-17

* equal contribution

1 Introduction

Parts of this introduction were based on the 2019 published review in the journal Current Opinion in Systems Biology: Light-microscopy methods in *C. elegans* research. Authors listed on the publication are Laura Breimann, Friedrich Preusser and Stephan Preibisch. LB and FP contributed equally but different paragraphs to the review. Only paragraphs written by LB were used for this introduction.

1.1 Structural Maintenance of Chromosomes Complexes regulate the 3D organization of the genome

Temporal and spatial regulation of gene expression is vital for multicellular organisms to gain distinct cellular identities during development and maintain specific cellular functions. Many factors contribute to proper gene regulation, and especially cis-regulatory elements have been widely studied, like transcription factor binding, DNA methylation, and histone modification (Gorkin et al., 2020; Cusanovich et al., 2018). Beyond these levels of regulation, the 3D architecture of the genome was proposed to regulate gene expression. During development, extensive chromatin reorganization was observed, suggesting that 3D chromatin architecture contributes to cell identity (Dixon et al., 2015; Rubin et al., 2017). However, there are still many open questions about how the 3D genome influences gene regulation.

In my thesis, I investigated the interplay of one chromatin organizing molecule, condensin DC, and gene regulation in the context of dosage compensation in *C. elegans*. Condensin DC spatially organizes the hermaphrodite X chromosomes and downregulates their transcription two-fold. However, how condensin DC regulates transcription mechanistically is not well understood and is a fascinating question. Here, I will summarize the current understanding of the 3D organization and the function of chromatin organizing complexes. Then I will give an overview of transcription regulation, and I will briefly discuss different methods to study gene regulation, emphasizing microscopy methods, image analysis, and *C. elegans* as a model organism for imaging. In the last part, I will focus on the mechanism of dosage compensation by condensin DC. Firstly, I will compare different dosage compensation strategies in different organisms and highlight recent publications that furthered our understanding of the dosage compensation pathway in *C. elegans*. Finally, I will discuss possible gene regulation mechanisms by condensin DC in respect to new findings.

1.1.1 Chromatin architecture and its role in gene regulation

The hierarchical organization of chromatin into different 3D structures is essential for many chromatin functions ranging from DNA replication to regulating gene expression (Figure 1) (Cavalli and Heard, 2019; Dekker and Mirny, 2016; Yu and Ren, 2016). Especially technical advances in imaging and biochemical methods have improved our understanding of the different length scales of chromatin architecture (Bickmore, 2012; Cavalli and Heard, 2019; Dekker and Mirny, 2016; Hnisz et al., 2017; Krijger and Laat, 2016; Lakadamyali and Cosma, 2020; Levine et al., 2014; Yu and Ren, 2016).

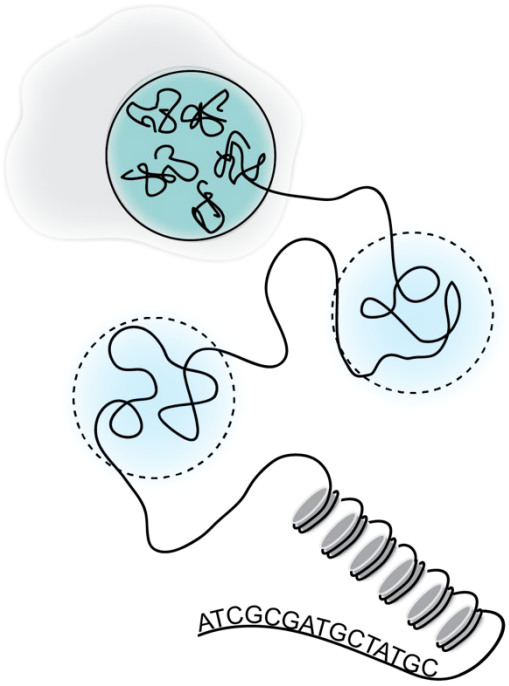

Figure 1 Hierarchical genome organization.
The genome is organized at different scales. At the smallest scale, the DNA sequence is wrapped around histones which form with additional proteins chromatin. Specific chromatin regions interact preferentially with themselves and thereby form chromatin domains or TADs. Active chromatin domains interact with other active chromatin domains and separate from inactive domains. These interactions between differentially active chromatin lead to the formation of A and B compartments. At the largest scale, single chromosomes separate from other chromosomes in the nucleus and form chromosome territories.

At the smallest scale, chromatin consists of a 2 nm DNA double helix wrapped around histone octamers that, together with other non-histone proteins, form the 10 nm chromatin fiber (Kornberg, 1974; Woodcock et al., 1976; Olins and Olins, 1974). Through histone positioning, modifications, and different variants, different proteins regulate chromatin function like gene regulation or DNA repair (Talbert and Henikoff, 2017; Lawrence et al., 2016; Hauer and Gasser, 2017).

Folding of the long chromatin fibers has been studied using genomic assays that map the 3D contacts between DNA sites. These revealed self-interaction contact domains termed topologically associated domains (TADs) (Dixon et al., 2012; Nora et al., 2012; Sexton et al., 2012; Rao et al., 2014). These TADs often consist of co-regulated genes and are separated from other TADs through boundaries that are strongly reduced in long-range *cis*-interactions (Dekker and Mirny, 2016; Krijger and Laat, 2016; Yu and Ren, 2016). TAD structures have been characterized on chromosomes of many model organisms like yeast (Hsieh et al., 2015; Mizuguchi et al., 2015), *C. elegans* (Crane et al., 2015), *Drosophila* (Sexton et al., 2012), zebrafish (Gómez-Marín et al., 2015), pig (Zhao et al., 2021) and human (Dixon et al., 2012). However,

examples of 3D architectures without detectable TADs structures have been reported in *Arabidopsis thaliana* that lack TAD structures, albeit showing TAD boundary-like elements (Wang et al., 2015).

The existence of highly condensed and less condensed areas in the nucleus was already observed with early microscopy (Monneron and Bernhard, 1969). Through the development of chromosome capture methods, including Hi-C, an organization of larger nuclear neighborhoods or compartments with different levels of transcription activity was suggested (Lieberman-Aiden et al., 2009). The two main compartments, A and B, are enriched for different markers. Chromatin in A compartments is enriched for active genes, early replicating, has a high density of genes, is enriched for H3K36me3, and is DNAse I hypersensitive (Lieberman-Aiden et al., 2009; Hiratani et al., 2008; Pope et al., 2014). In contrast, chromatin that falls into B compartments overlaps with lamin-associating domains, is late replicating, and has repressive epigenetic marks (Ryba et al., 2010; Cremer et al., 2000). Another possible determining factor for compartments could be the protein compositions within the compartment. In active compartments, factors involved with transcription and looping could be driving and reinforcing the compartment (Rao et al., 2017). Equally, in B compartments, proteins like heterochromatin protein 1α (HP1α) could promote the formation of a phase-separated compartment (Larson et al., 2017).

Beyond the compartments, single chromosomes occupy specific chromosome territories (CT) within the nucleus (Cremer and Cremer, 2001; Branco and Pombo, 2006). These CT are not random as radial CT positioning of some chromosomes appears to be evolutionarily conserved (Parada et al., 2003), and CT correlates with cell-type-specific functions like replication and transcriptional activity (Grasser et al., 2008; Takizawa et al., 2008). Furthermore, different CT form specific contacts during interphase to coordinate the expression of genes involved in a shared pathway (Maass et al., 2019). For example, the ribosomal RNA genes are encoded on five different human chromosomes and come together to form the nucleolus for ribosome assembly (McStay, 2016).

1.1.2 SMC complexes drive 3D chromatin architecture

To create specific contacts of sequences that are far apart in the linear DNA but in close proximity in 3D space, a model was proposed of an active chromatin extrusion process that loops distant sequences close together. This loop extrusion model has the central assumption of an active, ATP consuming motor that binds to DNA and starts creating loops by progressively extruding DNA (Fudenberg et al., 2016; Bouwman and Laat, 2015; Nichols and Corces, 2015; Sanborn et al., 2015; Nasmyth, 2001). This idea was supported by modeling approaches that

predict properties of the extruders like speed and processivity, and the amount of loop extruding factors determine the loop length and degree of compaction (Alipour and Marko, 2012; Goloborodko et al., 2016b; a). One of the main loop extruding factors are Structural Maintenance Complexes (SMCs).

SMCs are involved in many processes in the nucleus, from maintaining chromosome architecture (Hirano, 2012; Nasmyth, 2001), TAD formation (Crane et al., 2015; Zuin et al., 2014; Seitan et al., 2013), sister chromatid cohesion (Guacci et al., 1997; Michaelis et al., 1997; Nasmyth and Haering, 2009), DNA repair (Ström et al., 2004; Ünal et al., 2004), to chromosome condensation and dosage compensation (Crane et al., 2015; Chuang et al., 1994; Ercan, 2015).

A prominent feature of the general SMC structure is the ring shape (Gruber et al., 2003; Haering et al., 2002). The ring is formed in part by the two SMC proteins with long coiled-coil domains (~ 50 nm, Figure 2a) (Haering et al., 2002; Melby et al., 1998). The SMCs form a heterodimer hinge domain on one end and on the other end a head domain including two ATPases (Saitoh et al., 1994). The ATPase domains are connected by a kleisin subunit (Gruber et al., 2003; Haering et al., 2002; Schleiffer et al., 2003). Several regulatory proteins bind to the kleisin subunit called "HEAT repeat proteins associated with kleisins" (HAWKs) or "kleisin interacting tandem winged-helix elements" (KITEs) (Wells et al., 2017; Kinoshita et al., 2015; Yoshimura and Hirano, 2016; Piazza et al., 2014; Neuwald and Hirano, 2000; Palecek and Gruber, 2015).

SMC complexes are conserved from bacteria to humans (Hirano, 2016; Uhlmann, 2016; Ruiten and Rowland, 2018; Hassler et al., 2018). The eukaryotic SMC complexes are divided into Cohesin, Condensin, and SMC5/6, which regulate different chromatin processes (Figure 2b). Most prokaryotes and best studies in *Bacillus subtilis* have an Smc homodimer associated with a kleisin subunit, ScpA, which forms a subcomplex with another winged-helix domain protein ScpB without a eukaryotic homolog (Britton et al., 1998; Soppa et al., 2002). In contrast, the SMC complex in *Escherichia coli* is called MukBEF/MksBEF and is more closely related to SMC complexes of γ-proteobacteria (Niki et al., 1991).

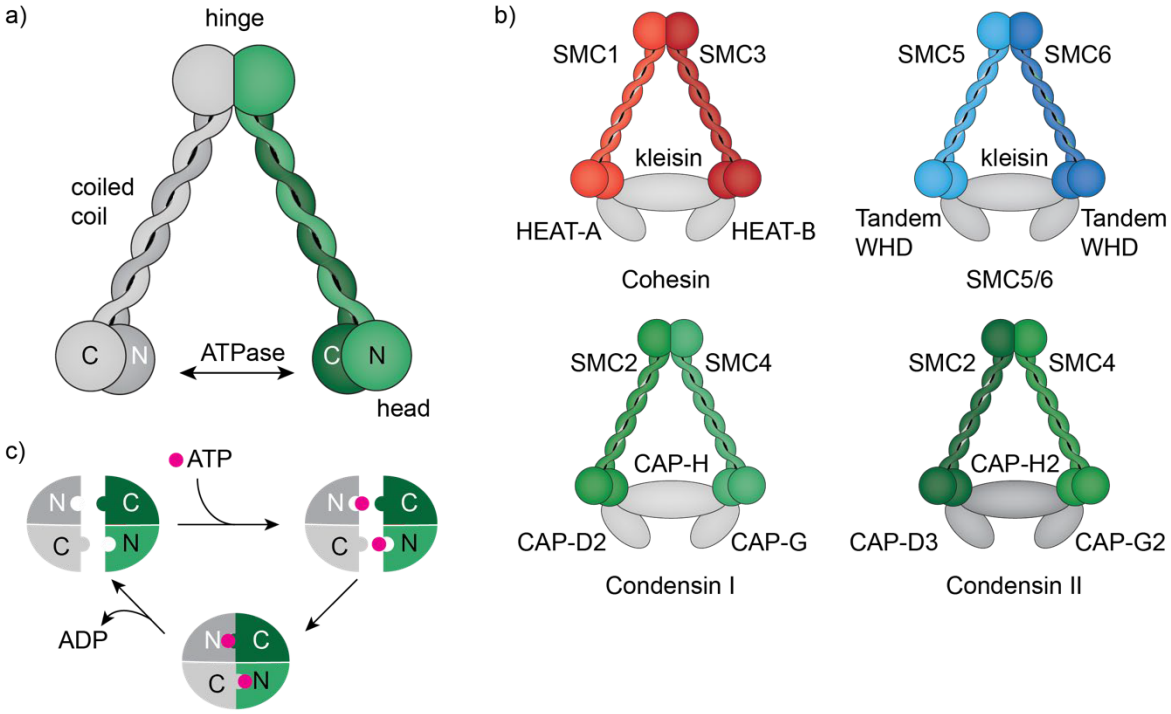

Figure 2 SMC protein complexes.
a) The core of the SMC complexes is formed by homo (for prokaryotes) or heterodimer (for eukaryotes) SMC proteins. The two SMC arms connect at the hinge domains. The hinge is connected to the head domain through coiled coils. The heads include the N- and C- terminal domains of the SMC proteins and form the ATPase domain. **b)** Subunits for cohesin, SMC5/6, and the two condensin complexes. **c)** The ATPase cycle of SMC head domains. First, the two heads come together through the binding of two ATP molecules. Then, the heads dissociate and release ADP, and new ATP molecules can bind.

1.1.3 SMC binding and function

Central to the function of SMCs in chromosome condensation, sister chromatid cohesion, enhancer-promoter loop formation, or DNA repair is their ability to bind to DNA. The binding and consequent functions rely on SMCs ATPase activity, for example, the compaction of DNA by condensin (Strick et al., 2004). The SMC ATPase domains have similarities to the ATP binding cassette (ABC) transporters which undergo global structural changes through the hydrolysis of ATP (Hopfner et al., 2000). Therefore, an ATP hydrolysis-induced conformational change was also proposed for SMCs. If ATP binds, the two ATPase heads can come together and engage (Figure 2c) (Lammens et al., 2004). The Walker A motif in the N terminus domain and the signature motif in the C terminal domain bind to the ATP molecule. The Walker B motif, also in the C terminal domain, contains the catalytic base for ATP hydrolysis (Hirano, 2006; Lammens et al., 2004). During the ATP hydrolysis, the heads can rotate, potentially leading to a rod-like or folded structure in the coiled-coil domain (Diebold-Durand et al., 2017; Bürmann et al., 2019).

The binding of ATP to SMCs seems essential for SMC's ability to associate with DNA as mutations in the Walker A motif prevent condensin from binding to DNA (Kinoshita et al., 2015). In

contrast, mutations in the Walker B motif diminishing ATP hydrolysis did not block SMC associations with DNA in many species (Vian et al., 2018; Kinoshita et al., 2015; Hirano and Hirano, 2004; Thadani et al., 2018; Hudson et al., 2008). Interestingly, a recent study found that the two ATPase sites of condensin have distinct roles in structuring chromosomes, where one site was the driver and the other the dampener of loop extrusion (Elbatsh et al., 2019). Taken together, the ATPase domains are essential for condensin and cohesin function, yet, how the energy of hydrolysis is translated into their molecular mechanisms remains unclear.

At least two ways were proposed how condensin and cohesin could associate with DNA. Firstly, through kleisin bound regulatory proteins, SMCs can bind directly to DNA through electrostatic interactions (Kschonsak et al., 2017; Li et al., 2018b). Secondly, it has been shown that condensin and cohesin can topologically entrap DNA inside their ring-shaped molecule (Haering et al., 2008; Cuylen et al., 2011). Recent publications suggest the entrapment of DNA mostly happens in the ring formed by the kleisin subunit with the two ATPase heads (K-compartment) and, if at all, DNA only transiently binds in the ring formed between the SMC subunits (S-compartment) (Nunez et al., 2019; Chapard et al., 2018). The two different binding modes could reflect a sequential binding mechanism. The SMC molecule first binds more loosely to DNA through electrostatic interactions mediated by regulatory proteins. Subsequently, it associates more stably by topologically entrapping DNA through activating the ATPase domain (Eeftens et al., 2017).

After binding to DNA, the SMC ATPase activity also plays a role in the translocation of SMCs along the DNA (Hu et al., 2011; Murayama and Uhlmann, 2014; Petela et al., 2018; Arumugam et al., 2003; Terakawa et al., 2017) and is required for DNA compaction (Eeftens et al., 2017; Strick et al., 2004; Kim et al., 2019c). One proposed model predicts that the ATPase activity of SMCs is essential for the formation of chromatin loops (Nasmyth, 2001). In the loop extrusion model, small loops are entrapped by SMCs and processively increase in size until a boundary element is reached or the SMC falls off DNA (Alipour and Marko, 2012). The loop extrusion mechanism has been observed *in vitro* for condensin (Ganji et al., 2018) and cohesin (Kim et al., 2019c; Davidson et al., 2019). Different *in vivo* and *ex vivo* approaches support this idea, including Hi-C (Naumova et al., 2013; Jimenez et al., 2021) and electron microscopy (Paulson and Laemmli, 1977). Additionally, modeling approaches largely agree with the proposed mechanism (Alipour and Marko, 2012; Goloborodko et al., 2016b; Fudenberg et al., 2016; Banigan and Mirny, 2020).

1.1.4 SMC5/6

The SMC5/6 complex is the least studied SMC complex (Piccoli et al., 2009). The complex consists of six subunits: the SMC subunits Smc5 and Smc6, as well as four regulatory proteins

Nse1, Nse2, Nse3, and Nse4 (Fousteri and Lehmann, 2000; Hazbun et al., 2003; Taylor et al., 2007). Its ATPase activity is critical for the topological entrapment of DNA (Kanno et al., 2015), and the yeast protein Nse5/6 is a negative regulator of the ATPase (Hallett et al., 2021). Recently it has been reported, that SMC5/6 binds to specific DNA structures like plectonemes and can compact DNA using the energy from ATP hydrolysis (Serrano et al., 2020; Gutierrez-Escribano et al., 2020).

So far, the role of SMC5/6 has frequently been implicated in several DNA repair pathways (Lehmann et al., 1995; Mengiste et al., 1999; Maria et al., 2007; Liu et al., 2015; Potts et al., 2006; Andrews et al., 2005). Furthermore, it also plays a role in repairing damaged replication forks (Branzei et al., 2006) or for the resolution of intertwined sister chromatids and repairing replication stress (Menolfi et al., 2015; Kegel et al., 2011).

1.1.5 Cohesin

Cohesin is a highly conserved member of the SMC family and functions in sister chromosome cohesion (Michaelis et al., 1997; Strunnikov et al., 1993; Guacci et al., 1997; Losada et al., 1998; Farcas et al., 2011), DNA repair (Ström et al., 2004; Ünal et al., 2004), replication (Tittel-Elmer et al., 2012) and gene regulation (Dorsett, 2007). After DNA replication, cohesin holds the two sister chromatids together to prevent entanglement (Nasmyth and Haering, 2009; Makrantoni and Marston, 2018). The cohesion between the two is only resolved during metaphase when all chromosomes are at the metaphase plate, and homolog chromosomes are attached with microtubules from opposite poles. The proper alignment deactivates the spindle assembly checkpoint, and the enzyme separase can cleave the cohesin ring bound mostly at the centromeres to release the sister chromatids (Nasmyth and Haering, 2009; Makrantoni and Marston, 2018; Hinshaw et al., 2017). The protease separase cleaves Scc1, the kleisin subunit, to trigger the metaphase-to-anaphase transition (Uhlmann et al., 2000). The complete loss of cohesin is lethal for cells as they fail to separate sister chromosomes and end up with aneuploidies (Michaelis et al., 1997).

The focus of cohesin research shifted in recent years to its role during interphase in gene regulation (Hadjur et al., 2009; Seitan et al., 2013; Sofueva et al., 2013; Zuin et al., 2014; Rao et al., 2017). Especially the role in establishing TADs and enhancer-loop formation was shown in several organisms (Fudenberg et al., 2016; Bortle et al., 2014; Kagey et al., 2010; Rao et al., 2014). Recent studies indicate that the looping of DNA by cohesin is also through an active extrusion mechanism (Davidson et al., 2016; Fudenberg et al., 2016; Gassler et al., 2017; Kim et al., 2019c; Wendt et al., 2008). If loop formation is disturbed through the loss of cohesin, gene expression can be dysregulated (Zuin et al., 2014; Seitan et al., 2013). If enhancer-promoter

loops are lost, affected genes reduce transcription, but when loops between a promoter and a repressive element are lost, genes gain transcriptional activity (Dorsett and Merkenschlager, 2013). If TAD formation is disrupted by deleting boundary regions, gene expression of flanking regions can be affected, which is especially problematic during development (Lupiáñez et al., 2015).

Regulators of cohesin binding and processivity also regulate the 3D organization of the genome. The loading and the processivity of cohesin are mediated by the kollerin complex consisting of NIPBL (Scc2 in yeast) and MAU2 (Scc4 in yeast) (Ciosk et al., 2000; Rhodes et al., 2017a; Nasmyth, 2011). The kollerin complex, together with DNA, promotes ATPase activity of cohesin (Haarhuis et al., 2017; Petela et al., 2018), which is required for its function (Arumugam et al., 2003; Hu et al., 2011; Vian et al., 2018). In contrast to the release of centromeric cohesin by separase, cohesin release from chromosome arms is regulated by acetylation (Chan et al., 2012). Eco1 acetylates Smc3 to prevent the association of the release factor WAPL (Wings apart-like subunit). WAPL collaborates with PDS5 (HEAT repeat-containing subunit) and Scc3 to open the Smc3-Scc1 gate and release cohesin from chromatin (Muir et al., 2020; Gligoris et al., 2014). Release of cohesin reduces cohesin-mediated loop extension (Gassler et al., 2017; Haarhuis et al., 2017; Wutz et al., 2017; Murayama and Uhlmann, 2015). Interestingly, a recent paper found that cohesin turnover was necessary for proper gene regulation and that WAPL depletion and, therefore, static binding of cohesin resulted in depletion of cohesin from cell-type-specific gene regulatory regions (Liu et al., 2021). This result underlines the importance of the dynamic binding of cohesin for proper gene regulation.

Many of the recent studies focused on cohesin activity and function using Hi-C in combination with genetic perturbation. Another approach to study the effect of NIPBL, WAPL, and CTCF on cohesin binding dynamics *in vivo* are FRAP and other live-cell imaging methods. In human cells, WAPL depletion leads to an increased residence time and the chromatin-bound fraction of cohesin (Kueng et al., 2006; Tedeschi et al., 2013) and decreases diffusion (Rhodes et al., 2017b). On the other hand, reducing the dosage of the NIPBL homolog in *Drosophila melanogaster* decreases the amount of stably bound cohesin without affecting its chromosomal residence time and, consistently, reducing the Pds5 dosage increases the amount of stable cohesin (Gause et al., 2010).

Cohesin-mediated loop extrusion is also restricted by the CCCTC binding factor (CTCF) (Parelho et al., 2008; Wendt et al., 2008) that localizes to the TAD boundaries in mammals (Rao et al., 2017; Schwarzer et al., 2017). Because the CTCF DNA motif is nonpalindromic, CTCF binds to it with a specific orientation. Cohesin interacts with its N-terminal domain of the CTCF protein and, therefore, only stops when it encounters a CTCF site in a specific orientation (Nora et al., 2020). Because of this direction sensitive interaction, the orientation of CTCF sites is critical for

the function as loop extrusion barrier and the ability to form a TAD boundary (de Wit et al., 2015; Gómez-Marín et al., 2015; Guo et al., 2015; Rao et al., 2014; Vietri Rudan et al., 2015; Nora et al., 2020; Sanborn et al., 2015). In summary, cohesin is required for TAD formation, and CTCF and cohesin bind TAD boundaries. The loading complex kollerin regulates the loading of cohesin, and the unloading factors WAPL with PDS5 control the loop length and dynamic binding of cohesin. Going forward, experiments studying the loop-extrusion *in vivo* and the contribution of different co-factors for processivity and how this regulates transcription will enhance our understanding of how cohesin regulates 3D chromatin and gene regulation.

1.1.6 Condensin

Condensin is another SMC family member that is evolutionary conserved and is essential for chromosome condensation and segregation during cell division (Hirano et al., 1997; Hirano, 2002; Chan et al., 2004; Cuylen and Haering, 2011; Houlard et al., 2015; Kinoshita and Hirano, 2017). Metazoans have two condensin isoforms, condensin I and II (Ono et al., 2003; Yeong et al., 2003) that bind to mitotic chromosomes at different cell cycle stages and can additionally be distinguished by their non-SMC subunits (Ono et al., 2004; Hirota et al., 2004). Condensin II is present in the nucleus throughout the cell cycle and can already bind to prophase chromatin and start condensing chromatin. The binding of condensin II creates long loops that shorten the length of the chromosome (Walther et al., 2018; Gibcus et al., 2018; Green et al., 2012). In contrast, condensin I is cytoplasmic and only associates with chromatin after the nuclear envelope breakdown (NEBD) when cells enter prometaphase (Hirota et al., 2004; Gerlich et al., 2006a). The long loops created by condensin II are subdivided into smaller loops through the binding of condensin I, which reduces the width of the chromosome arms (Walther et al., 2018; Gibcus et al., 2018; Green et al., 2012).

Analogous to all SMCs, condensin binds to open chromatin. Possibly nucleosome remodelers like the RSC complex in budding yeast could promote condensin loading by evicting nucleosomes (Chao et al., 2015; Hinshaw et al., 2015). A different possibility could be that loading is promoted by the interaction with a different DNA binding protein. Condensin physically interacts with TFIIIC and overlaps at TFIIIC binding sites in the genome (Bortle et al., 2014; Yuen et al., 2017; D'Ambrosio et al., 2008). TFIIIC is a conserved transcription factor that interacts with RNA Pol III to regulate tRNA and 5S rRNA expression (Cieśla et al., 2018). TFIIIC might interact as an insulator protein and contribute to 3D architecture formation (Noma et al., 2006; Raab and Kamakaka, 2010; Kirkland et al., 2013). In yeast, condensin was also required for 3D colocalization of tRNA genes (Haeusler et al., 2008; Iwasaki et al., 2010; Snider et al., 2014). Knock-down of TFIIIC reduces levels of condensin II on chromatin but not vice versa; therefore,

TFIIIC promotes the binding of condensin II. Additionally, chromatin marks might play a role in either condensin loading or binding. Condensin II binding colocalizes with H3K4me3 enrichment, and condensin II can physically interact with the mark (Yuen et al., 2017; Bortle et al., 2014; Cubeñas-Potts et al., 2017). Mitotic chromosomes are enriched for H4K20me1 at the beginning of prophase through the CDK1 phosphorylation-dependent removal of the H4K20me1 demethylase PHF8 and the activation of the histone methyltransferase Pr-Set7 (Liu et al., 2010; Houston et al., 2008; Nishioka et al., 2002; Karachentsev et al., 2005; Wu et al., 2010). The HEAT repeat domains of condensin II can bind to H4K20me1, and both overlap in their ChIP-seq profiles (Liu et al., 2010). After mitosis, Pr-Set7 is targeted for proteasome-mediated degradation, PHF8 associates again with chromatin and H4K20me1 levels drop, allowing the G1-S transition (Liu et al., 2010; Wu et al., 2010; Julien and Herr, 2004).

Not many proteins are known to regulate condensin activity, and in contrast to cohesin, condensin can extrude DNA *in vitro* using ATP without additional co-factors (Ganji et al., 2018). However, in yeast, CDK1 and PLK1 phosphorylation of condensin stimulate ATPase activity and DNA supercoiling (St-Pierre et al., 2009; Sutani et al., 1999). Additionally, depletion of the mitotic Aurora B kinase disrupts chromosome structure and compaction by condensin in *C. elegans* (Kaitna et al., 2002; Hagstrom et al., 2002), *D. melanogaster* (Giet and Glover, 2001), and in human cells for condensin I but not condensin II (Lipp et al., 2007; Takemoto et al., 2007; Lavoie et al., 2004). Whether the unloading of condensin is regulated by modification or other co-factors has not been identified yet.

Since condensin I stays in the cytoplasm until mitosis, the interphase functions of canonical condensins are mainly carried out by condensin II (Yuen and Gerton, 2018). In *D. melanogaster*, condensin II was shown to promote the formation of chromosome territories (Hartl et al., 2008; Bauer et al., 2012) and to influence the level to which chromosome territories can interact (Rosin et al., 2018). Interestingly a recent study in 24 eukaryotic species found that chromosome organization was dependent on the presence of condensin II subunits (Hoencamp et al., 2021). Condensin II was also detected in mouse embryonic stem cells at super-enhancers, and loss of condensin reduced the expression of critical genes for cell identity (Dowen et al., 2013). Condensin binding was also detected at the strongest TAD boundaries in mice (Bortle et al., 2014), and depleting condensin did disrupt TAD boundaries in *C. elegans* and *D. melanogaster* (Li et al., 2015; Crane et al., 2015). During mitosis, condensin I was also detected at active promoters in DT40 cells, and depletion of condensin I before mitosis led to a decreased expression in those genes during the G1 phase (Kim et al., 2019b). In budding yeast, tRNA genes are clustered in the nucleolus through condensin binding, and in fission yeast, Pol III and tRNA genes cluster at the centromere mediated by condensin (Iwasaki et al., 2010; D'Ambrosio et al.,

2008). Besides examples of regulating active genes, several links between condensin and silenced gene expression were reported. Examples include silencing genes in budding yeast (Wang et al., 2016a; Bhalla et al., 2002), the repression of homeotic genes in *Drosophila* (Lupo et al., 2001), transcription repression in *C. elegans* (Kranz et al., 2013), and the regulation of senescence (Yokoyama et al., 2015) or quiescence (Swygert et al., 2019).

1.2 Transcription regulation and methods to quantify expression

Transcription describes the copying of genetic information from DNA to RNA and is one of the most fundamental processes for a cell. Transcription is highly regulated to ensure proper temporal and spatial expression of genes. The central protein complexes for transcription are polymerases. In eukaryotes, three different RNA polymerases transcribe DNA into different classes of RNA (Roeder and Rutter, 1969; Sentenac, 2008). The critical protein for the transcription of coding genes is RNA Polymerase II (Pol II) (Cramer et al., 2000). To synthesize RNAs from genes, Pol II is recruited to promoter regions, opens the DNA duplex, and transcribes an RNA molecule until it reaches a termination signal. Pol II's mechanism of gene transcription is tightly regulated at many levels and includes the interplay of several molecular processes.

1.2.1 Posttranslational modifications of histone tails

Histone modifications are imperative for transcription regulation. The tails of histones, especially the N-terminal, are modified with various chemical groups, creating binding sites for different factors that can interact with chromatin or other proteins (Strahl and Allis, 2000). Furthermore, histone modifications can also alter the histone core. For instance, acetylation of H4K16 neutralizes the positive charge of the lysine, which weakens the interaction with the negatively charged DNA and increases the accessibility of DNA (Strahl and Allis, 2000). Not every histone modification can be associated with a downstream effect which might vary depending on the temporal or spatial context. However, a range of modifications is strongly associated with active transcription like H4K16ac, H3K4me3, and H3K27ac or repressed transcription like H3K9me3 and H3K27me3 (Heintzman et al., 2009; Ernst et al., 2011; Karlić et al., 2010).

1.2.2 Transcription regulation by sequence-specific transcription factors

Transcription factors (TFs) are necessary to establish cell identity. They drive the differentiation of cell types and can be used to force cells back into pluripotency through dedifferentiation (Takahashi and Yamanaka, 2016). TFs have two main domains, a DNA binding and a transcription activation domain (Ptashne, 1988). The DNA binding domain recognizes DNA sequences with different levels of specificity and stringency (Weirauch and Hughes, 2011; Lambert et al., 2018). The local sequence environment also influences the ability to bind the recognition sequence. Multiple copies of the recognition sequence, the spacing, and other TFs influence the efficiency of binding (Jolma et al., 2015; Lin et al., 2010; Swanson et al., 2010).

Another factor that influences binding is the chromatin context of the binding site. Nucleosome binding can block TF binding sites, and nucleosome remodelers can be recruited to these sites to open up specific TF binding sites (Soufi et al., 2015). TFs mainly bind either to promoter regions or distal elements like enhancers to activate or repress transcription. The transactivation domain mediates the function by recruiting other activating or repressing complexes. These complexes can modify the surrounding histones with active or repressive chromatin marks or remodel histones (Frietze and Farnham, 2011).

Many transactivating domains contain disordered domains. Disordered proteins recently gained much attention through the concept of phase separation (Hnisz et al., 2017). In this concept, the low complexity domains could condensate into a protein complex via weak interactions between multivalent molecules (Banani et al., 2017). These condensates have properties of liquid droplets, such as fast exchange of molecules, coarsening, and the possibility to fuse to other droplets. The assembly of these condensates could make transcription activation more efficient by increasing the local concentration of factors necessary for transcription initiation (Boehning et al., 2018).

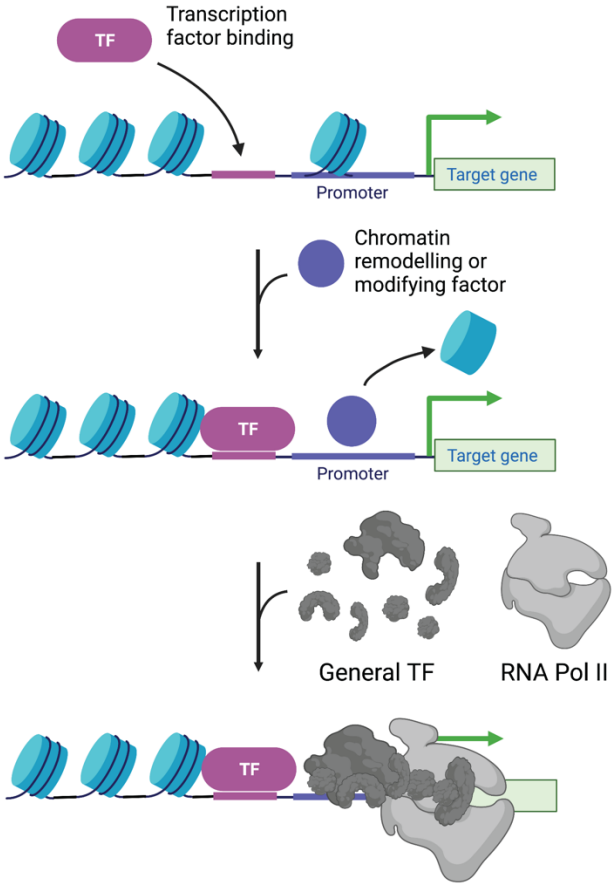

Figure 3 Model for transcription initiation regulation.
Initiation starts with the binding of gene-specific transcription factors (TFs). These can recruit chromatin remodeling or modifying factors. The recruited complexes can rearrange the promoter-proximal chromatin making it permissive for transcription. Next, the general TFs and RNA Pol II bind to the promoter region, forming the Pre-Initiation Complex (PIC). Figure created with BioRender.com.

1.2.3 Regulation of the transcription cycle

The transcription cycle is highly regulated by large protein complexes and can be separated into four main regulatory steps: initiation, elongation, termination, and recycling. In recent years, this sequential view on regulation was updated by a more dynamic and stochastic process of transcription regulation (Steensel and Furlong, 2019; Lu and Lin, 2019; Lu et al., 2018; Cramer, 2019).

During initiation, Pol II is recruited to genes. The process starts with the cooperative binding of different gene-specific transcription factors and general transcription factors (GTFs) to the promoter region and the recruitment of Pol II to the transcription start site (TSS) (Sainsbury et al., 2015; Thomas and Chiang, 2008; Haberle and Stark, 2018). This cooperative binding forms the pre-initiation complex (PIC), which can be further stabilized by Mediator complex binding (Kornberg, 2005; Cramer, 2019; Allen and Taatjes, 2015; Juven-Gershon et al., 2008). Next, 10-15 bp around the TSS are melted by a translocase subunit of the GTF TFIIH, and the template strand is placed in the active site cleft of Pol II (Wang et al., 1992; Schilbach et al., 2017; Kim et al., 2000; Grünberg et al., 2012). Finally, the Pol II starts transcribing the DNA into RNA by adding nucleotides to the growing RNA molecule by catalyzing the formation of a phosphodiester bond at its active site (Wang et al., 2006; Tinetti et al., 2007). After the first 30 bp, the PIC dissociates, and Pol II loses contact with the core promoter (Jonkers and Lis, 2015; Luse, 2013).

In many metazoans, it has been described that after PIC release and the start of elongation, the Pol II pauses again after ~50 bp (Rougvie and Lis, 1988; Tome et al., 2018). This stop in elongation has been described as promoter-proximal pausing, a genome-wide mechanism important for many eukaryotic genes, and a critical checkpoint for controlling the rate of RNA production (Adelman and Lis, 2012; Core and Adelman, 2019). However, in *C. elegans,* promoter-proximal pausing affected only a small proportion of genes and does not seem to be a central point for gene regulation (Kruesi et al., 2013; Maxwell et al., 2014).

Release from the paused state and the switch to productive elongation requires the phosphorylation and release of DRB sensitivity-inducing factor (DSIF) and negative elongation factor (NELF) (Adelman and Lis, 2012; Yamaguchi et al., 2013). Different elongation factors like the positive transcription-elongation factor-b (P-TEFb) promote elongation (Saunders et al., 2006; Vos et al., 2018). Additionally, elongating Pol II can encounter blocks that lead to pausing, backtracking, and termination (Landick, 2006). TFIIS will then release Pol II to continue elongation (Churchman and Weissman, 2011; Cheung and Cramer, 2011). The mRNA abundance can also be regulated by modulating the elongation rate (Shilatifard et al., 1996; Luo et al., 2012; Hou et al., 2019).

A transcription termination signal marks the end of transcripts. It triggers cleavage of the RNA, polyadenylation, and transcription termination (Richard and Manley, 2009; Moore and Proudfoot, 2009). Termination is critical for the transcription cycle as an unreleased Pol II interferes with productive transcription of the gene and stops recycling of the engaged Pol II (Eaton and West, 2020). The termination and polyadenylation machinery can influence the PIC assembly and therefore influence re-initiation efficiency through Pol II recycling (Mapendano et al., 2010). Additionally, the GTFs can stay bound to gene promoters to allow fast re-initiation of transcription (Shandilya and Roberts, 2012). Furthermore, gene looping of the 3'-end to the core promoter was observed (Lykke-Andersen et al., 2011; Kaderi et al., 2009).

The extended C-terminal domain (CTD) of the largest Pol II subunits (AMA-1 in *C. elegans*) is a central hub for regulation. Different model organism comprises a variable number of repeats of the sequence $Y_1S_2P_3T_4S_5P_6S_7$, e.g., 52 times in H. sapiens or 42 times in *C. elegans* (Allison et al., 1988; Rosonina and Blencowe, 2004). The different phases of the transcription cycle are characterized by distinct patterns of posttranslational modifications (PTMs) on the CTD, which serve as a binding platform for many factors involved in processes like RNA processing, histone modifications, or chromatin remodeling (Clapier et al., 2017; Bentley, 2014; Chen et al., 2018). Additionally, the long disordered CTD might also promote transcription initiation through phase separation (Lu et al., 2018; Kwon et al., 2014; Lu et al., 2019). Phase separation relies on the multivalent interactions of proteins with disordered regions that help to concentrate proteins in small droplets or condensates (Banani et al., 2017). Different microscopy assays have described transcription hubs or factories that could resemble such condensates (Tolhuis et al., 2002; Papantonis and Cook, 2013; Cisse et al., 2013; Buckley and Lis, 2014; Cho et al., 2018; Chong et al., 2018; Sabari et al., 2018). In this model, TFs with disordered regions could recruit Pol II via its CTD to initiate transcription (Boija et al., 2018; Kwon et al., 2014). Then phosphorylation of the CTD would disrupt self-association with the promoter condensate and release Pol II (Boehning et al., 2018). The phosphorylated CTD is a binding platform for many co-regulating and processing factors that bind to nascent RNA (Herzel et al., 2017; Battaglia et al., 2017). It was proposed that phosphorylated CTD, nascent RNA, and RNA binding proteins could form distinct condensates, termed "gene-body condensates" (Cramer, 2019; Guo et al., 2019). The model of initiation and elongation condensates supports a more dynamic transcription model. Condensates can form and dissolve rapidly by posttranslational modifications to alter the phase-separation properties of regulatory proteins.

1.2.4 Methods to study gene regulation

Our understanding of the regulation of gene transcription has been tremendously advanced by next-generation sequencing technology. Especially approaches capturing nascent transcription are informative about how genes are regulated. For example, using total RNA sequencing (without poly-A selection), the number of intronic reads can serve as a proxy for nascent transcription (Ameur et al., 2011). However, since most cellular transcripts are mRNAs, this is not a very efficient method to detect nascent transcription. A different technique to measure short-lived transcripts is transient transcriptome sequencing (TT-seq), where the incorporation of a labeled nucleotide is enriched before the sequencing reaction (Schwalb et al., 2016). Other methods that can study nascent transcripts are Global run-on sequencing (GRO-seq) and Precision Run-On Sequencing (PRO-seq), which are especially useful to map the location of active RNA polymerases or transcription start sites (TSSs) (Mahat et al., 2016; Core et al., 2008). Apart from this, approaches to study ongoing transcription include using Pol II binding measured by chromatin immunoprecipitation (ChIP-seq) as a proxy for active transcription (Wada et al., 2009). Alternatively, Pol II-associated RNAs can be purified and sequenced using native elongating transcript sequencing (NET-seq) (Nojima et al., 2015; Churchman and Weissman, 2011). While these approaches helped the field study many aspects of transcription regulation like poised Pol II close to promoters, it has become apparent in recent years that transcription is heterogeneous, and population-based methods fail to detect the differences in single cells or single organisms.

Differences in transcription between single cells may have consequences for the whole multi-cellular system or organism. New imaging methods allowed to study of single cells and their temporal discontinuous transcription. As markers of gene regulation, fluorescent proteins (FP) demonstrated that transcription of reporter genes in a population of genetically identical cells could vary considerably (Elowitz et al., 2002; Ozbudak et al., 2002). While fluorescent proteins helped to explore many aspects of gene regulation, measuring gene expression of FP is not a direct measurement of transcription and has limited sensitivity for minor fluctuations. By developing single-molecule fluorescent in-situ hybridization (smFISH) detection of RNA molecules, it became possible to study transcription and its variability in single cells (Raj et al., 2008; Femino et al., 1998). In smFISH, samples are fixed and hybridized with around 40 different 20 bp long fluorescently labeled oligonucleotide sequences complementary to a unique sequence of the target mRNA. These stained samples are imaged, and single spots can be localized, counted, and their intensity quantified. The application of smFISH for studying transcription yielded many insights into the mechanism of transcription regulation. It was discovered that transcription is a stochastic process with short, infrequent bursts of transcription resulting in significant variations in mRNA numbers (discussed below) (Raj et al.,

2006; Maamar et al., 2007). Several adjustments were made to the original smFISH method to decrease to cost of probes (Tsanov et al., 2016), reduce the hybridization time (Shaffer et al., 2013), or amplify the signal in different variations (Tavakoli et al., 2020; Wu et al., 2018; Marras et al., 2019; Wang et al., 2012). Especially in thick samples, amplification of the signal can increase the signal to noise ratio dramatically, however, precise quantification of transcription levels is obscured by signal amplification.

Additionally, live transcription methods were developed to better understand the dynamic aspect of transcription and study changes in the environment in a single cell over time. The transcription of a gene can be detected by adding a bacteriophage repeat sequence that forms stem-loops. These stem-loops can be recognized by a coat protein fused to a fluorescent protein (Beach et al., 1999; Bertrand et al., 1998). If the gene is expressed, the fluorescently labeled coat protein can bind to it during ongoing transcription and form a diffraction-limited spot. This fluorescent label allows the detection of promoters switching between inactive and active states and the number of RNAs produced from the integrated fluorescence intensity.

Since the described methods rely on designing probes against target genes or genetically modifying cells and organisms, their throughput is limited. Gene regulatory networks, however, can be complex, and an unbiased way of sampling more genes can give new insights into how pathways are connected. New methods that combine imaging with sequencing, termed spatial sequencing or spatial transcriptomics, offer great ways to study gene regulation with a high number of targets while preserving their spatial context (Ståhl et al., 2016). Several methods have been developed that either rely on a variation of FISH by using a binary code in several rounds of hybridization (Chen et al., 2015) or in situ sequencing where an amplicon is detected by a set of barcodes (Wang et al., 2018; Lee et al., 2014). While these methods promise exciting possibilities for high throughput assays, they are still being developed and can be technically challenging. For example, these methods rely on detecting barcodes for the same RNA between multiple rounds of labeling and washing. Especially registration of single points between multiple rounds is fundamental to detect the RNA correctly, but this can be challenging with samples deforming over the experimental time course.

1.2.5 Detection methods for single-molecule FISH spots

With the popularization of smFISH applications, the need for fast and precise detection of smFISH spots arose. Most available tools use a Gaussian fitting method to detect the centers of single spots (Thompson et al., 2002). While using Gaussian fitting algorithms results in precise localization in XYZ, they tend to have a relatively slow processing speed due to their iterative nature (Martens et al., 2018). Long computation times can be especially problematic for large

datasets or big volumes. Furthermore, different smFISH protocols and the use of different types of microscopes, such as epifluorescent, confocal, or lightsheet, can influence the appearance of single spots. Most current detection tools have a limited possibility to change critical parameters to allow detection across different samples (Tsanov et al., 2016; Mueller et al., 2013a; Lionnet et al., 2011; Raj et al., 2006). In conclusion, there is a need for a computationally efficient and freely accessible software tool to allow detection in large datasets with the possibility to adjust critical parameters.

1.2.6 Transcriptional bursting

Through advanced imaging methods, it has become apparent in the past two decades that transcription is an inherently stochastic process with discontinuous transcription leading to heterogeneous mRNA levels in a population of genetically identical cells (Raj and Oudenaarden, 2008). This variability is driven by intrinsic and extrinsic noise, which leads to stochastic bursts of transcription (Singh and Soltani, 2013; Swain et al., 2002). Extrinsic noise describes cell-to-cell differences in cell-specific factors such as enzyme levels, cell size, and cell cycle stage. In contrast, intrinsic noise describes the stochastic fluctuations of molecules involved in biochemical processes. Molecular noise is unavoidable, ubiquitous, and affects many cellular processes, but it can also bring advantages to the system. Gene expression noise can enable physiological regulation mechanisms like the coordinated expression of many genes as observed in yeast, where gene regulation in response to calcium was regulated by frequency-modulation (Cai et al., 2008). On a population level, gene expression noise can permit a wide range of probabilistic differentiation strategies (Losick and Desplan, 2008). Examples of stochastic cell fate decisions during development include the color vision photopigment selection in primates or olfactory receptor selection in mice (Johnston and Desplan, 2010). Gene expression noise can also facilitate evolutionary adaptation and generate diversity. A wide range of phenotypes can arise from a single genotype through stochastic gene expression, which can be advantageous in a fluctuating environment with selection pressures (Eldar and Elowitz, 2010).

Different models were used to fit the imaging data to infer the regulation of transcription bursting from smFISH or live transcription data. One commonly used model is the “random telegraph model” (Figure 4) (Raj et al., 2006; Peccoud and Ycart, 1995; Munsky et al., 2012). In this model, transcription bursting can be described by two characteristic values: the burst size and the burst frequency. The burst size describes the number of RNAs transcribed from one promoter during an active period, and the burst frequency describes the number of transcription bursts over time (Golding et al., 2005; Suter et al., 2011). Also, a third regulatory

phase was described in live-imaging studies that found a refractory period or transcriptionally silenced period between bursts (Tantale et al., 2016).

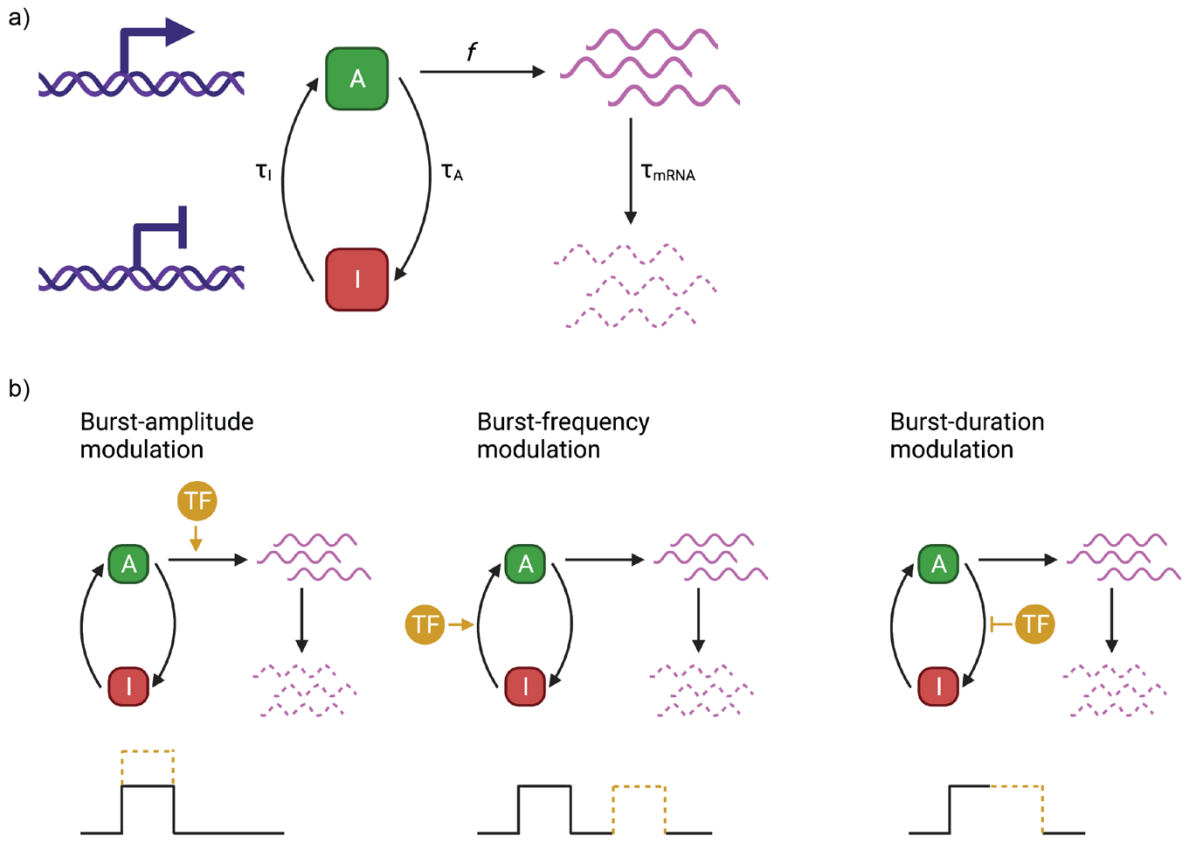

Figure 4 The telegraph model for transcription bursting.
a) The telegraph model describes the fluctuation of a promoter between the inactive (I) and active (A) state. In the inactive state, the promoter does not have transcriptional activity but could be poised for transcription. In the active state, the promoter actively transcribes the gene with a rate of *f*. The half-time of the produced mRNAs is described by τ_{mRNA}. The rate of switching between the active and inactive stages is described by τ_I and τ_A. **b)** Model of how TF binding can modulate transcription burst size, frequency, or duration. Figure adapted from (Li et al., 2018a) and created with BioRender.com.

These burst characteristics have been linked to several regulatory processes. To adapt cellular RNA levels to different cell sizes, it has been shown that mammalian cells modulate the burst size while burst frequency modulation was used to adapt transcription after DNA replication (Padovan-Merhar et al., 2015; Skinner et al., 2016; Kempe et al., 2015). To downregulate transcription of a gene, the associated promoter could either switch less often from inactive to active state and therefore reduce the burst frequency or destabilize the active state and reduce the burst size. Several molecular mechanisms have been suggested to regulate these two regulatory possibilities like TF binding, chromatin state, DNA topology, chromatin remodeling, enhancer looping, the stability of PIC and Pol II pausing. The burst frequency can be modulated by the rate of PIC initiation, while the burst size was regulated by the duration of Pol II

reinitiating (Yudkovsky et al., 2000; Hahn, 1998). In yeast, transcription was increased in two different ways and through two different promoter sequence mutations. Either mutating the TF binding site for more stable binding and increasing the burst size or increasing the burst frequency by mutating the promoter to nucleosome-disfavoring sequences (Dadiani et al., 2013). Promoter regulation in metazoans tends to be more complex, but a study found for the FOS gene that TF levels positively correlated with the frequency of FOS transcription burst (Senecal et al., 2014). Systematic mutation of the promoter elements in primary B cells found that different the regulation was either by burst size, frequency, or both and context-dependent (Hendy et al., 2017).

1.2.7 Imaging gene regulation in *C. elegans*

Many characteristics of the model organism *C. elegans* make it an appealing organism for imaging, including its size, transparency, and invariant cell lineage (Figure 5) (Nigon and Félix, 2017). These features allowed it early on to follow the complete cell linage using differential interference contrast (DIC) microscopy (Sulston and Horvitz, 1977; Sulston et al., 1983).

Undoubtedly, *C. elegans* had a central role in studying gene regulation when Green Fluorescent Protein (GFP) was first expressed in the roundworm (Chalfie et al., 1994). The use of GFP and other fluorescent proteins (FP) has been fundamental in reporter gene assays to study gene expression (Boulin et al., 2006). Reporter gene assays rely on the expression of an FP with a specific promoter sequence. In *C. elegans*, these reporters were either expressed from extrachromosomal arrays (Mello et al., 1991) or are stably integrated into the genome by bombardment (Praitis et al., 2001), the mosSCI system (Robert and Bessereau, 2007; Frøkjær-Jensen et al., 2012) or more recently also by CRISPR (Paix et al., 2015; Mouridi et al., 2017). Especially CRISPR is critical to study gene regulation as it allows to target endogenous genes with FP to keep the spatio-temporal expression of genes studied (Dickinson and Goldstein, 2016). While many characteristics of *C. elegans* make it an excellent organism for imaging, more biophysical and live imaging methods have been limited, probably because of challenges arising from body movement and relatively small nuclei. Studies on protein dynamics using Fluorescence Recovery After Photobleaching (FRAP) have been mostly limited to embryos (Daniels et al., 2010; Goehring et al., 2011). New variants of FP are continuously engineered and adapted for use in *C. elegans* (Lam et al., 2012; Redemann et al., 2011; Green et al., 2008). Recently, the use of HaloTag was demonstrated for *C. elegans* (Fan et al., 2019; Wu et al., 2019). This development is especially exciting for live transcription assays such as MS2 or PP7, considering that the integration of HaloTag reporters has improved live transcription studies in other organisms (Coleman et al., 2015; Stracy and Kapanidis, 2017).

A direct way to study expressed RNAs without requiring genomic engineering is to use RNA in-situ hybridization that uses antisense RNA probes to label expressed RNAs (Broitman-Maduro and Maduro, 2011). While this method detects qualitative transcription changes, counting single RNAs using smFISH is a more suitable technique to assess quantitative transcription changes (Raj et al., 2008; Ji and Oudenaarden, 2012; Ni et al., 2018; Bolková and Lanctôt, 2016). Especially applying smFISH in *C. elegans* embryos can be a powerful method since the staining protocol is straightforward and can be applied to large numbers of embryos. Additionally, the mRNA counts in staged embryos can be combined with the invariant lineage of *C. elegans* to get quantitative RNA counts at specific developmental time points (Charles et al., 2020).

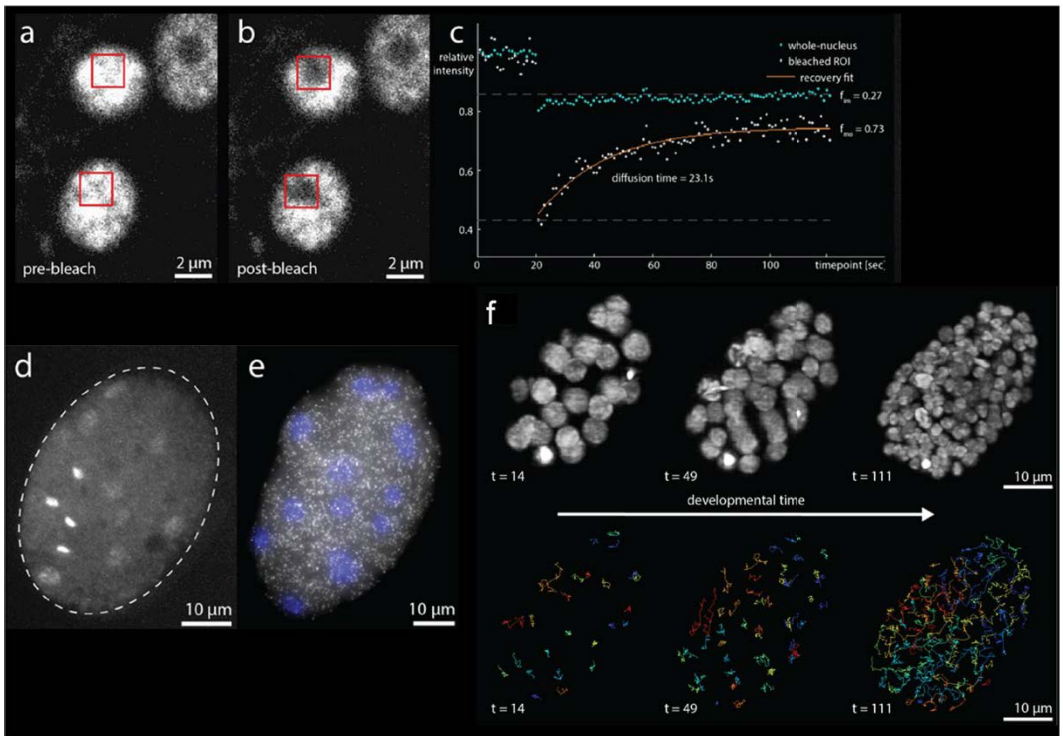

Figure 5 Examples of imaging approaches in *C elegans*.
a-c) FRAP analysis on H2B-mCherry in L1 larvae tail nuclei. Red boxes indicate areas used for bleaching and consequent fluorescent analysis. One example recovery curve is plotted in c. The mobile and immobile fractions are calculated by fitting the recovery curve. **d)** Early embryo expressing an H4K20me1 mintbody fused to GFP. Mitotic chromosomes show a strong signal for H4K20me1.**e)** Maximum intensity projection of a young *C. elegans* embryo labeled with smFISH probes against W04G3.5 mRNA (grayscale) and DAPI (blue). **f)** Maximum intensity projection of lightsheet microscopy images of *C. elegans* embryonic development at three different time points. Nuclei are marked with H2B-mCherry. The bottom row show tracks for segmented nuclei (5 min trajectories). Image modified from (Breimann et al., 2019).

1.3 An X-specific condensin in *C. elegans* serves as a model to study the role of 3D genome organization in gene regulation

A clear example of condensin-mediated gene regulation is the *C. elegans* dosage compensation system. Dosage compensation describes the regulatory process of equalizing the gene dosage between organisms with different copy numbers of sex chromosomes. Maintaining the proper gene dosage is crucial for normal cellular function and development, and failure to do so would be detrimental for the organism (Oromendia and Amon, 2014; Agrelo and Wutz, 2010). Different animals have evolved distinctive strategies to balance the dosage of sex chromosomes (Charlesworth, 1996). Relatively well-studied dosage compensation systems are in mammals, flies, and roundworms, as depicted in Figure 6. Mammals inactivate one of the two X in females to equalize gene dosage between XX females and XY males. *Drosophila* males (XY) upregulate their single X gene dosage two-fold to match it to the female (XX) dosage. In *C. elegans*, hermaphrodite worms (XX) downregulate both X by two-fold to match the male (X0) gene dose level. While the details vary, they also share general strategies for targeting the X chromosome for chromosome-wide gene regulation. In these systems, a large chromatin altering complex is targeted to one or two of the sex chromosomes (Straub and Becker, 2007). In addition, the complex controls gene expression only from the targeted X chromosomes and does not alter autosomal transcription (with a few exceptions). For the *Drosophila* and *C. elegans* systems, these complexes fine-tune the transcription by altering it two-fold. Also, the timing is crucial. The dosage compensation process starts during early development, and failure of the system is lethal.

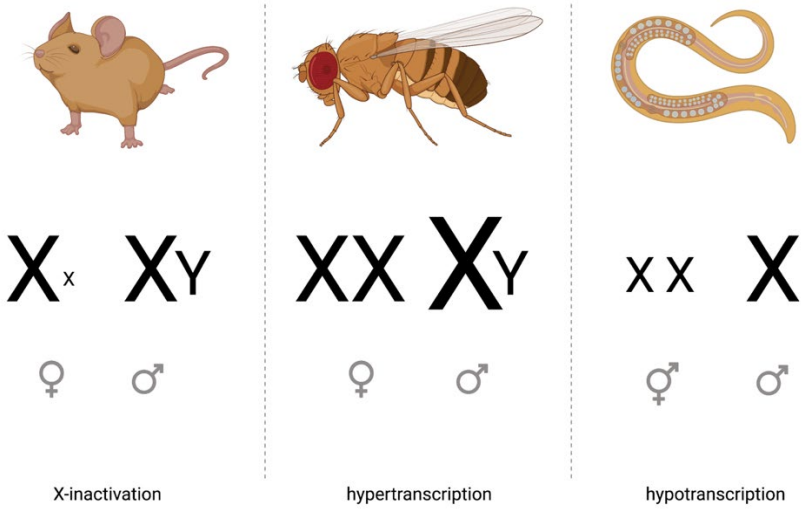

Figure 6 Examples of dosage compensation in different organisms.
Mammals, flies, and worms use a different mechanism to balance the gene dosage from different numbers of sex chromosomes. In mammals, females inactivate one X chromosome. In male flies, the single X is hyper-transcribed. The two X chromosomes of hermaphrodites are hypo-transcribed to match transcription to the single X in males in worms. Figure created with BioRender.com.

The mammalian strategy to dosage compensation is to silence one X chromosome in females to equalize the dosage to the XY males (Lyon, 1961; Brown et al., 1991). The inactive X is tightly packed into the Barr body, which can be observed using microscopy (Barr and Bertram, 1949; Ohno and Hauschka, 1960). The selection of which of the two X is inactivated is random (Galupa and Heard, 2016). The inactivation is accomplished through the cis-acting non-coding RNA Xist, which is transcribed from the X that will be inactivated (Xi) (Brown et al., 1991; Brockdorff et al., 1991). Xist then covers the whole length of the Xi chromosome and recruits chromatin modifiers and other factors for gene silencing (Brockdorff et al., 2020). As a result, the Xi loses histone modifications associated with active transcription and binding of RNA Pol II, and gains chromatin marks associated with silenced chromatin and DNA methylation (Brockdorff et al., 2020). Interestingly, an SMC-like protein, SmcHD1, was identified to play a role in X inactivation in mice (Blewitt et al., 2008). SmcHD1 is recruited to the Xi only after the onset of Xist expression and is thought to function in the maintenance of X inactivation by regulating higher-order chromatin structure (Gdula et al., 2019), while recent results suggest that the role in chromatin regulation may not be involved in gene silencing (Fierro et al., 2021).

The dosage compensation in *Drosophila* follows a different mechanism than the mammalian system. Male flies upregulate their single X chromosome two-fold to match the expression of the two X chromosomes of female flies (Gergen, 1987). If the dosage compensation mechanism fails, male-specific lethality is observed (Kuroda et al., 2016). The multi-subunit male-specific lethal complex (MSL), consisting of five proteins and one non-coding RNA, is targeted to the male X chromosome, where it enhances chromatin accessibility and increases transcription (Samata and Akhtar, 2018; Hamada et al., 2005). The MSL complex is targeted through its DNA binding subunit, MSL2, firstly to sites called PionX (pioneering sites on the X) and subsequently to other high-affinity sites (HAS) (Kelley et al., 1999; Alekseyenko et al., 2008; Dahlsveen et al., 2006; Straub et al., 2013; Villa et al., 2016). The expression of MSL2 during early development is repressed in female flies by the master regulator sex-lethal (Sxl) (Pomiankowski et al., 2004). Once bound to the entry site, the MSL complex spreads to nearby active genes through its subunit MSL3, which can bind to H3K36me3, the histone mark associated with active genes (Larschan et al., 2007; Sural et al., 2008). The existing 3D chromatin architecture of the X chromosome facilitates the binding to nearby genes, and their transcription upregulation correlates with their proximity (Schauer et al., 2017). Subsequently, the male X is hyperacetylated at H4K16 by a subunit of the MSL complex, the acetyltransferase MOF (males absent on the first) (Hilfiker et al., 1997), which weakens the binding of nucleosomes, opens the chromatin fiber, and allows transcription to be more efficient (Dunlap et al., 2012; Larschan et al., 2011). It has been proposed that the MSL complex regulates expression by controlling transcription elongation (Smith et al., 2001).

1.3.1 Dosage compensation in *C. elegans*

C. elegans uses yet another molecular mechanism for dosage compensation: the dosage compensation complex (DCC), which contains the specialized condensin DC binds to the two X chromosomes of the hermaphrodite and downregulates transcription of both X chromosomes by about two-fold (Meyer and Casson, 1986; Albritton and Ercan, 2018). The binding of the DCC to the X chromosomes is also responsible for compacting their volume by 40% (Lau et al., 2014). Furthermore, the DCC regulates chromatin architecture on the X chromosome. Hi-C analysis of the *C. elegans* genome revealed that TAD structures were most prominent on the X chromosome and dependent on the binding of the DCC (Crane et al., 2015; Brejc et al., 2017; Anderson et al., 2019). Notably, most of the TAD boundaries coincided with strong DCC binding sites (Crane et al., 2015). Together, this supports a hypothesis where the DCC binding to the X chromosome condenses the chromosome, changes the 3D architecture of the X, and downregulates transcription of X-chromosomal genes.

1.3.2 The dosage compensation complex (DCC) regulates X chromosome gene expression

C. elegans has, besides the canonical condensin I and II complexes, a third condensin complex, condensin DC, that shares many subunits with condensin I and forms together with additional proteins the dosage compensation complex (DCC) as depicted in Figure 7 (Chu et al., 2002; Pferdehirt et al., 2011; Yonker and Meyer, 2003). The DCC is targeted to both X of hermaphrodite cells, binds and compacts the chromosomes, and down-regulates transcription by two-fold (Lau et al., 2014; Jans et al., 2009; Kruesi et al., 2013; Kramer et al., 2015).

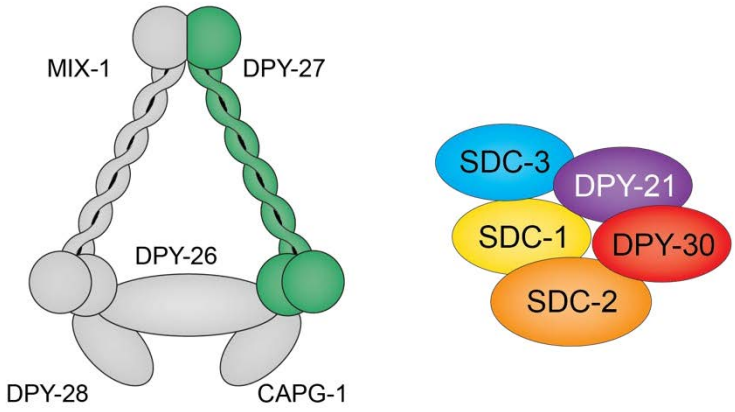

Figure 7 The C. elegans Dosage Compensation Complex (DCC).
The DCC consists of the SMC subunit condensin DC and the non-SMC-proteins SDC-1, SDC-2. SDC-3, DPY-21, and DPY-30. Condensin DC shares most subunits with condensin I but has the unique subunit DPY-27.

The DCC consists of five condensin and five non-condensin subunits. The condensin part of the complex shares four subunits with condensin I (Lieb et al., 1996; Dawes et al., 1999; Csankovszki et al., 2009b; Lieb et al., 1998; Chuang et al., 1996). The SMC protein MIX-1 (mitosis and X associated) and the regulatory subunits DPY-26, DPY-28 (dumpy: shorter than wild-type), and CAPG-1 (chromosome associated polypeptides) are all part of condensin I and involved chromosome segregation during mitosis (Plenefisch et al., 1989b; Lieb et al., 1998). The condensin DC-specific subunit is DPY-27, which is an SMC protein and replaces SMC4 (Chuang et al., 1994). Both MIX-1 and DPY-27 contain ATPase domains (Chuang et al., 1994; Lieb et al., 1998). The two SMC subunits are bound to the kleisin subunit DPY-26. The two HEAT repeat-containing subunits are DPY-28 and CAPG-1 (Yoshimura and Hirano, 2016). The DCC's non-SMC proteins have regulatory functions and include SDC-1, SDC-2, SDC-3 (sex determination and dosage compensation defect), DPY-30, and DPY-21.

While the mammalian and fly dosage compensation mechanism includes a lncRNA, no RNA component has been identified to play a role in the worm dosage compensation mechanism. Most non-SMC DCC proteins are essential for the worm, and mutations in SDC-2, SDC-3, and DPY-30 cause XX-specific lethality (Villeneuve and Meyer, 1987; Nusbaum and Meyer, 1989; DeLong et al., 1993; Hsu and Meyer, 1994). However, DPY-21 or SDC-1 are not essential for dosage compensation, and knock-down of these proteins causes partial lethality and strong phenotypes (Villeneuve and Meyer, 1987; Hodgkin, 1983a).

Apart from their function in dosage compensation, several DCC proteins also play a role in other pathways. SDC-1, for instance, binds to the autosomal gene *her-1* and strongly reduces the expression in the sex determination pathway (Trent et al., 1991; Chu et al., 2002; Yonker and Meyer, 2003). DPY-30 is also part of the MLL/COMPASS complex that functions in gene activation through H3K4 methylation (Pferdehirt et al., 2011; Hsu and Meyer, 1994). DPY-21 was recently described to have a Jmj-C demethylase activity. It is crucial for X-specific demethylation of H4K20me2 to H4K20me1. The knock-out of DPY-21 causes partial lethality, a strong dumpy phenotype (shorter and broader body size), and the loss of H4K20me1 enrichment on the X chromosomes in hermaphrodite worms (Brejc et al., 2017; Kramer et al., 2015; Vielle et al., 2012; Yonker and Meyer, 2003). DPY-21 also has been implicated in the regulation of Dauer arrest, metabolism pathways, and higher-order chromosome structure in meiotic nuclei (Dumas et al., 2013; Webster et al., 2013; Brejc et al., 2017; Delaney et al., 2017).

In summary, the DCC and its role in chromosome-wide gene regulation for dosage compensation is a great model for studying the basic mechanism of gene regulation by condensins. Since condensins' role in mitosis is essential, teasing apart its role in the two pathways is difficult. Mutations of condensin I and II additionally cause mitosis problems (Martin et al., 2016; Nishide and Hirano, 2014; Woodward et al., 2016). Furthermore, the recruitment of condensin to

chromosomes is not well understood. In contrast, several aspects of condensin DC loading are known and can help elucidate potential general mechanisms. Furthermore, the chromosome-wide gene regulation of DCC can serve as a model of how genes can be co-regulated over long distances.

1.3.3 Developmental timing of dosage compensation

The start of *C. elegans* dosage compensation is around the 30 cell stage as measured by immunofluorescence when the before diffuse staining of the condensin DC subunit DPY-27 starts to localize to the X chromosomes (Chuang et al., 1994). Embryos defective for dosage compensation die late in embryogenesis, suggesting this to be a critical developmental timepoint for proper gene dosage (Plenefisch et al., 1989a). However, dosage compensation continues throughout embryogenesis, and genes might not reach a complete dosage compensation until the L1 stage (Kramer et al., 2015).

To ensure hermaphrodite exclusive targeting of the X chromosomes by the DCC, sex-specific transcription programs need to be activated. In *C. elegans,* this happens by assessing the X to autosome ratio through specific elements on the X chromosomes and autosomes (Figure 8). The maternal to zygotic transcription activation in *C. elegans* happens around the 3-4 cell embryo (Edgar et al., 1994; Baugh et al., 2003; Seydoux and Fire, 1994; Seydoux and Dunn, 1997). In males, the X to A ratio leads to low repression and thus the expression of *xol-1* (XO lethal) around the 28-cell stage. The XOL-1 kinase is the master regulator for sex determination and dosage compensation (Gladden and Meyer, 2007). XOL-1 represses through an unknown mechanism the transcription of *sdc-2*, the loading factor for the DCC, and essential for dosage compensation (Miller et al., 1988; Dawes et al., 1999). In hermaphrodites, *xol-1* expression is repressed, which in turn fails to repress *sdc-2* expression, and consequently, the dosage compensation complex including SDC-2 can assemble.

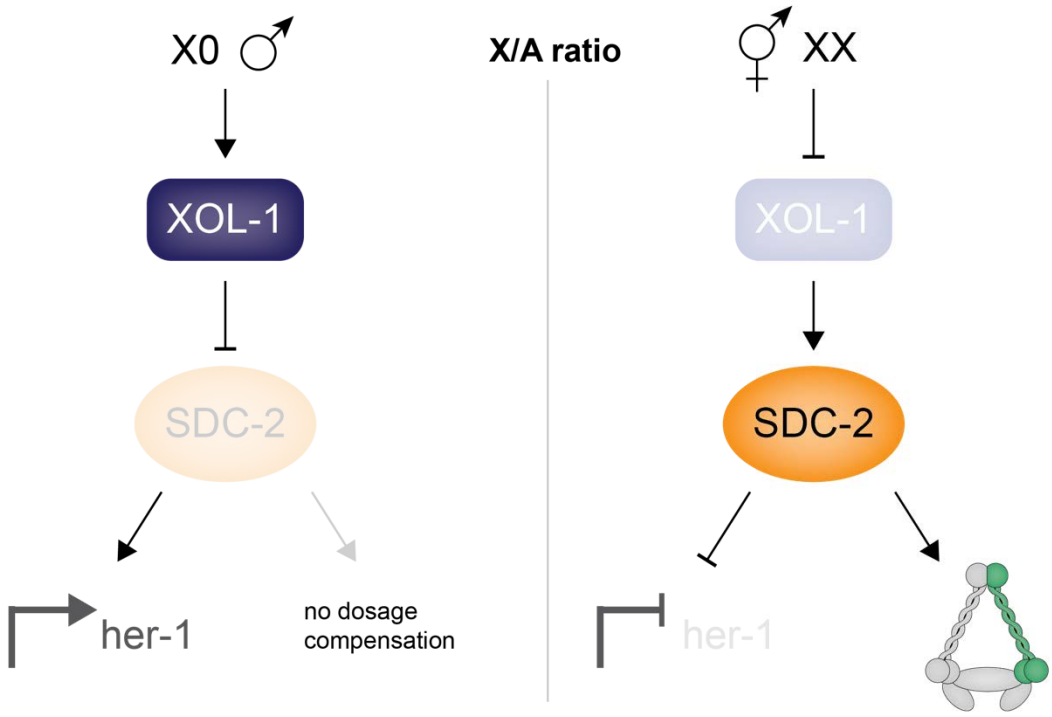

Figure 8 Model for sex determination in *C. elegans.*
The ratio of X chromosomes to autosomes determines if the *xol-1* expression is promoted or repressed. In males, *xol-1* is expressed and acts negatively on the expression of *sdc-2.* Without the expression of *sdc-2*, *her-1* is expressed, and male development is initiated. In hermaphrodites, the ratio of X chromosomes to autosomes repressed the expression of *xol-1* and therefore promotes the expression of *sdc-2.* SDC-2 is required for binding of the DCC to the X chromosome and the *her-1* locus.

At the 40-cell stage, SDC-2 is expressed and binds to the X chromosomes independent of other DCC subunits (Figure 9) (Chuang et al., 1996; Davis and Meyer, 1997; Dawes et al., 1999). SDC-2 is a large 344 kDa protein and the only DCC member that is not maternally loaded, but sex-specifically expressed at the 40-cell stage (Plenefisch et al., 1989a; Dawes et al., 1999). Subsequently, the DCC complex can assemble. First, SDC-3 binds, which need SDC-2 for binding to the X chromosome (Davis and Meyer, 1997). These two proteins might serve as the loading complex for condensin DC. Then DPY-30 binds and promotes the binding of the remaining DCC subunits to the X chromosome (Hsu et al., 1995; Pferdehirt et al., 2011). SUMOylation of the subunits SDC-3, DPY-27, and DPY-28 promotes robust DCC assembly and function (Pferdehirt and Meyer, 2013). Around the 100-cell stage, H4K20me1 is enriched explicitly on the X chromosomes (Vielle et al., 2012; Liu et al., 2011; Wells et al., 2012). The enrichment is mediated by the DCC subunit and H4K20me2 demethylase DPY-21 (Brejc et al., 2017). The binding of the DCC and dosage compensation of the X chromosome continuous throughout development until the adult stage, and the majority of X chromosomal genes are dosage compensated entirely only after the comma stage of embryogenesis (Kramer et al., 2015).

The binding of the DCC is restricted to the X chromosome, with one exception. The DCC also binds to one location on chromosome V, the *her-1* gene, essential for male development. In hermaphrodites, the complex binds to the gene and downregulates its transcription by ~20 fold to ensure no male developmental program is started (Trent et al., 1991; Yonker and Meyer, 2003). Interestingly, the demethylase DPY-21 is not located at the *her-1* gene (Yonker and Meyer, 2003). Thus, the more than two-fold downregulation and absence of DPY-21 could suggest DPY-21 involvement in regulating DCC's strength of gene regulation.

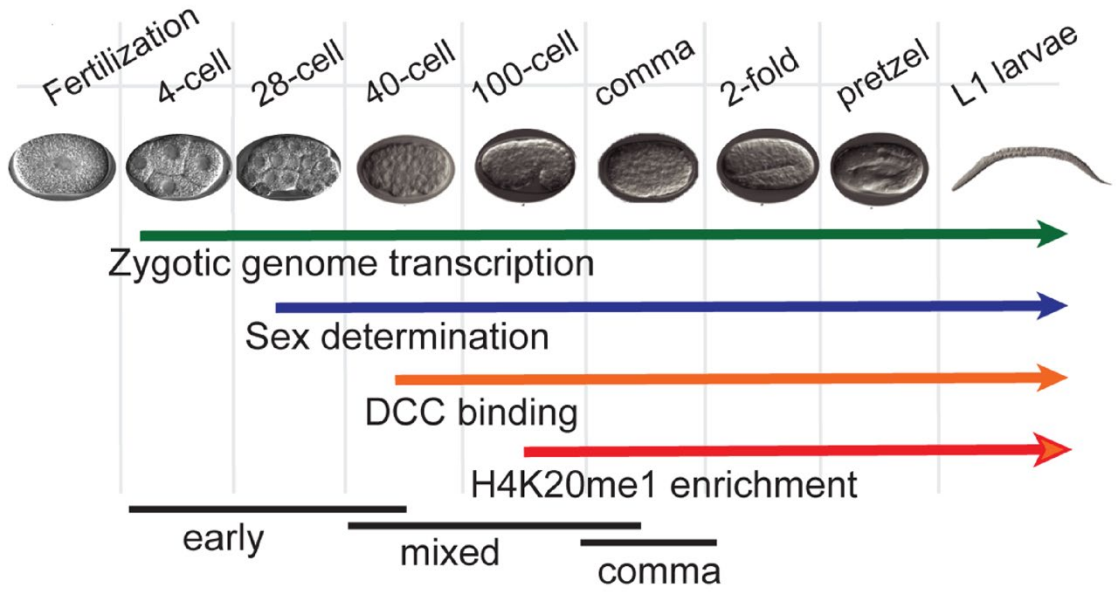

Figure 9 Developmental timing of dosage compensation.
The zygotic genome is activated around the 4-cell stage, followed by sex-specific gene expression around the 28-cell stage. Next, the DCC starts binding to the X chromosome at the 40-cell stage. Finally, X-specific enrichment of H4K20me1 is detectable at the 100-cell stage. Image from (Kramer et al., 2015).

1.3.4 Recruitment and Spreading of DCC

The binding of DCC can be detected across the whole length of the ~17 Mb X chromosomes (Chuang et al., 1994; Dawes et al., 1999; Ercan et al., 2009; Kranz et al., 2013; Jans et al., 2009; Ercan et al., 2007). However, DCC binds more strongly to enhancers, gene promoters, and a specific DNA motif. ChIP-chip and extrachromosomal recruitment assays found that a 12-bp DNA motif, termed 'recruitment element on X' or *rex* site, is necessary to recruit the DCC complex (Figure 10a) (Ercan et al., 2007; Jans et al., 2009; McDonel et al., 2006). There are ~60 recruitment sites on the X chromosome, each consisting of one or more *rex* sites, and their orientation is not essential for their function (Albritton et al., 2017; Jimenez et al., 2021). While *rex* sites are enriched on the X chromosome, they are also present on the autosomes, comparable to MSL recruitment in *Drosophila* (Alekseyenko et al., 2008, 2012). How does the system ensure

that the DCC is only targeted to the X chromosomes and not the autosomes? The recruitment to the X chromosome is structured hierarchically and cooperatively. Strong recruitment sites, consisting of *rex* motif clusters (at least two motifs within 200 bp), are the initial binding sites for DCC and are only present in the X chromosomes (Figure 10b) (Albritton et al., 2017). From there, the DCC can spread to weaker recruitment sites, enhancers, and gene promoters (Ercan et al., 2009, 2007; Kruesi et al., 2013). Besides having motif clusters, strong recruitment sites often overlap with high occupancy transcription factor target (HOT) sites and are marked by DNA sequences encoded for high nucleosome occupancy (Albritton et al., 2017). Seventeen strong *rex* sites are distributed over the length of the X chromosome spaced about 1 Mb apart and interspersed with weaker recruitment sites (Albritton et al., 2017). Intermediate and weak recruitment sites have less clustered motifs and overlap more frequently with tRNA genes which might be a general conserved feature of condensin binding (Kranz et al., 2013; Haeusler et al., 2008; Kim et al., 2019b; D'Ambrosio et al., 2008). Single weaker recruitment sites from the X chromosome ectopically integrated onto autosomes fail to recruit the DCC. However, the insertion of several *rex* sites placed at ~50 kb distance was able to robustly recruit the DCC underlining the cooperation of different *rex* sites for DCC recruitment (Albritton et al., 2017).

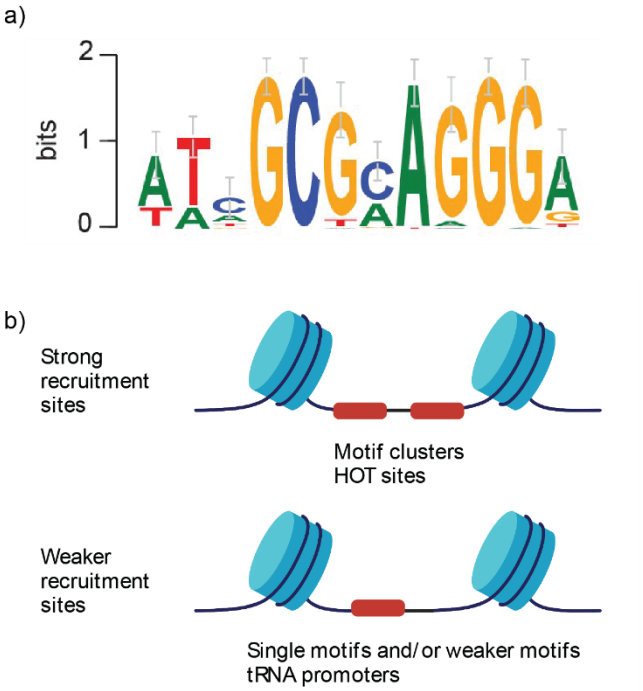

Figure 10 Recruitment elements of the X chromosome.
a) The 12-bp recruitment motif enriched on the X chromosome was identified using high-resolution SDC-2 ChIP-seq data. Figure from (Albritton et al., 2017). **b)** Different features differentiate strong recruitment sites from weaker recruitment sites. Strong recruitment sites are only found on the X chromosome, often include sequence motif clusters, and often overlap with HOT sites. On the other hand, weaker recruitment sites on the X chromosome and autosomes tend to have only single and weaker motifs or overlap with tRNA genes. Figure adapted from (Albritton and Ercan, 2018) and created with BioRender.com.

Deleting a single *rex* site reduced DCC binding to the ~1 Mb surrounding chromatin area weakly but significantly (Figure 11a) (Albritton et al., 2017). This effect was particularly pronounced for the leftmost and rightmost *rex* sites. Possibly the loss of internal *rex* sites can be compensated by neighboring rex sites. Interestingly, deletion of *rex-41* at the end of the X chromosome also slightly increased transcription from genes within a 500 kb window (Figure 11b) (Albritton et al., 2017). In contrast, in a recent paper, deletion of eight strong *rex* sites did not result in detectable expression changes close or far from the deleted *rex* sites using a gene expression change analysis with a 400 kb sliding window (Anderson et al., 2019). However, the data suggested that the *rex* site deletions shortened lifespan, possibly through gene expression changes around the two leftmost deleted *rex* sites (Anderson et al., 2019). Nevertheless, transgenes integrated at different locations on the X were transcriptionally downregulated, but repression did not correlate with their distance to the nearest *rex* site (Wheeler et al., 2016). How *rex* sites and their proximity to genes influence transcription remains an interesting open question.

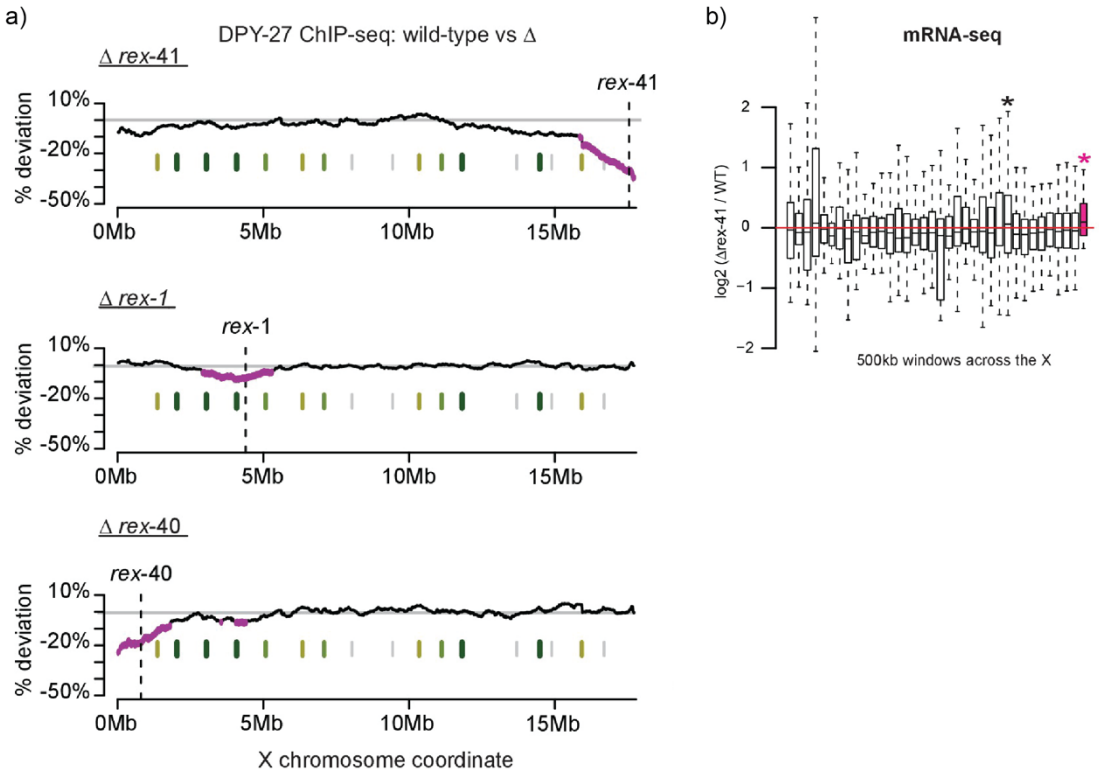

Figure 11 Contribution of single recruitment sites for DCC binding and function.
a) Deletion of single rex sites reduces binding of DPY-27 as measured by ChIP-seq. A sliding window analysis (window size 2Mb across each DPY-27 peak) was used to show differences in binding of DPY-27 in wild-type and single rex-site deletion strains. Pink regions have significantly less DPY-27 binding. Green bars indicate TAD boundaries. **b)** mRNA-seq analysis for the rex-41 deletion strain. The boxplots show a log2 ratio between the deletion strain and wild-type worms for 500 kb windows across the X chromosome. The rightmost window shows increased transcription in the rex-41 deletion strain. Figures from (Albritton et al., 2017).

After the initial binding of the DCC to strong rex sites, DCC spreads over the whole length of the X chromosome. DCC spreading is not sequence-specific as it can spread into autosomal regions when fused to the X chromosome (Ercan et al., 2009). The spreading into the autosomal region reduces with distance, suggesting that the DCC falls off chromatin and is not replenished as recruitment sites lack on the autosome. Additionally, the spreading of condensin DC is bidirectional and can reach long distances (~1 Mb) (Jimenez et al., 2021). Nonetheless, the spreading mechanism by which the DCC reaches other parts of the X after loading is not fully understood.

There are different models for the spreading mechanism which are not mutually exclusive. Measurements of binding dynamics across different species suggest that condensin binding is dynamic (Gerlich et al., 2006a; Oliveira et al., 2007; Walther et al., 2018; Robellet et al., 2015; Leonard et al., 2015). One possibility is that the DCC falls off and rebinds dynamically and thereby 'hops' to different DNA sequences that are close in 3D space. A different model would suggest that condensin topologically entraps DNA and spreads linearly on chromatin. The autosomal fusion experiments, where condensin linearly spreads onto the autosomal region, support this model (Ercan et al., 2009). The linear decay of DCC binding from the X:A fusion site suggests that DCC can translocate on DNA until it falls off. However, it does not exclude an active unloading mechanism. Additionally, if condensin encounters a bulky obstacle (>1400 kDa), it can be blocked *in vivo* (Jimenez et al., 2021). While this suggests that condensins could only form loops until the next chromatin-binding protein blocks them, it has been shown that condensins can transverse each other *in vitro* and in prokaryotes *in vivo* (Kim et al., 2019a; Brandão et al., 2020). Alternatively, the DCC could once bound, actively extrude chromatin loops until it reaches weaker recruitment sites and gene promoters, thereby bringing distant sequences in close proximity.

Interestingly, Hi-C analysis revealed that at least some of the strong *rex* sites function as TAD boundaries on the X chromosome, which were eliminated with an SDC-2 knock-down or the deletion of the overlapping *rex* sites (Crane et al., 2015; Anderson et al., 2019). *De novo* inserted *rex* sites on autosomes can also bind condensin DC and form loop anchored TAD-like domains (Jimenez et al., 2021; Albritton et al., 2017). Interestingly, modeling and experiments in prokaryotes suggested that while condensins could transverse each other, it would still reduce their translocation rate and if too many condensins collide, a block would emerge (Brandão et al., 2020; Anchimiuk et al., 2020). The ability of strong *rex* sites to load condensin DC would probably create an obstacle and, therefore, might reflect their ability to insulate TADs (Albritton et al., 2017; Crane et al., 2015). Finally, DCC movement could also be coupled to active transcription. The RNA Pol II could push condensin DC along the chromosome (Lengronne et al., 2004; Glynn et al., 2004; Wang et al., 2005; Racko et al., 2017; Borrie et al., 2017; Ocampo-

Hafalla et al., 2016; Gullerova and Proudfoot, 2008). Interestingly DCC binding is enriched a convergent gene ends (Ercan et al., 2007). In addition, there are many more DNA translocating enzymes such as helicases or translocases that use ATP and could be involved with the spreading of condensin DC (Briggs and Fischer, 2014; Stigler et al., 2016).

The above-discussed spreading mechanisms are not mutually exclusive and could reflect differential context-dependent condensin regulation. While many of the reported findings provide an insight into the static binding, an understanding of the dynamics of DCC is missing. More recently, and primarily through imaging methods, a more dynamic view on TADs and chromatin loop structures emerged (Hansen et al., 2018; Lazar-Stefanita et al., 2017; Golfier et al., 2020; Zhao et al., 2020). In addition, links between the dynamics of SMC molecules and their function in gene regulation have been proposed (Liu et al., 2021; Kriz et al., 2021). Therefore, studying the dynamics of condensin DC binding to the X chromosome and how this influences the gene regulation on the X is key to our understanding.

1.3.5 Mechanism of X chromosome repression

Although many studies tried to elucidate different aspects of dosage compensation in *C. elegans*, the mechanism of gene downregulation is not well understood. Specifically, how the DCC can regulate gene dosage on the one hand for genes over the entire length of the X chromosome and on the other hand with an average two-fold reduction is an exciting enigma.

Regulation of gene dosage could happen at several levels. On the protein level, the localization, stability, and degradation of proteins could be modulated (Varshavsky, 2012; Foot et al., 2017; Pizarro and Norambuena, 2014; Colón et al., 2017). A substantial effect on the protein abundance can also be accomplished by altering protein translation (Ingolia et al., 2009; Bastet et al., 2018). Apart from this, mRNA transport and stability are also critical for controlling the transcriptome (Munchel et al., 2011; Sieburth and Vincent, 2018; Bicknell and Ricci, 2017). Given that the DCC targets the X chromosome directly, it is more likely that the regulation happens at the transcription level.

The DCC binds to about 75% of promoters of active genes on the X chromosome (Ercan et al., 2007). While binding of DCC generally correlates with the transcriptional activity of the associated gene and open chromatin, as measured by H3K4me3 and H3K27ac enrichment, they are not strictly coupled (Street et al., 2019; Ercan et al., 2009). Additionally, DCC binding does not directly correlate with the transcription downregulation of the bound gene (Jans et al., 2009). Furthermore, the DCC-mediated repression appears to be chromosome-wide and not gene-specific as 43% of dosage-compensated genes lack DCC binding (Jans et al., 2009), and no

large groups of genes escape from dosage compensation (Kramer et al., 2016, 2015). In summary, this data indicates that dosage compensation acts in transcription regulation in a chromosome-wide mechanism.

1.3.6 The role of histone modifications for DCC function

Several histone modifications are associated with the X chromosomes in *C. elegans* hermaphrodites. During development, the two X chromosomes are enriched explicitly for H4K20me1 while losing H4K16ac marks (Vielle et al., 2012; Wells et al., 2012; Kramer et al., 2015). The decrease of H4K16ac is mediated by the deacetylase SIR-2.1 and depends on the enrichment of H4K20me1 (Wells et al., 2012). The X chromosome-specific enrichment of H4K20me1 is mediated by the DCC subunit DPY-21, an H4K20me2 demethylase (Brejc et al., 2017). How these histone modifications and additional modifications generally associated with active and repressed transcription might be involved in gene regulation is discussed in more detail below.

The histone modification H4K16ac is vital for dosage compensation in fruit flies. In *Drosophila,* H4K16ac is enriched in the male X chromosome and plays a central role in transcription upregulation. Intriguingly, in *C. elegans,* the hermaphrodite X chromosomes which are transcriptionally downregulated are depleted for H4K16ac by the deacetylase SIR-2.1 (Wells et al., 2012). Depletion of *sir-2.1* de-condenses the hermaphrodite X chromosomes, similar to a DCC mutation (Lau et al., 2014). However, it is questionable if the decrease of H4K16ac is directly involved with transcription regulation. For example, RNAi-mediated knockdown of *sir-2.1* does not genetically interact with DCC mutants (Wells et al., 2012). Additionally, while H4K16ac drives the male X decondensation, depleting *mys-1*, the H4K16 histone acetyltransferase decreased male X transcription only mildly (Lau et al., 2016). The mild transcription phenotypes suggest that H4K16ac is not a significant histone modification of X chromosome transcription regulation.

The depletion of H4K16ac is downstream of the enrichment of H4K20me1 at the X chromosomes (Vielle et al., 2012; Wells et al., 2012). H4K20me1 is a conserved histone modification and plays a role in mitotic chromatin compaction, gene silencing, preventing DNA damage, and mammalian X inactivation (Nishioka et al., 2002; Beck et al., 2012; Karachentsev et al., 2005; Kohlmaier et al., 2004). Three enzymes are known to regulate the different methylation states of H4K20 in *C. elegans*: the methyltransferases SET-1 and SET-4, as well as the X-specific demethylase DPY-21, which is also part of the DCC (Brejc et al., 2017). SET-1 (PR-Set7 in mammals) is the histone methyltransferases responsible for catalyzing the conversion of H4K20 to H4K20me1 (Nishioka et al., 2002; Vielle et al., 2012). SET-4 (Suv4-20h1/2 in

mammals) is responsible for converting H4K20me1 to di- and tri-methylated H4K20 (H4K20me2/3) associated with DNA replication and DNA damage repair or heterochromatin, respectively (Schotta et al., 2004; Vielle et al., 2012; Jørgensen et al., 2013).

DPY-21 is a Jmj-C domain-containing demethylase that catalyzes the demethylation of H4K20me2 to H4K20me1 and physically interacts with the DCC (Brejc et al., 2017). Indeed, in the X;A fusion experiments, when DCC spreads into the autosomal region, H4K20me1 enriches on the autosome (Vielle et al., 2012). Moreover, depletion of H4K20me1 through mutations in *set-1*, *set-4*, or *dpy-21* leads to a decondensation of the X chromosomes, similar to H4K16ac depletion (Lau et al., 2014; Brejc et al., 2017). Additionally, these mutations also increase transcription of X-linked genes but not all to the same level (Kramer et al., 2015; Brejc et al., 2017). The most substantial transcription upregulation was observed for the knock-out of *dpy-21*. Interestingly, mutating the active site did not de-repress genes to the same extent, suggesting that DPY-21 also has a noncatalytic activity (Kramer et al., 2015; Brejc et al., 2017).

While dosage compensation is affected in *dpy-21* KO worms, it is not lethal compared to the KO of most other DCC subunits. This difference suggests that DPY-21 and H4K20me1 may contribute to the dosage compensation mechanism but cannot explain all observed dosage compensation phenotypes. Moreover, the enrichment of H4K20me1 on the X chromosome is delayed compared to binding of the DCC during embryogenesis (Kramer et al., 2015). Interestingly, the *set-4* mutations also decreased expression from all autosomes, suggesting that H4K20me1 might contribute to X chromosome down-regulation in a non-specific way (Kramer et al., 2015). Nonetheless, H4K20me1 could regulate the binding of the DCC to the X chromosome through its HEAT-repeat-containing subunit. In mammalian cells, condensin II subunits N-CAPD3 and N-CAPG2 were found to bind to H4K20me1, which is enriched on chromosomes during mitosis, potentially increasing loading efficiency (Liu et al., 2010). In summary, while H4K20me1 is a distinct histone modification on the X chromosomes and the parallels to mitotic chromatin are intriguing, a precise mechanism on how the mark might influence dosage compensation is still missing. Especially the disconnect of the catalytic and noncatalytic activities of DPY-21 needs to be addressed.

It is unlikely that the DCC accomplishes transcription downregulation by placing repressive histone modifications and recruitment of repressive transcription factors. DCC binding did not overlap with repressive transcription modifications like H3K27me3 or H3K9me3 (Street et al., 2019). Moreover, the level of repressive marks on the X nor binding of transcription repressors is affected by DCC depletion (Street et al., 2019). Similarly, H3K9me3 depletion had no specific effect on DCC or Pol II binding (Street et al., 2019). Overall, these results indicate that repressive histone modifications are not central for dosage compensation in *C. elegans*.

While DCC might not increase repressive histone modification, it could decrease active transcription marks. Possible active histone modifications include H3K4me3, which is enriched at transcription start sites and associates with active transcription (Barski et al., 2007; Vermeulen et al., 2010; Vastenhouw et al., 2010) and H3K27ac, which is associated with transcription activation, probably by controlling TF binding and Pol II release from promoters (Stasevich et al., 2014). DCC binding sites on the X chromosome coincide with ATAC-seq peaks (assay for transposase-accessible chromatin using sequencing) at promoters and enhancers that contain active histone marks such as H3K4me3 and H3K27ac, and binding of RNA Pol II, MDT-15 (Mediator subunit), and CBP-1 (CBP/p300 homolog) (Daugherty et al., 2017; Street et al., 2019). Conversely to the repressive histone modifications, DCC depletion caused an increase of active histone modifications, specifically on the X chromosome (Street et al., 2019). DCC-mediated reduction of H3K4me3 was also observed in the autosome region when fused to an X chromosome (Street et al., 2019). How does DCC reduce active marks at promoters? Surprisingly, while DCC reduces H3K27ac, it did not reduce the binding of CBP-1, the putative enzyme for this modification (Street et al., 2019). Possibly DCC recruits a deacetylase analogous to SIR-2.1 for H4K16ac. Nonetheless, the observed changes in histone modifications might be downstream of the effect of the DCC (Howe et al., 2017).

Besides histone tail modifications, histone variants are also involved in transcription regulation. The conserved histone variant H2A.Z regulates DCC targeting to the X chromosome (Petty et al., 2009). H2A.Z is enriched at many promoters and enhancers genome-wide and is involved in establishing transcriptionally permissive chromatin and regulating transcription (Weber and Henikoff, 2014). In yeast, H2A.Z is deposited to the TSS by the conserved chromatin remodeling complex SWR1 (Mizuguchi et al., 2004). Eviction of the mark is less well understood, but Pol II and CTD phosphorylation by CDK7 might be involved in its turnover (Ranjan et al., 2020). In *C. elegans,* H2A.Z (HTZ-1) is depleted on the hermaphrodite X chromosomes, while reducing overall HTZ-1 levels leads to ectopic binding of DCC to autosomes (Petty et al., 2009; Whittle et al., 2008). Therefore HTZ-1 might regulate the recruitment of DCC to promoters, and additionally, DCC might directly or indirectly remove HTZ-1 from promoters on the X.

1.3.7 Regulation of TF binding for DCC function

A possible mechanism of transcription downregulation could be the general exclusion of active TFs and Pol II from X chromosomal promoters. This exclusion could be realized through an overall conformation change, and in fact, the X chromosomes are more compacted than other chromosomes (Lau et al., 2014). In this model, the DCC would indiscriminately reduce the binding of proteins to the X chromosome through compaction and therefore reduce

transcription activation. Supporting this idea is that chromatin is highly condensed during mitosis, and condensin binding to promoters displaces TFs and histone modifications (Martínez-Balbás et al., 1995; Segil et al., 1996; Gottesfeld and Forbes, 1997; Ginno et al., 2018). Moreover, to maintain the memory of the transcription program, condensin needs to be excluded from promoters to prevent compaction and exclusion of TFs (Xing et al., 2005, 2008). Nevertheless, in the case of the DCC, a recent study could not confirm this and found that DCC depletion did not affect the binding of the PHA-4 transcription factor, the cohesin loader PQN-85 (Scc2 homolog), nor the putative H3K27 acetyltransferase CBP-1 (Street et al., 2019). However, these findings all stem from ChIP-seq experiments, which might miss more dynamic changes in the binding of these factors. Nonetheless, whether compaction directly regulates transcription is unclear, as, in bacteria, Pol II could still transcribe genes in highly condensed chromatin (Janissen et al., 2018).

The binding of DCC to promoter sequences could also physically inhibit the binding of specific active TFs or Pol II. While this might contribute to downregulation, this cannot be the primary dosage compensation mechanism since not all promoters of compensated genes are bound by the DCC (Ercan et al., 2007).

1.3.8 Transcription regulation of DCC

In wild-type *C. elegans*, Pol II accumulates towards the 3' end of genes. This accumulation of Pol II could suggest that regulation of elongation or termination of transcription might be a critical step. However, using Global run-on sequencing (GRO-seq) and ChIP-seq, it was shown that the DCC specifically reduces Pol II binding at promoter regions (Kruesi et al., 2013; Pferdehirt et al., 2011; Kramer et al., 2015). Furthermore, the DCC also accumulates at the TSS of X-linked genes (Ercan et al., 2007), which would suggest that initiation of transcription might be affected by the DCC.

It is unlikely that the DCC affects promoter release of Pol II, which would probably lead to an increase of Pol II binding before or around the TSS, which is not observed using ChIP or GRO-seq regions (Kruesi et al., 2013; Pferdehirt et al., 2011; Kramer et al., 2015).

A different possibility for the DCC to regulate transcription could be at the level of Pol II re-initiation, and therefore, disruption of efficient transcription. DCC could reduce active histone marks and remove GTF from promoter regions through a direct or indirect mechanism. GTFs like TFIID can bind to modifications such as H3K4me3 (Vermeulen et al., 2007). Indeed, a recent study found that DCC reduces active histone modifications, including H3K4me3 from the X chromosomes (Street et al., 2019). However, if these changes in histone modifications are sufficient and directly linked to transcription regulation remains to be seen.

A different model could involve the formation of positive supercoils in DNA. For PIC assembly, DNA is melted to load Pol II onto the template strand. Negative supercoils facilitate the melting of DNA strands (Parvin and Sharp, 1993). Condensin DC could interfere with transcription initiation by introducing positive supercoils at the promoter region (Kimura and Hirano, 1997).

In summary, regulation of the transcription cycle is complex, with many possibilities of how the DCC could down-regulate transcription. Primarily regulating transcription initiation through histone modifications, reduced transcription activators, or positive supercoiling are promising aspects of studying to understand the mechanism of dosage compensation.

1.3.9 The 3D architecture of the X chromosome

The 3D structure of chromatin has been associated with gene regulation. For example the organization of genes that are co-regulated into TADs (Rodríguez-Carballo et al., 2019). Boundaries between TADs insulate different regulatory units and show some conservation between different cell types and species (Fudenberg et al., 2017; Vietri Rudan et al., 2015; Nagano et al., 2013). In some cases, disruption of TAD boundaries can lead to misregulation of genes (Lupiáñez et al., 2015; Narendra et al., 2016). However, in other cases, disruption of TAD boundaries did not alter gene expression (Rodríguez-Carballo et al., 2017). A common feature of TAD boundaries is the presence of CTCF sites that serve as anchors for cohesin. Yet, depleting CTCF from cells and thereby dissolving TADs has a moderate or negligible effect on transcription depending on the system (Nora et al., 2016; Kubo et al., 2021)

Interestingly, no CTCF or CTCF-like protein was found in *C. elegans* and other nematodes (Heger et al., 2009). The 3D structure of the *C. elegans* genome is also different from other eukaryotes. Autosomes do not show clear TAD-like structures, which could be connected to the lack of CTCF and therefore missing loop anchors for cohesin (Gabdank et al., 2016; Crane et al., 2015). Interestingly, the hermaphrodite X chromosomes show a higher-order structure similar to TADs, which are dependent on the DCC (Crane et al., 2015). Some of the TAD boundaries coincide with *rex* sites. While deleting several of these *rex* sites disrupted the TAD structure of the X, transcription changes could not be detected using bulk measurements, albeit some changes to worm aging were detected (Anderson et al., 2019).

In conclusion, *rex* sites on the X chromosome function as TAD boundaries to promote a higher-order chromatin structure dependent on the DCC. However, if the 3D chromatin structure of the X directly regulates genes is unclear.

1.3.10 Positioning of chromosome in the nucleus

Radial positioning in the nucleus can be important for transcription regulation. Active developmentally regulated genes are enriched in the nuclear interior (Meister et al., 2010). The nuclear periphery has two regulatory environments. Firstly, the nuclear lamina, where silenced genes are anchored (Ikegami et al., 2010; Towbin et al., 2012; González-Aguilera et al., 2014). Secondly, the nuclear pores are associated with active domains through a transcription-dependent mechanism (Rohner et al., 2013; Ikegami and Lieb, 2013).

Through imaging, it has been reported that the hermaphrodite X chromosomes do not contact the nuclear pores, which is dependent on the DCC, suggesting a model where the reduced access to nuclear pores reduces transcription on the X chromosome (Sharma et al., 2014; Sharma and Meister, 2015). In contrast, the male X chromosome was associated with nuclear pores (Sharma et al., 2014). However, other labs could not reproduce these results and instead found that the X of both sexes was positioned more centrally (Snyder et al., 2016) or found no preference for localization altogether (Wheeler et al., 2016). These differences could arise from different cell types and stages of worms used and technical limitations of the fixing and staining protocols (Askjaer, 2014). Moreover, it is unclear if the radial position of the X chromosome influences transcription downregulation in hermaphrodites. In experiments using mutants involved in tethering chromatin to the nuclear membrane (*met-2*, *set-25*, and *cec-4*), the X chromosome was released into the nucleus radial center but showed little effect on X-linked gene expression (Snyder et al., 2016; Bian et al., 2020) nor binding of Pol II to TSSs (Street et al., 2019).

1.4 Aims of this thesis

The 3D chromosome organization by SMC molecules and the functional consequences of this organization have been a focus of research in the last two decades. Nevertheless, especially the role of condensins in gene regulation remains a topic with many open questions. The *C. elegans* dosage compensation system offers the unique opportunity to study how a condensin complex regulates gene expression without interfering with condensin's essential function in the cell cycle progression. In *C. elegans,* the Dosage Compensation Complex (DCC) spatially organizes the X chromosomes and down-regulates transcription chromosome-wide, and yet transcription is unchanged when many TAD boundaries are lost. Moreover, while many regulatory proteins contribute to dosage compensation, their contribution to transcription downregulation is unclear. Thus, how the DCC mechanistically regulates transcription is not well understood and a fascinating open question.

The work of my thesis is divided into two parts (Figure 12). Firstly, I study how the binding dynamics of condensin DC influence gene regulation. Secondly, I characterize the transcription of X-linked genes during embryogenesis and how the depletion of different DCC subunits influences transcription bursting.

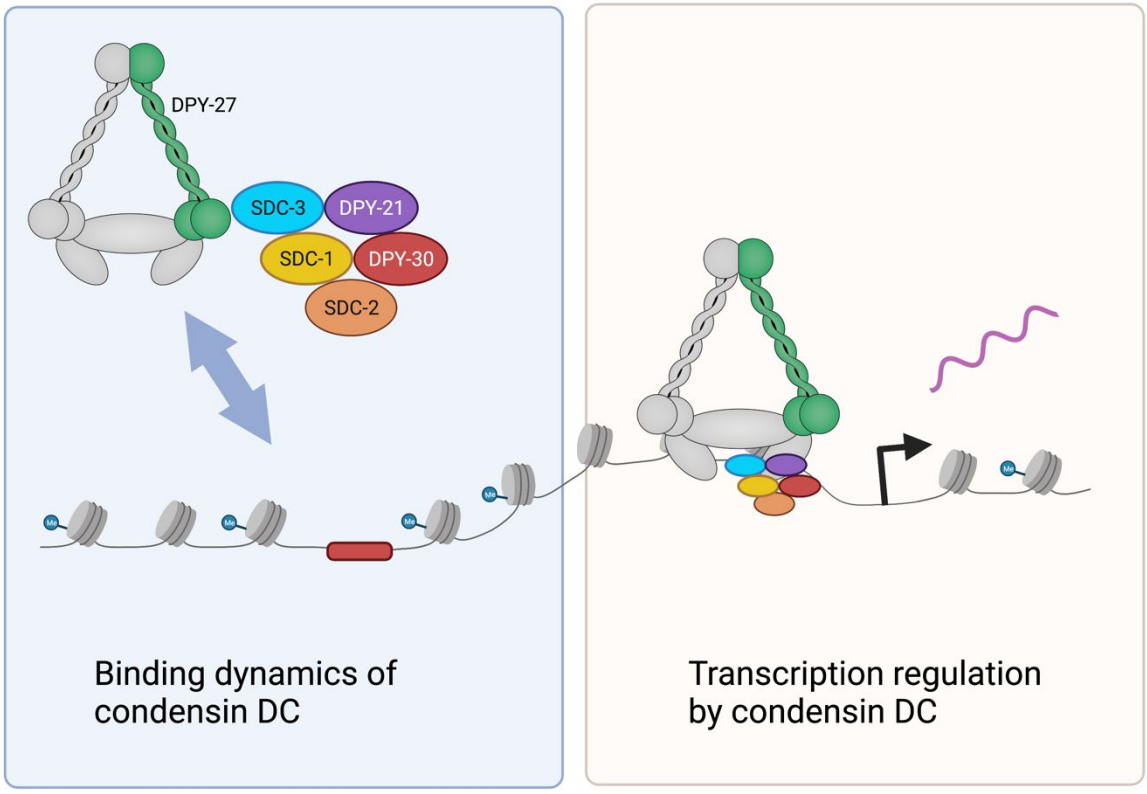

Figure 12 Model for the aims of this thesis.

Aim 1: Characterize the dynamics of condensin DC binding using FRAP.

In the first part of my thesis, I set out to study the regulators of condensin DC dynamics using FRAP and how changes to binding dynamics influence gene regulation. Condensin DC is the core protein complex of the DCC and essential for X chromosome gene regulation. I first asked how fast condensin DC exchanges once localized to the X chromosome using FRAP. The ATPase domains of SMC molecules are essential for the binding and translocation of the complex in many systems. I wanted to characterize how the ATPase domain of the condensin DC-specific subunit DPY-27 influences condensin DC binding to the X chromosome. HEAT repeat-containing condensin subunits can bind to H4K20me1. I wanted to study if condensin DC can bind H4K20me1 i*n vitro* and if removing the mark influences DCC binding dynamics *in vivo*. In summary, this study reveals that condensin DC's binding dynamics are a critical aspect of transcription regulation in live cells.

Aim 2: Characterize the expression and stochastic bursting of DCC-regulated genes on the X chromosome using smFISH.

In the second part of my thesis, I aimed to characterize the transcription of X-linked genes during embryogenesis to gain insight into how the DCC controls gene regulation for dosage compensation. Considering that transcription is stochastic, I aimed to detect the transcription heterogeneity between different embryos of X-linked genes and how uniform the timepoint of dosage compensation is. Furthermore, to study dosage compensation regulation, I addressed how single rex sites contribute to transcription regulation and different subunits of the DCC. Finally, I asked how the DCC regulates nascent transcription and transcription bursting.

Transcription has been described as an inherently stochastic process, therefore studying gene regulation in single cells and single embryos is necessary to detect characteristic differences in transcription. To this end, I aimed to establish a smFISH setup to study transcription with high spatial and temporal resolution in many single embryos, albeit with a limited number of genes. Furthermore, to overcome current limitations in the analysis of such smFISH images, an additional aim of my thesis was to develop a staining and detection pipeline to detect single transcripts in thousands of embryos across the entire embryogenesis. Taken together, in the second part of my thesis, I aimed to study the mechanism of transcription regulation by using smFISH and to develop a pipeline to detect and stage many embryos.

2 A noncatalytic activity of the H4K20 demethylase DPY-21 and the ATPase domain of DPY-27 regulate condensin DC binding

This chapter is based on the 2021 preprint: *A noncatalytic activity of the H4K20 demethylase DPY-21 regulates condensin DC binding*. Authors listed in the publication are Laura Breimann*, Ana Karina Morao*, Jun Kim, David Sebastian Jimenez, Nina Maryn, Krishna Bikkasani, Michael J Carrozza, Sarah E Albritton, Maxwell Kramer, Lena Annika Street, Kustrim Cerimi, Vic-Fabienne Schumann, Ella Bahry, Stephan Preibisch, Andrew Woehler, Sevinç Ercan. *Authors contributed equally to this paper.

2.1 Research Motivation

Structural maintenance of chromosomes (SMC) complexes are evolutionarily conserved proteins that regulate chromosome structure through the energy from ATP hydrolysis (Hirano, 2016). Condensin, a conserved SMC member, compacts DNA to facilitate DNA segregation during mitosis and is additionally involved in genome organization to regulate transcription during interphase (Paul et al., 2018a). One of the prevailing models in the field is the loop extrusion model, where molecular motors like condensin extrude DNA to processively compact it while forming loops (Goloborodko et al., 2016b; Cacciatore and Rowland, 2019). In contrast to cohesin, chromatin factors and proteins regulating condensin binding and loop extrusion processivity are either unknown or not well characterized (Paul et al., 2018b). In this chapter, I will discuss how we use condensin DC from the *Caenorhabditis elegans* dosage compensation system to study condensin binding dynamics and factors that regulate this dynamic.

In *C. elegans,* dosage compensation is mediated by condensin DC which is part of the larger dosage compensation complex (DCC) (Albritton and Ercan, 2018). While most subunits of condensin DC are shared with condensin I, the SMC-4 is replaced by the specific subunit DPY-27 (Chuang et al., 1994). In the current model, the DCC subunits SDC-2 along with SDC-3 and DPY-30 recruit the complex to a small number of recruitment elements on the X *(rex*) (Csankovszki et al., 2004; Jans et al., 2009; Albritton et al., 2017). The complex spreads linearly along the X chromosome from the initial *rex* sites, binding to weaker *rex* sites and accumulates at active promoters, enhancers, and other accessible regulatory sites (Street et al., 2019; Ercan et al., 2009). Condensin DC binding to the X chromosomes regulates their compaction, 3D architecture, and gene expression (Jimenez et al., 2021; Rowley et al., 2020; Crane et al., 2015; Anderson et al., 2019; Lau et al., 2014).

One DCC member is the Jumonji domain-containing histone demethylase DPY-21 that converts H4K20me2 to H4K20me1 (Brejc et al., 2017; Yonker and Meyer, 2003), resulting in increased H4K20me1 on the X chromosome (Vielle et al., 2012; Wells et al., 2012). Downstream of this increase is the deacetylation of H4K16 mediated by SIR-2.1 (Wells et al., 2012). Additionally, condensin DC and DPY-21 are also required for lower levels of H3K27ac on the X chromosome (Street et al., 2019). Interestingly, mitotic chromatin in metazoans also has an increase of H4K20me1 and decreased acetylation levels (Schmitz et al., 2020), providing a link between canonical condensin and condensin DC binding to chromatin. This parallel of condensin binding and increase in a specific histone modification poses the question if histone modifications might act as regulators for condensin binding or binding dynamics.

In this work, I aim to study the dynamics of condensin DC binding *in vivo.* For this, I aim to elucidate the importance of the ATPase domain for condensin DC binding. Additionally, I aim to

study the effect of several mutants that regulate H4K20 methylation and H4K16 acetylation on condensin DC's binding dynamics and function. To study these possibilities, I present work establishing a fluorescence recovery after photobleaching (FRAP) assay in *C. elegans* intestine cells using a GFP-tagged DPY-27.

2.2 Author contribution statement

The FRAP protocol and analysis were developed by Andrew Woehler, Kustrim Cerimi, Vic-Fabienne Schumann, and myself. FRAP experiments were performed by Kustrim Cerimi and myself and analyzed by myself. Image intensity analysis was developed by Ella Bahry and myself and performed by myself. The heat-shock expression worm lines were created by Krishna Bikkasani and crossed for FRAP by Mandy Terne and myself. The DPY-27::HaloTag line was created by Lena Annika Street and crossed for analysis by myself. ChIP-seq experiments were performed by Ana Karina Morao, Jun Kim, Nina Maryn, and Lena Annika Street. Ana Karina Morao performed immunoprecipitation and western blot experiments. *In vitro* binding assay was performed by Michael J Carrozza. Sarah E Albritton and Maxwell Kramer performed the RNA-seq experiments. David Sebastian Jimenez analyzed RNA-seq and performed the Hi-C experiments. Jun Kim performed HI-C analysis. Dumpiness measurements were conducted by myself. I supervised and instructed Kustrim Cerimi and Vic-Fabienne Schumann. Sevinç Ercan and I wrote the preprint with edits by Ana Karina Morao, Jun Kim, and David Sebastian Jimenez. Final manuscript figures were prepared by myself. Stephan Preibisch and Andrew Woehler gave comments on the final manuscripts. Stephan Preibisch, Andrew Woehler, and Sevinç Ercan supervised the project.

2.3 Results

2.3.1 Establishment and characterization of a DPY-27::GFP expression system

To detect condensin DC binding *in vivo*, we wanted to measure the dynamics of DPY-27, the SMC4 homolog that distinguishes condensin DC from I, using fluorescence recovery after photobleaching (FRAP) (Figure 13a). The FRAP technique has previously been successfully applied to uncover the binding dynamics of different SMC members in different organisms (Gerlich et al., 2006a; Elbatsh et al., 2019; Gerlich et al., 2006b; Rhodes et al., 2017a; Walther et al., 2018; Oliveira et al., 2007; Borgmann et al., 2013). Our initial approach was to tag DPY-27 endogenously with a HaloTag at the C-terminus using CRISPR/Cas9 genome editing. We were able to generate a DPY-27::HaloTag strain that was phenotypically wild-type. Since the loss of DPY-27 results in lethal or dumpy worms, we were confident that the tagged protein conserved

the protein function. Using Halo ligand labeling, I detected subnuclear localization of DPY-27::HaloTag, which is typical for the DCC's X-specific localization (Figure 13b) (Csankovszki et al., 2004; Jans et al., 2009). However, I could not photobleach the signal of different ligands when bound to DPY-27::HaloTag, and therefore this construct was not suitable for FRAP. Since DPY-27 is not highly expressed, tagging DPY-27 endogenously with GFP resulted in an insufficient fluorescent signal for FRAP. Thus we decided to use a heat-shock expression system to induce expression of DPY-27::GFP in sufficient amounts for usage in a FRAP assay. To characterize the expression from the heat-shock promoter, I observed the expression and localization of DPY-27::GFP at different time points after a 1-hour heat shock of 35°C (illustrated in Figure 13c). After 3 hours, the protein was expressed and localized to the nucleus. I detected robust localization to one or two subnuclear positions only after 8 hours and subsequently used this time point for my FRAP analysis (Figure 13b). The subnuclear localization of DPY-27::GFP overlapped with the localization of endogenously tagged DPY-27::HaloTag and therefore suggested that DPY-27::GFP correctly localizes to the X chromosomes (Figure 13b).

Next, we used immunoprecipitation (IP) analysis to validate that the GFP tagged version of DPY-27 could still form the complete condensin complex (Figure 13d). We found that DPY-27 could still bind to condensin DC subunits MIX-1 and DPY-26, thus we concluded that the GFP tag did not disrupt complex formation.

To test whether DPY-27::GFP could still bind to the same sites on the X chromosome, we used ChIP-seq analysis using either antibodies against the GFP tag or DPY-26, the kleisin subunit (Figure 13e). We could confirm that DPY-27::GFP was enriched on the X chromosome at the same locations as DPY-26.

With these results, we were confident that the GFP tag did not disrupt the complex formation or the X-specific binding of DPY-27 and used this worm strain to study condensin DC binding dynamics *in vivo*.

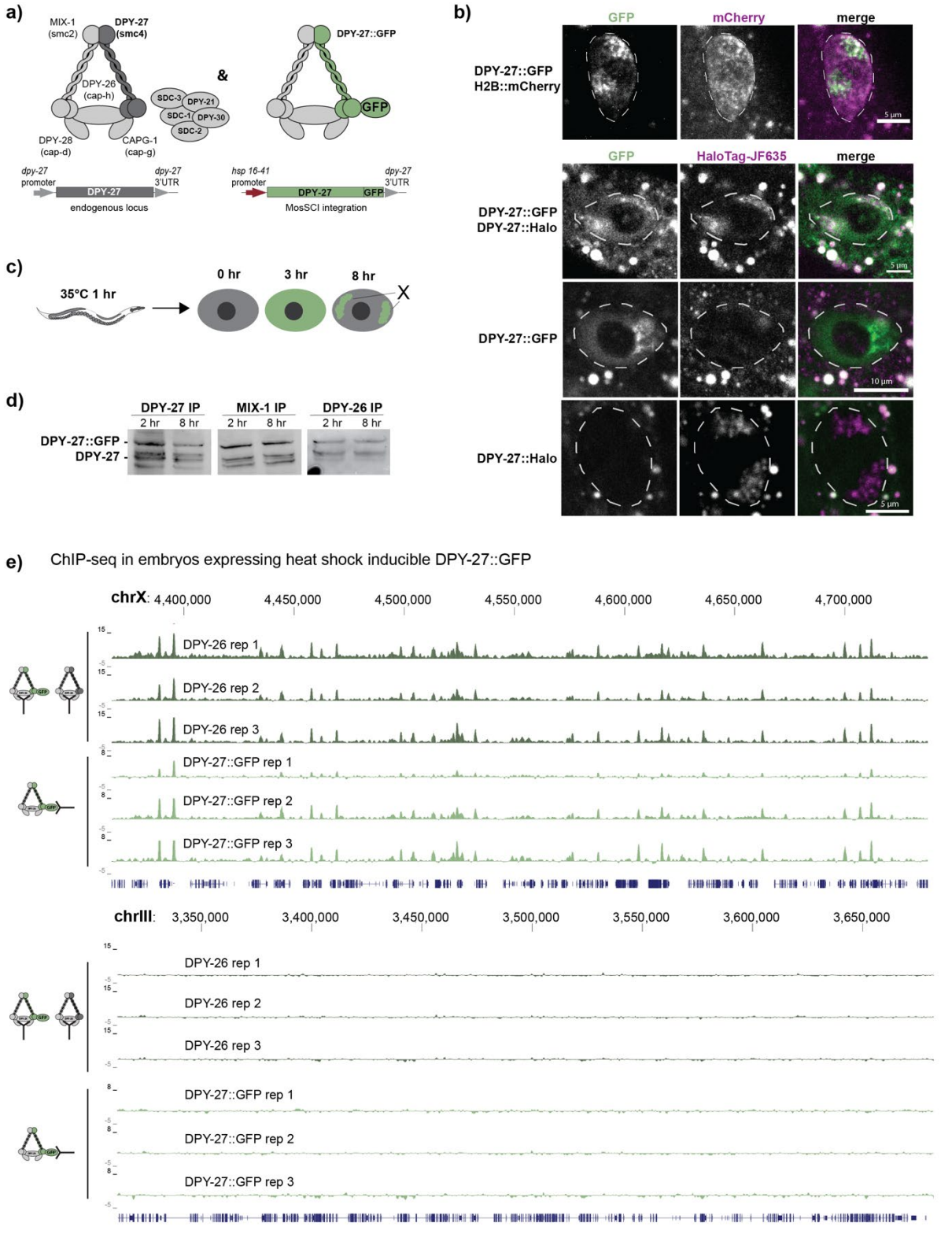

Figure 13 Validation of expression system for GFP tagged DPY-27
a) The left panel illustrates the condensin DC subunits and the rest of the DCC subunits. The right panel indicates the expression of GFP tagged DPY-27 under the control of a heat-shock inducible promoter at the Chr II MosSCI site. **b)** DPY-27::GFP subnuclear localization to the X chromosomes after heat-induced expression (top row) was validated by colocalization with the endogenously tagged DPY-27::Halo stained with JF635 HaloTag ligand (bottom panel). The bottom two rows show that the GFP and JF635-Halo signals are specific and do not bleedthrough. The fluorescent images depict intestine nuclei after feeding JF635-Halo ligand in homozygous worms expressing heat-shock inducible DPY-27::GFP or endogenously Halo-tagged DPY-27. Both worm lines were stained with JF635-Halo ligand and heat-

shocked. White dotted lines mark nuclei. **c)** Illustration of worms heat shocked for 1 hour at 35°C and fluorescence followed in the large intestinal cells. DPY-27::GFP subnuclear localization is apparent after 8 hours of recovery. **d)** DPY-27::GFP binding with condensin DC was validated by co-immunoprecipitation with MIX-1 and DPY-26. Young adult worms were used for IP either 2 or 8 hours after heat shock at 35°C for 1 hour. The ratio of GFP tagged DPY-27 to the endogenous protein in the DPY-27 IP lane indicates the relative abundance of each protein. The ratio in the other lanes indicates the relative interaction of endogenous and DPY-27::GFP with IPed subunit. **e)** Validation of DPY-27::GFP localization specifically to the X chromosomes by ChIP-seq. DPY-27::GFP ChIP-seq analysis was performed in three replicates using an anti-GFP antibody in embryos. DPY-26 ChIP-seq was used as a positive control in the same extracts. Figure modified from (Breimann et al., 2021).

2.3.2 Establishment of a FRAP analysis method

With the generated hsp::DPY-27::GFP expressing worm line, we performed FRAP experiments in intestine nuclei of living but anesthetized *C. elegans* adults. In order to extract relevant measurements from our experiments and compare different mutant conditions, we established a reliable and reproducible image analysis pipeline using MATLAB and Python. The first step in the script stabilizes minor worm movements within acquired images of one experiment as even anesthetized worms can move in the microscope. Next, we implemented a manual selection of nuclei outlines to exclude bright intestinal spots typical in the intestine of adult worms, as depicted in Figure 14a. The most accurate way of detecting the position of the actual bleached area is not using the selected bleach position from the microscope but detecting the bleached area directly from the data. Therefore, the bleached area is detected by subtracting the average of five post bleach images from five pre- bleach images (Figure 14b). Since we used a GFP for fluorescence detection, we encountered high acquisition bleaching. This unintended bleaching was normalized by detecting the loss of fluorescence signal in the nucleus during the experiment. The degradation of the signal was fitted, and this correction was used to normalize the fluorescence signal in the bleach point (Figure 14c). The normalized fluorescence intensity was fit with a monoexponential curve, and the mobile and immobile fractions were calculated (Figure 14d). To monitor if the monoexponential curve fitting best represented the acquired data points, the coefficient of determination (R^2) was calculated to determine the goodness of fit. Fluorescent intensity recovery curves for each experimental condition were collected for a minimum of 30 nuclei from at least three independent experiments.

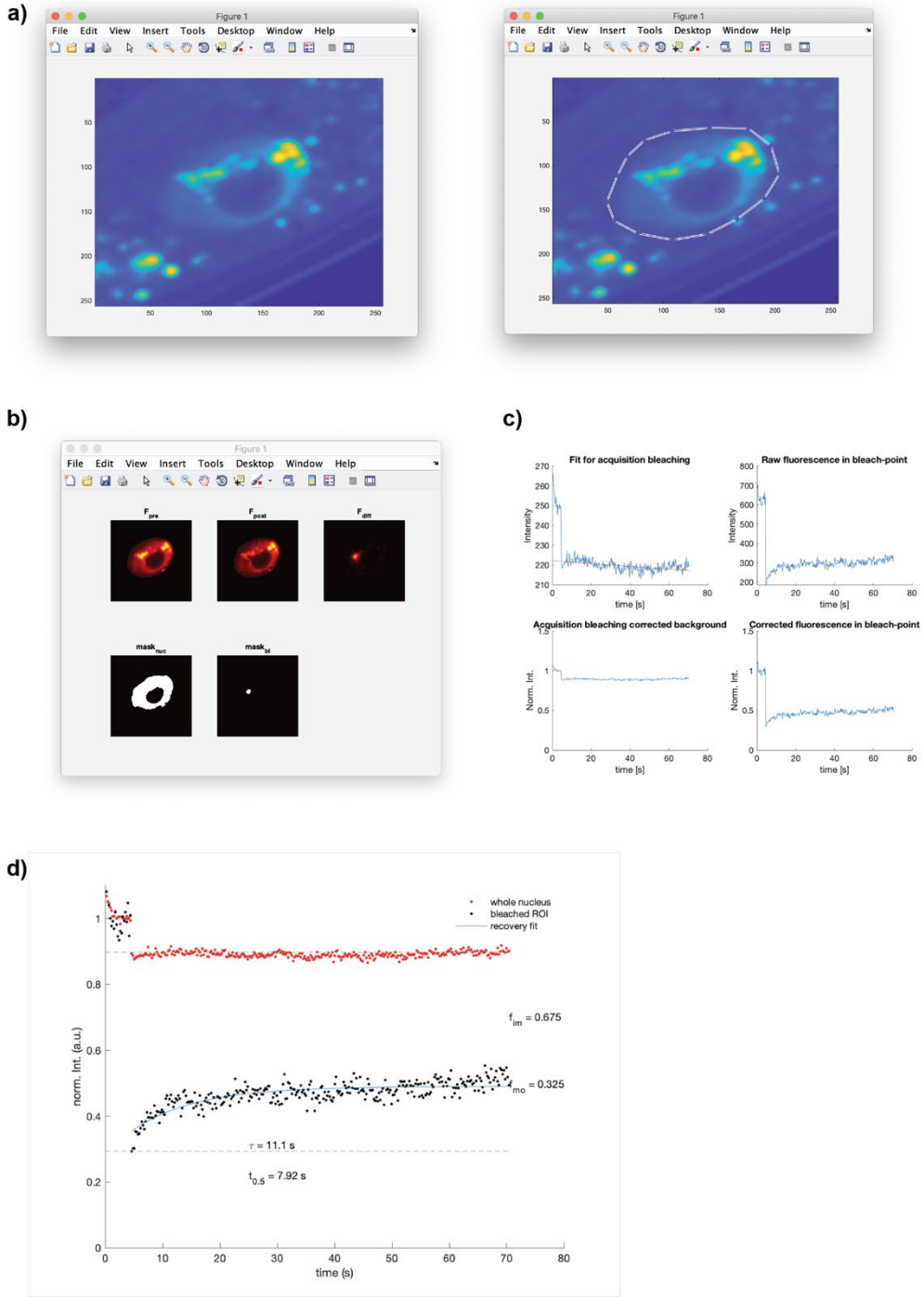

Figure 14 Overview of image analysis script for FRAP images in MATLAB
a) For precise detection of the fluorescence in each *C. elegans* intestine nuclei, the analysis script includes a manual selection step. **b)** The bleach-point mask ($mask_{bl}$) is detected automatically in the difference of pre (F_{pre}) and post (F_{post}) bleach images. **c)** The fluorescence intensity is corrected for the acquisition bleaching after fitting the background signal. This normalization is applied to the detected fluorescence in the bleach point. **d)** The normalized fluorescence intensity in the bleach-point (black) and the rest of the nucleus (red). The mobile (f_{mo}) and immobile (f_{im}) fractions are determined by fitting a monoexponential curve (blue line). Figure modified from (Breimann et al., 2021).

2.3.3 FRAP measurement of condensin DC binding *in vivo*

We chose to perform FRAP in the large intestinal nuclei of adult *C. elegans* (Figure 15a). These nuclei are polyploid and therefore larger than other nuclei in adult worms, which facilitates detection of the subnuclear localization of the complex. Previous characterizations of condensin DC binding were performed in intestine nuclei using immunofluorescence microscopy (Yonker and Meyer, 2003; Csankovszki et al., 2004; Wells et al., 2012; Brejc et al., 2017). Additionally, expression in intestine nuclei was more reproducible as the heat-shock expression in embryos was very variable (Breimann et al., 2021).

To characterize the binding dynamics in intestine cells, I compared the DPY-27::GFP recovery to free NLS::GFP and histone H2B::GFP (Figure 15a-d). Measuring the fluorescence recovery after bleaching for a given fluorescently tagged protein typically results in two quantitative measurements. Firstly, the percentage of the recovered signal at the bleached area represents the proportion of mobile molecules that replaced the bleached molecules. Secondly, the time needed for recovery represents how the molecule moves through the cell or nucleus. Fast recovery indicates movement purely by diffusion, which can be slowed down if the molecule can transiently bind cofactors or cellular structures like chromatin. The stable binding of the molecule is reflected in a very high immobile fraction (Mueller et al., 2013b).

The freely diffusing NLS::GFP did indeed show a high mobile fraction and fast recovery half-time (Figure 15b-d). In contrast, the binding of H2B::GFP was very stable and showed a low mobile fraction (Figure 15a-b). The recovery of H2B-GFP was much longer than the observed experimental timeframe, and therefore, a recovery half-time was excluded from the recovery half-life plot. A similar observation was made for FRAP experiments in human cell lines, where very low mobile fractions for H2B-GFP (4%) were reported with a recovery half-life of over 2 hours (Kimura and Cook, 2001).

The mobile fraction for DPY-27::GFP was ~30%, with a recovery half-time of ~2.6 seconds. Comparing results from different experimental set-ups with different analysis strategies and, of course, from the different organisms can be challenging as different approaches can influence the results significantly (Mazza et al., 2012). However, comparing our findings to results from *Saccharomyces cerevisiae* for Smc4 show similar half-time recoveries of ~ 2 and ~6 seconds in the G1 and M phase, respectively (Thadani et al., 2018). The residence times of human condensin I and II are much longer in the range of ~2-10 min (Walther et al., 2018; Gerlich et al., 2006a). However, the binding was variable throughout the cell cycle for condensin I but not condensin II, which binds to chromatin also during interphase and has a residence time of >5 min with a mobile fraction of 40% (Walther et al., 2018; Gerlich et al., 2006a). Condensin I only binds to chromatin during mitosis and has a residence time of ~3 min with a mobile fraction of

80% (Walther et al., 2018; Gerlich et al., 2006a). In summary, our results indicate condensin DC has a similar recovery half time to yeast but a smaller mobile fraction than human condensin I or II with a shorter recovery half-life.

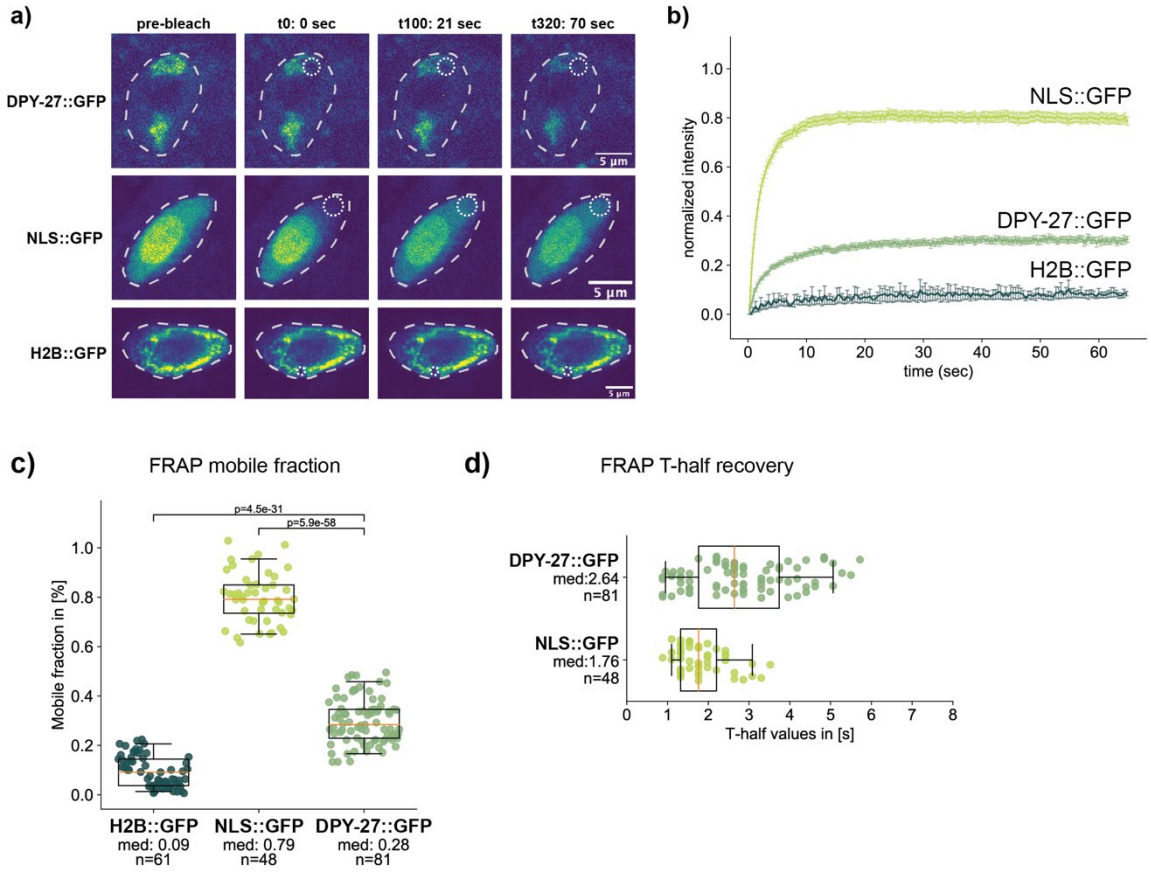

Figure 15 Fluorescence recovery after photobleaching (FRAP) analysis of condensin DC binding
a) FRAP sequence for intestine nuclei of adult *C. elegans* worms expressing either DPY-27::GFP, NLS::GFP, or H2B::GFP. The first column of images depicts the first image of the pre bleach series (a total of 20 images). The second column shows the first image after the single-point bleach with the bleached area indicated by the small dotted circle. The two following columns depict two-time points after the bleach point, t100 (21 seconds) and t320 (70 seconds). The scale bars correspond to 5 µm. **b)** Mean FRAP recovery curves from wild-type DPY-27::GFP, H2B::GFP, and NLS::GFP expressing worms. Error bars denote the standard error of the mean (s.e.m.). Number of bleached single intestine nuclei (from at least 3 biological replicates) for each experiment is n = 81 for DPY-27::GFP, n = 48 for NLS::GFP and n= 61 for H2B::GFP. **c)** Mobile fractions for the different GFP tagged proteins or free GFP. The mobile fraction is the lowest for H2B::GFP and the highest for NLS::GFP. The mobile fraction for DPY-27::GFP is ~28%. P values are from an independent two-sample t-test. **d)** FRAP half-time recovery values for the bleach curves of Figure 15b. The half-time recovery for NLS::GFP shows a shorter diffusion time than DPY-27::GFP. H2B::GFP is not shown due to the very low recovery of the fluorescence signal during the experimental time frame. Figure modified from (Breimann et al., 2021).

2.3.4 A conserved mutation to the DPY-27 ATPase domain eliminates its binding in the presence of the wild-type protein

Condensin and other SMC molecules have two head domains that can come together in the presence of ATP, hydrolyze two molecules of ATP and finally dissociate again (Hirano, 2016). In order to test if ATP hydrolysis is vital for condensin DC binding dynamics, we inserted a walker

B mutation (E to Q, Figure 16a) that nearly eliminates ATP hydrolysis in humans (Vian et al., 2018), *Xenopus* (Kinoshita et al., 2015), yeast (Hirano and Hirano, 2004; Thadani et al., 2018), and chicken (Hudson et al., 2008).

While DPY-27(EQ)::GFP was expressed similarly to DPY-27::GFP after 3 hours, it failed to localize to the X chromosome after 8 hours like the wild-type complex (Figure 16b). Furthermore, the levels of the ATPase mutant decreased after 8 hours compared to the levels of DPY-27::GFP.

The observation that the ATPase domain is essential for X localization was supported by the ChIP-seq analysis comparing binding of DPY-27::GFP and DPY-27(EQ)::GFP in embryos (Figure 16c). In contrast to the wild-type protein, the ATPase mutant failed to bind to the X chromosomes in the presence of the endogenous DPY-27.

To rule out that the ATPase mutation leads to problems in complex formation, we performed an IP comparing the wild-type and EQ mutant complex (Figure 16d). Both GFP-tagged proteins were still capable of binding to the condensin DC subunits MIX-1 and DPY-26. However, the co-IP of DPY-27::GFP with the kleisin subunit DPY-26 was more robust than DPY-27(EQ)::GFP suggesting that the ATPase mutation might affect the interaction to the kleisin subunit. Proteins that cannot form the complex (Figure 16d) or bind to DNA (Figure 16c) may be degraded over time, as observed in Figure 16b. Nevertheless, a significant fraction of DPY-27(EQ)::GFP protein could bind to other complex subunits. Thus, the EQ mutant's failure to localize to the X chromosomes indicates that ATP hydrolysis is required for the stable association of condensin DC with the X chromosomes.

To study if the expression of the ATPase mutant has a dominant-negative effect on X-linked gene expression, we performed mRNA-seq experiments. Indeed, embryos with induced expression of DPY-27(EQ)::GFP showed a slightly higher expression of X-linked genes than in DPY-27::GFP or wild-type worms (Figure 16e). Possibly the overexpression of the ATPase mutant negatively regulates condensin DC similar to the negative regulator SMCL-1 an SMC-like protein with an ATPase hydrolysis mutation similar to the EQ mutation (Chao et al., 2017).

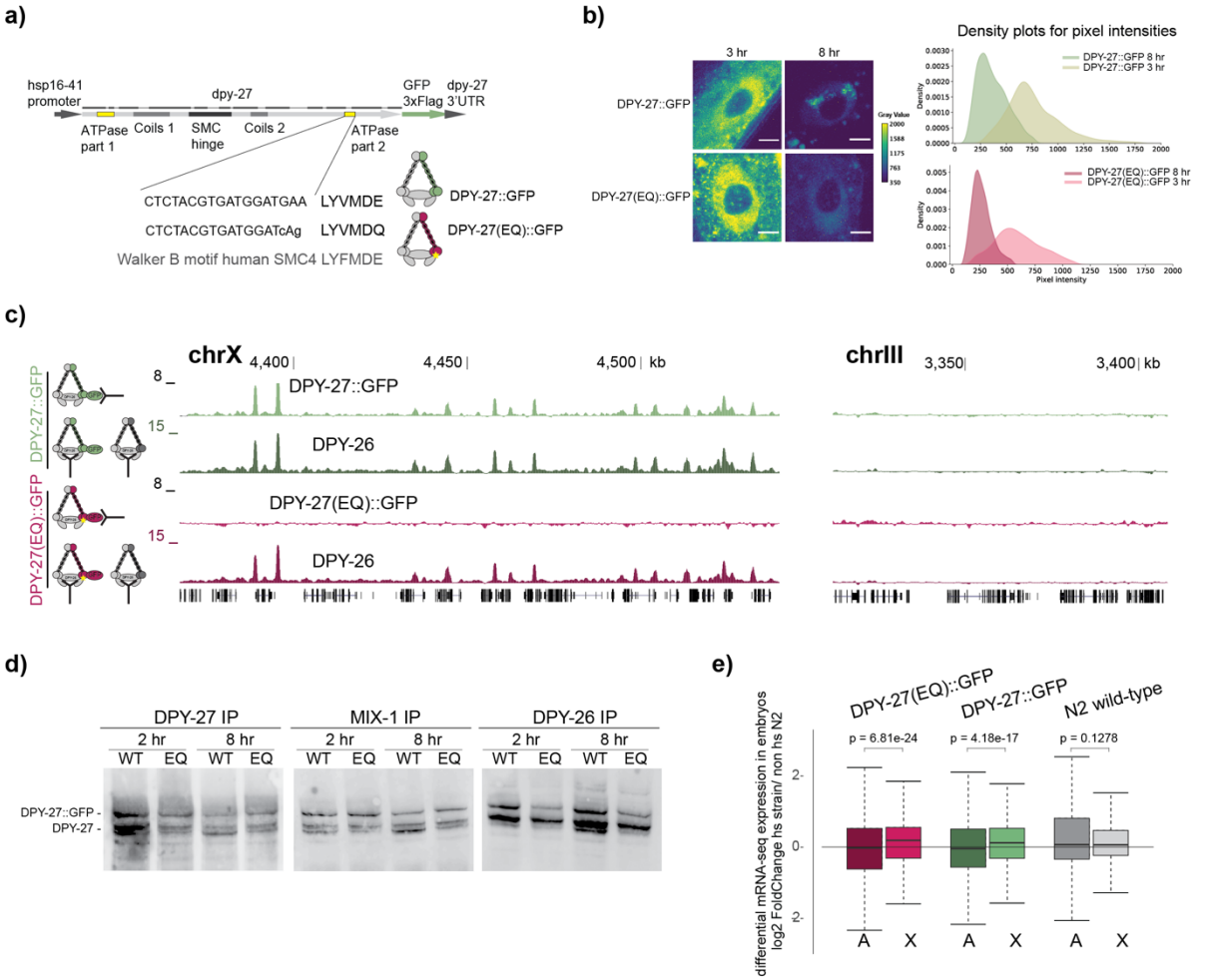

Figure 16 The effect of a conserved SMC ATPase mutation on DPY-27 binding, function, protein stability, and complex formation

a) Heat shock inducible GFP tagged *DPY-27(EQ)*. The DNA sequence coding for the conserved Walker B motif and the E to Q mutation are shown below. **b)** Localization of the wild-type and EQ ATPase mutant DPY-27::GFP proteins in intestine cells. Adults were heat-shocked at 35°C for 1 hour and recovered for either 3 or 8 hours. Unlike DPY-27::GFP, ATPase EQ mutant did not show subnuclear localization. Additionally, the ATPase mutant was present only in a very low amount after the 8-hour recovery suggesting degradation of nonfunctional DPY-27. The right panel quantifies the GFP signal's pixel intensities in the nuclei after 3 and 8 hours of recovery from heat shock. The intensities were recorded from at least three biological replicates in adult intestine cells. For wild-type, DPY-27::GFP 21 images were used for the 3-hour intensity curve and 26 for the 8 hours recovery time point. For the intensity curves of DPY-27(EQ)::GFP, 44 images were used for the short time point and 36 images for the long recovery time point. The scale bar corresponds to 5 µm. **c)** ChIP-seq analysis of wild-type and ATPase mutant DPY-27(EQ)::GFP using the anti-GFP antibody in embryos. ChIP against DPY-26 was used as a positive control in the same extracts. Unlike the wild-type protein, ATPase mutant failed to bind the X, and both did not localize to the autosomes; a representative region from chromosome III is shown on the right panel. **d)** Co-immunoprecipitation analysis of condensin DC subunits. Protein extracts were prepared from larvae that were heat-shocked for 1 hour at 35°C and recovered at room temperature for 2 hours or 8 hours. Immunoprecipitated (IP) proteins were blotted by an anti-DPY-27 antibody. Comparing GFP tagged DPY-27, and the EQ mutant to the endogenous protein indicates the relative interaction of the GFP tagged proteins with the IPed condensin subunit compared to endogenous. **e)** Log2 fold changes in mRNA-seq between heat-shocked strains and non-heat-shocked wild-type embryos, collected after 30 min heat shock at 35°C followed by 2-hour recovery. P values are from a Wilcoxon–Mann–Whitney test. Figure modified from (Breimann et al., 2021).

2.3.5 ATP hydrolysis is required for stable association of condensin DC to the X chromosomes

We wondered if the ATPase mutant could still interact with DNA in an ATPase-independent way that would not lead to the loading of the molecule onto DNA and therefore be too transient for ChIP-seq analysis (Figure 16c). We performed FRAP and compared the binding of DPY-27(EQ)::GFP to binding the wild-type protein after *sdc-2* RNAi (Figure 17a). SDC-2 recruits condensin DC to the X chromosome, and loss of the protein leads to complete loss of condensin DC binding to the X chromosomes (Kranz et al., 2013).

Using FRAP, we found that DPY-27(EQ)::GFP had slightly lower mobility than the complex in the *sdc-2* RNAi condition (Figure 17a-b). This difference suggests that the ATPase mutant could still transiently associate with chromatin but not bind to DNA. Possibly the complex interacts with SDC-2 but then fails to use ATP hydrolyses to bind DNA functionally. Interestingly, the half-time recovery was unchanged between the three conditions (Figure 17d). The unchanged recovery half-time between these conditions suggests that the FRAP measurement predominantly captures the rapid exchange of free molecules at the binding sites.

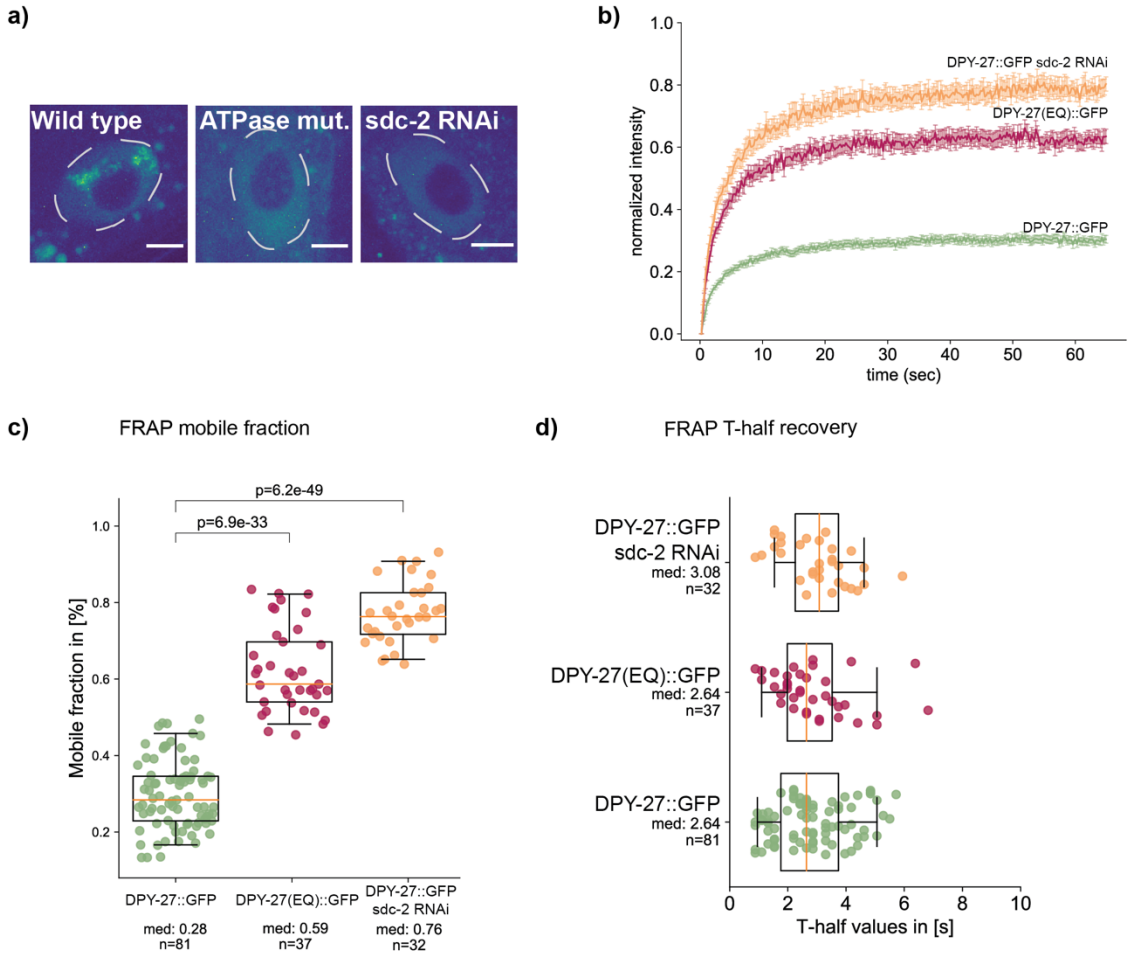

Figure 17 The ATPase mutant affects binding similar to the loss of the recruiter SDC-2

a) Microscopy images depicting example pictures of intestine nuclei used for FRAP analysis. Unlike DPY-27::GFP, ATPase EQ mutant did not show subnuclear localization, similar to when condensin DC recruiter SDC-2 was knocked down. Scale bars correspond to 5 µm. **b)** Mean FRAP recovery curves from DPY-27::GFP, DPY-27(EQ)::GFP and DPY-27::GFP upon *sdc-2* RNAi. FRAP was performed ~8 hr after the heat shock. Error bars denote s.e.m.. Number of bleached single intestine nuclei (from at least 3 biological replicates) for each experiment is n = 81 for DPY-27::GFP, n= 37 for DPY-27(EQ)::GFP and n= 32 for DPY-27::GFP *sdc-2* RNAi. **c)** FRAP analysis of mobile fractions corresponding to curves depicted in part b. P values are from an independent two-sample t-test. **d)** FRAP analysis of T-half recovery time corresponding to curves depicted in part b. Figure modified from (Breimann et al., 2021).

2.3.6 Recombinant DPY-28 HEAT repeat domain bind to histone H3 and H4 peptides *in vitro*

We wanted to test if chromatin and specifically histone modifications could regulate the binding dynamics of condensin DC. To test this hypothesis, we focused on two histone modifications: H4K20me1 which is enriched explicitly on the X chromosome, and H4K16ac depleted from the X chromosomes as depicted in Figure 18a. Several enzymes are known to regulate these marks genome-wide and are also associated with dosage compensation: The methyltransferases SET-1 and SET-4, and the deacetylase SIR-2.1 (Figure 18a) (Kramer et al., 2015; Wells et al., 2012). Additionally, the X-specific H4K20me2 demethylase activity of DPY-21 was recently identified (Brejc et al., 2017).

We hypothesized that condensin DC could interact with chromatin via its HEAT repeat domains (Figure 18b). HEAT repeats are amphiphilic helical protein structural motifs that, in the context of the SMC subunits CAP-G and CAP-D, are interspersed with intrinsically disordered regions (IDRs) (Yoshimura and Hirano, 2016). In *Xenopus* cell-free egg extracts, the HEAT subunits of condensin I regulated dynamics chromosome axes assembly (Kinoshita et al., 2015). The HEAT repeats could support unspecific condensin binding to DNA and activate its ATPase function for ectopic entrapment of DNA (Piazza et al., 2014; Hara et al., 2019). The HEAT subunits could also support condensin-condensin interactions via its IDRs leading to phase separation during mitosis (Yoshimura and Hirano, 2016; Piazza et al., 2014). Notably, the HEAT repeat subunits of condensin II interacted with monomethylated H4K20 peptides (Liu et al., 2010). Intriguingly, H4K20me1 is enriched specifically during mitosis (Wu et al., 2010; Liu et al., 2010).

We wanted to test if condensin I/DC could bind to H4K20me1 and other histone tails via the HEAT repeat domains. The HEAT repeats of CAP-G (yeast Ycg1) are predicted to bind to DNA (Kschonsak et al., 2017). Therefore, we focused on the CAPD-2 homolog DPY-28. We identified HEAT repeat domains of DPY-28 using homology to the human homolog hCAP-D2 and pfam predictions for HEAT repeats (Figure 18c).

Using a recombinant protein of the HEAT subunits, we performed an *in vitro* in-solution peptide binding assay (Figure 18e). We tested H4 peptides (23 aa N-terminal) that were either unmodified, mono, di, or trimethylated at lysine 20 and unmodified or tetra-acetylated H3

(K4,9,14,18) or H4 (K5,8,12,16) (Table 5). The recombinant DPY-28 HEAT repeat domains preferentially interacted with unmodified 23 aa H4 and 20 aa H3 N-terminal peptides. The acetylation of the H3 and H4 tails reduced the binding of the recombinant protein. The binding was also sensitive to the methylation status at the lysine 20 position. Unmethylated or monomethylated peptides interacted well with the recombinant protein, but further methylation decreased binding in this assay. These results suggest that histone modifications can potentially regulate condensin DC interaction with chromatin.

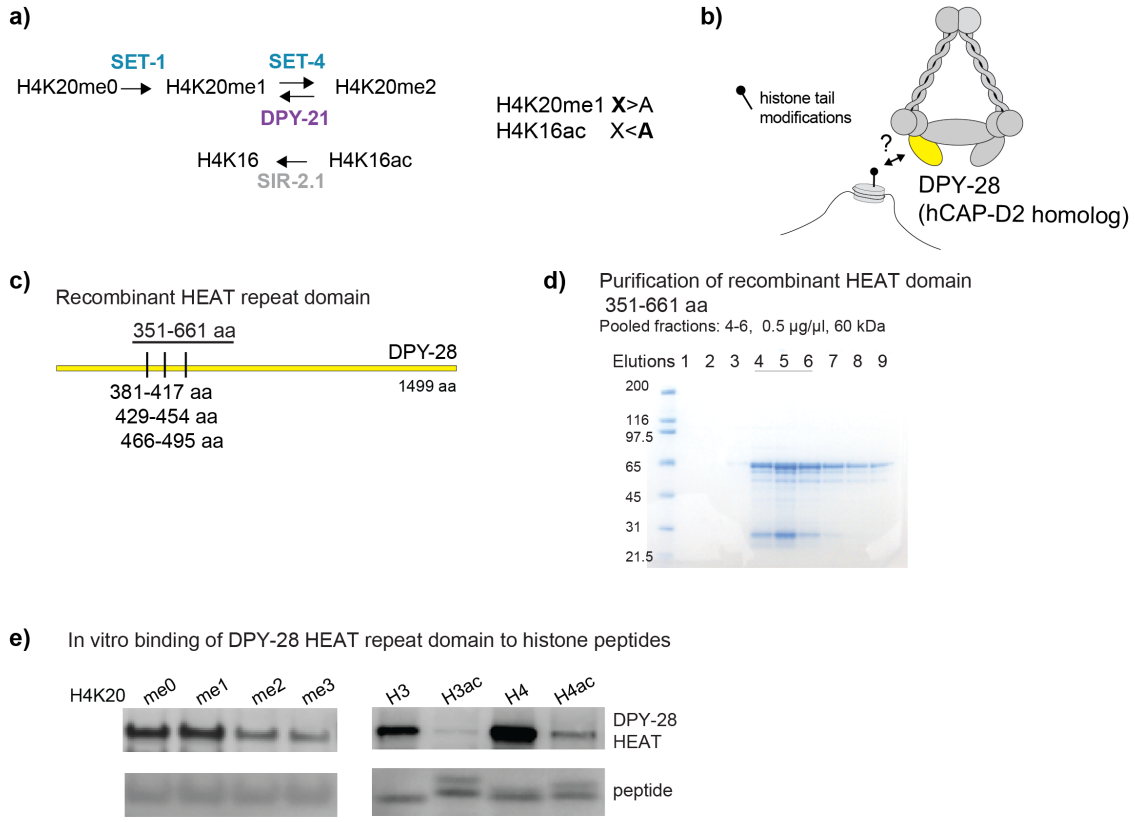

Figure 18 Condensin DC may interact with histone tails via its DPY-28 subunit
a) Enzymes that regulate H4K20 methylation and H4K16 acetylation. In hermaphrodites, H4K20me1 is increased, and H4K16ac is reduced on the dosage compensated X chromosomes compared to autosomes. *Dpy-21* null is *(e418)* allele with a premature stop codon that eliminates the protein (Yonker and Meyer, 2003), *Dpy-21(JmjC) is (y607)* allele, a point mutation that nearly abolishes H4K20me2 demethylase activity without eliminating the protein itself (Brejc et al., 2017). *Set-4* null is *(n4600),* a knockout allele that eliminates H4K20me2/3 (Delaney et al., 2017). *Sir-2.1* null is *(ok434),* a knockout allele that increases H4K16ac (Wells et al., 2012). **b)** Cartoon depicting possible interaction of the HEAT repeat-containing domain of DPY-28 (homologous to human hCAPD-2) with histone tail modifications. **c)** Three HEAT repeats annotated by pfam are shown as tick marks. The amino acids 351-661 were purified and used in peptide binding. **d)** Elutions of GST-DPY-28 HEAT repeat domain recombinant protein, predicted to be ~60 kDa. Fractions 4-6 were pooled for peptide binding assay. **e)** In solution peptide binding assay was performed using GST-tagged DPY-28 HEAT domain and biotinylated histone N-terminal tail peptides with indicated modifications. The recombinant protein was incubated with peptides bound to magnetic streptavidin beads, and bound fractions were analyzed using western blot. The streptavidin signal below indicates the amount of peptide in each fraction. Figure modified from (Breimann et al., 2021).

2.3.7 SET-4, SIR-2.1, and catalytic activity of DPY-21 do not regulate condensin DC binding

While the *in vitro* peptide binding assay results suggest that histone modifications could potentially regulate the binding of condensin DC to chromatin, previous studies using ChIP-seq showed little effect on DPY-27 binding to the X chromosome in chromatin modifier mutants (Kramer et al., 2015; Brejc et al., 2017; Wells et al., 2012; Vielle et al., 2012). However, a slight reduction of DPY-27 at promoters was observed in the *dpy-21* null mutant (Kramer et al., 2015). A recent study found that the binding of condensin DC correlated with the reduction of active histone modification at gene regulatory elements (Street et al., 2019). Therefore we tested if the loss of the H4K16 deacetylase SIR-2.1 influenced condensin DC binding. For this, we performed ChIP-seq analysis in the *sir-2.1* null embryos and could not observe a significant difference in the binding of DPY-27 compared to wild-type, *dpy-21* null, or *set-4 null* (Figure 19a-b). The loss of the SIR-2.1 did lead to a slight X chromosomal derepression (Figure 19c) and moderate dumpiness, a phenotype associated with dosage compensation problems (Figure 19d), but overall the effect was only mild.

Interestingly, published RNA-seq data suggested that the derepression of the X chromosome was different between a *dpy-21* null and *dpy-21(JmjC)* catalytic mutant (Figure 19c) (Kramer et al., 2015; Brejc et al., 2017). The catalytic and null mutants reduced H4K20me1 enrichment on the X to the same extent (Brejc et al., 2017). I compared the dumpiness phenotype in the *dpy-21* null and the *dpy-21(JmjC)* mutant and found that the null mutant had the more pronounced dumpy phenotype (Figure 19d).

Thus, DPY-27 binding sites on the X chromosome are not regulated by the activity of SET-4 or SIR-2.1. Loss of DPY-21 affects binding levels to some promoters but overall had a similar binding pattern compared to wild-type (Kramer et al., 2015). Intriguingly, the catalytic and noncatalytic activities of DPY-21 affect derepression and dumpiness phenotype differently.

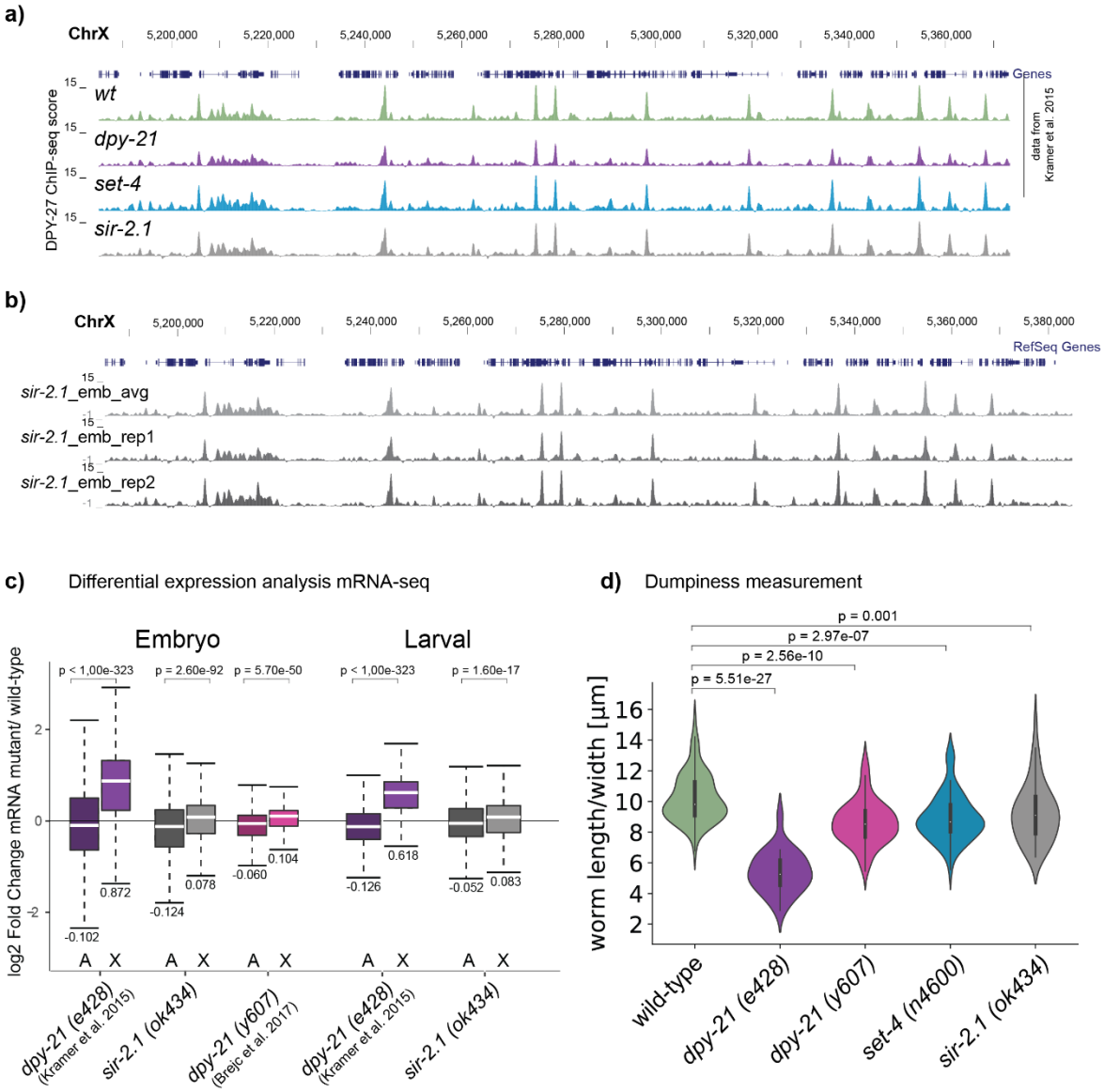

Figure 19 *set-4*, *sir-2.1*, and catalytic activity of *dpy-21* does not regulate condensin DC binding
a) UCSC genome browser shot of a representative region showing similar DPY-27 ChIP-seq patterns in wild-type and *sir-2.1*. Data from wild-type N2, *dpy-21* null, *set-4* null are from (Kramer et al., 2015) and are plotted for comparison. **b)** UCSC genome browser shot of a representative region showing similar DPY-27 ChIP-seq patterns in *sir-2.1* replicates. **c)**mRNA-seq analysis comparing published *dpy-21 (e428)* from (Kramer et al., 2015), *dpy-21(JmjC)* data from (Brejc et al., 2017), and new data in *sir-2.1* null mutant in embryos (left) and larvae (right). The level of X chromosome derepression compared to autosomes was compared in different mutants using log2 expression ratios compared to wild-type. Significant X chromosome upregulation was tested by a Wilcoxon–Mann–Whitney test. Median values of each group of genes are shown below each boxplot. **d)** Dumpiness phenotype analysis of wild-type and different mutant worms. The length divided by the width of young adult worms was calculated as a proxy for their dumpiness level from two biological replicates. The following number of worms were used for each condition: wild-type: n= 102; *dpy-21(e428)*: n= 24; *dpy-21(y607)*: n= 67; *set-4 (n4600)*: n= 69; *sir-2.1(ok434)*: n= 51. P values are from an independent two-sample t-test. Figure modified from (Breimann et al., 2021).

2.3.8 DPY-21 has a noncatalytic activity that increases the mobile fraction of condensin DC

Since we saw little to no changes in binding for the histone modifier mutants using ChIP-seq, I wanted to test if the dynamics of condensin DC binding changes in the histone modifier mutants using the established FRAP method. In worms with a *set-1* knockdown, *sir-2.1* null, and *dpy-21 (JmjC)* mutations, DPY-27 FRAP recovery was not significantly different from the recovery in wild-type worms (Figure 20a-c). The *set-4* null worms showed a slight decrease in their mobile fraction. This result is difficult to interpret as set-4 null mutations also changed transcription genome-wide (Kramer et al., 2015), and the observed decrease in mobile fraction might be a secondary effect. Therefore, the small or no change in binding dynamics of these mutants suggests that *set-1*, *set-4*, *sir-2.1,* and the catalytic activity of *dpy-21* act downstream of condensin DC binding to contribute to X chromosome repression.

In contrast, I did find a striking change in condensin DC binding for the *dpy-21 null* mutant (Figure 20a-b). The *dpy-21 null* mutant reduced the mobile fraction of DPY-27::GFP from ~30% to ~10% (Figure 20b). Similar to H2B-GFP, T-half recovery of DPY-27::GFP in *dpy-21 null* was much longer than the experimental timeframe and therefore excluded from the analysis (Figure 20c). To test if the substantial change in the mobile fraction was due to a change of free and unbound DPY-27::GFP in the *dpy-21 null* mutant, I bleached fluorescence signal outside the X chromosome area (Figure 20d). The recovery half time and mobile fraction were not significantly different between the two conditions suggesting that the observed effect is specific to binding to the X chromosome. These findings suggest that DPY-21 functions in increasing the proportion of mobile molecules on the X chromosome that is not dependent on its ability to demethylate H4K20me2. Consequently, DPY-21 might have two functional roles in dosage compensation. Firstly, upstream of binding, it increases the exchange of condensin DC and then secondly, downstream of DCC binding, it increases the H4K20 monomethylation specifically on the X. Both functions appear to contribute to dosage compensation, however, the noncatalytic activity seems to be the more substantial contribution for dosage compensation (Figure 19c-d).

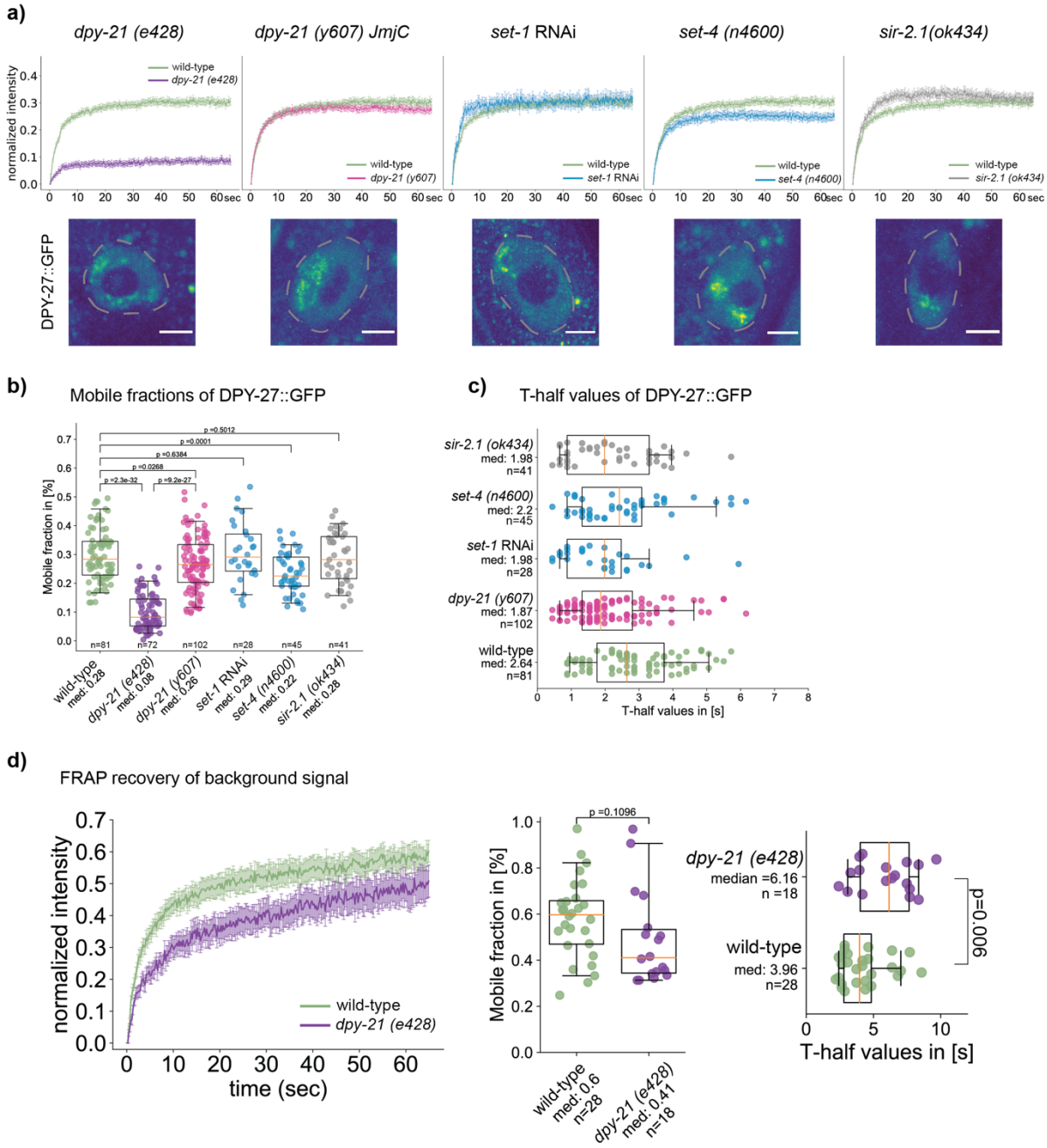

Figure 20 DPY-21 null but not catalytic mutant reduces the proportion of mobile condensin DC
a) Mean FRAP recovery curves of DPY-27::GFP in either wild-type (green) or different mutant conditions. Error bars denote s.e.m.. Number of bleached single intestine nuclei (from at least 3 biological replicates) for each experiment is n = 81 for wild-type, n = 72 for *dpy-21 (e428)*, n = 102 for *dpy-21 (y607), set-1 RNAi* n = 28, *set-4 (n4600)* n = 45, *sir-2.1 (ok434)* n= 41. Corresponding images of intestine nuclei for each mutant condition are depicted under each FRAP curve. Scale bar = 5 µm. **b)** Mobile fractions calculated from individual replicate FRAP recovery curves in panel a. P values are from an independent two-sample t-test. The number of used images of nuclei is noted under each boxplot. **c)** T-half recovery time calculated from individual replicate FRAP recovery curves in panel a. The T-half value for *dpy-21 (e428)* is not included in the plot due to the very low recovery during the experimental time frame. **d)** Mean FRAP recovery curves for background DPY-27::GFP in wild-type and *dpy-21 (e428)* mutant worms. FRAPs were performed 8 hours after a 1-hour heat shock at 35°C. Unlike panel a, the bleach point was placed outside the X chromosomal area. Error bars for the bleach curves denote s.e.m. Number of bleached single intestine nuclei (from 2 biological replicates) for each experiment is n = 28 for wild-type and n = 18 for *dpy-21 (e428)*. The middle panel depicts the mobile fractions for the background recovery. The right panel depicts the T-half recovery times for the background recovery. P values are from an independent two-sample t-test. Figure modified from (Breimann et al., 2021).

2.3.9 The loss of DPY-21 increases DPY-27 binding to the X chromosomes

Previous work studied the DPY-27 distribution in *dpy-21* null mutants using immunofluorescence microscopy and did find an increase in X chromosome volume but no difference in binding (Lau et al., 2014; Brejc et al., 2017). Using the endogenous expression of DPY-27::Halo, we tested if the reduction of mobile fraction we observed for *dpy-21* null also resulted in a different binding pattern compared to wild type (Figure 21a-b). Through careful segmentation of the X chromosomal signal in 3D and measurement of intensity, we did indeed observe stronger puncta of the DPY-27 signal at the X chromosomal domain in the *dpy-21* null mutant, which appears as a long tail of high pixel intensities in the distribution (Figure 21b).

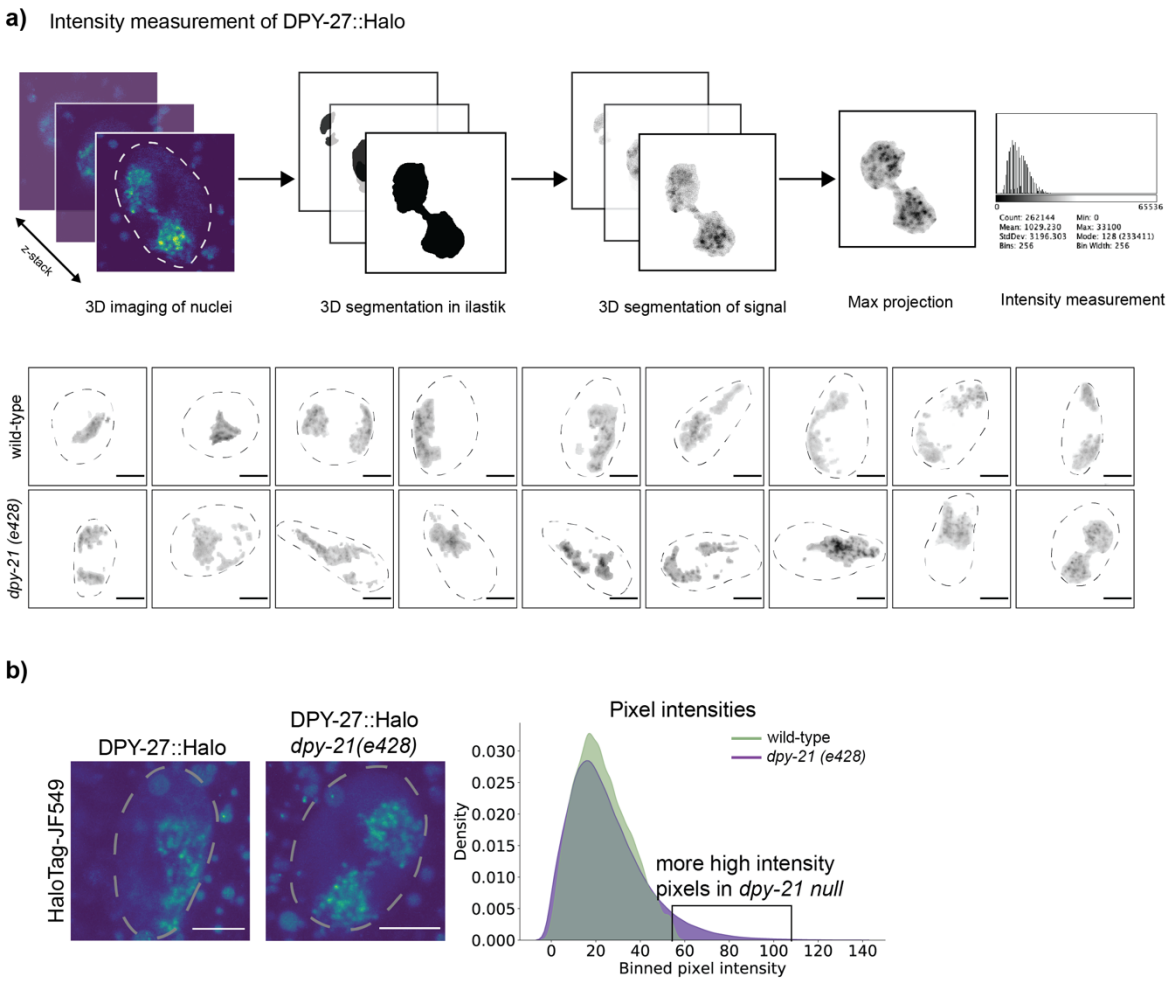

Figure 21 Loss of DPY-21 increases binding of DPY-27 to the X chromosomes
a) Analysis of the fluorescence intensity of endogenously tagged DPY-27::Halo, for wild-type and *dpy-21 (e428)* worms. The top row shows the analysis pipeline for the 3D segmentation of the HaloTag-JF549 signal. Z-stacks of intestine nuclei were imaged and segmented in 3D using ilastik (Berg et al., 2019). The resulting mask segmented the fluorescent signal in 3D, and from max projections, binned intensities were obtained. The bottom row depicts example images of 3D segmented and max projected nuclei of the wild-type and mutant worms. The scale bar corresponds to 5 µm, and all images are calibrated to the same gray values. **b)** Analysis of endogenous DPY-27::Halo fluorescent intensity enrichment on the X chromosome compared in wild-type and *dpy-21* null worms. The left panel depicts two example nuclei (marked with a dotted line). Scale bar corresponds to 5 µm. For the wild-type worms, 17 images were analyzed. For the *dpy-21(e428)*, mutant images of 31 nuclei were analyzed. The right panel shows the binned mean pixel fluorescence intensity for the two conditions. Figure modified from (Breimann et al., 2021).

2.3.10 3D DNA contacts as measured by Hi-C does not change significantly in the *dpy-21* null

Since the *dpy-21* null mutation decreased the fraction of mobile DPY-27 molecules at the X chromosomes, we wondered if DPY-21 might be an unloading factor similar to the cohesin unloader WAPL (Haarhuis et al., 2017). We reasoned that in this model, condensin DC would be stuck at the X chromosome in the *dpy-21* null mutant, which could change the condensin DC-dependent 3D architecture of the X chromosome (Crane et al., 2015). We performed Hi-C in *dpy-21* null embryos and analyzed in parallel published Hi-C data in the catalytic *dpy-22 (JmjC)* mutant (Brejc et al., 2017) (Figure 22).

Although we observed a reduction in insulation in some strong *rex* sites that act as TAD boundaries, the overall structure of the X chromosome appeared unchanged between wild type and *dpy-21* null mutant conditions (Figure 22a). Additionally, the range of interactions between locations on the X chromosome and locations in the autosomes was similar between wild type and *dpy-21* null mutants (Figure 22b-c). In contrast, the published data on the catalytic *dpy-21 (JmjC)* mutant showed a reduction of long-range interactions on X chromosomes and autosomes (Brejc et al., 2017) (Figure 22b-c).

Since condensin DC binds only to the X chromosome, we highlighted the X-specific contacts by normalizing the contact frequency across the same distance on the X to autosomes (Figure 22d-e). This analysis reaffirmed that the DNA contacts on the X chromosome between 50 kb to 1 Mb range are most frequent. In the *dpy-21* null mutant, the range of contacts did not significantly change from wild-type (Figure 22d). However, the *dpy-21 (JmjC)* mutant did show a shift to shorter contacts enriched on the X chromosomes (Figure 22e). Strong *rex* sites on the X chromosome interact in wild-type, overlapping with TAD boundaries (Figure 22a,d). While the *dpy-21* null mutation reduces the *rex-rex* interactions, the *dpy-21 (JmjC)* mutant had an even greater loss of *rex-rex* interactions. These results suggest that DPY-21 demethylase activity and, therefore, an increase of H4K20me1 at the X chromosome changes the X-enriched DNA contacts and that loss of the DPY-21 protein can partially compensate for these changes.

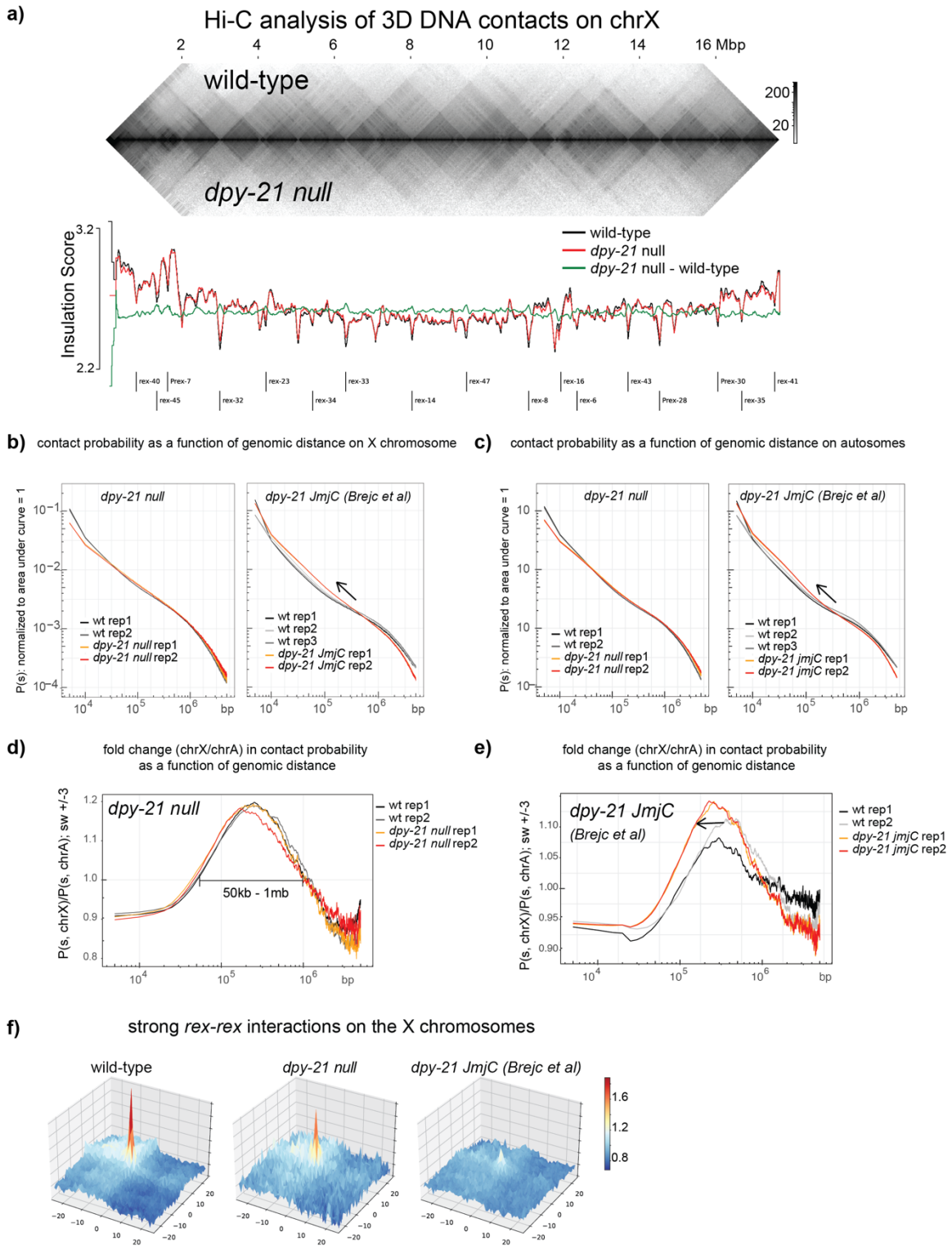

Figure 22 Hi-C analysis of 3D DNA contacts in the *dpy-21* null and *JmjC* mutant embryos
a) Hi-C contact probability heatmap and insulation scores of chromosome X for wild-type and the *dpy-21* null mutant. The insulation scores for wild-type, mutant, and mutant minus wild-type are displayed below the contact probability map. Additionally, the location of strong *rex* sites is annotated. **b)** The distance decay curve for the X chromosomes, showing the relationship between 5 kb binned genomic separation (s) and average contact probability (P(s)). Each plot is normalized to unity. *JmjC* mutant data was downloaded and analyzed with the same parameters as the *dpy-21* null, using corresponding wild-type data (Brejc et al., 2017). **c)** For the autosomes, a distance decay curve showing the relationship between 5 kb binned genomic separation (s) and average contact probability (P(s)). Each plot is normalized to unity. *JmjC* mutant data was downloaded and analyzed with the same parameters as the *dpy-21* null,

using corresponding wild-type data (Brejc et al., 2017). **d)** X-A normalized distance decay curve for *dpy21* null. For every genomic separation s, the unity normalized contact probability of X-chromosome, P(s,chrX), is divided by autosomes, P(s,chrA). A moving average of +/- 3 bins is applied for plotting. **e)** X-A normalized distance decay curve for *JmjC* mutant. For every genomic separation s, the unity normalized contact probability of X-chromosome, P(s,chrX), is divided by autosomes, P(s,chrA). A moving average of +/- 3 bins is applied for plotting. Wild-type replicate number three from (Brejc et al., 2017) was an outlier and excluded from the analysis. **f)** Meta-'dot' plot showing the average strength of interactions between pairs of *rex* sites on a distance-normalized matrix. For 17 strong *rex* sites, a total of 33 *rex-rex* pairs located within 3 Mb of each other were used. Figure modified from (Breimann et al., 2021).

2.4 Discussion

The *C. elegans* condensin DC complex shares four out of five subunits with the canonical condensin I complex (Csankovszki et al., 2009a). In condensin DC, the SMC protein DPY-27 replaces the SMC-4 subunit (Hagstrom et al., 2002; Csankovszki et al., 2009a). DPY-27 and SMC-4 are highly conserved proteins and share high sequence similarity with other SMCs, especially at the ATP binding domains (Chuang et al., 1994) (Figure 16a). *In vitro* and *in vivo* studies have shown that SMC complexes require their ATPase activity (Hirano, 2016; Hassler et al., 2018). We could show that a single amino acid mutation, which reduced ATP hydrolysis in other organisms, eliminated DPY-27 binding to the X chromosome (Figure 16, Figure 17). This finding underlines that SMC activity is conserved in condensin DC (Wood et al., 2010; Lau and Csankovszki, 2015; Albritton and Ercan, 2018).

The binding of DPY-27 to the X chromosome was eliminated in the ATPase mutant, suggesting that the hydrolysis of ATP is required for the stable association of condensin DC (Figure 16, Figure 17). While the ATPase activity of SMCs is conserved between many organisms, the consequence of the different ATPase mutants may be different for different SMC complexes and in between organisms. In *Xenopus* extracts, blocking the ATP hydrolysis function via the EQ mutation in SMC-2 and SMC-4 did not abolish loading of the complex to chromosomes analyzed using immunofluorescence (IF) (Kinoshita et al., 2015). Similarly, in chicken cell culture and yeast, the EQ mutant in SMC-2 or SMC-4 did not affect binding but did prevent proper chromosome compaction (Hudson et al., 2008; Thadani et al., 2018). In *Bacillus subtilis,* the EQ mutant SMC was bound to *parS* loading sites but had reduced spreading along the chromosome as observed using ChIP-seq analysis (Minnen et al., 2016). In mammalian cells, the EQ mutant affected cohesin binding more at CTCF sites than at loading sites (Vian et al., 2018). Thus different forms of binding of SMC molecules might be driven by different functions of the ATPase cycle.

While the mutated Walker B motif is highly conserved, it is possible that the mutation did not abolish ATP hydrolysis but affected the ATPase differently. To investigate that the wild-type condensin DC can indeed function as an ATPase and that the EQ mutation causes a decrease in ATP hydrolysis, performing *in vitro* assays would be the way to test this. For example, an *in vitro*

binding assay using a nonhydrolyzable ATP analog or an isothermal titration calorimetry assay of ATP biding to different DPY-27 mutants, including the EQ mutant, would provide evidence if the EQ mutant in DPY-27 is an ATP binding or ATP hydrolysis mutant (Hirano and Hirano, 2004; Hassler et al., 2019).

2.4.1 The ATPase activity may be required for the formation and stability of condensin DC

Besides its role in binding, the ATPase activity might also contribute to the formation and stability of the SMC complex *in vivo*. One possibility is that the ATPase activity controls significant structural changes triggered by the cycle of ATP binding and hydrolysis (Lee et al., 2020). No defects in complex formation with the ATPase mutant were detected using pull-down experiments in chicken cells (Hudson et al., 2008). However, in budding yeast, an ATP binding mutant showed reduced interactions between the SMC-4 and kleisin subunit (Thadani et al., 2018), and in *B. subtilis,* a crosslinking assay revealed a reduced interaction between the SMC homodimer and the ScpA bridging protein (Wilhelm et al., 2015). In our experiments, we also noticed a reduced interaction between the kleisin subunit and DPY-27(EQ) which might be responsible for the degradation of protein over time (Figure 16b). Similarly, a reduced protein level was also reported in budding yeast for the ATP binding mutant (Thadani et al., 2018). Together, these observations suggest that the function of the ATP domain can also affect the formation and stability of the condensin complexes *in vivo*.

2.4.2 Enrichment and depletion of H4K20me1 and H4K16ac on the X chromosomes have little effect on condensin DC binding *in vivo*

Human condensin II might interact with histones via its HEAT repeat domains in CAP-D3 and CAP-G2 (Liu et al., 2010). We also found that the condensin I/DC subunit DPY-28 could interact with histone H3 and H4 tail peptides in a manner sensitive to the modifications tested (Figure 18). However, mutants that increased or decreased the X enriched histone modification H4K20me1 or the X depleted histone modification H4K16ac did not affect condensin DC binding to the X chromosome as measured by ChIP-seq and FRAP (Figure 19, Figure 20).

Condensin prefers to bind to free DNA *in vitro* (Piazza et al., 2014; Kschonsak et al., 2017; Kong et al., 2020) and accumulate at accessible regions *in vivo* (Jeppsson et al., 2014; Uhlmann, 2016). A recent study found that condensin can extrude DNA fragments containing 3-4 nucleosomes, and the presence of nucleosomes even increased the velocity of condensin II *in vitro* (Kong et al., 2020). Nucleosomes could potentially stimulate the ATPase-dependent movement of condensin

in vivo. Additionally, different modifications on histone tails, histone variants as well as linker histone were suggested to modulate condensin binding (Kimura and Hirano, 2000; Kim et al., 2009; Liu et al., 2010; Tada et al., 2011; Tanaka et al., 2012; Yuen et al., 2017; Petty et al., 2009; Choppakatla et al., 2020). Our results suggested only a small contribution of H4K20me1 and H4K16ac to dosage compensation, but potentially the combined effect of these modifications together with other modifications, variants, or linker histones on the X chromosome might regulate condensin DC binding and function.

2.4.3 A noncatalytic activity of DPY-21 regulates the dynamics of condensin DC binding and is required for transcription repression on the X chromosomes

DPY-21 is a subunit of the Dosage Compensation Complex and demethylates H4K20me2 to H4K20me1 through the action of the JmjC domain (Yonker and Meyer, 2003; Brejc et al., 2017). The null and JmjC mutation have different consequences for condensin DC binding, and gene repression suggestion a catalytic and structural role for DPY-21 (Brejc et al., 2017). The catalytic demethylase activity acts downstream of condensin DC binding and contributes to X chromosome repression. Our results show that DPY-21 has an additional noncatalytic activity that acts upstream of condensin DC binding, increasing the mobile fraction of the complex on the X chromosome, which is critical for transcription repression.

One hypothesis of how DPY-21 could regulate the proportion of mobile condensin DC could be that DPY-21 removes condensin DC from chromatin directly or indirectly. This role would be similar to the cohesion unloader WAPL, where Hi-C analysis showed enrichment of longer-range cohesin-mediated 3D contacts (Haarhuis et al., 2017; Nuebler et al., 2018). Hi-C analysis of the catalytic *dpy-21 (JmjC)* mutant showed diminished long-range interactions between *rex* sites (Brejc et al., 2017). Our Hi-C analysis for the complete loss of DPY-21 rescued the X-enriched long-range interaction, including to some extent between *rex* sites. These different Hi-C results would suggest that the noncatalytic activity of DPY-21 may counteract the catalytic activity of DPY-21 for establishing long-range chromatin contacts. It is difficult to address how a single protein might have opposing effects because it is unclear how DPY-21 interacts with condensin DC and other DCC proteins and if DPY-21 has additional catalytic activities. Since there is no good model of how histone modifications can affect 3D DNA contacts, we speculate that *dpy-21(JmjC)* might regulate properties of the chromatin fiber to promoter-long range interactions. The noncatalytic activity may reduce condensin DC residence on chromatin and thereby decreasing the range of 3D interactions. Together, these two activities largely cancel each other and contribute to the fine-tuning of condensin DC binding dynamics for proper dosage compensation.

How do these different activities contribute to dosage compensation regulation? The catalytic activity of DPY-21 enriches H4K20me1 specifically on the X chromosome, consequently leading to a reduction of H4K16ac. This specific profile of histone modifications might reduce the binding of transcription activators, contributing to the 2-fold gene repression on the X chromosomes. Our analysis suggests that a noncatalytic activity of DPY-21 regulates the dynamics of condensin DC binding to chromatin. In the *dpy-21* null mutant, the fraction of mobile condensin DC was reduced, and the ChIP-seq enrichment was lower at promoters compared to wild-type. WAPL ablation and, therefore, cohesin binding stabilization resulted in increased binding of cohesin overall but decreased binding to specific promoters leading to loss of gene expression (Liu et al., 2021). The dynamic turnover of condensin DC possibly contributes to the specific binding to promoter sites and repressing transcription initiation for dosage compensation.

In summary, we found an additional noncatalytic activity for DPY-21 in regulating the dynamic binding of condensin DC. Loss of DPY-21 results in derepression of the X chromosome by ~2-fold but changes the X-enriched 3D contacts only minimally as measured by Hi-C. Possibly, this discrepancy lies in Hi-C measuring the changes between different equilibrium states rather than the changes of dynamic loop formation in a system. Perhaps for condensin DC-mediated gene regulation, the dynamic formation of loops via binding and unbinding of loop-extrusion factors is more important than the location and size of the loops. Thus, we conclude that the noncatalytic activity of DPY-21 regulates condensin DC binding to the X chromosome, which is vital for its function in transcription repression (Figure 23).

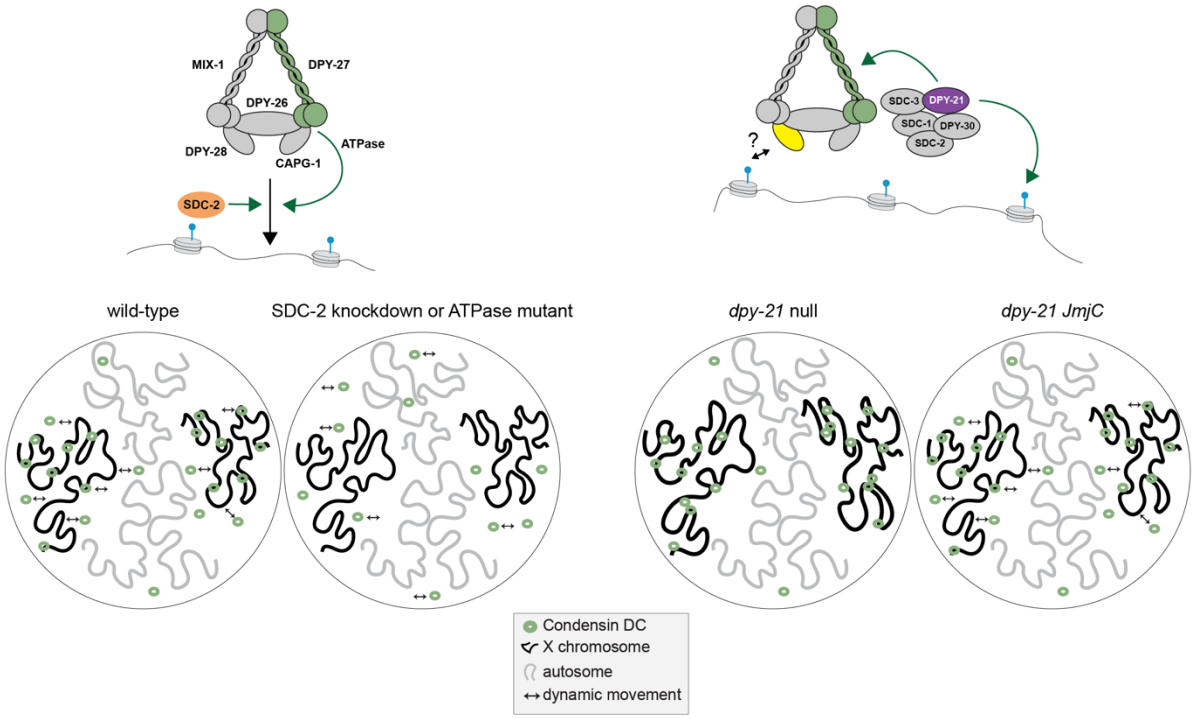

Figure 23 Model for regulation of condensin DC binding
In a wild-type hermaphrodite cell, condensin DC binds dynamically to the X chromosomes. This binding is disrupted by a knockdown of its recruiter SDC-2 or a single amino acid mutation in the ATPase domain of DPY-27. Condensin DC may interact with histone tails through HEAT-repeats within DPY-28. The H4K20me2 demethylase DPY-21 has a dual function in X chromosome repression. The catalytic activity increases H4K20me1 on the X and contributes to repression downstream of condensin DC. The noncatalytic activity of DPY-21 increases the turnover of condensin DC molecules, which is vital for transcription repression. In the *dpy-21* null condition, both catalytic and noncatalytic activities are eliminated, resulting in stronger X chromosome derepression. Figure modified from (Breimann et al., 2021).

2.5 Methods

2.5.1 Strains and Worm Growth

Unless noted, worms were grown and maintained using standard methods at 20-22°C on NGM plates containing OP50-1 strain of *E. coli* as food.

Table 1 List of strains used in chapter 2

strain name	strain genotype	short description
N2	wild type	wild type laboratory strain
CB428	dpy-21(e428) V	*dpy-21* null
MT14911	set-4 (n4600) II	*set-4* null
ERC47	ersSi12[hsp16-41::dpy-27::GFP::3xFlag, unc-119(+)] II; unc-119(ed3) III	promoter_hsp::dpy-27::GFP in mossci Chr II site
ERC55	ersSi21[hsp16-41::dpy-27[EQ-TR]::GFP::3xFlag, unc-119(+)] II; unc-119(ed3) III	promoter_hsp::dpy-27 EQ TR mutation::GFP in mossci Chr II site
VC199	sir-2.1(ok434) IV	*sir-2.1* null
ERC76	ers53[dpy-27::halo] III	dpy-27::halo endogenous location fully complementing function with tag and 11 aa deletion
TY5686	dpy-21(y607)	dpy-21*(jmjC*) catalytic mutant (Brejc et al. 2017)
RW10993	unc-119(ed3) III; itIs37 IV; stIs10116; wgIs94.	H2B::mCherry
EG8961	oxSi255 I; oxTi81 him-5(e1490) V	H2B::GFP
EG8899	oxTi951 I; unc-119(ed3) III	Free GFP with NLS
strains derived for FRAP analysis by crossing		
SPL7	RW10993 X ERC55	ATPase mutant with H2B::mCherry
SPL8	RW10993 X ERC47	Wild-type with H2B::mCherry
SPL13	SPL8 X TY5686	*dpy-21(jmjC*) catalytic mutant with DPY-27::GFP
SPL14	SPL8 X MT14911 (set-4 null)	*set-4* null with DPY-27::GFP
SPL15	SPL8 X CB428 (dpy-21 null)	*dpy-21* null with DPY-27::GFP
SPL16	SPL8 X VC199	Sir-2.1 null with DPY-27::GFP
SPL17	ERC47 X ERC76	Endogenous dpy-27::halo with DPY-27::GFP
SPL18	RW10993 X ERC76	Endogenous dpy-27::halo with H2B::mCherry
SPL19	CB428 X ERC76	Endogenous dpy-27::halo with *dpy-21* null

Generation of DPY-27::GFP and DPY-27(EQ)::GFP strains: An inducible GFP-tagged copy of DPY-27 was expressed from the chrII MosSCI site (~8.4 Mb) (Frøkjær-Jensen et al., 2008) under the control of a heat-shock inducible *hsp 16-41* promoter and the *dpy-27* 3' UTR. The *hsp 16-41* promoter was amplified from pCM1.57 using primers SE123 F&R, and *dpy-27* 3'UTR was amplified from genomic DNA using primers SE124F&R and were inserted into pCFJ151 at the XhoI site. The resulting plasmid contained a SphI site between the promoter and the 3' UTR, which was used for NEB Infusion cloning with the full-length *dpy-27* and a GFP-3xflag sequence. Amplification of the *dpy-27* sequence was done from genomic DNA using the primers SE135F&R.

A GFP-3x flag sequence was amplified from a plasmid kindly provided by Susan Strome, using primers SE136 F&R. The ATPase mutagenesis of DPY-27 was performed by incorporating the E to Q mutation at the conserved ATPase domain as shown in Figure 16.

Generation of DPY-27::Halo strain: The CRISPR/Cas9 system was used to insert the Halo tag at the C-terminus of DPY-27 (Dokshin et al., 2018). A 20 bp crRNA (LS37) was designed to target the end of the last *dpy-27* exon. The dsDNA donors consisting of a 15 bp flexible linker (GlyGlyGlyGlySer) and the Halo tag flanked by 35 bp homology arms were generated by PCR using 5' SP9 (TEG) modified primers AM29F&R and pLS19 as a template. The injection mix containing *S.pyogenes* Cas9 3NLS (10 µg/µl, IDT), crRNA (2 nmol, IDT), tracrRNA (5 nmol, IDT), dsDNA donors, and pCFJ90 (pharynx mCherry marker). About 40 F1s positive for the co-injection marker were transferred to individual plates and allowed to have progeny. F2 progeny was screened by PCR with primers LS40F&R. Sanger sequencing of positive PCR products showed in-frame insertion of the Halo tag along with 18 bp of unknown sequence that did not affect the function of the tagged protein.

Table 2 List of primers

F primer	*R primer*	*Forward Sequence*	*Reverse Sequence*
DPY 28 351F	DPY-28	atgcGGATCCGAACGAGCCGAAAAGCCA	atgcGAATTCTCAATCGTCCA TTTGGGTTAG
SE123F	SE123R	GCAGGAATTCCTCGActgcaggtcgactctag a	Atatattacttcaatatttttttctaccggtacc
SE124F	SE124R	attgaagtaatatattttaaac	CACCGTACGTCTCGAttaggaa attatttttgat
SE135F	SE135R	gtattggtaccggtagaaaaaatATGCAGCCGTT TAAAAGACG	ATGTCTGCTTCTTCGCACAC
SE136F	SE136R	CGAAGAAGCAGACATATGAGTAAAGGA GAAGAACTT	gtttaaaatatattacttcaatTCACT TGTCATCGTCATCC
SE127		gatgacgacaagggcagc	
SE128		cgggcctgagatccacac	
SE129		GCAAAGGATGAAGTTCGG	
SE130		TGAACTGAAAGAGGCTGG	
SE131		ATCACGCACTGGAAGCTC	
SE132		AATTGCAAACTTCAACGg	
SE133		AAGATGTTGACAAGTTCC	
SE134		TCGAGGAGGAGATCAAAC	
SE101F	SE101R	cAgATCGATGCGGCACTGGAC	ATCCATCACGTAGAGGGGTG
LS37		ACACGGCGTTGAACGACAAT	
AM29F	AM29R	CATCTCCACCACCAATCGTCGTCCAACG T CGCGTGCGAAGAAGCAGACATgggggagg a ggatcgGAAATCGGTACAGGCTTTCC	Ttttcaaaatttagtttaaaatatattact tcaatTTATCCGGAGATCTCGA GGGTGG
LS40F	LS40R	TGGACAGTACGTGATGCAAAG	CGATGAGCCAGTAAGAAGACG

2.5.2 RNAi conditions

For RNAi experiments, bacteria strains from the Ahringer RNAi library were verified by sequencing and used for knockdown experiments (Table 3). Single colonies of bacteria were picked and grown in 10 mL LB with 50 µg/mL ampicillin overnight (at 37°C shaking at 300 rpm), then transferred to a 400 mL LB with 50 µg/mL ampicillin culture and after 2 hours when the culture reached OD ~1 induced with 0.1 mM ITPG and grown for another 3 hours. Bacteria were concentrated 10-fold and seeded onto 10 cm NGM plates supplemented with 50 µg/mL ampicillin, 2 µg/mL tetracycline, and 1mM IPTG. Worms were synchronized by bleaching, and L1s were placed on the seeded plates. Worms were used for FRAP experiments after 72 hours at 20°C (young adult stage). RNAi knockdown experiments were controlled using an embryonic lethal positive condition, pop-1, and the number of progeny for worms with pop-1, experimental condition (if germline was able to form) or empty vector were scored 24 hours after the FRAP experiments. Additionally, FRAP experiments for the *set-1* RNAi condition were performed in germline-less worms.

Table 3 List of RNAi bacteria strains

Sequence name	Targeted gene
control	empty vector
W10C8.2	*pop-1*
T26A5.7	*set-1*
C35C5.1	*sdc-2*

2.5.3 Genomic Data Access

The genomic data is available at Gene Expression Omnibus (GEO) series number GSE169458.

2.5.4 ChIP-seq

For the ChIP-seq analyses of GFP tagged DPY-27 in embryos, gravid adults were heat-shocked at 35°C for 30 min and transferred to room temperature for two hours for recovery. Embryos were collected by bleaching, and ChIP was performed as described previously (Ercan et al., 2007). Two micrograms of anti-GFP (Abcam ab290) and anti-DPY-26 antibodies were used with 1-2 mg of embryo extract. Detailed antibody information is given in Table 4. The ChIP-seq analysis of the *sir-2.1* mutant strain was performed in early L3 larvae by hatching embryos in M9 overnight. The next day, L1s were plated on NGM media containing HB101 bacteria and incubated at 20°C for ~24 hours. ChIP in larvae was performed by grinding frozen larvae a few minutes in mortar and pestle cooled in liquid nitrogen, followed by crosslinking in PBS containing 1%

formaldehyde for 10 min quenching with 125 mM glycine for 5 min and preparing ChIP extract as in embryos. Two micrograms of anti-DPY-27 were used with 1-2 mg of extract per ChIP. Half of the ChIP DNA and approximately 20-80 ng of the input control DNA were used to make Illumina TruSeq libraries as previously described (Albritton et al., 2017). For each data set, at least two biological replicates were generated. Single-end sequencing was performed in Illumina HiSeq500 or NextSeq.

Table 4 List of antibodies

Target	Antibody	Antibody information	Antigen	Reference
DPY-27	JL00001	Rabbit polyclonal	1-409 aa	(Ercan et al., 2007)
DPY-26	JL00003	Rabbit polyclonal	740-1262 aa	(Ercan et al., 2009)
MIX-1	JL00004	Rabbit polyclonal	837–1244 aa	(Ercan et al., 2009)
GFP	ab290	Rabbit polyclonal	Recombinant full-length protein corresponding to GFP	abcam

ChIP-seq data analysis: We used bowtie2 version 2.3.2 to align 50-75 bp single-end reads to WS220 with default parameters (Langmead and Salzberg, 2012). Bam sorting and indexing was performed using samtools version 2.1.1 (Ramirez-Gonzalez et al., 2012). BamCompare tool in Deeptools version 3.3.1 was used to normalize for the sequencing depth using CPM and create ChIP/Input ratios with a bin size of 10 bp and 200 bp read extension (Ramírez et al., 2016). Only reads with a minimum mapping quality of 20 were used, and mitochondrial DNA, PCR duplicates, and blacklisted regions were removed (Ho et al., 2014). The average coverage data was generated by averaging ChIP-Input enrichment scores per 10 bp bins across the genome.

2.5.5 mRNA-seq

mRNA-seq analysis of *sir-2.1* null mutant strain VC199 was performed as described in and compared to previously published mRNA-seq data (Kramer et al., 2015). Briefly, embryos and L2/L3 larvae were collected for at least three biological replicates. After collection, worms were stored in Trizol (Invitrogen). RNA was purified using the manufacturer's protocol after freeze-cracking samples five times. RNA was cleaned up using a Qiagen RNeasy kit, and mRNA was purified using Sera-Mag Oligo (dT) beads (Thermo Scientific) from 1 µg of total RNA. Stranded Illumina libraries were prepared as described (Kramer et al., 2015), and sequencing was done with Illumina HiSeq-2000 to produce single-end 50-75 bp reads. We aligned reads to the WS220 genome version using Tophat version 2.1.1 with default parameters (Kim et al., 2013). Count data were calculated using HTSeq version 0.6.1 (Anders et al., 2015) and normalized using the R package DESeq2 (Love et al., 2014).

2.5.6 Hi-C

CB428 (*dpy-21(e428))* gravid adults were bleached to isolate embryos, which were crosslinked in 50 mL M9 containing 2% formaldehyde, washed with M9 and PBS, and pelleted at 2000 g 1 min to store at -80°C. Approximately 50 µl of the embryo pellet was resuspended and crosslinked a second time using the same conditions, washed once with 50 mL 100mM Tris-Cl pH 7.5 and twice with 50 mL M9. The embryo pellet was resuspended in 1 mL embryo buffer (110 mM NaCl, 40 mM KCl, 2 mM CaCl2, 2 mM MgCl2, 25 mM HEPES-KOH pH 7.5) containing 1 unit chitinase (Sigma) and digested approximately 15 minutes. Blastomeres were then washed with embryo buffer twice by spinning at 1000g 5 min. The pellet was resuspended in 1 mL Nuclei Buffer A (15 mM Tris–HCl pH 7.5, 2 mM MgCl2, 0.34 M Sucrose, 0.15 mM Spermine, 0.5 mM Spermidine, 1 mM DTT, 0.5 mM PMSF, 1xCalbiochem Protease Inhibitor cocktail I, 0.25% NP-40, 0.1% Triton X-100), centrifuged at 1000 g for 5 minutes at 4°C then resuspended in 1.5 mL Nuclei Buffer A. The embryos were dounced ten times with a loose pestle A and ten times with a tight pestle B. The cellular debris was spun down 1 min at 200 g. The supernatant containing nuclei was kept on ice. The pellet was resuspended in 1.5 mL Nuclei Buffer A, and the douncing process was repeated four times. Each supernatant was checked for absence of debris by DAPI stain and pooled and spun down at 1000 g for 10 mins at 4°C. Approximately ~20 µl of nuclei were used to proceed to the Arima Hi-C kit, which uses two 4-base cutters, DpnII (^GATC) and HinfI (G^ANTC), followed by KAPA Hyper Prep Kit for library preparation per the protocol provided by Arima. Paired-end Illumina sequencing was performed with Nextseq or Novaseq.

Hi-C data analysis: 150bp reads were trimmed using fastx toolkit version 0.0.14 to match replicates generated by 100-bp paired-end sequencing. The Hi-C data was mapped to ce10 (WS220) reference genome using default parameters of the Juicer pipeline version 1.5.7 (Durand et al., 2016). Because Hi-C data generated from the Arima Hi-C kit used two restriction enzymes, dpnII (^GATC) and hinfI (G^ANTC), while the published Hi-C data used only one, dpnII (^GATC), the corresponding restriction sites files were used for the juicer pipeline. The inter_30.hic outputs were converted to h5 using the hicConvertFormat of HiCExplorer version=3.5.1 for genome-wide normalization and sample-to-sample depth normalization (Wolff et al., 2018, 2020; Ramírez et al., 2018). The inter_30.hic files were first converted to cool files, and the correction method was removed using the --correction_name none option. Then, cool files were converted to h5 files to be used in HiCExplorer. The replicates of the same experimental condition were combined using hicSumMatrices. The count values of each replicate were normalized to match those of the most shallow matrix using hicNormalize with the option --smallest. The same method was used for the summed matrices. Lastly, the hicCorrectMatrix function was applied to each matrix to correct for sequencing bias with the

following parameters: --correction_method ICE, -t 1.7 5, --skipDiagonal, --chromosomes I II III IV V X. The distance decay curves were generated by computing the average contact for a given distance using the 5000 bp-binned normalized matrix using hicPlotDistVsCounts with parameters --perchr, maxdepth 20,000,000. The outputs from --outFileData were plotted in R. The curves were normalized to unity to compare different samples by setting the sum of contacts in the distance range of 5000 bp to 4 Mb range to 1 for each chromosome. To analyze X-specific changes, we calculated P(s,chrX)/P(s,chrA) by dividing the P(s) of the X chromosome by the average P(s) of all autosomes at every distance, s. The insulation scores were computed using the 10kb-binned normalized matrix with the function hicFindTADs using parameters: --correctForMultipleTesting fdr, --minDepth 80000, --maxDepth 200000, --step 40000. The meta-loops were computed using the 10 kb-binned normalized matrix with the hicAggregateContacts function of hicexplorer with parameters: --range 100000:3000000, --avgType mean, --transform obs/exp, --plotType 3d, --vMin 0.8 --vMax 2 --BED 17 strong *rex*es (Albritton et al., 2017). A 400 bp window for the 17 strong *rex* sites was defined as center regions with an additional 250 kb of up and downstream regions.

2.5.7 Immunoprecipitation and Western blots

Immunoprecipitations (IPs) of GFP-tagged DPY-27 proteins were performed from protein extracts prepared using 200 µL of young adult worms heat-shocked at 35°C for one hour and let to recover at 20°C for the indicated times. Worms were dounced in lysis buffer (40 mM HEPES pH 7.5, 10% glycerol, 150 mM NaCl, 1 mM EDTA, and 0.5% NP-40) complemented with protease inhibitors (Calbiochem cocktail I) and sonicated for 5 min (30 sec on and 30 sec off in a Bioruptor). Extracts were centrifuged at 17,000 g for 15 min at 4°C, and 2 mg of protein were incubated overnight with 2-3 µg of the indicated antibody. Immunocomplexes were collected with protein A Sepharose beads at 4°C for 2 hours. Beads were washed thrice with 1 mL of immunoprecipitation buffer (50 mM HEPES-KOH pH 7.6, 1 mM EDTA, 0.05% Igepal, and 150 mM NaCl). IPed proteins were eluted by boiling in SDS sample buffer and analyzed by SDS-PAGE and immunoblotting using an anti-DPY-27 antibody (1:2000). Detection was performed using ECL Plus reagents (#PI80196, ThermoFisher).

2.5.8 Worm size analysis

Quantification of the worm size was performed in young adults. Worms were allowed to lay eggs for 4 hours, and the progeny was grown at 20°C to the young adult stage. Worms were washed with M9, anesthetized with 10 mM levamisole, and placed on a fresh NGM plate without OP50 to

achieve an even and clear background. Worms were singled with an eyelash, and images of about 30 worms were acquired using a Dino-Lite eyepiece camera (AM7025X) on a Zeiss stereomicroscope with a 1X magnification. For analysis, the background was subtracted using Fiji (Schindelin et al., 2012) with a rolling ball radius of 50 px (light background). The Fiji plugin WormSizer (Moore et al., 2013) was used to analyze the worms' size and width, and plots were created using Python (https://github.com/ercanlab/2021_Breimann_et_al).

2.5.9 Heat shock, fluorescent labeling, and mounting worms for imaging

JF549-HaloTag and JF635-HaloTag ligands were a generous gift from Luke D. Lavis and Jonathan B Grimm (Grimm et al., 2017, 2015) and were incorporated into worms by feeding based on (Wu et al., 2019) with the following modifications. L4 worms were washed and collected in small eppendorf tubes with 200 µl M9, concentrated OP50, and 2.5 µM HaloTag dye. Tubes rotated at RT for about 17 hours, and worms were then placed on fresh OP50 plates for at least 4 hours to reduce the background signal of the unbound HaloTag ligand.

For imaging experiments using the heat shock inducible DPY-27::GFP, worms were grown to young adult stage and heat-shocked for 1 hr at 35°C and recovered at RT for 8 hr (unless otherwise labeled). Worms were settled in M9 at 4°C for 10 min, and 40 µl were transferred to a well depression microscopy slide with the addition of 10 µl of 50 mM levamisole (LGC). After 10 minutes, the worms were transferred onto a 10% agarose pad on a microscope slide and covered with a 1.7 µm objective slide (high precision, no.1.5H, Marienfeld). Excess liquid was removed using a lab tissue (Kimtech precision wipe), and the edges of the objective slide were sealed with a two-component silicone glue (picodent twinsil speed).

2.5.10 Confocal microscopy and FRAP

Confocal imaging and FRAP were performed on a scanning confocal microscope (Leica SP8) using an HC PL APO 63x 1.3 NA glycerol objective (Leica) and Leica Application Suite X (version 3.5.5.19976). For wGFP, the white light laser was set to 482 nm with 10-15% laser intensity, and the emission detection was set to 488 - 520 nm with a HyD hybrid photodetector and gain of 162%. For JF549, the white light laser was set to 549 nm with 10% laser intensity, and the emission detection was set to 554-651 nm with a HyD detector and gain of 200% and gating between 0.3 - 6.0. For JF635, the white light laser was set to 633 nm with 10% laser intensity, and the emission detection was set to 638-777 nm with a HyD detector and gain of 100% and gating between 0.30 - 6.00.

For FRAP in the intestine nuclei, 20 pre bleach images were acquired, followed by a point bleach (smallest possible bleach spot) of 700 ms with 100 % laser power and subsequent acquisition of ~500 recovery images using 10-15% laser power. The scan speed was set to 600 Hz, with bidirectional scanning (phaseX: 29.752) in a frame size of 256 x 256 pixels (Pixel dwell time 0,002425 s). The pinhole was set to 1 AU, and a 7x digital zoom was used to zoom in to single intestine nuclei of young adult worms. The FRAP experimental protocol, including videos, can be found here: https://dx.doi.org/10.17504/protocols.io.bpkymkxw

2.5.11 FRAP data analysis

Image analysis of the fluorescence recovery at the bleach point was performed using a custom-written script in MATLAB (MathWorks). First, lateral drift in pre- and post-bleach image stacks was corrected using DFT-based sub-pixel image registration (Guizar-Sicairos et al., 2008). The area of each intestine nucleus was then manually segmented. The bleached region was determined by automated thresholding (Otsu's Method) of an image of the difference of the mean pre-bleach images and the mean of the first five post-bleach images. Acquisition bleaching was detected in the mean intensity of the whole nucleus region of interest in the post-bleach images. This decrease in intensity was fitted with a monoexponential decay and used to correct the acquisition bleaching during fluorescence recovery. To correct for differences in initial intensity and extent of photobleaching, to compare different datasets directly, each acquisition bleaching corrected curve was normalized to an initial value of 1 and an immediate post-bleach value of 0. To estimate the fraction of fluorescent proteins that can diffuse into the bleached region during the experiment's time course (mobile fraction) and the recovery time constant (τ), the post bleach recovery was fitted with monoexponential function with nonlinear least-squares-based fitting. The recovery half-time (t1/2), corresponding to the time required to recover half of the fluorescence maximum, is estimated directly from the data. The mean normalized relative intensity of all repeats for each experimental condition was calculated and plotted for each time point with the standard error of the mean using Python. The MATLAB analysis script can be found here: https://github.com/ercanlab/2021_Breimann_et_al

2.5.12 Intensity distribution analysis

To compare the protein expression and X-enrichment of DPY-27::GFP and DPY-27(EQ)::GFP images were recorded at 3 and 8 hours after a 1-hour heat-shock at 35°C. 2D images were manually segmented for the nuclear region, and pixel intensity values for the GFP tagged proteins were recorded for at least 20 images per condition. To compare the average density of

pixel intensities per condition, the pixel intensities were binned to ranges of 20, summed for all images of one condition, and divided by the number of used images using Python.

To compare image intensities of endogenous DPY-27::Halo in wild-type and *dpy-21 null* conditions, worms were stained with HaloTag-JF549, as described above, and z-stack images were recorded to capture the complete intestinal nuclei. To compare DPY-27::Halo enrichment at the X chromosome between different conditions, the HaloTag signal was segmented in 3D using autocontex pixel classification in ilastik, resulting in a simple segmentation that assigns the most probable class for each pixel (Berg et al., 2019). Using Fiji (Schindelin et al., 2012), a binary 3D mask was created from the ilastik segmentation using Otsu's method to segment the HaloTag signal. Binned pixel intensities were recorded from both conditions, and density plots were created using Python https://github.com/ercanlab/2021_Breimann_et_al.

2.5.13 Recombinant protein and peptide binding assay

The DNA encoding for amino acids 351-661 of the DPY-28 protein was amplified from cDNA using the primers DPY 28 351F & DPY-28 660R (Table 2). According to the manufacturer's protocol, the cDNA template was prepared from total RNA using SuperScript III (Invitrogen). The PCR product was digested with BamHI and EcoRI and cloned into corresponding sites in pGEX-5X-2. The plasmid was transformed to a BL21 codon + *E. coli* strain to be induced with 1 mM IPTG for 3 hours at 25°C and purified using standard GST protein purification using GE Healthcare Glutathione Sepharose 4B based on the manufacturer's protocol, and the protein amount was quantified using a Bradford assay. The peptides were kindly provided by Brian Strahl (Table 5). Briefly, 60 µl of the magnetic streptavidin beads (Dynabeads M280; Invitrogen) were washed twice with 1 mL recombinant protein binding buffer (rPBB) (50 mM Tris pH 8, 0.3 M NaCl, 0.1% Igepal CA360) and incubated rotating 1 hour with 1 nmol peptide at 4°C. The beads were washed twice with rPBB and incubated with 40 pmol of recombinant protein for 3 hours, rotating at 4°C. The beads were washed 5 min thrice with rPBB and resuspended in 30 µl SDS buffer, and 15 µl was run on a 4-12% Bis-Tris MOPS gel (Invitrogen) transferred to a PVDF membrane and was blocked with 1XPBST (0.1%Tween-20) containing 5% dry milk. Bound peptides were visualized using an anti-GST antibody (GE 27-4577-50) 1:2,000, Anti-goat-HRP (Promega V8051) 1:10,000 ECL-Plus (GE), and the Typhoon Scanner.

Table 5 Peptides used for in solution peptide pull-down assay

		Sequence
H3 unmodified	H3 1-20	$AR^{2}TK^{4}QTAR^{8}K^{9}S^{10}TGGK^{14}APRK^{18}QL$-K(Biot)-$NH_2$
H3 tetra acetyl	H3 1-20	ARTK(Ac)QTARK(Ac)STGGK(Ac)APRK(Ac)QL-K(Biot)-NH_2
H4 unmodified	H4 1-23	Ac-$SGRGK^{5}GGKGLGKGGAKRHRK$VLR-Peg-Biot
H4 tetra acetyl	H4 1-23	Ac-SGRGK(Ac)GGK(Ac)GLGK(Ac)GGAK(Ac)RHRKVLR-Peg-Biot

H4K20me0	SGRGKGGKGLGKGGAKRHRKVLR-Peg-Biot
H4K20me1	SGRGKGGKGLGKGGAKRHRK(Me)VLR-Peg-Biot
H4K20me2	SGRGKGGKGLGKGGAKRHRK(Me2)VLR-Peg-Biot
H4K20me3	SGRGKGGKGLGKGGAKRHRK(Me3)VLR-Peg-Biot

3 Mechanism of transcription repression by an X-specific condensin complex in C*. elegans*

Parts of this chapter are based on the 2021 preprint: ***RS-FISH: Precise, interactive and scalable smFISH spot detection using Radial Symmetry***. Authors listed in the publication are Ella Bahry*, Laura Breimann*, Leo Epstein*, Klim Kolyvanov, Kyle I. S. Harrington, Timothée Lionnet, Stephan Preibisch
*Authors contributed equally to this paper.

3.1 Research Motivation

Condensins are essential for chromosome compaction and have been implicated in transcription regulation. The mechanistic foundation of their transcription regulatory function is poorly understood (Kim, 2021; Paul et al., 2018a). A clear paradigm to address this question is the X-specific condensin DC in *C. elegans*, which specifically binds to and represses X chromosomes in XX hermaphrodites by 2-fold. Although many studies tried to elucidate different aspects of dosage compensation in *C. elegans*, the mechanism of transcription repression is not well understood. Specifically, how the DCC mediates an average two-fold reduction of genes transcribed at different levels over the entire length of the X chromosome is an exciting enigma. The DCC binds to about 75% of promoters of active genes on the X chromosome (Ercan et al., 2007). While binding of DCC generally correlates with the transcriptional activity of the associated gene and open chromatin, as measured by H3K4me3 and H3K27ac enrichment, they are not strictly coupled (Street et al., 2019; Ercan et al., 2009). Additionally, DCC binding does not directly correlate with the transcription downregulation of the bound gene (Jans et al., 2009). DCC-mediated repression appears to be chromosome-wide and not gene-specific as 43% of dosage-compensated genes lack DCC binding (Jans et al., 2009), and no large groups of genes escape from dosage compensation (Kramer et al., 2016, 2015).

In this part of the thesis, I aim to understand the effect of condensin DC on transcript numbers and transcription dynamics in single embryos across embryonic development. I want to measure the changes in transcription kinetics between wild-type and DCC mutant embryos to contribute to our understanding of how transcription repression during dosage compensation functions. For this, we use an imaging approach based on widefield single-molecule RNA fluorescence in situ hybridization (smFISH) and analyze the data using a novel single-molecule detection approach and advanced machine learning approaches to identify and stage vast numbers of embryos to their developmental time point.

3.2 Author contribution statement

The smFISH staining and imaging protocol was adapted and executed by me. In some experiments, the preparation of worms for the experiments was assisted by Andrea Grybowski and Mandy Terne. The analysis pipeline was developed by Ella Bahry, Klim Kolyvanov, Leo Epstein, Marwan Zouinkhi, Stephan Preibisch, and myself. Specifically, the segmentation of embryos was developed by Ella Bahry, Stephan Preibisch, and myself. Ella Bahry and I developed the staging of embryos. The spot detection using RS-FISH was developed and performed by Ella Bahry, Klim Kolyvanov, Marwan Zouinkhi, Stephan Preibisch, and myself.

Timothée Lionnet created simulated data to benchmark the RS-FISH plugin. The benchmark of RS-FISH against FISH-quant results was performed by Ella Bahry, Leo Epstein, Kyle I. S. Harrington, and myself. Stephan Preibisch and Timothée Lionnet developed the RS-FISH algorithm. The preprint manuscript was written by Stephan Preibisch and myself, with input from all co-authors. Leo Epstein and I developed the intron detection. The image postprocessing was developed by Klim Kolyvanov, Marwan Zouinkhi, Stephan Preibisch, and myself. Sevinç Ercan and I made the target gene selection. Final analysis of smFISH spots per embryo was developed and performed by myself. Sevinç Ercan and Stephan Preibisch supervised the project.

3.3 Results

3.3.1 SmFISH based analysis of dosage compensation target genes in single *C. elegans* embryos

Transcription has been described as inherently stochastic in many organisms (Tunnacliffe and Chubb, 2020). Thus, to quantitatively analyze transcription throughout embryogenesis, I decided to use a high-throughput imaging-based approach. C*. elegans* embryos are difficult to synchronize experimentally, but imaging detects nuclei counts through DAPI staining, allowing embryos to be developmentally staged. Additionally, the use of intronic smFISH probe sets enables the detection of nascent transcription to characterize transcription parameters, in part because smFISH can detect RNA at much lower concentrations than sequencing approaches. Furthermore, the spatial context of images enables the identification of individual transcription sites. To detect transcription changes in thousands of embryos, I established a protocol and pipeline to stain, image, and process images from single embryos (Figure 24). In the first few paragraphs, I will describe the establishment of the smFISH protocol and the analysis pipeline. Subsequently, I will present our results detecting transcription during embryogenesis and how we extract transcription parameters.

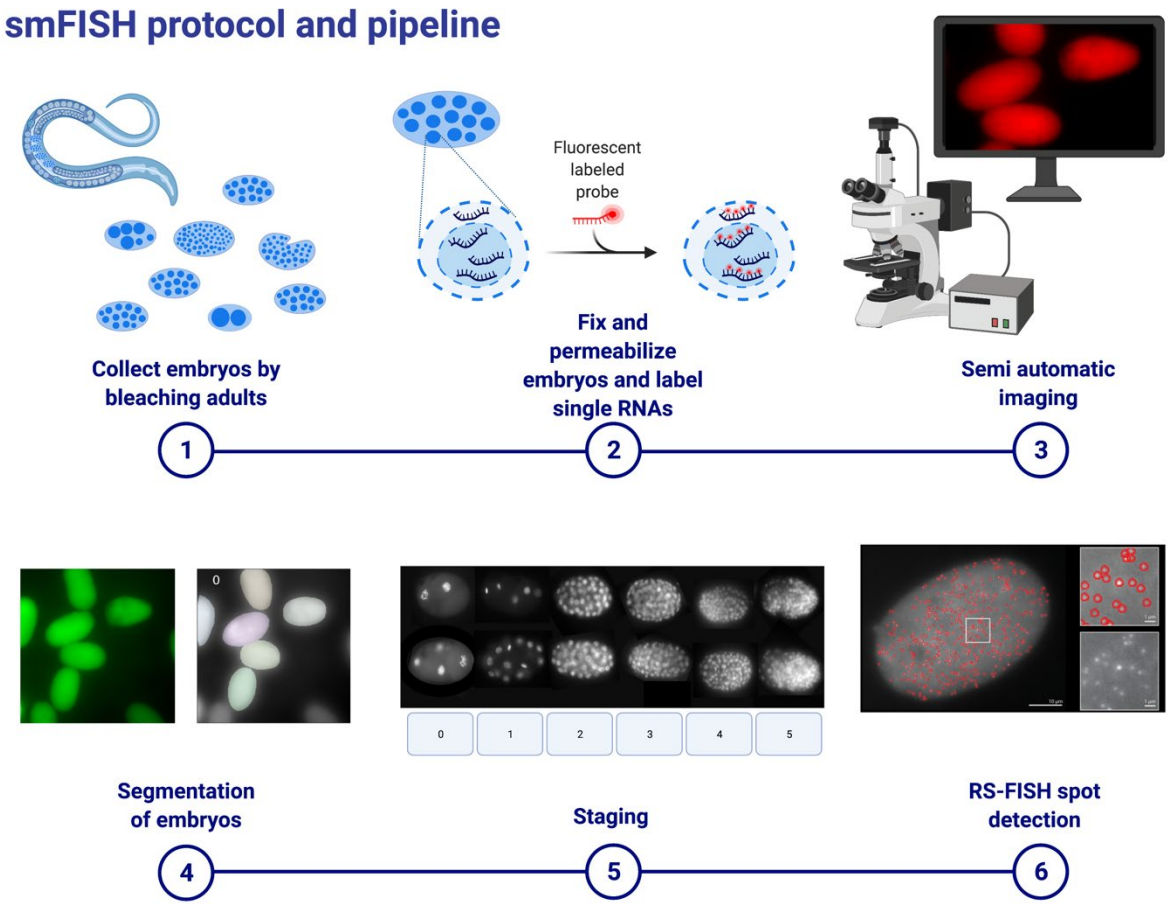

Figure 24 smFISH protocol and pipeline overview.
(1) Embryos are collected by bleaching adult worms. (2) The embryos are fixed, permeabilized, and labeled with smFISH probes. (3) A semi-automatic imaging approach captures z-stacks of thousands of embryos. (4) Single embryos are segmented by a machine learning approach. (5) Staging embryos into specific bins is done using an autoencoder. (6) smFISH spots are detected in 3D using RS-FISH. Created with BioRender.com.

3.3.2 Collection, smFISH labeling, and imaging of single embryos

To detect transcription changes during the establishment of dosage compensation, I collected embryos from *C. elegans* adult hermaphrodites via bleaching and washing off older embryos from plates. For labeling single RNA molecules using smFISH, I designed probes for several X chromosomal and autosomal genes (in more detail on page 107). I used NIS elements software to semi-automatically image thousands of embryos, each with five channels and 90 z-positions (Figure 25). With this approach, I created a dataset containing 11.326 images with 16.077 single embryos. Each embryo in this dataset was labeled with smFISH probes against three different genes, resulting in 48.231 images that were used for single spot detection. The scale of this dataset exceeded any manual image analysis approaches, and therefore we developed a high throughput image analysis pipeline.

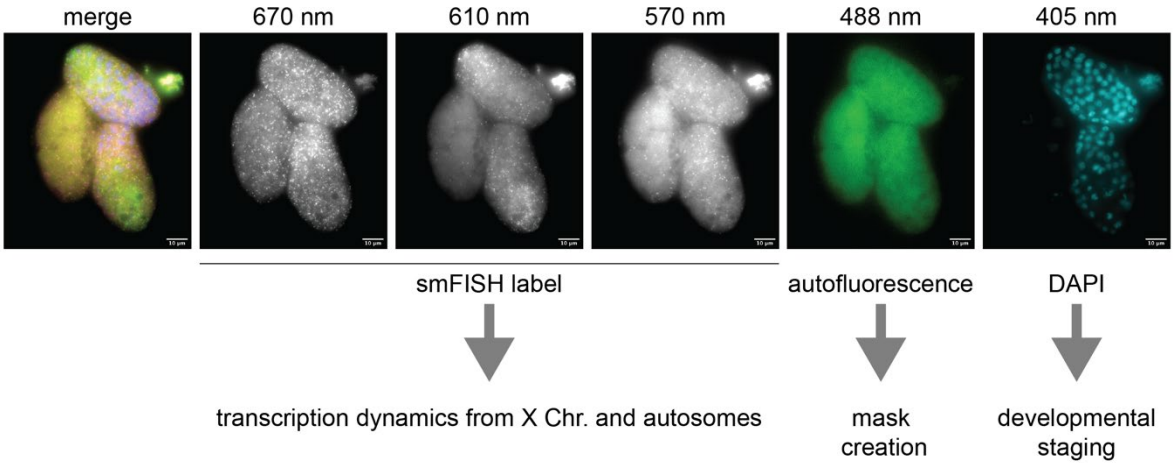

Figure 25 smFISH labeling of *C. elegans* embryos
C. elegans embryos labeled with three smFISH probe sets and DAPI. The 488 nm channel is imaged for instance segmentation of single embryos. The DAPI channel is used for the developmental staging of embryos.

3.3.3 Segmentation of embryos

To reduce imaging time while capturing several embryos, I adjusted the number of embryos mounted on each slide to contain several embryos in each field of view without "overcrowding" the microscopy slide. However, to detect transcription in single embryos, we needed to segment tens of thousands of embryos reliably. For this, we established a semi-automatic instance segmentation pipeline, where each instance represents a single embryo. A convolutional neural network (StarDist, (Schmidt et al., 2018)) then detects the outline of all embryos, and single instance masks are confirmed for accuracy manually. The manual selection of the masks is not strictly necessary in the vast majority of cases due to the incredible performance of StarDist, however, it does offer the opportunity to assess if the embryos were preserved during the staining protocol and sort out broken embryos. To allow easy segmentation, each embryo was imaged using the GFP channel (λ 488 nm). While no specific label was fluorescent in this channel, the relatively high autofluorescence of *C. elegans* embryos allowed to capture an even signal of the outline of the embryo (Figure 25).

Our first step was to create a large training dataset with accurately segmented embryos. First, we used a random forest classifier (trained with 588 hand segmented embryos) which created rough binary masks for 2D max projections of the GFP channel differentiating embryos and background (Figure 26a). These binary masks were then used to fit an ellipsoid constrained by the expected sizes of embryos. We created a custom-written selection tool, with which I was able to screen the fitted ellipsoids and correct the shape if necessary (Figure 26a). We created a dataset of about 5000 embryo masks through this method, from which 1374 were selected as input to train and test the StarDist network. The selection only included images in which all embryos were segmented with good masks.

In the next step and to optimize mask creation, we used StarDist (Schmidt et al., 2018), a deep convolutional neural network that predicts for each pixel the distance to its object boundary (in our case, the edge of each embryo) to automatically create binary masks for instance segmentation (Figure 26b). The ground-truth dataset, created through the ellipsoid fitting, was split into training (85% - 1168 images) and validation (15% - 206 images) datasets. The 206 images in the validation dataset included 247 single embryos. Our StarDist network correctly identified 100% (true-positive) of the 247 embryos but found ~3% of other objects like dirt or broken pieces (false-positive). To exclude false-positive detections and exclude embryos with low signal-to-noise smFISH staining ratios, I manually curated the predicted masks alongside the smFISH labels and DAPI staining (Figure 26c). Finally, for each selected embryo, the original image was cropped around each embryo (40 pixels padding) to reduce the size of the dataset and isolate individual embryos. With this approach, we found 16077 single embryos in 11326 images. The final masks are used for staging each embryo and after smFISH spot detection to filter out spots found in neighboring embryos or outside dirt pieces.

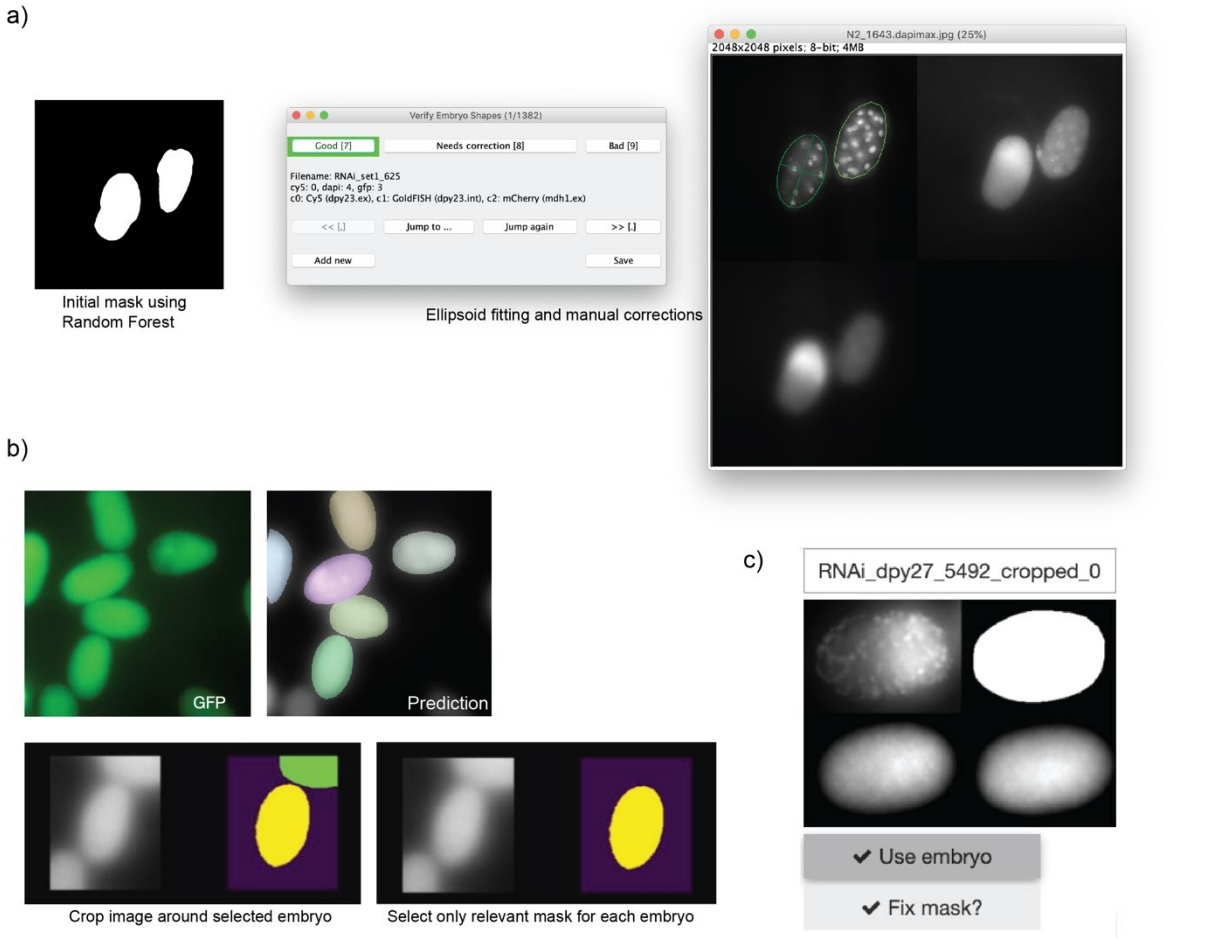

Figure 26 Development of instance segmentation pipeline for *C. elegans* embryos.
a) Creation of a training dataset using random forest classification and ellipsoid fitting. To find all embryos in an acquired image, 2D max projections of GFP images are first segmented using a random forest algorithm resulting in a rough binary mask. These masks are the basis for an ellipsoid fitting approach. Each fitted ellipsoid is manually curated and edited if necessary through a custom-written Fiji tool. **b)** Instance segmentation using StarDist. The neural network

was trained by the ground truth data created in the ellipsoid fitting. The network predicted masks on the 2D max projections of GFP images. Masks for single embryos are curated, and the original image is cropped around each segmented embryo. **c)** Screenshot of the selection tool to inspect the binary mask (top right), the integrity of the embryo according to the DAPI staining (top left), and smFISH signal-to-noise (bottom row, two different channels).

3.3.4 Staging fixed *C. elegans* embryos

Dosage compensation is established during embryogenesis (Kramer et al., 2015). To capture changes in transcription regulation during development, it is crucial to stage embryos according to their developmental time-point when detecting transcription counts for each embryo. In contrast to RNA-seq methods, imaging transcription using smFISH has the advantage of being able to image and count all nuclei using a DAPI staining. Since *C. elegans* is a stereotypic organism, the nuclei count is directly linked to its developmental time point (Sulston et al., 1983; Hench et al., 2009). While it is theoretically possible to pinpoint every embryonic stage beginning from a single nucleus up to 558 nuclei at the end of embryogenesis, this endeavor would be tremendously challenging (Bao et al., 2006; Wang et al., 2016b). Nuclei have different shapes and sizes and, embryos in later embryonic stages show very densely packed nuclei, making it very hard to count each nucleus correctly. Through the training of deep neuronal networks, the staging of embryos can be vastly sped up. However, for reliable predictions, an extensive and well-annotated training dataset for each prediction class is necessary for most algorithms. Therefore, we grouped different developmental stages into bins to reduce the annotation effort and maximize the correctness of stage prediction. I decided to group embryos into six carefully chosen, meaningful bins and annotated a training dataset where each bin contained 24 examples (Figure 27a).

The bin boundaries reflect essential milestones during embryogenesis and dosage compensation establishment. I selected embryos with one to four nuclei for the first bin ("bin 0"). This timespan captures the moment before zygotic genome activation (ZGA) for most genes and, therefore, detects each gene's maternal load (Edgar et al., 1994; Baugh et al., 2003; Seydoux and Fire, 1994; Seydoux and Dunn, 1997). Next, bin 1 includes embryos with 5 - 30 nuclei. In this bin, embryos started zygotic transcription and underwent sex determination, and consequently, hermaphrodites expressed SDC-2, which is needed for the DCC to localize to the X chromosome (Miller et al., 1988; Dawes et al., 1999). The next bin includes embryos with nuclei from 31-99 nuclei. The DCC localizes to the X chromosome in this bin and starts repressing genes (Chuang et al., 1996; Davis and Meyer, 1997; Dawes et al., 1999). We expect a gradual downregulation as in mRNA-seq data, as some genes were not fully down-regulated until the L1 stage (Kramer et al., 2015). The next bin includes embryos from 100-149 nuclei. DCC binding to the X chromosome at this stage increases the X-specific level of H4K20me1 (Vielle et al., 2012; Liu et al., 2011; Wells et al., 2012). The next bin is large, including embryos with nuclei from 150 -534. In these stages,

the nuclei are dense, and counting accurately is difficult (Figure 27a). After this stage in bin 5, nuclei hardly divide anymore, but embryos undergo several detectable morphological changes and, therefore, are straightforward to label and classify into one bin.

Based on these bins, I annotated a training dataset using a custom-written ImageJ macro (Figure 27b, macro by Ella Bahry). I annotated ~100 embryos with this approach, but we had a strong class imbalance due to the initial random sampling of embryos. However, using the initial prediction in an active learning approach (the user is asked to provide further training data if prediction performance is bad for specific cases), we avoided random sampling in further iterations and thus annotated specifically stages with previously fewer examples to even out the classes (Figure 27c).

For stage prediction of each embryo, we used an autoencoder-based deep learning classification method (Figure 27d) (Kramer, 1991). First, the entire dataset (input) was used to train an autoencoder network in an unsupervised way to learn the underlying features of the images for reconstruction (reconstructed input). For this, images were preprocessed by masking the embryo, selecting the middle 21 slices of the z-stack, and copied with slight modifications (augmentation) to increase the amount of data for training. From these preprocessed images, small tiles (64x64) were extracted and used for training and classification. The pre-trained encoder part was coupled with a classifier part to predict embryo stages in the next step. The classifier was trained with the previously annotated training dataset. For each tile, a stage was predicted, and the majority vote of the same staged tiles determined the stage bin of each embryo. We created improved datasets for manual annotation from the first iteration of this prediction, and the stage prediction with improved class balance was rerun.

With this approach, we reached sufficient prediction accuracy of the different embryonic stages (Figure 27e). As expected, early embryonic stages are more accurately predicted than older stages, which is also true for the manual staging of embryos. While this approach has some uncertainty, especially for older embryonic stages, the ability to stage thousands of embryos automatically in a short time outweighs the benefits of the manual approach.

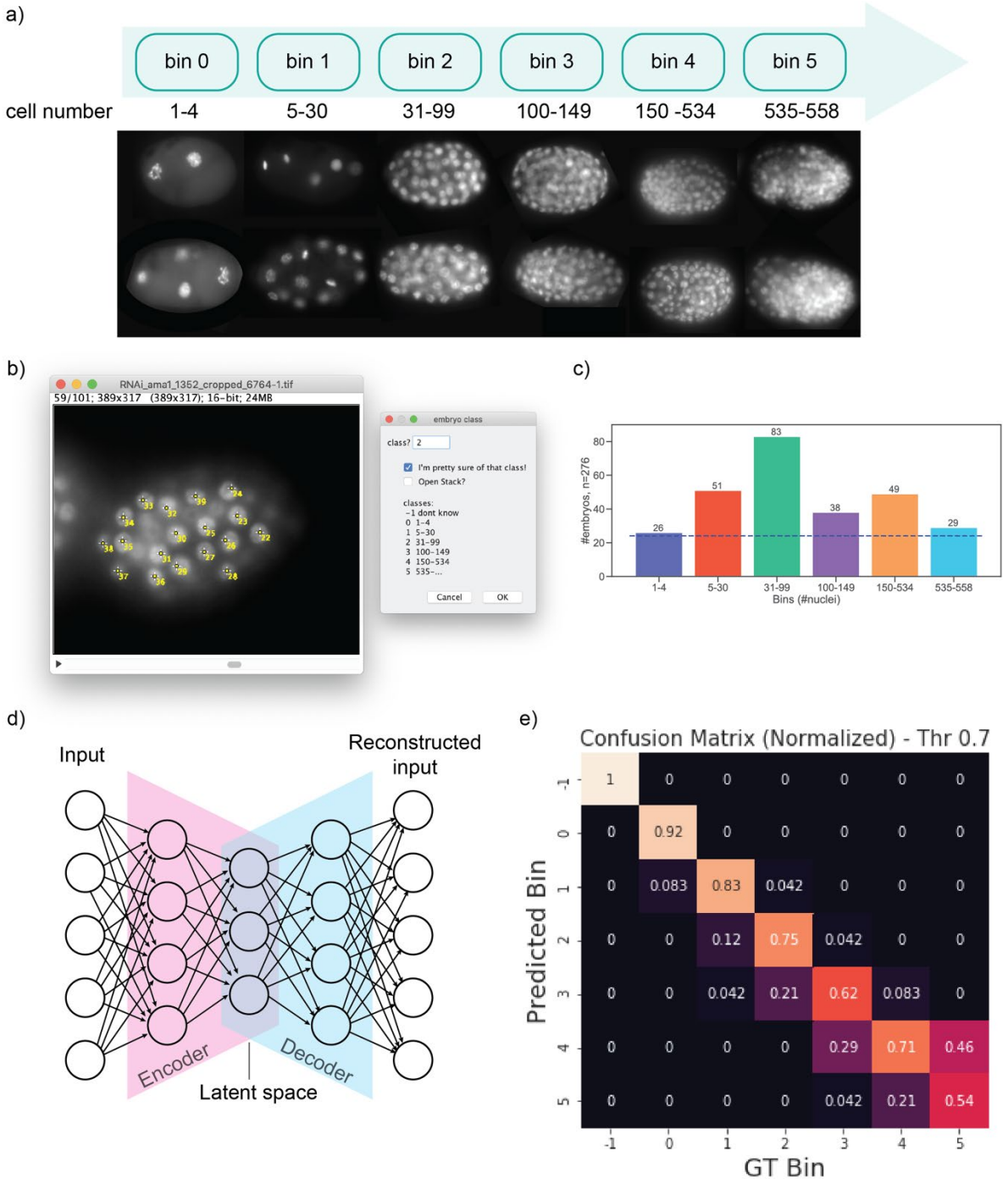

Figure 27 Prediction of embryonic stages using an autoencoder.
a) Grouping all developmental stages into six bins with the included nucleus count labeled below each bin and additional example images of DAPI stained embryos. **b)** Custom-written ImageJ macro for manual stage annotation of training data. **c)** Count of annotated example images of each bin. The bin with the lowest count was used as a cut-off for all bins to have equal-sized training data. **d)** Illustration of an autoencoder architecture that was used for prediction of the stage bin. **e)** Confusion matrix for the predicted bins against a set of ground truth (GT) bins. Values closer to 1 represent better predictions for the bin.

3.3.5 Detection of smFISH spots in 3D embryos

In many organisms, transcription was described as a stochastic process leading to cell-to-cell and organism variation in mRNA and protein levels (Raj and Oudenaarden, 2008). In order to

detect robust changes in dosage compensation within these variations throughout the embryonic development for several mutants, I created a dataset with over 10.000 embryos. Each of these embryos was stained with three different smFISH probe sets and was captured in 3D, creating a large and complex dataset. Detecting smFISH spots in this large dataset using available tools was challenging due to their limitations to scale to large datasets. Therefore, we developed the Fiji plugin RS-FISH for precise and fast spot detection in 3D.

Most automatic spot detection approaches work with a Laplacian of Gaussian or difference of Gaussian filter to enhance single spots, localize single spots by local maxima and intensity thresholding and finally improve accurate detection by Gaussian fitting (Mueller et al., 2013a; Trcek et al., 2015). While the Gaussian fitting algorithms can detect spots in 3D accurately, they tend to be slow due to their iterative nature. Furthermore, many of the available tools are written in the MATLAB environment, making it hard to use with large datasets with thousands of images or samples with large volumes. Therefore, we developed a spot detection plugin for the open-source platform Fiji/ImageJ (Schindelin et al., 2012).

During the plugin development, we prioritized the precise detection of close spots in 3D and efficient scaling to large datasets. We achieved this by deriving a 3D version of a radial symmetry algorithm that, in contrast to Gaussian fitting, works in a non-iterative fashion (Figure 28a) (Parthasarathy, 2012). Through fast processing speed, we were able to additionally add a robust outlier removal using Random Sample Consensus (RANSAC) (Fischler and Bolles, 1987). With this, RS-FISH can detect points in 3D accurately and fast, separate close detections, and ignore outlier pixels that would disrupt the localization of single points (Figure 28b).

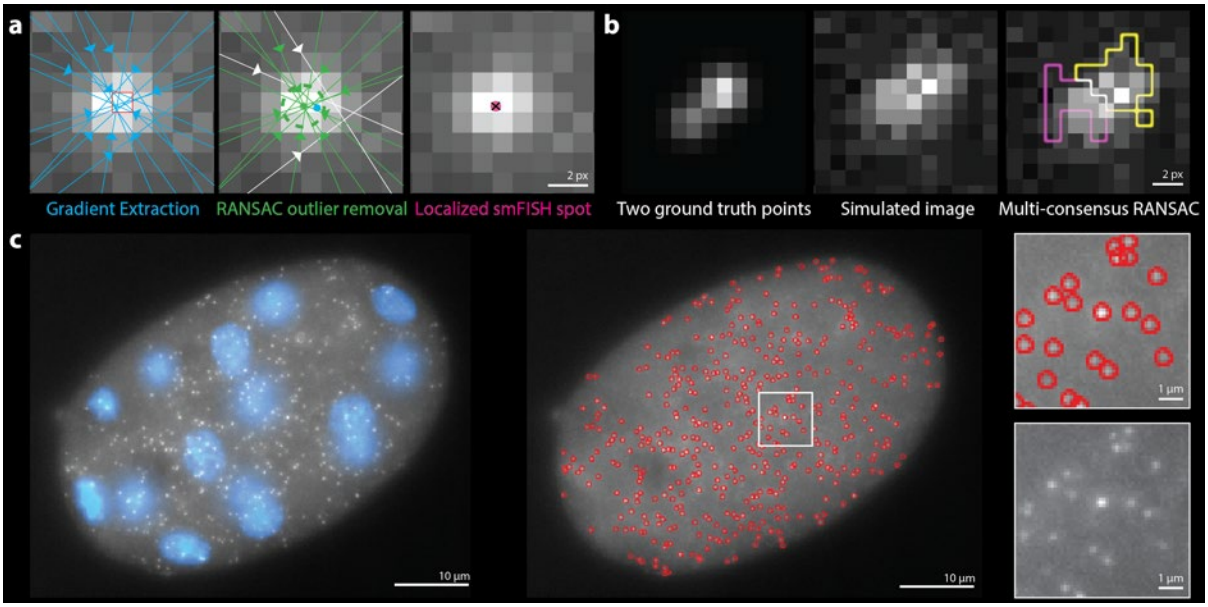

Figure 28 Precise and fast spot detection with RS-FISH.

a) Illustration of spot detection principle. Gradients of intensity are detected in the image in 3D. A RANSAC outlier removal step removes gradients that do not cross in the middle. This allows for precise localization of the smFISH spot in 3D. **b)** The multi-consensus RANSAC allows the separation of close spots. **c)** *C. elegans* embryo stained with DAPI (blue) and smFISH for dpy-23 (gray). RS-FISH can detect single spots in the whole embryo stack. Image from (Bahry et al., 2021).

In order to test the plugin and benchmark it against other available tools, we decided to create a set of images with artificial points with known XYZ locations and different levels of noise. We ran a grid search of reasonable detection parameters and found that our tool had a comparable accuracy as FISH-quant, a commonly used tool for smFISH spot detection (Table 6) (Mueller et al., 2013a). Importantly, we tested the detection speed using several smFISH labeled *C. elegans* embryo images and found that the speed was about 13x increased for our plugin compared to FISH-quant (Table 6, Figure 28c). The faster processing speed is especially advantageous for the large dataset I created. This dataset spans several genes and mutants and includes 11326 images (5 channels, ~90 z positions each). We processed the dataset in 70 minutes through an extension of the tool using cloud computing (AWS).

Table 6 Localization and speed comparison of RS-FISH and FISH-quant.
The first row compares the percentage of smFISH spots missed in simulated datasets, and the second row compares the localization error for the identified spots. The last row compares the computation speed for real 3D volumes of smFISH acquisitions of entire *C. elegans* embryos. From (Bahry et al., 2021).

	RS-FISH	**FISH-quant / BigFish**
smFISH spots missed (avg/median/stdev)	1.10% / 0.00% / 1.92%	2.99% / 0.00% / 7.75%
smFISH spot localization error (avg/median/stdev)	0.40px / 0.21px / 0.44px	0.34px / 0.27px / 0.27px
smFISH processing speed increase for 3D volumes (relative speedup factor)	13.7x	1x

To increase the signal-to-noise of the smFISH spots and remove the often uneven backgrounds that can appear using the microscope camera, we applied per plane a median filter (sigma of 19) to the images and subtracted the median filtered image from the original (Figure 29a). The resulting image was used for spot detection using RS-FISH (Figure 29b). The detected spots were filtered with the previously created binary masks (Figure 29c). To accurately compare mRNAs counts between different embryos and within one embryo depending on the position relative to the microscope objective, we decided to correct the signal intensity for any depth-dependent signal loss (Figure 29d). For this, we detected the signal intensity of each spot per z position and fitted it with a quadratic function along z. We corrected the slope of intensities over z with this quadratic fit to achieve equal signal intensity for spots from the beginning to the end

of the stack covering each embryo. Additionally, we normalized the detected counts to compare detections between embryos and genes (Figure 29e). Therefore, we fitted the histogram of detected counts with a gamma distribution. Since we expected that most detected spots are single mRNA molecules, we set the center of the fit to 1 to quantify mRNA counts between embryos.

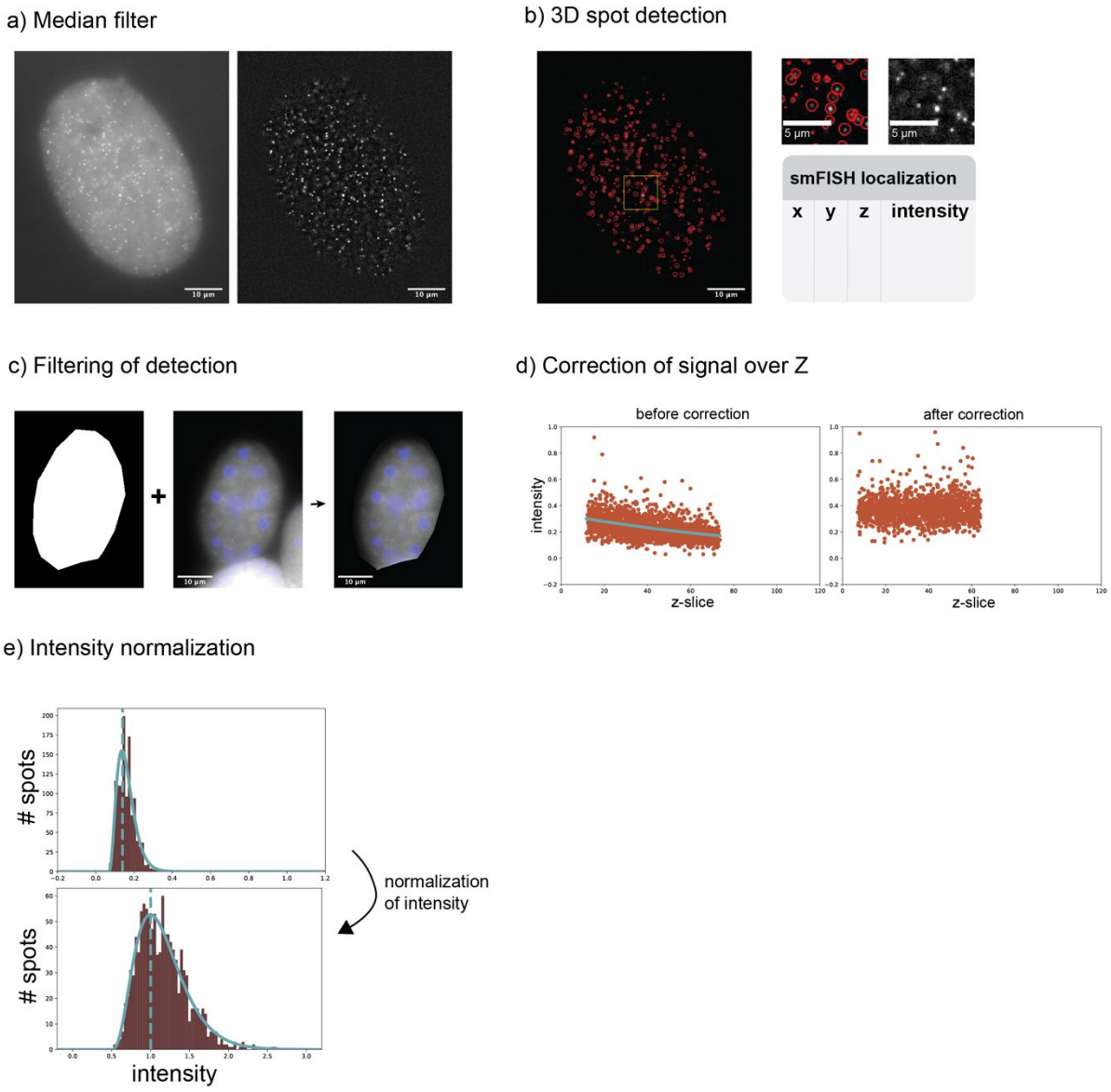

Figure 29 Pre- and Postprocessing steps for single spot detection.
a) Before spot detection, a median filter is applied to the images and subtracted from each slice. This step enhances the spots and reduces intensity differences introduced by the microscope camera. **b)** After detecting single spots using RS-FISH (red circles). **c)** The detected spots for each embryo are filtered by the binary mask to exclude spots from neighboring embryos in the field of view. **d)** The average intensity of the signal of single spots is reduced deeper in the tissue. To correct this, a quadratic function is fit to the distribution and normalized to ensure an equal intensity of signal throughout the embryo. **e)** The distribution of detected spots is fitted with a gamma distribution and normalized so that the maximum of the distribution is at 1 making the intensity values comparable between different images.

With this imaging and analysis pipeline, we can image thousands of single embryos labeled with smFISH probes, stage them to their developmental time-point and detect single RNAs with high accuracy. Each RNA detection is normalized to compare detections between embryos. This approach allows me to study the variability and timing of dosage compensation in single embryos and detect relative changes in transcription parameters between wild-type and DCC mutant conditions.

3.3.6 Selection of dosage compensation target genes

To detect transcription changes on the X chromosome using smFISH, we selected target genes that can be used to design smFISH probe sets for RNA detection. For this, we selected genes expressed during embryogenesis using published RNA-seq data (Kramer et al., 2015) (Table 7). Detection of mRNAs using smFISH has a limitation for genes with very high transcript numbers, and therefore we excluded genes with very large FPKM numbers. Next, we were interested in selecting genes that show a significant upregulation after DCC loss like *dpy-23*, and in contrast, genes with a mild effect after DCC depletion like *rab-6.2*. Another essential criterion for gene selection is the length of the transcript. For efficient labeling using smFISH, it is favorable to use 48 probes when possible. Each probe is 20 nt long and is placed with leaving a space of 2 nt. Therefore we excluded short genes from our selection.

Table 7 X chromosomal genes selected for smFISH analysis. FPKM data from (Kramer et al., 2015)

gene	Chr	transcript length (nt)	N2 FPKM		Vector RNAi FPKM	RNAi DPY-27 FPKM	DPY-21 KO FPKM		Mature RNA		Nascent RNA	
			Early embryo	Comma embryo	Mixed embryo	Mixed embryo	Early embryo	Mixed embryo	# of probes	Fl	# of probes	Fl
dpy-23	X	1980	68,64	76,93	61,98	79,23	66,81	89,03	48	Q670	48	Q570
sdc-2	X	9247	27,79	10,26	14,65	21,54	25,26	14,21	48	Q670	48	Q570
wdr-5.2	X	2040	23,06	34,85	29,67	39,67	13,66	30,47	48	Q570	-	-
W04G3.5	X	1253	0,40	301,11	211,60	247,45	16,97	240,51	48	Q670	46	Q570
nhr-1	X	2554	26,16	78,24	78,27	96,19	25,12	98,31	48	Q670	48	Q570
rab-6.2	X	913	53,11	206,39	178,36	193,41	42,31	170,27	41	Q670	46	Q570
C16H3.3a	X	2746	15,36	93,92	78,74	92,47	37,19	73,96	48	Q670	48	Q570

A different factor for gene selection was their position on the X chromosome (Figure 30). Strong *rex* sites are thought to be the initial binding sites for the DCC from which the complex can spread to bind to weaker *rex* sites and gene promoters (Albritton et al., 2017; Jimenez et al., 2021). We were interested in studying the reported absence of a correlation between repression and distance to a *rex* site. Therefore we selected genes close to *rex* sites that were deleted or inserted using CRISPR (Albritton et al., 2017). This includes *dpy-23* (*rex-1* deletion), and *nhr-1, rab-6.2* and *C16H3.3a* (*rex-41* deletion) as well as *wdr-5.2* (*rex-8* insertion).

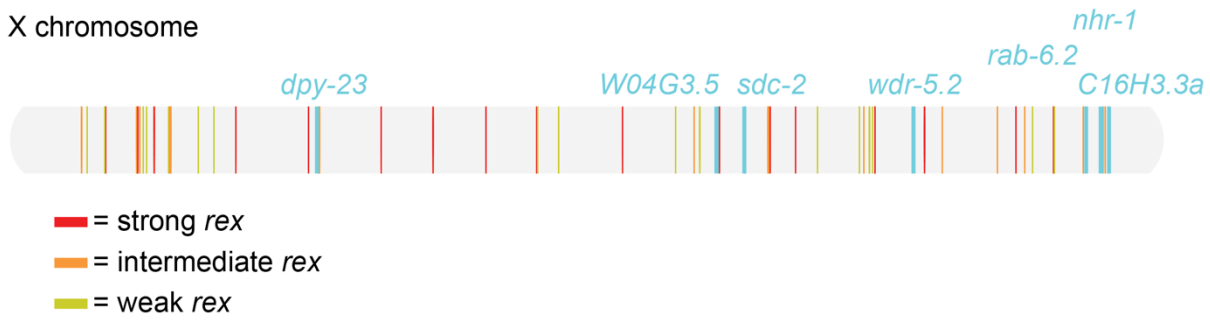

Figure 30 Position of genes on the X chromosome used for smFISH analysis
Illustration of the X chromosome with the relative location of genes (in blue) used for smFISH. The location of rex sites and their capability of recruiting the DCC. The DCC binds first to strong rex sites and consequently spreads to intermediate and weak rex sites. Classification of rex sites from (Albritton et al., 2017).

3.3.7 Selection of control genes

Studying gene regulation within the X chromosome dosage compensation system has the advantage of autosomes serving as internal controls. The selection of control genes followed similar rules as the X chromosomal genes (Table 8). Namely, genes are expressed throughout embryogenesis and are not too highly expressed. As expected, autosomal genes do not show a significant upregulation upon the depletion of DCC proteins.

Table 8 Autosomal control genes selected for smFISH analysis. FPKM data from (Kramer et al., 2015)

gene	Chr	transcript length (nt)	N2 FPKM		Vector RNAi FPKM	RNAi DPY-27 FPKM	DPY-21 KO FPKM		Mature RNA		Nascent RNA	
			Early embryo	Comma embryo	Mixed embryo	Mixed embryo	Early embryo	Mixed embryo	# of probes	Fl	# of probes	Fl
pha-4	V	2158	62,82	218,16	152,80	148,14	54,13	160,52	46	Q670	48	Q570
mdh--1	V	1149	123,26	588,64	634,14	599,16	121,53	601,70	41	C610	-	-
ama-1	IV	6020	271,49	92,02	92,88	99,41	255,66	104,29	48	C610	48	Q570
dpy-27	III	4677	58,82	77,45	69,78	26,95	80,74	56,82	48	C610	-	-

3.3.8 smFISH probe design

Probes were designed using the Stellaris Probe designer web tool (Biosearch Technologies) specifically for *C. elegans*. The probe designer avoids sequences rich in GC or repetitive sequences to ensure efficient and specific binding of the probes. If possible, the maximum amount of probes (48 per order) was selected for each exonic or intronic sequence. The number and color of probes are listed in Table 7 and Table 8. The complete sequences can be found in the Appendix. Probes were designed to have at least two nt space in between neighboring probes to avoid quenching. For exonic or intronic probe design, sequences listed at wormbase.org were used, and splice regions were masked with "n" nucleotides to avoid probes in these areas. An example of the distribution of exonic and intronic probes for DPY-23 mRNA can be found in

Figure **31**.

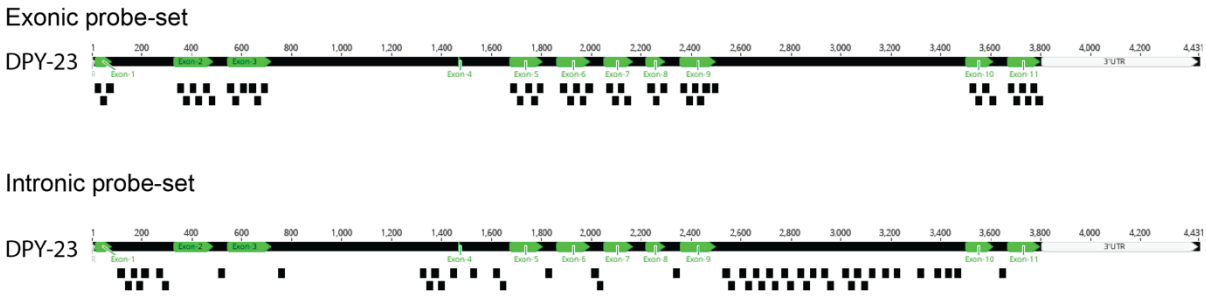

Figure 31 smFISH probe design example for exonic and intronic probes for DPY-23 mRNA

3.3.9 Specificity of smFISH detection

To maximize the number of genes and detect transcription from the autosome and the X chromosome simultaneously, I designed probes labeled with three different fluorophores (Quasar 570, CAL Fluor Red 610, and Quasar 670). To separate the detection from the three wavelengths (λ 570 nm, 610 nm, and 670 nm), I selected filter sets with narrow bandwidths (Figure 32a). To test the specificity of the detected signal, I stained embryos using smFISH probes for three different genes labeled with different fluorophores. I detected single RNA molecules for the three different genes with no bleed-through of signal between the channels (Figure 32b). Therefore, simultaneously detecting three probe sets is possible, and co-localization of signals in different channels is not the result of bleed-through between them.

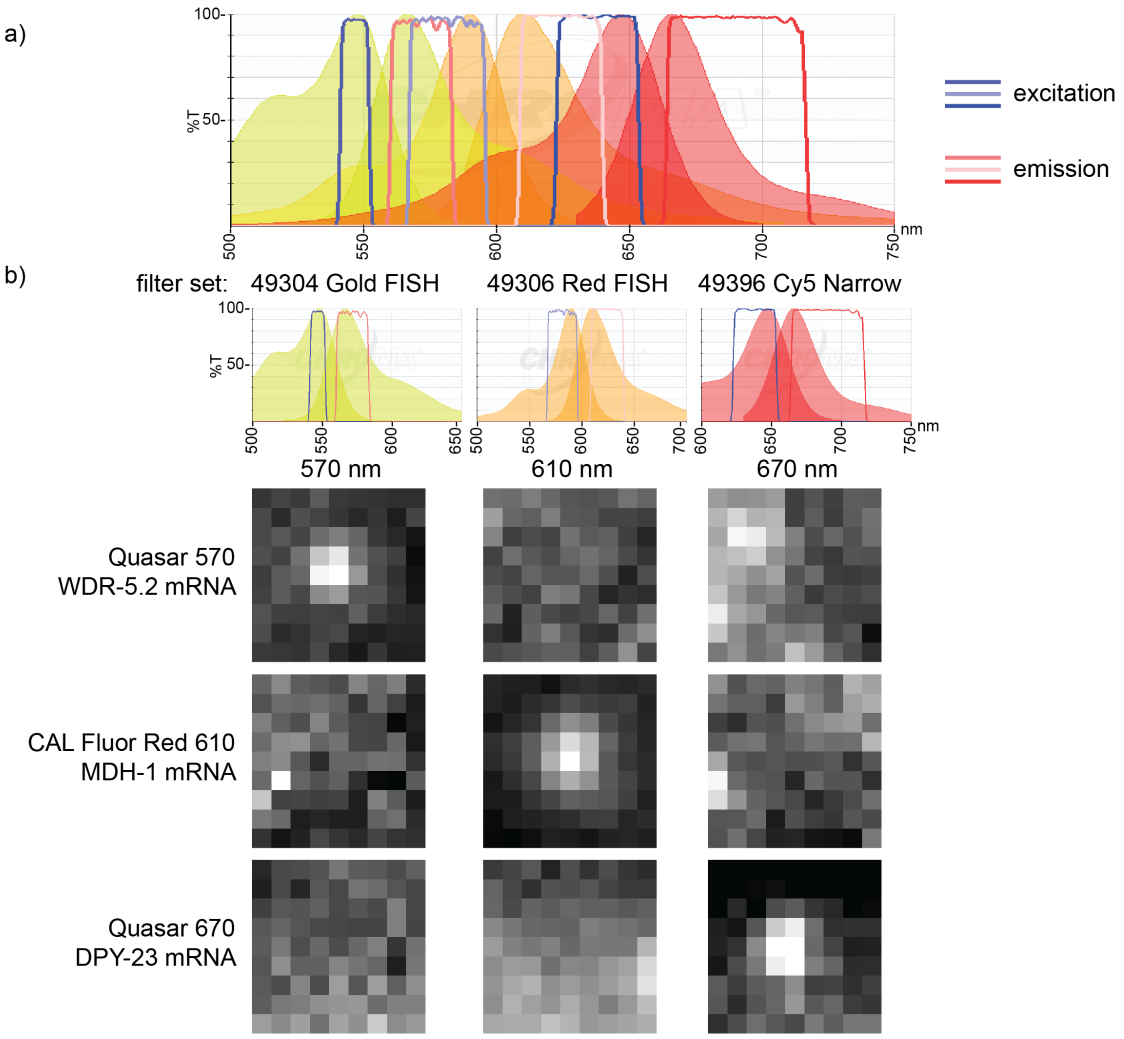

Figure 32 Spectral specificity of smFISH fluorophores.
a) Curves of the fluorescent spectra of the three smFISH fluorophores (Quasar 570, CAL Fluor Red 610, and Quasar 670) and filter bandwidth for the three filters (Gold FISH, Red FISH, Cy5 Narrow) to specifically detect them. Spectra were created using the Chroma Spectra Viewer. **b)** Fluorescent images of smFISH spots for three different mRNAs with three different fluorophores. Images of the same spot in the different channels show the specificity of the signal and low bleed-through.

3.3.10 RNA Pol II knock-down efficiently blocks new transcription in *C. elegans* embryos

I wanted to validate that I can detect transcription changes using the established smFISH assay. For this, I depleted worms of AMA-1, the large subunit of *C. elegans* RNA Pol II (Figure 33a). The X chromosomal gene *sdc-2* is not maternally loaded and only transcribed during embryogenesis in hermaphrodites (Plenefisch et al., 1989a; Dawes et al., 1999). Using smFISH, strong transcription sites for *sdc-2* are visible in young embryos (Figure 33b). The knock-down of AMA-1 reduces the presence of these active transcription sites (Figure 33b).

Using the quantitative smFISH pipeline, I detected the transcription of SDC-2 mRNA in wild-type and *ama-1* RNAi embryos throughout embryogenesis (Figure 33c). SDC-2 mRNA is strongly transcribed from the 5-30 nuclei time-point on in wild-type embryos. *Ama-1* RNAi embryos do not show these high transcript levels for most of the embryogenesis. Interestingly, higher

transcript levels of SDC-2 in *ama-1* RNAi embryos are observed at the end of embryogenesis. Knock-down of *ama-1* is lethal for embryos. *Ama-1* RNAi may select against embryos with stronger knockdown so that embryos with higher AMA-1 levels have a better chance of survival. Since I select for intact embryos during the analysis, I might filter out dead embryos at this stage. Additionally, embryos do not feed and therefore do not take up fresh RNAi bacteria. It is unclear how long the effect of RNAi persists during embryogenesis, as previously performed sequencing experiments did not have this temporal resolution.

DPY-23 mRNA is maternally loaded, and wild-type embryos with 100-534 nuclei have the highest total number of DPY-23 transcripts. Since *ama-1* RNAi leads to germline formation defects, I only started feeding L3/L4 worms with *ama-1* RNAi bacteria. This relatively short time of RNAi exposure allows worms to form germlines and embryos but reduces the knockdown of maternally deposited mRNAs. Nevertheless, a clear knock-down of the X-linked DPY-23 (Figure 33c) and the autosomal MDH-1 mRNAs is visible for embryos from 5 nuclei (Figure 33d). The stability of DPY-23 mRNA is possibly higher than MDH-1 mRNA, and therefore more DPY-23 mRNA persists in the embryos. It is challenging to treat embryos with transcription inhibition substances to observe mRNA decay like α-amanitin or actinomycin-D since the eggshell of embryos shields the embryos from many substances.

With this test, I saw that I could detect transcription changes throughout embryogenesis and use RNAi treatment of the parental generation to knock-down proteins of interest.

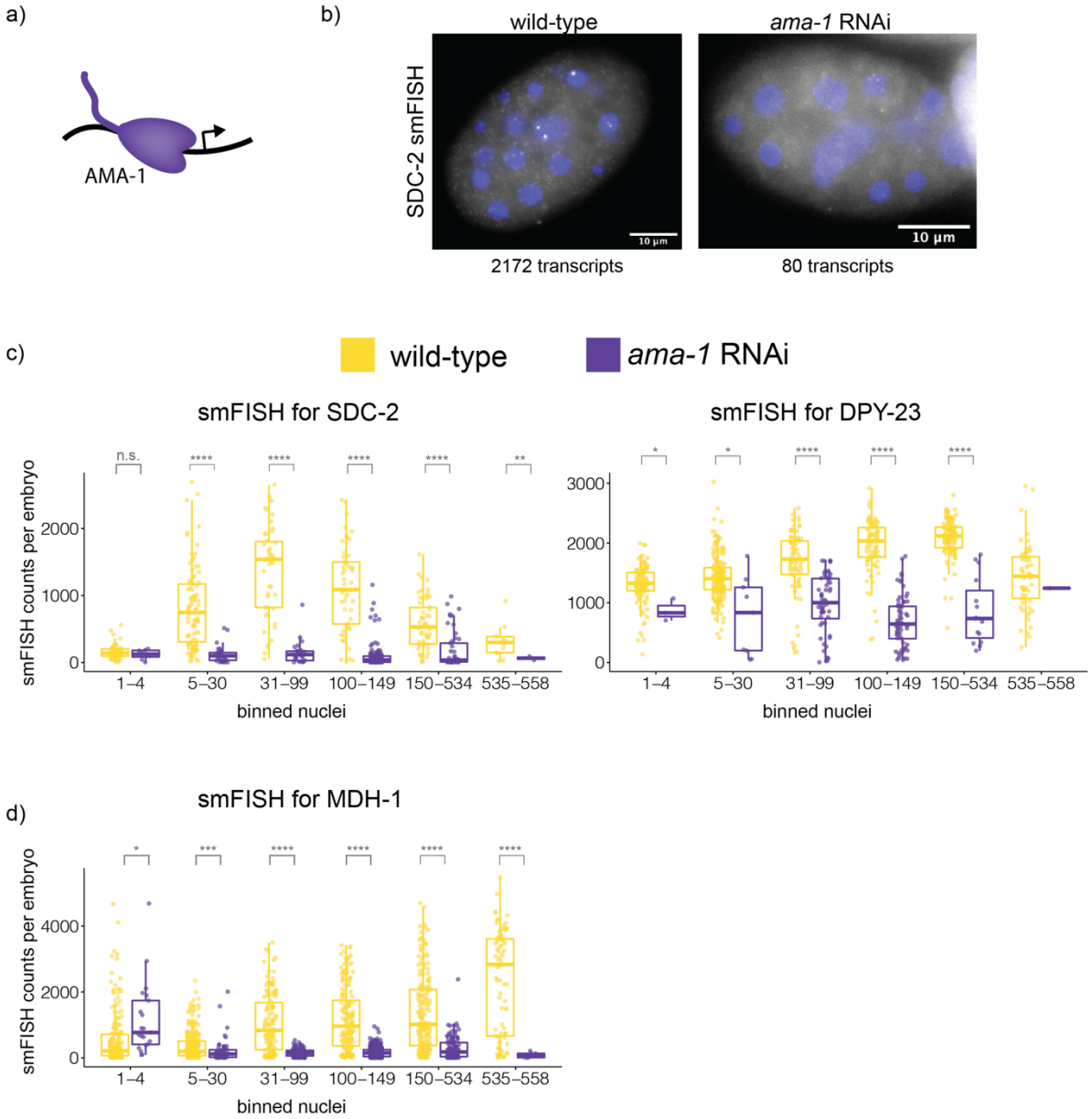

Figure 33 Detection of smFISH in wild type and *ama-1* RNAi embryos
a) Cartoon of the RNA Pol II with the largest *C. elegans* subunit AMA-1 **b)** Example images of either wild type or *ama-1* RNAi embryos, labeled with SDC-2 smFISH. The number of detected smFISH spots for each example is written under the image. **c)** Plots for smFISH detection X chromosomal mRNAs (SDC-2 and DPY-23). Each spot represents the total mRNA count for one embryo, plotted against the binned nuclei number for wild type (yellow) or *ama-1* RNAi (dark purple). **d)** Plot as in c but for the autosomal mRNA MDH-1. Significant P-values from Welch's unequal variances t-test are noted above the wild-type vs. knock-down condition for each time-point. P-values are denoted as n.s. ($P > 0.05$), * ($P \leq 0.05$), ** ($P \leq 0.01$), *** ($P \leq 0.001$) and **** ($P \leq 0.0001$). If one of the samples had too few points, no P-value was calculated.

3.3.11 Knock down of *sdc-2* leads to X specific transcription increase

The DCC subunit SDC-2 is the first factor to bind to the X chromosome and essential for loading the DCC onto the X chromosome (Figure 34a). Knock-down of *sdc-2* is lethal and leads to a two-fold upregulation of transcription from the X chromosome as detected by RNA sequencing methods (Jans et al., 2009; Kruesi et al., 2013). I used *sdc-2* RNAi to knock-down the DCC loader

and observed the transcription upregulation of X-linked genes. SDC-2 mRNA is highly expressed during early embryogenesis. RNAi against *sdc-2* only affects the mRNA, therefore transcription sites are still visible for SDC-2 smFISH in *sdc-2* RNAi embryos, but the total SDC-2 mRNA count is reduced (Figure 34b).

Using the smFISH pipeline, I observed the *sdc-2* knock-down during embryogenesis using smFISH probes for SDC-2 mRNA (Figure 34c). Similar to *ama-1* RNAi (Figure 33c), I could knock-down the SDC-2 mRNA, but since de novo transcription was not blocked, the knock-down does not reduce SDC-2 mRNA as strongly. Also, similar to DPY-23 smFISH in *ama-1* RNAi (Figure 33c), the mRNA counts increase again in the last two bins, suggesting that the RNAi is less effective in late embryonic stages (Figure 34c).

The X-linked gene *dpy-23* is more expressed in the *sdc-2* RNAi condition than a mock RNAi treatment in later embryo stages. Experiments using RNAi bacteria are typically performed using plates with different compositions than for standard *C. elegans* growth and maintenance. Therefore, comparing results from RNAi treatments to mock RNAi treatments using the same RNAi plates is favorable. Unfortunately, not all my experiments had results for mock RNAi treatment but were used as a comparison whenever possible.

Using the mock RNAi treatment as a comparison, it is clear that the *sdc-2* RNAi leads to the transcription upregulation of DPY-23 mRNA from the 30 cell stage. Expression of the autosomal control gene *mdh-1* shows some variability between the *sdc-2* RNAi and mock RNAi conditions; however, there is no apparent transcription upregulation in the mutant condition (Figure 34c).

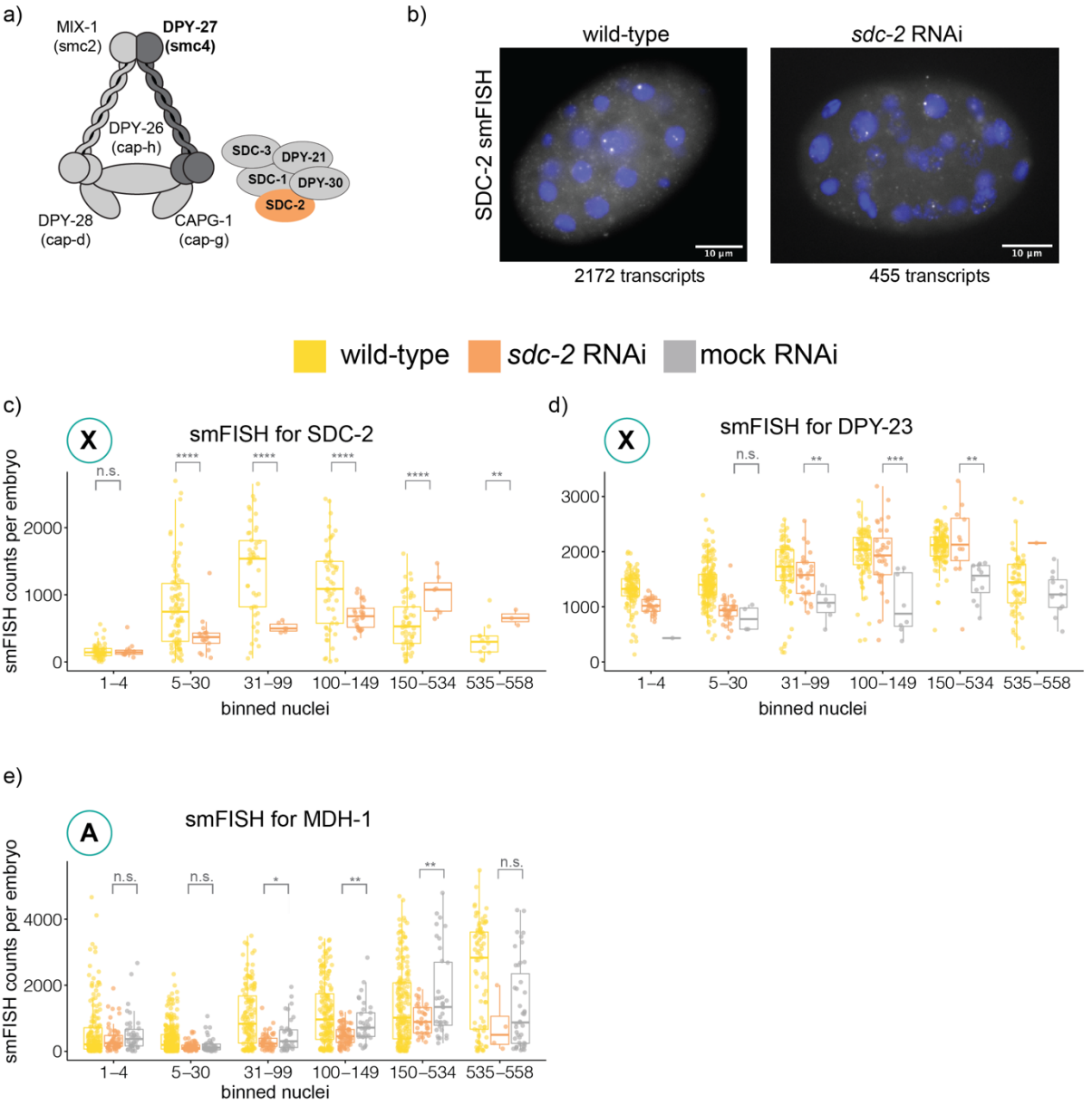

Figure 34 Detection of smFISH in wild type and *sdc-2* RNAi embryos
a) Cartoon of the DCC complex highlights the subunit SDC-2 **b)** Example images of either wild type or sdc-2 RNAi embryos, labeled with SDC-2 smFISH. The number of detected smFISH spots for each example is written under the image. **c)** Plots for smFISH detection X chromosomal mRNA SDC-2. Each spot represents the total mRNA count for one embryo, plotted against the binned nuclei number for wild type (yellow), *sdc-2* RNAi (orange), or mock RNAi (gray). **d)** Plot as in c but for the X chromosomal mRNA DPY-23. **e)** Plot as in c but for the autosomal mRNA MDH-1. Significant P-values from Welch's unequal variances t-test are noted above the wild-type vs. knock-down condition for each time-point. P-values are denoted as n.s. ($P > 0.05$), * ($P \leq 0.05$), ** ($P \leq 0.01$), *** ($P \leq 0.001$) and **** ($P \leq 0.0001$). If one of the samples had too few points, no P-value was calculated.

3.3.12 Loss of DPY-27 specifically increases X chromosomal transcription

DPY-27, the SMC4 homolog, is the only condensin DC-specific subunit that is not shared with condensin I (Figure 35a). Progeny of homozygous *dpy-27* null mutant worms die in late embryonic and early larval stages (Hodgkin, 1983b; Meyer and Casson, 1986; Plenefisch et al., 1989b). I used *dpy-27* RNAi to knock-down condensin DC (Figure 35b,d). The X chromosomal

mRNAs SDC-2, DPY-23, and RAB-6.2 show specific upregulation in later embryonic stages, especially in the 150-534 nuclei bin in the *dpy-27* RNAi condition. The transcription dynamics throughout embryogenesis of these three genes are remarkably different, but all are upregulated at a similar time-point in my analysis. However, the upregulation of the X-linked genes is reduced in the last time-point. *Dpy-27* RNAi has partial lethality for embryos, and a selection effect of less affected embryos or fewer siRNAs in late embryonic stages could explain this trend. Nevertheless, the smFISH detection of DPY-27 mRNA in *dpy-27* RNAi suggests that the knock-down of *dpy-27* was efficient (Figure 35d).

The autosomal mRNA MDH-1 is not as affected by the *dpy-27* RNAi, highlighting the specific effect of DPY-27 on the X chromosome (Figure 35e).

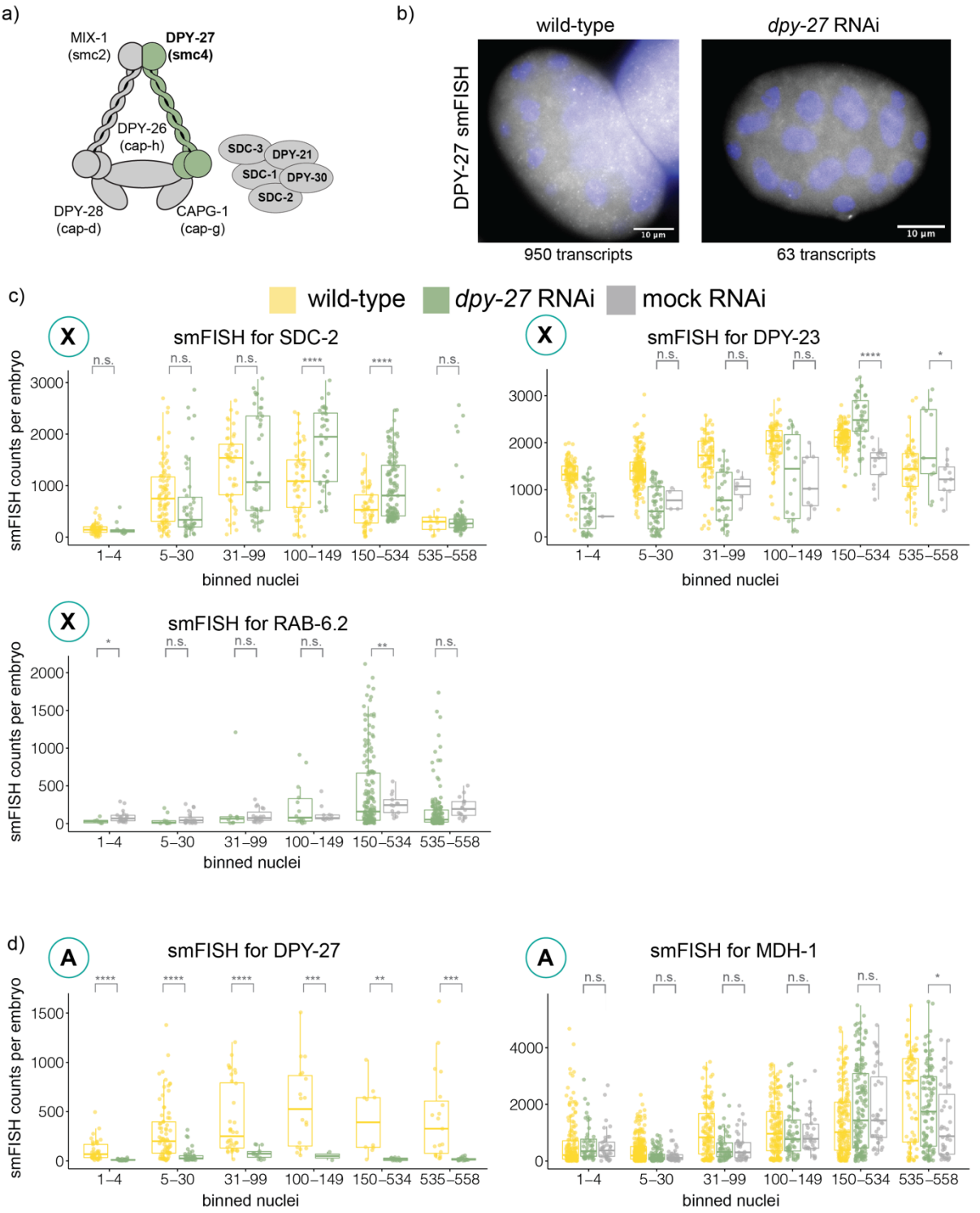

Figure 35 Detection of smFISH in wild type and *dpy-27* RNAi embryos
a) Cartoon of the DCC complex with a highlight on the condensin DC subunit DPY-27 **b)** Example images of either wild type or *dpy-27* RNAi embryos, labeled with DPY-27 smFISH. The number of detected smFISH spots for each example is written under the image. **c)** Plots for smFISH detection X chromosomal mRNAs (SDC-2, DPY-23, and RAB-6.2). Each spot represents the total mRNA count for one embryo, plotted against the binned nuclei number for wild type (yellow), *dpy-27* RNAi (green), or mock RNAi (gray). **d)** Plot as in c but for the autosomal mRNA MDH-1 and DPY-27. Significant P-values from Welch's unequal variances t-test are noted above the wild-type vs. knock-down condition for each time-point. P-values are denoted as n.s. ($P > 0.05$), * ($P \leq 0.05$), ** ($P \leq 0.01$), *** ($P \leq 0.001$) and **** ($P \leq 0.0001$). If one of the samples had too few points, no P-value was calculated.

3.3.13 Loss of DPY-21 increases transcription from X chromosomes and autosomes

The jumonji demethylase DPY-21 is part of the DCC and specifically demethylates H4K20me2 to H4K20me1 at the X chromosomes (Figure 36a) (Brejc et al., 2017). DPY-21 loss is not lethal for the worms, and therefore a homozygous null line is viable but has a pronounced dumpy phenotype (Figure 19d).

Similar to *sdc-2* RNAi and *dpy-27* RNAi, the *dpy-21* null condition shows upregulation of X chromosomal genes in the bin of 150-534 nuclei, albeit not as strongly (Figure 36b).

However, the autosomal mRNA MDH-1 is also affected in the *dpy-21* null embryos (Figure 36c). DPY-21 was previously implicated in other pathways like metabolic regulation (Webster et al., 2013). The malate-dehydrogenase MDH-1 could be directly or indirectly affected by the loss of DPY-21. More autosomal genes should be analyzed to test if the upregulation of *mdh-1* is gene-specific or if *dpy-21* loss generally affects autosomal genes.

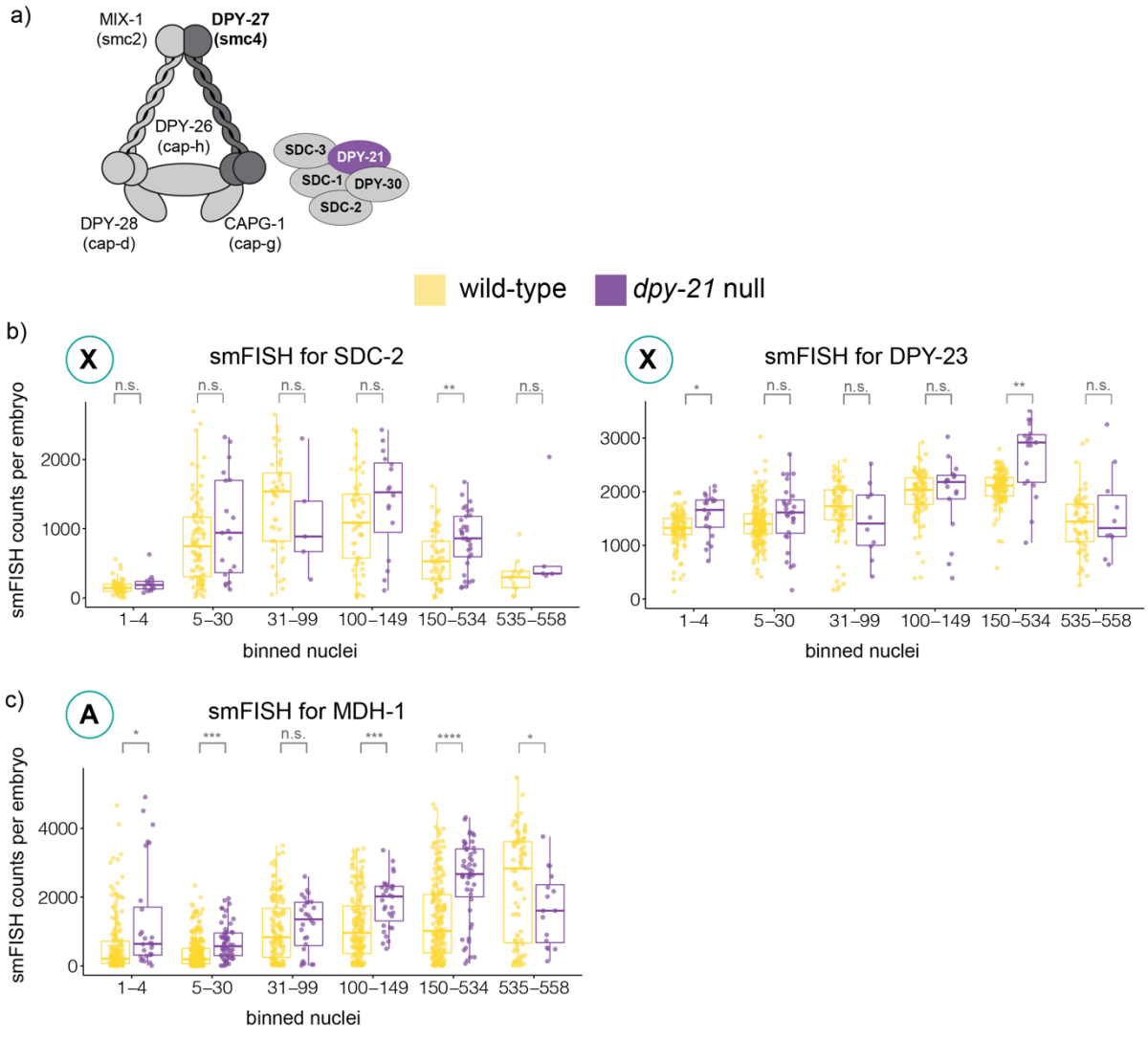

Figure 36 Detection of smFISH in wild type and *dpy-21 null* embryos

a) Cartoon of the DCC complex highlights the subunit DPY-21 **b)** Plots for smFISH detection of X chromosomal mRNAs (SDC-2 and DPY-23). Each spot represents the total mRNA count for one embryo, plotted against the binned nuclei number for wild type (yellow) or *dpy-21* null (purple). **c)** Plot as in b but for the autosomal mRNA MDH-1. Significant P-values from Welch's unequal variances t-test are noted above the wild-type vs. knock-down condition for each time-point. P-values are denoted as n.s. ($P > 0.05$), * ($P \leq 0.05$), ** ($P \leq 0.01$), *** ($P \leq 0.001$) and **** ($P \leq 0.0001$).

3.3.14 Loss of *rex* sites can influence transcription locally

We were interested in testing if the presence of *rex* sites influences transcription locally and if the distance to single *rex* sites influences the time-point of repression. Previous studies removed single *rex* sites using CRISPR and observed a reduction of DPY-27 binding to a local region of ~1 Mb around the deletion site (Albritton et al., 2017). Interestingly, deletion of *rex-41* at the end of the X chromosome also slightly increased transcription from genes within a 500 kb window (Albritton et al., 2017). In contrast, in a recent paper, deletion of eight strong *rex* sites did not result in detectable expression changes close or far from the deleted *rex* sites using a gene expression change analysis with a 400 kb sliding window (Anderson et al., 2019). However, the data suggested that the *rex* site deletions shortened lifespan, possibly through gene expression changes around the two left-most deleted *rex* sites (Anderson et al., 2019). It is likely that RNA-seq is not sensitive enough to detect small transcription changes in a heterogeneous population.

We asked if the deletion of *rex-1* influences the transcription of *dpy-23,* which is located at a distance of ~6 kb. Therefore we compared wild-type with *rex-1* deletion embryos. Using different fluorophores, we quantified transcription of three genes in identical embryos: The X-linked genes *dpy-23* and *wdr-5.2* and the autosomal gene *mdh-1* (Figure 37a).

As observed with the previous knock-down experiments, transcription of *dpy-23* is specifically upregulated in the later embryonic stages in the *rex-1* deletion strain (Figure 37b). Strikingly, transcription of the *wdr-5.2* that is far in the genomic distance is mostly not affected in the *rex-1* deletion strain. Similarly, the autosomal gene *mdh-1* shows no transcription upregulation.

This result suggests that the absence of a *rex* site could regulate dosage compensation locally. In contrast to RNA-seq, our method detects transcription changes in single embryos at specific time-points and therefore is more sensitive to changes that might be missed in a population-based method.

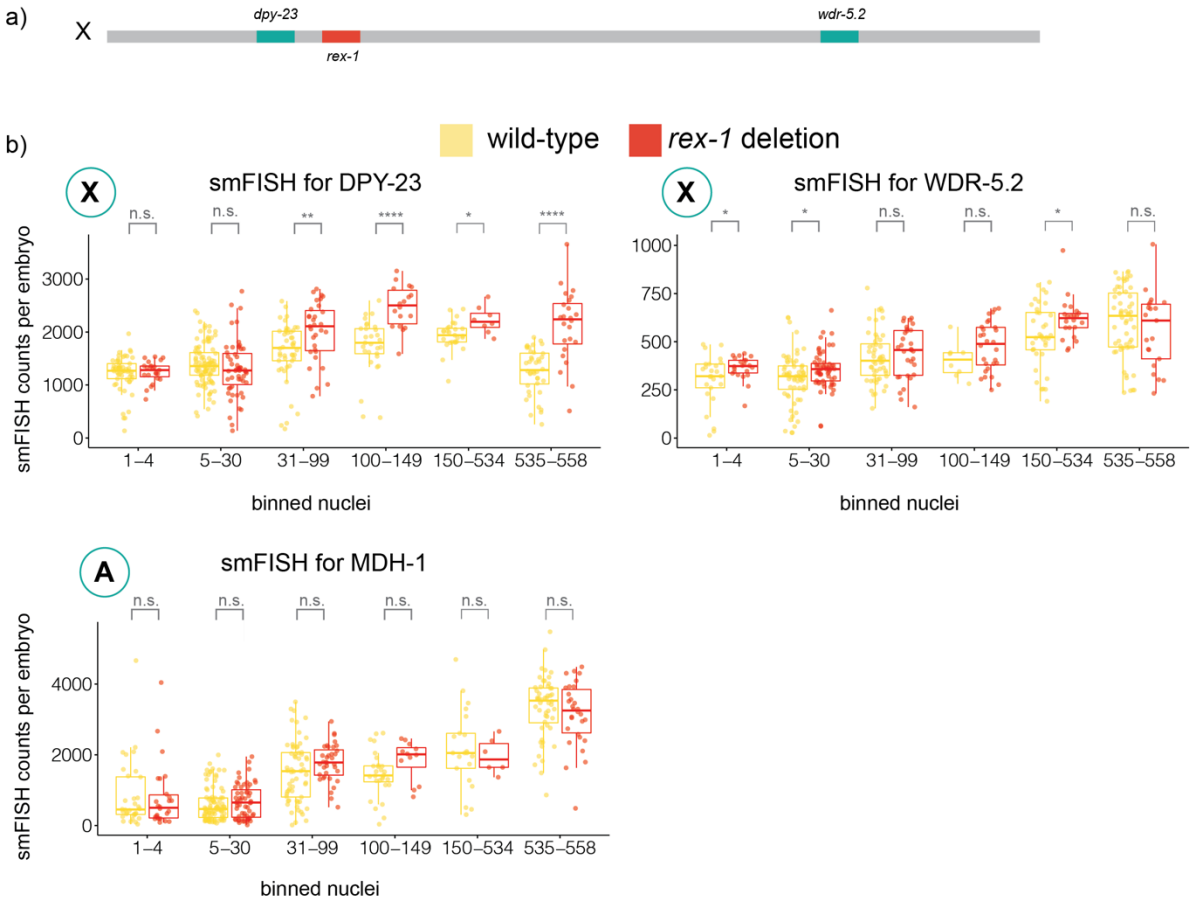

Figure 37 Influence of single *rex* sites on dosage compensation
a) Cartoon of the X chromosome with approximate locations of the genes *dpy-23* and *wdr-5.2* (~10 Mbp away) and the location of *rex-1*. **b)** Plots for smFISH detection X chromosomal mRNAs (DPY-23 and WDR-5.2) and one autosomal mRNA (MDH-1) in wild-type and *rex-1* deletion strains. Each spot represents the total mRNA count for one embryo, plotted against the binned nuclei number for wild type (yellow) or *rex-1* deletion (red) strains. Significant P-values from Welch's unequal variances t-test are noted above the wild-type vs. deletion condition for each time-point. P-values are denoted as n.s. ($P > 0.05$), * ($P \leq 0.05$), ** ($P \leq 0.01$), *** ($P \leq 0.001$) and **** ($P \leq 0.0001$).

3.3.15 Determining transcription bursting kinetics

Transcription bursting parameters can be directly extracted from single cells using smFISH imaging and mathematical modeling (Halpern et al., 2015). Previously an approach using co-staining of introns and exons to identify sites of active transcription has been used to infer transcription kinetics of the selected genes (Halpern et al., 2015; Halpern and Itzkovitz, 2016). Therefore I designed probes to intronic sequences of my genes of interest (Figure 31). With this strategy, I detected spots with high intensity in the exon and intron channels (Figure 38a). However, the detection of intronic spots was not always limited to the nucleus. It could be that the genome annotation for *C. elegans* was incomplete, and thus unannotated exons could result in unspecific intron-probe binding. Alternatively, a form of intron retention could lead to unspliced or post-transcriptionally spliced introns. A similar observation was made by the Murray lab (U Penn, unpublished).

Due to the lack of specific intron labeling, we decided to use the normalized exon signal of each embryo and set a threshold for high-intensity spots (Figure 38b). Our normalization strategy set the maximum of the fitted curve over all detected spots to an intensity of one. We chose to set the transcription site detection threshold to 1.7 to distinguish the site of transcription, which should capture sites with less than two full-length RNAs. Visual inspection of the normalized intensities of several co-stained transcription sites confirmed this threshold.

Transcription kinetics can be inferred from the fluorescent intensities at transcription sites. In the two-state random telegraph model, an increase in transcription can be accomplished by increasing the frequency of transcription (how often a promoter is turned on) or by increasing the burst rate (the number of RNAs produced at a transcription site) (Figure 38c) (Peccoud and Ycart, 1995; Lenstra et al., 2015). These parameters can be approximated through mathematically modeling (Halpern et al., 2015; Raj et al., 2008). Previously published models inferred frequency from the fraction of active promoters per cell (f), which the ratio of active transcription sites (TSS) and the number of genetic loci of the gene (n). The burst size (μ) is approximated from the RNA Pol II occupancy (M_{SUM}) at the promoters and the speed of RNA Pol II (v) by the length of the gene (l). RNA Pol II occupancy (M) is calculated from the intensity of a single transcription site (I_{TSS}) divided by correction factors for the probe position (η), inferred RNA Pol II occupancies ($\varkappa$), and the intensity of a single mRNA (I_{mRNA}).

However, these modeling approaches were developed for single cells or tissue sections of clearly countable single cells, including their boundaries and nuclei. Additionally, experimental measurements for the RNA Pol II occupancies ($\varkappa$) or speed of RNA Pol II (v) have been primarily performed in mammalian systems, and measurements for *C. elegans* are missing (Singh and Padgett, 2009; Darzacq et al., 2007). I wanted to study how the transcription kinetics change between the wild-type and DCC mutant embryos in my experiments. We expect polymerase speed and length of genes to stay constant between these two conditions. Thus we can analyze the change of transcription rate (f) through the relative change of active transcription sites between conditions (Figure 38d). To study if single promoters increase their transcription rate, we looked at the average RNA Pol II occupancy at a single transcription site (M) between mutant and wild-type embryos.

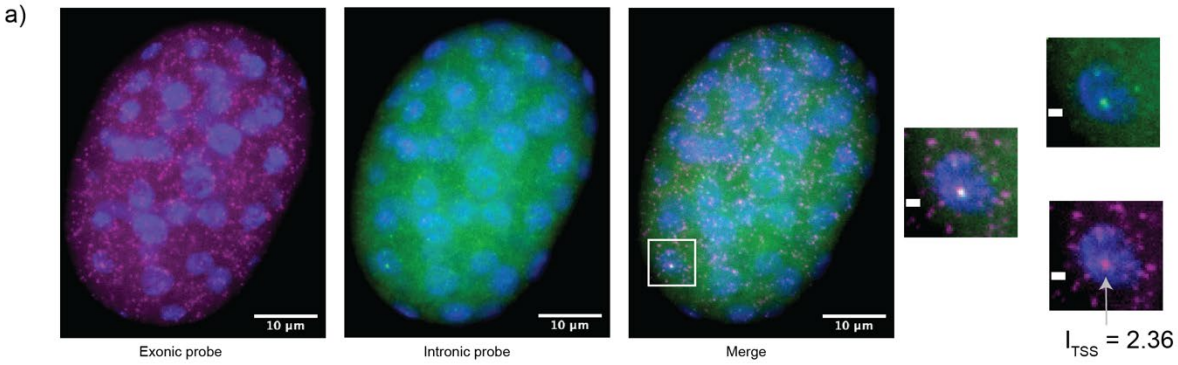

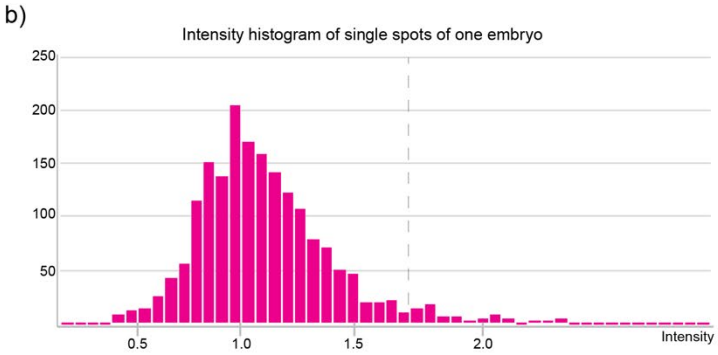

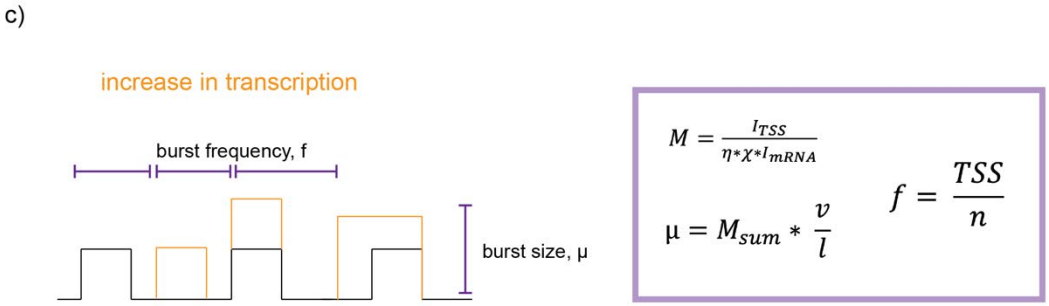

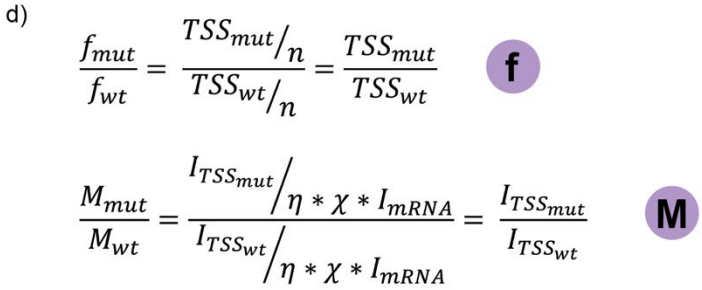

Figure 38 Detection nascent transcription and calculation bursting parameters
a) Example image of a single embryo labeled with smFISH for the exonic and the intronic sequence. A highlight of a single nucleus with one bright transcription site. The normalized transcription site intensity (ITSS) is 2.36. The scale bar of the zoom-in is 1 µm. **b)** Histogram of the normalized exon intensities of all detected spots for the embryo displayed in part a. The cut-off for high-intensity spots is set to 1.7 (indicated by the dotted line). **c)** Two state random telegraph model of bursting characteristics. Transcription can increase through a higher burst frequency (f) or burst size (µ). M = RNA Pol II occupancy, ITSS = intensity at a single promotor, η = correction factor of probe position, ϰ = inferred RNA Pol II occupancy, ImRNA = intensity of a single mRNA, v =speed of transcription, l = gene length, TSS = number of active transcription sites, n = number of genomic loci. Models previously defined by (Halpern et al., 2015). **d)** Detection of relative changes in bursting characteristics between a mutant (mut) and wild type (wt) condition.

3.3.16 Transcription frequency modulation in *dpy-27* RNAi embryos

The transcription of X chromosomal genes was upregulated in late embryonic stages in *dpy-27* RNAi embryos compared to wild-type embryos (Figure 35). To study the promoter states that lead to these transcription changes, I used the approach of detecting relative changes in burst frequency (f) and RNA Pol II occupancy (M) measured by the average number of nascent transcripts at one promoter, which is related to the burst rate (μ) between wild-type and mutant embryos (Figure 38d).

Interestingly, all X chromosomal genes increase burst frequency in later stages in *dpy-27* RNAi compared to control conditions (Figure 39a). The average number of transcripts per TSS is relatively unchanged between most conditions for *dpy-23* and *rab-6.2*. Transcription of *sdc-2* seemed to be influenced by changes in burst frequency and burst size. SDC-2 is transcribed from the X chromosome, and the protein SDC-2 itself is a subunit of and is required for binding of the DCC. Therefore, transcription of *sdc-2* might be regulated by a feedback loop with different transcription kinetics. Additionally, a mock RNAi control is missing for this sample which might influence the results. Nevertheless, consistent with the idea that dosage compensation regulates transcription frequency, the burst frequency changes for *sdc-2* were also significantly increased.

The autosomal gene *mdh-1* has less significant changes in burst frequency and the average number of transcripts per promoter (Figure 39b).

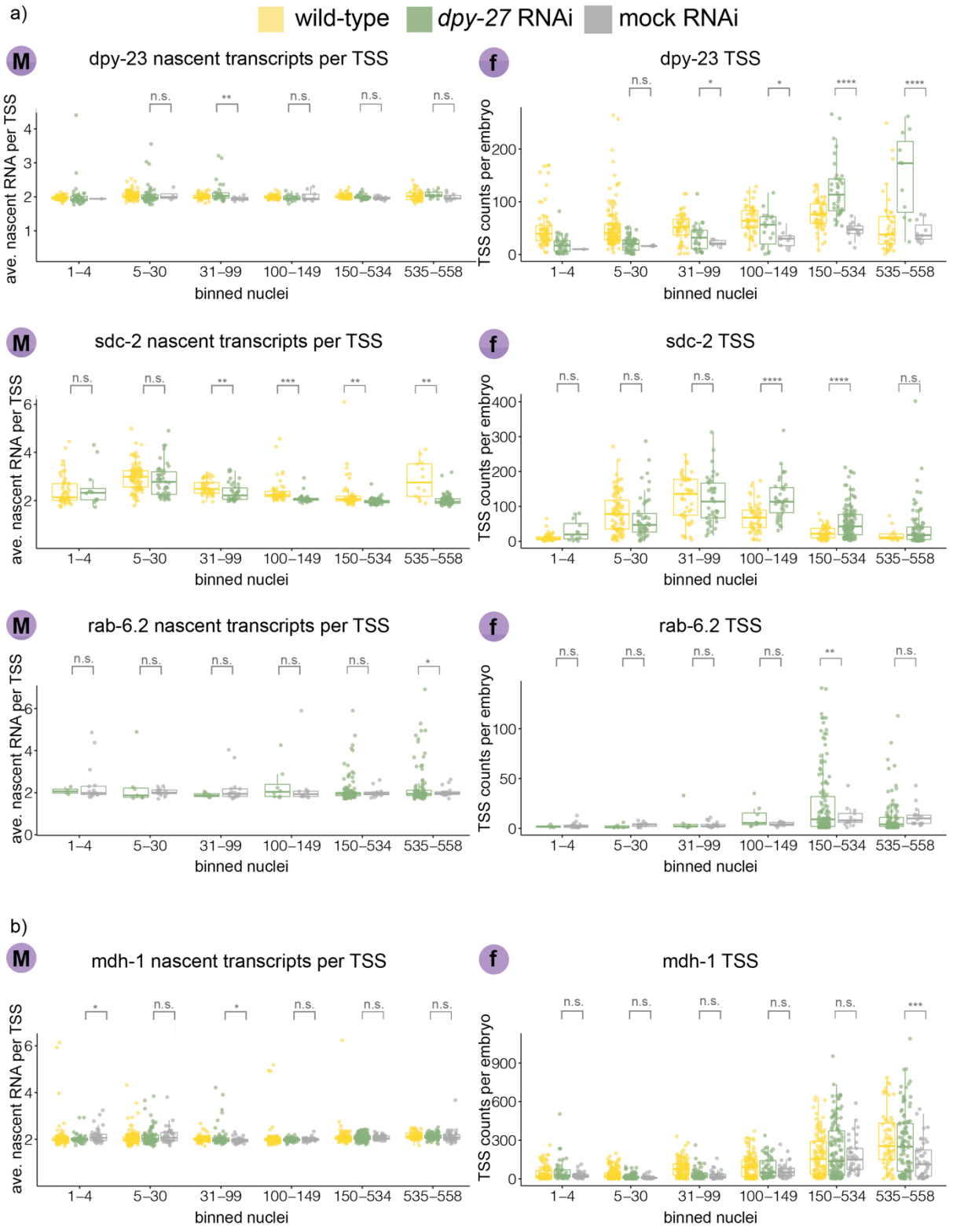

Figure 39 Detection of transcription parameters in dpy-27 RNAi and control embryos
a) Relative transcription parameter changes for X chromosomal genes for wild-type (yellow), *dpy-27* RNAi (green), and mock RNAi (gray) conditions**.** The first column (M) shows the average number of nascent transcripts per TSS. The second column (f) shows the number of actively transcribing promotors. **b)** As in part a but for the autosomal gene *mdh-1***.** Significant P-values from Welch's unequal variances t-test are noted above the wild-type vs. knock-down condition for each time-point. P-values are denoted as n.s. ($P > 0.05$), * ($P \leq 0.05$), ** ($P \leq 0.01$), *** ($P \leq 0.001$) and **** ($P \leq 0.0001$). If one of the samples had too few points, no P-value was calculated.

3.3.17 Influence of threshold selection for transcription parameter approximation

Sites of nascent transcription are typically detected by co-staining of exonic and intronic smFISH probes (Halpern et al., 2015). Due to the unspecific labeling of cytoplasmic RNAs with the intron probe, we decided to use an intensity threshold to detect sites with high intensity (Figure 38b). This approach assumes that active transcription sites transcribe more than one RNA simultaneously when actively transcribing (Raj and Oudenaarden, 2008).

To test if choosing a different threshold influences the contribution of burst frequency or size modulation for *dpy-23* in *dpy-27* RNAi and control conditions, I repeated the analysis in Figure 39 using different thresholds (Figure 40a). All three selected thresholds still recapitulate the main finding that for *dpy-23,* the frequency of transcription activation is vital for transcription upregulation in the *dpy-27* RNAi condition (Figure 40b). The threshold of 1.5 seems to be overestimating the number of active transcription sites per embryo as the number of transcription sites increases significantly in younger embryos. Nevertheless, this is true for all thresholds with varying degrees and a downside from relying on intensity measurements for TSS detection. Possibly using a machine learning approach in the future that combines the detection of intronic and exonic probes in an area of high DAPI intensity could lead to a refined detection of transcription sites.

In the absence of alternative TSS detection possibilities, I continued using an intensity threshold of 1.7 to detect sites of nascent transcription and infer transcription parameters.

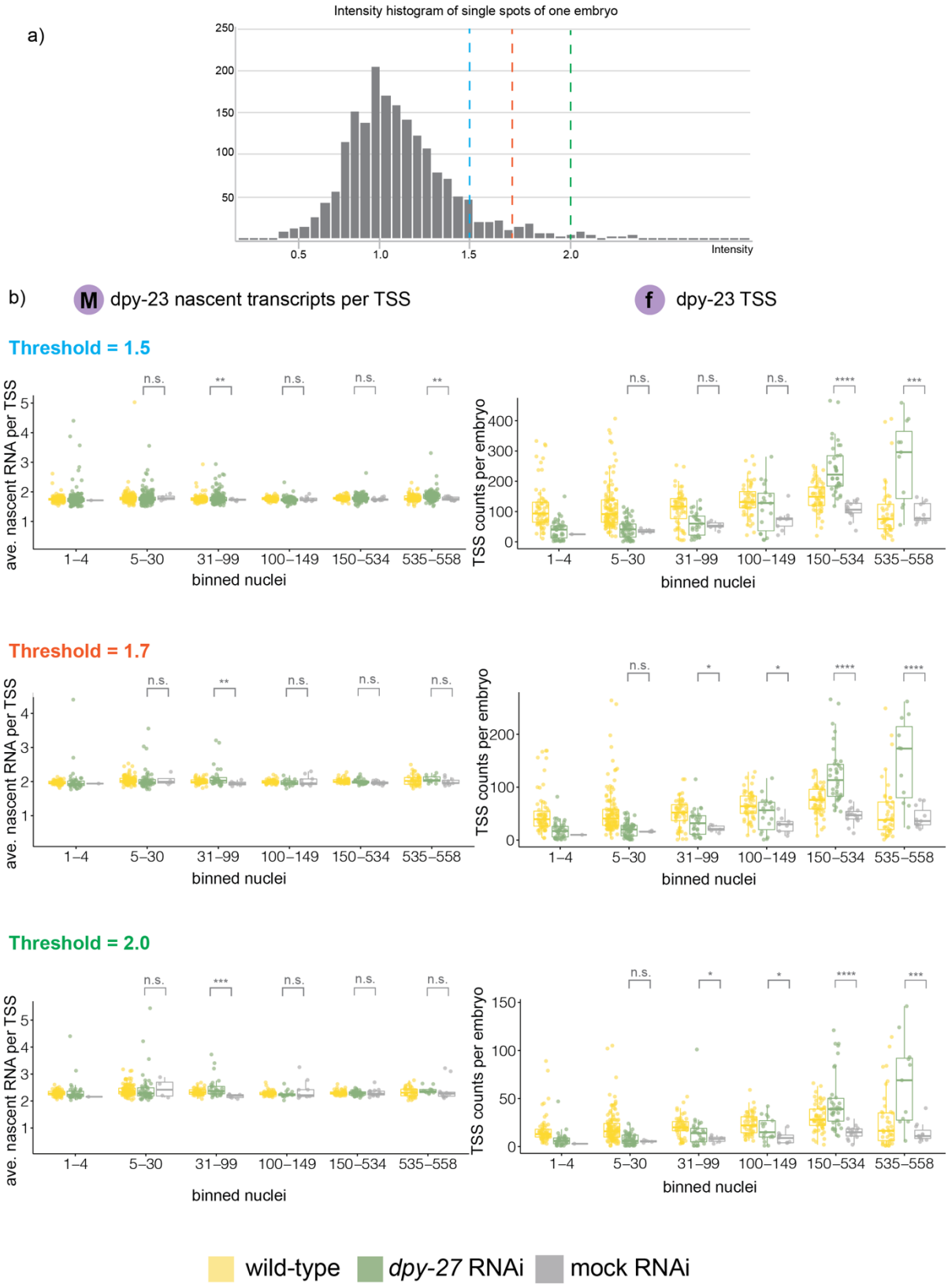

Figure 40 Validation of threshold selection

a) Histogram of the normalized exon intensities of all detected spots for one embryo. Different cut-offs for detection of high-intensity spots were selected at 1.5 (blue), 1.7 (red), and 2.0 (green). **b)** Relative transcription parameter changes for X chromosomal genes for wild-type (yellow), *dpy-27* RNAi (green) and mock RNAi (gray) conditions**.** The first column (M) shows the average number of nascent transcripts per TSS. The second column (f) shows the number of actively transcribing promotors. Three different thresholds were selected to classify transcription sites in the dataset. Significant P-values from Welch's unequal variances t-test are noted above the wild-type vs. knock-down condition for

each time-point. P-values are denoted as n.s. (P > 0.05), * (P ≤ 0.05), ** (P ≤ 0.01), *** (P ≤ 0.001) and **** (P ≤ 0.0001). If one of the samples had too few points, no P-value was calculated.

3.3.18 Transcription parameter changes for *dpy-21* null embryos

Transcription of the X chromosomal genes *dpy-23* and *sdc-2*, as well as the autosomal gene *mdh-1*, were upregulated in *dpy-21* null embryos compared to wild-type (Figure 36). Similar to the *dpy-27* RNAi condition (Figure 39), the transcription upregulation of DPY-23 mRNA is achieved through increased frequency of active transcription sites and not through increasing the transcriptional output of each promoter (Figure 41a).

SDC-2 mRNA was only mildly upregulated in *dpy-21* null embryos. (Figure 36). The transcription frequency is not much affected, and the average number of RNAs per TSS is reduced in the *dpy-21* null condition, similar to the results in the *dpy-27* RNAi condition (Figure 39).

Transcription of the autosomal gene *mdh-1* was also increased in *dpy-21* null embryos (Figure 36). Like DPY-23, transcription increased by increasing burst frequency in *dpy-21* null compared to wild-type embryos (Figure 41c).

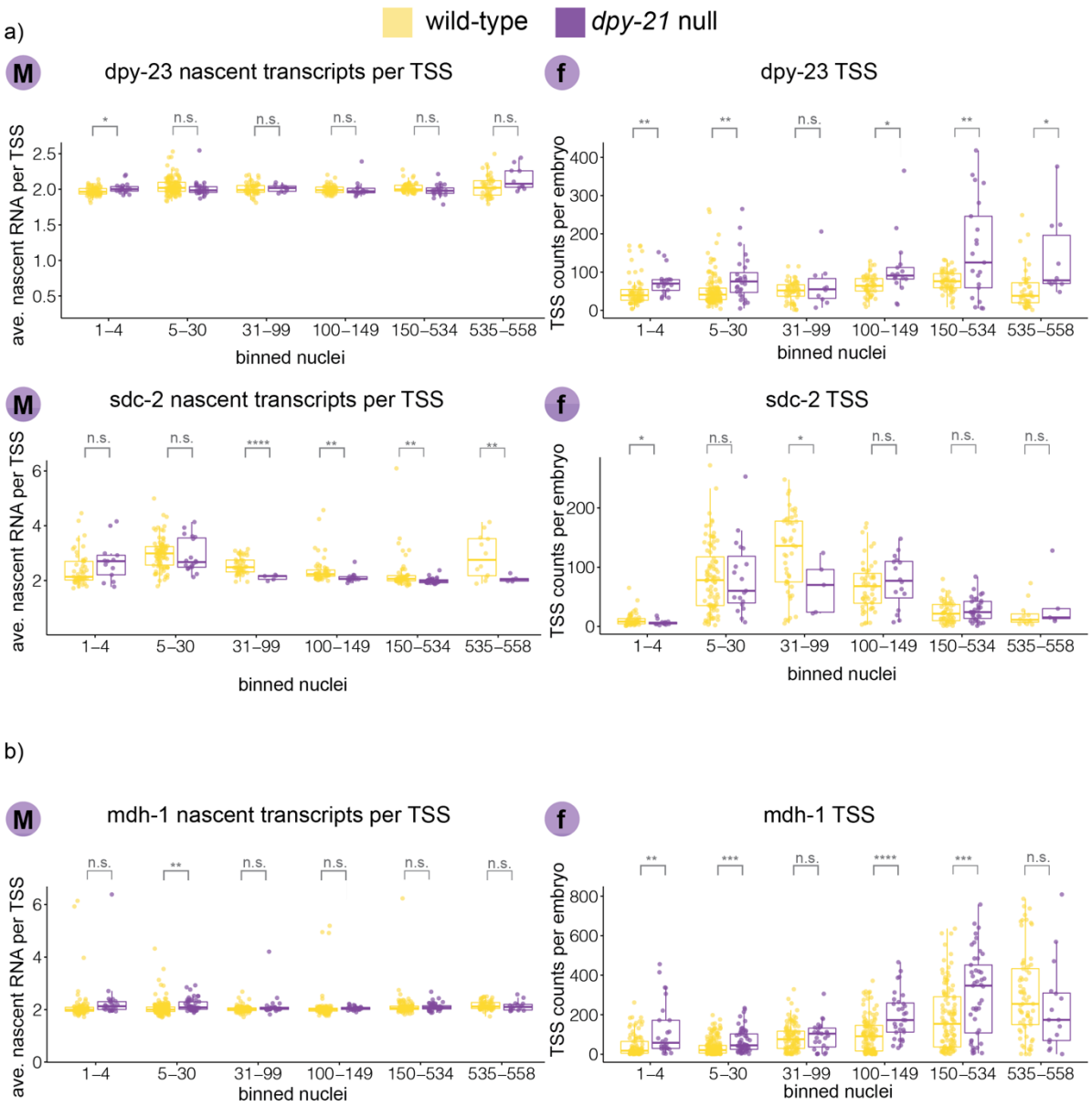

Figure 41 Detection of transcription parameters in *dpy-21* null and wild type embryos
a) Relative transcription parameter changes for X chromosomal genes for wild-type (yellow) and *dpy-21* null (purple) conditions**.** The first column (M) shows the average number of nascent transcripts per TSS. The second column (f) shows the number of actively transcribing promotors. **b)** As in part a but for the autosomal gene *mdh-1***.** Significant P-values from Welch's unequal variances t-test are noted above the wild-type vs. knock-down condition for each time-point. P-values are denoted as n.s. ($P > 0.05$), * ($P \leq 0.05$), ** ($P \leq 0.01$), *** ($P \leq 0.001$) and **** ($P \leq 0.0001$).

3.3.19 Transcription parameter changes for *sdc-2* RNAi embryos

The knock-down of *sdc-2* increased the transcription of *dpy-23* in later embryonic stages (Figure 34). Also, in the *sdc-2* RNAi condition, *dpy-23* transcription increased through burst frequency modulation (Figure 42a). The transcription parameters of the autosomal gene *mdh-1* do not show the same burst frequency modulation (Figure 42b).

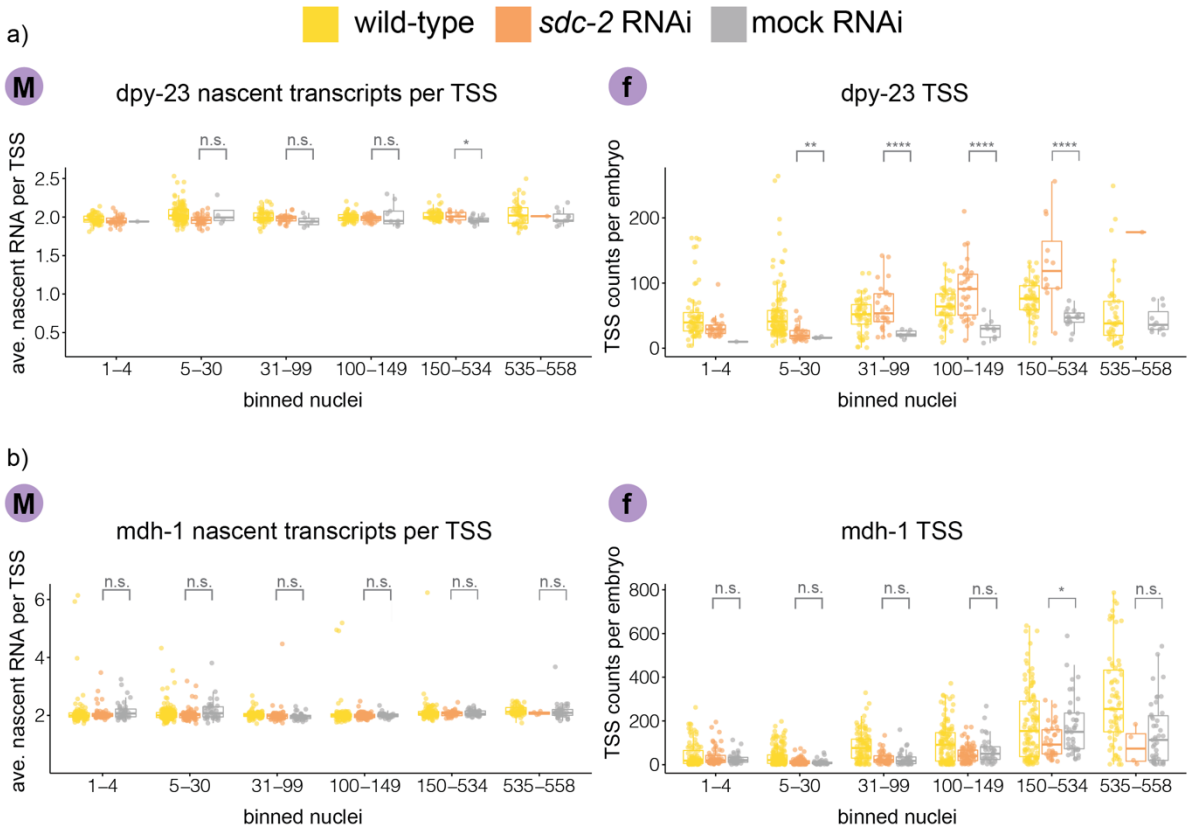

Figure 42 Detection of transcription parameters in *sdc-2* RNAi and control embryos
a) Relative transcription parameter changes for the X chromosomal gene *dpy-23* for wild-type (yellow), *sdc-2* RNAi (orange), and mock RNAi (gray) conditions**.** The first column (M) shows the average number of nascent transcripts per TSS. The second column (f) shows the number of actively transcribing promotors. **b)** As in part a but for the autosomal gene *mdh-1***.** Significant P-values from Welch's unequal variances t-test are noted above the wild-type vs. knock-down condition for each time-point. P-values are denoted as n.s. ($P > 0.05$), * ($P \leq 0.05$), ** ($P \leq 0.01$), *** ($P \leq 0.001$) and **** ($P \leq 0.0001$). If one of the samples had too few points, no P-value was calculated.

3.4 Discussion

The dosage compensation system in *C. elegans* reduces transcription from both X chromosomes in hermaphrodites by about 2-fold (Meyer and Casson, 1986; Albritton and Ercan, 2018). Central to the transcription repression is the binding of the dosage compensation complex (DCC) to the X chromosomes. The mechanism of transcription regulation is not well understood. In this work, I used an imaging approach based on widefield single-molecule RNA fluorescence in situ hybridization (smFISH) and machine learning to detect transcription dynamics throughout embryonic development. We obtained thousands of smFISH images for a set of condensin DC-regulated and control genes in wild-type or DCC mutant embryos and extracted mature and nascent RNA counts in 3D, which we used to determine transcription burst characteristics.

3.4.1 Detection of transcription with high spatial and temporal resolution

The use of smFISH has been widely applied to quantify transcription parameters in single cells or tissue sections (Halpern et al., 2015; Miura et al., 2019; Wan et al., 2021). Studying transcription using smFISH in developing organisms has many advantages but constitutes a challenging experimental, microscopy, and image analysis problem. *C. elegans* is an optimal organism for imaging due to its transparent body and fixed lineage. SmFISH has been applied to detect transcription in *C. elegans* embryos however, previous studies either used smFISH qualitatively (Harterink et al., 2011; Nishimura et al., 2015), with low throughput (Raj et al., 2010; Seidel et al., 2011) or quantified transcription only in early embryos (Charles et al., 2020; Parker et al., 2020). A quantitative and high throughput study of transcription in *C. elegans* embryonic development has lacked so far.

The imaging and image analysis pipeline we developed allows detection of transcription in vast numbers of single embryos throughout embryonic development. Especially staging of later embryonic stages is challenging, but unsupervised deep learning (autoencoder) and carefully chosen, differently sized bins allowed us to detect transcription changes in late stages. We found that transcriptional changes of X chromosomal genes occur mostly late in embryogenesis (Figure 35). We know from RNA-seq data that transcription repression happens throughout development but might not reach total repression until the L1 stage (Kramer et al., 2015). Even though DCC binding to the X chromosome is seen from the 40 cell stage on (Dawes et al., 1999; Chuang et al., 1996), I observed transcription regulation started only from the 100 or 150 cell stage on in most experiments. To refine the detection of the exact time points, the last two bins could be split into smaller bins to achieve a higher temporal resolution. Alternatively, a probabilistic atlas from high-resolution lightsheet data of a developing *C. elegans* embryo could be used to map smFISH images to their developmental time-point.

3.4.2 Heterogeneity of transcription and dosage compensation

Transcription is a stochastic process leading to differential mRNA and proteins levels between cells and organisms with the same genetic background and sharing the same environment (Raj and Oudenaarden, 2008; Tunnacliffe and Chubb, 2020). Even transcription in the deterministic organism *C. elegans* with a fixed lineage and cell numbers was described as stochastic in reaction to mutations (Raj et al., 2010) during development (Lee et al., 2019) and might be critical to determine the lifespan of the animal (Rea et al., 2005). Such fluctuations in gene expression can be advantageous for an individual in an isogenic population (Urban and Johnston, 2018).

We observe variability for all genes in wild-type and DCC mutant conditions. Interestingly, the expression of *rab-6.2* seems to have higher variability in the *dpy-27* RNAi condition (Figure 35c). While this needs to be confirmed with a larger control sample size, it is interesting that the DCC seems to reduce transcription noise from this promoter specifically. It would be fascinating to see if more genes show high transcription noise in a DCC mutant condition as an increase in transcription noise in reaction to mutations has been observed before (Raj et al., 2010).

For our analysis, we assumed that transcription from both alleles is similarly affected by the depletion of the DCC proteins. Generally, it is not clear if dosage compensation affects both X chromosomes to the same extent and if regulation of the same alleles is coupled or uncoupled. It would be interesting to study if transcription from the two alleles is similarly affected upon DCC depletion. The SNP density of *C. elegans* is very low, so it is challenging to design different probes for different alleles. One possibility would be combining two different live transcription systems (e.g., MS2 and PP7) and cross animals to observe transcription from two different alleles simultaneously.

3.4.3 The role of *rex* sites for transcription regulation

The DCC is first recruited at ~60 recruitment elements on the X (*rex*) sites (Albritton et al., 2017). We found that transcription of the *dpy-23* gene is misregulated when deleting the close-by *rex* site, *rex-1* (Figure 37). Transcription of *dpy-23* was specifically increased from the 31 -99 cell stage on and stayed elevated throughout embryogenesis. This result agrees with the finding of Albritton et al. that found deletion of rex-41 increased transcription locally while decreasing condensin DC binding using RNA-seq in a mixed embryo sample (Albritton et al., 2017). Conversely, Anderson et al. observed no transcriptional changes locally or X chromosome-wide when deleting eight strong *rex* sites (Anderson et al., 2019). While it is unclear where this difference comes from, there are several possible explanations. Firstly, their eight *rex* site

deletions did not include *rex-1* nor *rex-41,* so that it could be something specific about these *rex* sites. Additionally, while they did take great care of matching the RNA-seq data to an expression reference, RNA-seq in mixed embryo populations might not have the resolution to detect dynamic transcription changes during embryogenesis. While they detected no transcription changes, they identified changes in lifespan when deleting two *rex* sites on the left arm, which might be caused by transcription changes that were missed in the analysis approach.

My results suggested that *dpy-23* expression is upregulated until the end of embryogenesis. It would be interesting to follow the transcription dynamic into larval stages to test if there is a time-point where transcription is repressed again in the *rex-1* deletion strain. Since the transcription repression in dosage compensation does not reach the full level until the L1 stage, as measured by RNA-seq, there may be a later time-point when *dpy-23* transcription is dosage compensated in the deletion strain resulting in equal levels of DPY-23 mRNA between wild-type and *rex-1* deletion strains.

With this first experiment, we could show that at least the loss of *rex-1* influences dosage compensation locally and potentially temporally. It would be interesting to test if more *rex* sites can influence dosage compensation by including other *rex* deletion strains in our analysis. Additionally, it would be fascinating to test if *de novo* insertion of a *rex* site would repress transcription further or earlier.

3.4.4 Dosage compensation through burst frequency modulation

Our data suggest that dosage compensation functions through transcription frequency modulation. Modulation of the burst frequency was a common mechanism observed for the regulation of developmental genes in *Drosophila* embryos (Bakker et al., 2020; Hoppe et al., 2020; Bothma et al., 2014; Fukaya et al., 2016; Garcia et al., 2013; Holloway and Spirov, 2017; Little et al., 2013). Different transcription regulatory elements have been associated with modulation of burst frequency, burst size, or both.

One element to modulate burst size is, for example, the promoter sequence. TATA-containing sequences resulted in larger bursts than promoters lacking the TATA sequence (Larsson et al., 2018; Hornung et al., 2012; Tantale et al., 2016).

What could be the mechanism leading to a reduced burst frequency in *C. elegans* dosage compensation? TF binding and histone modifications have been associated with modulating either burst frequency or burst size depending on each example.

There are reports for burst frequency modulation for TF binding (Friedrich et al., 2019; Lammers et al., 2020; Larson et al., 2013; Senecal et al., 2014; Mir et al., 2017) but also for burst size modulation (Suter et al., 2011; Dar et al., 2012; Rullan et al., 2018; Donovan et al., 2019). However, linking TF binding kinetics to transcription burst kinetics is still technically challenging (Megaridis et al., 2018). The DCC could impair the binding of specific activating TFs to the X chromosomes to modulate the burst frequency. However, so far, no general exclusion of activating TFs could be found from the X chromosome (Street et al., 2019).

Different histone deacetylases reduced transcription either by burst size or burst frequency alteration (Weinberger et al., 2012; Chen et al., 2019; Batenchuk et al., 2011). In one study, acetylation of histones, especially H3K27ac at promoter regions, affected burst frequency modulation (Nicolas et al., 2018). Potentially it could also be less about the modification, but the location of the histone modification as one study suggested that the location of the histone modification would change whether the burst size or frequency is affected. In this report, promoter-localized histone modifications (e.g., H3K4me) were associated with burst size and frequency alteration, while gene body histone modifications (e.g., H3K79me) were associated with bust frequency modulation (Wu et al., 2017). Deacetylation of the X chromosomes could contribute to the observed burst frequency modulation. However, loss of the H4K16 deacetylase SIR-2.1 increased X chromosomal transcription only slightly (Figure 19). Potentially other histone deacetylases work in combination to decrease transcription from the X chromosome, or a different deacetylase is the key driver for dosage compensation. The DCC could function in recruiting the deacetylase to the X chromosomes to modulate burst frequency.

Nucleosome occupancy at TSS has been associated with changing burst frequency (Dey et al., 2015). Possibly the DCC reduces access of specific nucleosome remodelers to reduce the opening of promoter regions, or alternatively, it could change the topological stress at promoters blocking histone eviction and DNA duplex opening (Teves and Henikoff, 2014; Corless and Gilbert, 2016). It was proposed that condensin DC might increase negative supercoiling at TSS to repress transcription (Kimura and Hirano, 1997; Hagstrom et al., 2002). However, a recent paper only found evidence for DCC-dependent negative supercoiling at *rex* sites but not at X-chromosomal TSSs (Krassovsky et al., 2021).

There are many examples of enhancer sequences and enhancer-promoter contacts modulating the burst frequency (Fukaya et al., 2016; Chen et al., 2019; Larsson et al., 2018; Bothma et al., 2014; Hoppe et al., 2020; Walters et al., 1995). Accordingly, an experiment forcing the looping of an enhancer to a promoter only affected the burst frequency, not the burst size (Bartman et al., 2016). Some enhancer-promoter contacts at TAD boundaries are dependent on the dynamic binding of cohesin (Rao et al., 2017; Hansen et al., 2016). Depleting cohesin can dissolve these contacts with a simultaneous decrease in nascent transcription of genes close to the boundary

(Thiecke et al., 2020). Strikingly it was also observed that cohesin could alter burst frequency at genes close to TAD boundaries (Luppino et al., 2020). Possibly cohesin dynamically binds at TAD boundaries to help regulate gene expression. Maybe dynamic binding of condensin DC to the X chromosome disrupts enhancer-promoter contacts and thereby decreases burst frequency.

In summary, we found that the DCC reduces the burst frequency of X chromosomal genes to achieve dosage compensation. We speculate that the DCC could disrupt promoter-enhancer contacts or recruit yet unknown factors like additional histone deacetylases to the X chromosome to reduce the frequency of transcription initiation.

3.5 Methods

3.5.1 Strains and Worm Growth

Unless noted, worms were grown and maintained using standard methods at 20-22°C on NGM plates (1L: 980 ml Milli-Q water, 3 g NaCl, 20 g agar, 2.5 g peptone, 1 ml 1 M CaCl2, 1 ml 5 mg/ml cholesterol in ethanol, 1 ml 1 M MgSO4 and 25 ml 1 M KPO4 buffer) containing OP50-1 strain of *E. coli* as food.

Table 9 Worm strains used in chapter 3

strain name	strain genotype	short description	SOURCE
N2	wild type	wild type laboratory strain	CGC
CB428	dpy-21(e428) V	dpy-21 null	CGC
SEA12	ers20[delX:4394846-4396180]; knuIs6[pSE-02 undisclosed(400bprex-1SNP), unc-119(+))] I; unc-119(ed3) III	rex-1 deletion strain	(Albritton et al., 2017)

3.5.2 RNAi conditions

RNAi plates (RNAi plates (1L), 3g NaCl, 17g bacto agar, 3g bacto peptone, 975ml water, autoclave, cool and add: 1ml cholesterol (5mg/ml in EtOH), 1ml 1M $CaCl_2$, 1ml 1M $MgSO_4$, 25ml 1M K phosphate buffer, 1ml IPTG (1mM final concentration, made freshly), 1ml Amp (50mg/ml stock), 1ml Tet (12mg/ml stock)) were prepared freshly and usually not stored longer than one month in the dark. Bacteria (from the Ahringer library) were sequenced before use. Single clones of bacteria were picked and cultured in a 5 ml overnight culture (LB + Amp Kan) at 37°C and shaking at 400 rpm. The next day, the small culture was added to typically 200 mL LB (Amp Kan) and continued shaking for 2-4 hours when the density of the culture reached OD 1. Then 1 ml IPTG was added to the culture, and incubation continued for 2 hours. To reduce the bacteria volume by 1/10, bacteria were spun down at 1000 g and resuspended in M9 to have about 400 µl of bacteria per plate (very dense).

Worms were grown to the adult stage and bleached to retrieve embryos. Embryos were placed in a 15 ml tube with M9 at RT and were shaking overnight. The next day, starved L1s were placed on the freshly prepared RNAi plates and placed at 20°C in the dark. For *ama-1* RNAi, L3/L4 were placed on RNAi bacteria to allow germline formation. After three days, adult worms were collected, and embryos were extracted as described below.

Table 10 Bacteria strain used for RNA interference

Sequence name	Targeted gene
control	empty vector
W10C8.2	*pop-1*
C35C5.1	*sdc-2*
R13G10.1	*dpy-27*
F36A4.7	*ama-1*

3.5.3 smFISH staining in *C. elegans* embryos

This protocol for smFISH labeling in *C. elegans* embryos was adapted from the Raj lab (Raj et al., 2008) protocol with some modifications.

3.5.3.1 Probe design

All used smFISH probe sets (Custom Stellaris® RNA FISH Probe Set) were designed and manufactured by Biosearch Technologies using the Stellaris probe designer web tool (Biosearch Technologies) specifically for *C. elegans*. Probes were designed to target exons or introns and labeled Quasar 670, CAL Fluor Red 610, or Quasar 570. Typically far-red dyes performed better due to the autofluorescence of *C. elegans* embryos and especially in older stages. If possible, the maximum amount of probes (48 per order) were selected for each exonic or intronic sequence. The number and color of probes are listed in Table 7 and Table 8. The complete sequences can be found in the Appendix. Probes were designed to have at least two nt space in between neighboring probes to avoid quenching. For exonic or intronic probe design, sequences listed at wormbase.org were used, and splice regions were masked with "n" nucleotides to avoid probes in these areas.

3.5.3.2 Preparation of worms

Worms were synchronized by either bleaching or egg-laying and grown to the adult stage. At this step, it is crucial to have non-starved, healthy adult worms in sufficient amounts. Typically, at least 5 x 6 cm plates full of worms were used to collect embryos.

3.5.3.3 Collection of embryos

For embryo collection, worms and older embryos were washed off plates using M9 and collected in a 35 µm nylon filter. Worms were washed at least three times with H2O, then carefully

transferred to a falcon tube using M9 and allowed to settle down. The supernatant was removed, and 5 ml freshly prepared bleaching solution was added to the worms. The dissolving of the adult worms was closely observed, and after 3 minutes, the tubes were spun at 3000 g for 1 min to collect the embryos. The supernatant was quickly removed, and the embryo pellet was vortexed. Then 10 ml of 1x PBS (with 0.05% of Triton X-100) were added, and the tube was centrifuged again for 3 min at 3000 g. This step was then repeated two more times until a clean embryo extract was left in the tube.

3.5.3.4 Fixing and permeabilization

Embryos were resuspended in 1 ml fixation solution and incubated at RT for 15 min while rotating. Next, the tube was submerged into liquid nitrogen for 1 minute to freeze crack the embryo eggshells. The tube was then transferred to a beaker with RT water to thaw, and once it was fully thawed, it was kept on ice for an additional 20 minutes. After this incubation, the tubes were spun down at 3000 g for 3 minutes, and the supernatant was removed, and the embryos were washed twice with 1 ml of 1x PBS (with 0.05% of Triton X-100). The embryos were resuspended in 70% EtOH and kept at 4 °C for at least 24 hours. Embryos can be kept at 4 °C for at least several months.

3.5.3.5 smFISH staining

For smFISH staining of the previously fixed embryos, tubes were centrifuged at 3000 g for 3 minutes, and ethanol was carefully removed. The pellet can be loose at this step, so removing supernatant should also be done in two stages. Embryos were then resuspended in 1 ml wash buffer and vortexed. Tubes were centrifuged, as above, and the supernatant was removed. The embryos were then resuspended in 50 µl hybridization solution, and 1 µl of each probe set (12.5 µM stock solution) was added directly to the sample. Tubes were then vortexed lightly and incubated at 37°C in the dark overnight. The next day, 0.5 ml of the wash buffer was added, the tubes vortexed and centrifuged to remove the supernatant. Next, 1 ml of wash buffer was added, and samples were incubated at 37°C for 30 minutes. After that, tubes were centrifuged again to remove the supernatant, and the embryo pellet was vortexed before adding 1 ml wash buffer. In this step, DAPI (5 ng/mL) was added to the wash buffer, and tubes were incubated at 37 °C for 30 minutes. The wash buffer was removed after centrifugation, and samples were washed once with 2x SSC.

3.5.3.6 Buffer

Collection buffer M9: 5.8 g Na2HPO4, 3.0 g KH2PO4, 0.5 g NaCl, 1.0 g NH4Cl, Nuclease-free water to a final volume of 1000 ml

1x PBS (DEPC treated + autoclave + 0,05% of Triton X-100)

Fixing buffer: 4% paraformaldehyde (PFA) in 1xPBS (DEPC treated + autoclave + 0,05% of Triton X-100)

Bleaching stock solution: 2.5 ml 4N NaOH, 2.5 ml 5% NaClO, 5 ml Nuclease-free water, freshly made

Washing buffer: 40 ml nuclease free water, 5 ml deionized formamide, 5 ml 20x SSC

Hybridization solution: 50 µl H20 (RNAse free), 37.5 µl ethylene carbonate (EC) 5 mg/ml, 25 µl formamide (at RT), 12.5 µl SDS (dissolved), 125 µl dextran sulphate 10 %

3.5.3.7 Mounting

To mount the stained embryos, most of the liquid was removed from the tubes. About 15 µl of dense embryos (in 2x SSC) were used per glass slide and spread onto a coverslip (#1.5, 22 x 22 mm). The sample was left to dry for about 15 minutes, and then 15 µl of ProLong™ Diamond Antifade Mountant (Thermo Fisher) was added to the sample. The glass slide (SuperFrost, VWR) was pressed with the embryos and mounting media onto the coverslip. Slides were left at RT in the dark for 24 hours before sealing the sides with nail polish and then stored at 4°C. Images were then acquired within two weeks of preparing the sample.

3.5.4 Imaging smFISH embryos

Embryos were imaged on a Nikon Ti inverted fluorescence microscope with an EMCCD camera (ANDOR, DU iXON Ultra 888), Lumen 200 Fluorescence Illumination Systems (Prior Scientific), and a 100x plan apo oil objective (NA 1.4) using appropriate filter sets (Gold FISH, Red FISH, Cy5 Narrow, GFP, DAPI). Images were acquired with 90 z-stacks positions with 200 nm step-width using Nikon Elements software.

3.5.5 Instance segmentation

Ellipsoid fitting was performed with a custom-written java script. StarDist was used for the creation of 2D binary masks (Schmidt et al., 2018). Analysis scripts can be found here: https://github.com/PreibischLab/nd2totif-maskembryos-stagebin-pipeline/blob/master/2_stardist_predict.py

3.5.6 Staging of embryos

Staging of different embryos into selected age bins was done by training an autoencoder for stage prediction. Around 150 embryos were first hand-staged into different bins and used to train the network. Scripts can be found here: https://github.com/PreibischLab/nd2totif-maskembryos-stagebin-pipeline/blob/master/4_stage_prediction.py

3.5.7 RS-FISH analysis

Detection of single RNA spots in 3D was performed using the Fiji plugin RS-FISH. For this, images were preprocessed by subtracting a duplicated and median filtered (sigma 19) image from the raw image to increase single spots and smooth background signals. Spot detection was performed using RS-FISH (https://github.com/PreibischLab/RS-FISH). The settings used for detection were: -i0 0, -i1 65535, -a 0.650, -r 1, -s 1.09, -t 0.001, -sr 2, -ir 0.3, -e 0.5116, -it 33000, -bg 0. Spots were filtered using binary masks to exclude spots found from neighboring embryos. To correct for z-dependent signal loss, a quadratic function was fit to the detected spots and used to correct the spot intensity throughout the embryo. All found detections were fitted with a gamma function, and the maximum of the curve was set to 1 to normalize intensity detection between different embryos.

3.5.8 Plotting and statistical analysis

Plotting of detected spots was performed using custom-written scripts in R using ggplot2 and ggpubr. To test if mutant and wild-type conditions had significantly different RNA levels or intensities, a Welch's unequal variances t-test was used in R. Significant P-values were indicated in the plots as n.s. ($P > 0.05$), * ($P \leq 0.05$), ** ($P \leq 0.01$), *** ($P \leq 0.001$) and **** ($P \leq 0.0001$). If one of the samples had too few points, no P-value was calculated.

4 Discussion

4.1 Noncatalytic functions of histone modifiers

The DCC-subunit DPY-21 is a jumonji demethylase specific for H4K20me2 (Brejc et al., 2017). The results of our study suggest that DPY-21 increases the dynamics of condensin DC on the X chromosome, which is vital for its function in dosage compensation. Intriguingly, this function was preserved in the DPY-21 catalytic mutant, suggesting an additional noncatalytic function for DPY-21. Several histone modifiers enzymes have noncatalytic functions or noncatalytic subunits.

One example of noncatalytic functions is noncatalytic subunits of histone remodeling complexes (Längst and Manelyte, 2015). The number of noncatalytic subunits increased throughout evolution (Kadoch and Crabtree, 2015), and several functions were identified for noncatalytic subunits. One role might be to increase the binding specificity of the complex (Moshkin et al., 2006). Other roles include mediating protein-protein interactions. For example, the SWI/SNF complex subunit BRM can repress transcription independent of its catalytic activity by binding to the TF CLK and recruiting repressive complexes (Kwok et al., 2015; Jordán-Pla et al., 2018). The histone methyltransferase EZH2 of the polycomb repressive complex 2 (PRC2) also has a noncatalytic function in stabilizing PRC2 or even PRC2 independent function in DNA damage repair (Kim et al., 2015; Koyen et al., 2020). A different example for stabilizing protein interactions is the methyltransferase Trr (mammalian MLL3/4) which is canonically responsible for depositing H3K4me1 at enhancers. However, Trr catalytic-inactivating mutations only changed transcription minimally due to the presence of a small region capable of stabilizing the H3K27 demethylase UTX (Rickels et al., 2020; Wang et al., 2017). A different noncatalytic function is the stimulation of the catalytic function. For example, flies' ESC-E(Z) complex has critical noncatalytic subunits to stimulate the catalytic methyltransferase activity (Ketel et al., 2005).

Other demethylases also show noncatalytic activities. For example, the Lysine-specific demethylase 1 (LSD1 or KDM1A) canonically demethylates histone targets to regulate gene expression (Lee et al., 2005). Beyond histone targets, LSD1 also demethylates a range of non-histone targets (Gu et al., 2020). More recently, a range of noncatalytic activities for LSD1 has been discovered, including the role of LSD1 as a scaffolding protein, destabilizing other proteins by promoting self-ubiquitylation, inhibiting autophagy, or protecting other proteins from proteasome-dependent degradation (Gu et al., 2020; Miller et al., 2020).

JmjC domain-containing demethylases have a range of noncatalytic activities. Kdm2b the H3K36 demethylase recruits PRC1 to unmethylated CpG islands via its zinc finger domain and independent of the catalytic activity (He et al., 2013). Similarly, the H3K36 demethylase dKDM4A in Drosophila regulates heterochromatin position-effect variegation which is not dependent on the demethylase activity (Colmenares et al., 2017). In fission yeast,

overexpression of the histone demethylase Epe1 causes heterochromatin defects by recruiting the histone acetyltransferase complex SAGA independently of the demethylase activity (Bao and Jia, 2019).

The noncatalytic activity of DPY-21 could include serving as a scaffold protein for other proteins that might regulate condensin DC binding to chromatin. So far, structural work is only limited to 407 aa that included the JmjC domain. Secondary structure prediction tools suggest that the rest of the 1641 aa long protein is highly unstructured and might include coils. Intrinsically disordered proteins and domains promote protein-protein and protein-nucleic acid interactions (Davey, 2019). Additionally, there is evidence that other proteins might bind to DPY-21, like the protein kinase SGK-1 (Webster et al., 2013). As a scaffold protein, DPY-21 could recruit factors that increase the mobility of condensin DC. This function would not be disrupted in the catalytic mutant, which could explain our finding that the catalytic mutant did not change condensin DC binding dynamics.

4.2 Condensin DC as an adapted stress-sensing repressive complex?

Condensins were first characterized in their role in mitotic chromosome condensation. Subsequently, several reports have described roles for condensin in transcriptional regulation during interphase. Many examples describe a role in general transcription repression for condensins, with a few reports also describing a transcription promoting function for condensin. Condensins activating transcription role is thought to function through looping of distant loci to the promoter (Haeusler et al., 2008; Iwasaki et al., 2010; Yuen et al., 2017). This looping could also contribute to the formation of transcription hubs, possibly by phase separation (Ryu et al., 2021).

However, there are more examples of condensins broadly down-regulating transcription. For example, condensins mediate the global downregulation of genes in budding yeast after a heat shock (Lancaster et al., 2021). Condensins also drive chromatin compaction and gene repression in quiescent yeast cells (Swygert et al., 2019). Similarly, cellular quiescence is disrupted in mouse T cells, where chromatin is de-compacted, and transcription increased after condensin II depletion (Rawlings et al., 2010). In *C. elegans*, condensin II was also involved with global transcription repression in germline cells in L1 larvae in response to starving (Belew et al., 2021).

Condensin DC represses transcription from both hermaphrodite X chromosomes by ~2-fold. It is possible that condensin DC adapted the evolutionarily conserved function of condensins to react to environmental stimuli (like heat and nutrition stress) to repress transcription broadly. If so,

condensin DC evolved to have several adaptations. Firstly, it is only targeted to the hermaphrodite X chromosomes through the sex-specific expression of the loading factor SDC-2 and the unique attributes of *rex* sites on the X chromosome. Secondly, the repression of transcription only reaches on average 2-fold. Potentially condensin DC is a less effective condensin molecule than condensin I/II or is negatively regulated to avoid complete repression. Thirdly, it evolved to be constantly "on" or in other words, no stress activation signal is needed to induce repression by condensin DC. Canonical stress sensing could function via post-translational modifications or by binding co-factors. Condensin DC might have lost or gained modifications or binding partners to activate the repressive function constantly. Studying the interactome of condensin DC might be helpful to reveal other binding partners that could be involved in such regulation.

4.3 Reconciling condensin DC binding dynamics with transcription regulation

In the first part of my thesis, I found that the dynamic of condensin DC binding is vital for transcription regulation. In the second part of my thesis, I found that dosage compensation might be regulated via burst frequency modulation. How can these two findings be reconciled into one dosage compensation model?

A recent paper found that loss of cohesin dynamics reduced cohesin at promoters and led to transcription misregulation (Liu et al., 2021). In this paper, they depleted the cohesin unloader WAPL, which leads to accumulation of cohesin on chromatin but paradoxically also to loss of cohesin at promoter regions. They proposed a model where cohesin turnover by loading and off-loading was essential to mediate enhancer-promoter contacts instead of static cohesin binding to chromatin.

Similarly, the dynamic binding of condensin DC to the X chromosomes might be more important than the static binding to specific promoter regions. In this model, condensin DC could disrupt transcription promoting contacts, remove polymerase from promoters, or continuously change the histone modifications at a promoter site. For instance, if condensin DC would disrupt enhancer-promoter contacts, the burst frequency could be reduced, leading to the X-linked 2-fold gene repression. In this model, depleting condensin DC from the X chromosome via *sdc-2* or *dpy-27* RNAi would increase burst frequency because condensin DC lacks from the X chromosome, and contacts are not disrupted. In the *dpy-21* null mutant, condensin DC would bind to the X chromosome but with changed dynamics. In this case, condensin DC might not efficiently disrupt contacts to reduce burst frequency. A more refined map of gene regulatory

contacts on the X chromosomes using Micro-C combined with single-molecule live imaging could reveal changes of sub-TAD interaction upon DCC-depletion (Hsieh et al., 2020).

4.4 Future directions

4.4.1 Does condensin DC reduce transcription frequency via regulating enhancer-promoter interactions?

The genome of *C. elegans* is very compact, with about 25% protein-coding sequences with many genes arranged in operon sequences (Reinke et al., 2013). The Cis-acting regulatory sequences of *C. elegans* are likely very close to the promoter region of genes. Often the minimal set of cis-acting sequences is found within 2 kb of the promoter (Reinke et al., 2013). Studies on enhancer sequences in *C. elegans* are often limited to single genes or lack functional validation (Chen et al., 2013; Stec et al., 2021). If most enhancer sequences are indeed very close to the promoter, enhancer-promoter loops might be very small. High-resolution chromatin conformation maps are necessary to test if condensin DC disrupts specific contacts on the X chromosome to modulate the burst frequency.

4.4.2 Does condensin DC reduce RNA Pol II reinitiation to reduce transcription?

After RNA Pol II completely transcribed a gene, several mechanisms support the reinitiation of RNA Pol II at the same promoter. GTF can remain bound at the promoter region to facilitate the PIC formation for a successive round of transcription (Sarge and Park-Sarge, 2005). Additionally, the terminal region of a gene can interact with the promoter region through gene looping to allow rapid reinitiation (Kaderi et al., 2009; Calvo and Manley, 2003). Condensin DC could function in disrupting such contacts to reduce transcription initiation. Possibly high-resolution microscopy could help to test if, after DCC depletion, the X chromosome shows more gene looping while genes are derepressed.

REFERENCES

Adelman, K., and J.T. Lis. 2012. Promoter-proximal pausing of RNA polymerase II: emerging roles in metazoans. *Nature Reviews Genetics*. 13:720–731. doi:10.1038/nrg3293.

Agrelo, R., and A. Wutz. 2010. X inactivation and disease. *Semin Cell Dev Biol*. 21:194–200. doi:10.1016/j.semcdb.2009.09.017.

Albritton, S.E., and S. Ercan. 2018. Caenorhabditis elegans Dosage Compensation: Insights into Condensin- Mediated Gene Regulation. *Trends in Genetics*. 34:41–53. doi:10.1016/j.tig.2017.09.010.

Albritton, S.E., A.-L. Kranz, L.H. Winterkorn, L.A. Street, and S. Ercan. 2017. Cooperation between a hierarchical set of recruitment sites targets the X chromosome for dosage compensation. *eLife*. 6:e23645-29. doi:10.7554/elife.23645.

Alekseyenko, A.A., J.W.K. Ho, S. Peng, M. Gelbart, M.Y. Tolstorukov, A. Plachetka, P.V. Kharchenko, Y.L. Jung, A.A. Gorchakov, E. Larschan, T. Gu, A. Minoda, N.C. Riddle, Y.B. Schwartz, S.C.R. Elgin, G.H. Karpen, V. Pirrotta, M.I. Kuroda, and P.J. Park. 2012. Sequence-Specific Targeting of Dosage Compensation in Drosophila Favors an Active Chromatin Context. *Plos Genet*. 8:e1002646. doi:10.1371/journal.pgen.1002646.

Alekseyenko, A.A., S. Peng, E. Larschan, A.A. Gorchakov, O.-K. Lee, P. Kharchenko, S.D. McGrath, C.I. Wang, E.R. Mardis, P.J. Park, and M.I. Kuroda. 2008. A Sequence Motif within Chromatin Entry Sites Directs MSL Establishment on the Drosophila X Chromosome. *Cell*. 134:599–609. doi:10.1016/j.cell.2008.06.033.

Alipour, E., and J.F. Marko. 2012. Self-organization of domain structures by DNA-loop-extruding enzymes. *Nucleic Acids Research*. 40:11202–11212. doi:10.1093/nar/gks925.

Allen, B.L., and D.J. Taatjes. 2015. The Mediator complex: a central integrator of transcription. *Nat Rev Mol Cell Bio*. 16:155–166. doi:10.1038/nrm3951.

Allison, L.A., J.K. Wong, V.D. Fitzpatrick, M. Moyle, and C.J. Ingles. 1988. The C-terminal domain of the largest subunit of RNA polymerase II of Saccharomyces cerevisiae, Drosophila melanogaster, and mammals: a conserved structure with an essential function. *Mol Cell Biol*. 8:321–329. doi:10.1128/mcb.8.1.321.

Ameur, A., A. Zaghlool, J. Halvardson, A. Wetterbom, U. Gyllensten, L. Cavelier, and L. Feuk. 2011. Total RNA sequencing reveals nascent transcription and widespread co-transcriptional splicing in the human brain. *Nat Struct Mol Biol*. 18:1435–1440. doi:10.1038/nsmb.2143.

Anchimiuk, A., V.S. Lioy, A. Minnen, F. Boccard, and S. Gruber. 2020. Fine-tuning of the Smc flux facilitates chromosome organization in B. subtilis. *Biorxiv*. 2020.12.04.411900. doi:10.1101/2020.12.04.411900.

Anders, S., P.T. Pyl, and W. Huber. 2015. HTSeq—a Python framework to work with high-throughput sequencing data. *Bioinformatics*. 31:166–169. doi:10.1093/bioinformatics/btu638.

Anderson, E.C., P.A. Frankino, R. Higuchi-Sanabria, Q. Yang, Q. Bian, K. Podshivalova, A. Shin, C. Kenyon, A. Dillin, and B.J. Meyer. 2019. X Chromosome Domain Architecture Regulates Caenorhabditis elegans Lifespan but Not Dosage Compensation. *Developmental Cell*. 51:192-207.e6. doi:10.1016/j.devcel.2019.08.004.

Andrews, E.A., J. Palecek, J. Sergeant, E. Taylor, A.R. Lehmann, and F.Z. Watts. 2005. Nse2, a Component of the Smc5-6 Complex, Is a SUMO Ligase Required for the Response to DNA Damage. *Mol Cell Biol*. 25:185–196. doi:10.1128/mcb.25.1.185-196.2005.

Arumugam, P., S. Gruber, K. Tanaka, C.H. Haering, K. Mechtler, and K. Nasmyth. 2003. ATP hydrolysis is required for cohesin's association with chromosomes. *Current Biology*. 13:1941–1953. doi:10.1016/j.cub.2003.10.036.

Askjaer, P. 2014. Modern techniques for the analysis of chromatin and nuclear organization in C. elegans. *WormBook*. 1–35. doi:10.1895/wormbook.1.169.1.

Bahry, E., L. Breimann, L. Epstein, K. Kolyvanov, K.I.S. Harrington, T. Lionnet, and S. Preibisch. 2021. RS-FISH: Precise, interactive and scalable smFISH spot detection using Radial Symmetry. *Biorxiv*. 2021.03.09.434205. doi:10.1101/2021.03.09.434205.

Bakker, R., M. Mani, and R.W. Carthew. 2020. The Wg and Dpp morphogens regulate gene expression by modulating the frequency of transcriptional bursts. *eLife*. 9:R429-26. doi:10.7554/elife.56076.

Banani, S.F., H.O. Lee, A.A. Hyman, and M.K. Rosen. 2017. Biomolecular condensates: organizers of cellular biochemistry. *Nat Rev Mol Cell Bio*. 18:285–298. doi:10.1038/nrm.2017.7.

Banigan, E.J., and L.A. Mirny. 2020. The interplay between asymmetric and symmetric DNA loop extrusion. *Elife*. 9:e63528. doi:10.7554/elife.63528.

Bao, K., and S. Jia. 2019. Noncatalytic Function of a JmjC Domain Protein Disrupts Heterochromatin. *Epigenetics Insights*. 12:2516865719862249. doi:10.1177/2516865719862249.

Bao, Z., J.I. Murray, T. Boyle, S.L. Ooi, M.J. Sandel, and R.H. Waterston. 2006. Automated cell lineage tracing in Caenorhabditis elegans. *Proceedings of the National Academy of Sciences*. 103:2707–2712. doi:10.1073/pnas.0511111103.

Barr, M.L., and E.G. Bertram. 1949. A Morphological Distinction between Neurones of the Male and Female, and the Behaviour of the Nucleolar Satellite during Accelerated Nucleoprotein Synthesis. *Nature*. 163:676–677. doi:10.1038/163676a0.

Barski, A., S. Cuddapah, K. Cui, T.-Y. Roh, D.E. Schones, Z. Wang, G. Wei, I. Chepelev, and K. Zhao. 2007. High-Resolution Profiling of Histone Methylations in the Human Genome. *Cell*. 129:823–837. doi:10.1016/j.cell.2007.05.009.

Bartman, C.R., S.C. Hsu, C.C.S. Hsiung, A. Raj, and G.A. Blobel. 2016. Enhancer Regulation of Transcriptional Bursting Parameters Revealed by Forced Chromatin Looping. *Molecular Cell*. 1–12. doi:10.1016/j.molcel.2016.03.007.

Bastet, L., P. Turcotte, J.T. Wade, and D.A. Lafontaine. 2018. Maestro of regulation: Riboswitches orchestrate gene expression at the levels of translation, transcription and mRNA decay. *Rna Biol*. 01–34. doi:10.1080/15476286.2018.1451721.

Batenchuk, C., S. St-Pierre, L. Tepliakova, S. Adiga, A. Szuto, N. Kabbani, J.C. Bell, K. Baetz, and M. Kærn. 2011. Chromosomal Position Effects Are Linked to Sir2-Mediated Variation in Transcriptional Burst Size. *Biophys J.* 100:L56–L58. doi:10.1016/j.bpj.2011.04.021.

Battaglia, S., M. Lidschreiber, C. Baejen, P. Torkler, S.M. Vos, and P. Cramer. 2017. RNA-dependent chromatin association of transcription elongation factors and Pol II CTD kinases. *Elife*. 6:e25637. doi:10.7554/elife.25637.

Bauer, C.R., T.A. Hartl, and G. Bosco. 2012. Condensin II Promotes the Formation of Chromosome Territories by Inducing Axial Compaction of Polyploid Interphase Chromosomes. *PLoS genetics*. 8:e1002873-12. doi:10.1371/journal.pgen.1002873.

Baugh, L.R., A.A. Hill, D.K. Slonim, E.L. Brown, and C.P. Hunter. 2003. Composition and dynamics of the Caenorhabditis elegans early embryonic transcriptome. *Development*. 130:889–900. doi:10.1242/dev.00302.

Beach, D.L., E.D. Salmon, and K. Bloom. 1999. Localization and anchoring of mRNA in budding yeast. *Curr Biol*. 9:569-S1. doi:10.1016/s0960-9822(99)80260-7.

Beck, D.B., H. Oda, S.S. Shen, and D. Reinberg. 2012. PR-Set7 and H4K20me1: at the crossroads of genome integrity, cell cycle, chromosome condensation, and transcription. *Genes & Development*. 26:325–337. doi:10.1101/gad.177444.111.

Belew, M.D., E. Chien, M. Wong, and W.M. Michael. 2021. A global chromatin compaction pathway that represses germline gene expression during starvation. *J Cell Biol*. 220:e202009197. doi:10.1083/jcb.202009197.

Bentley, D.L. 2014. Coupling mRNA processing with transcription in time and space. *Nat Rev Genet*. 15:163–175. doi:10.1038/nrg3662.

Berg, S., D. Kutra, T. Kroeger, C.N. Straehle, B.X. Kausler, C. Haubold, M. Schiegg, J. Ales, T. Beier, M. Rudy, K. Eren, J.I. Cervantes, B. Xu, F. Beuttenmueller, A. Wolny, C. Zhang, U. Koethe, F.A. Hamprecht, and A. Kreshuk. 2019. ilastik: interactive machine learning for (bio)image analysis. *Nat Methods*. 16:1226–1232. doi:10.1038/s41592-019-0582-9.

Bertrand, E., P. Chartrand, M. Schaefer, S.M. Shenoy, R.H. Singer, and R.M. Long. 1998. Localization of ASH1 mRNA particles in living yeast. *Molecular Cell*. 2:437–445. doi:10.1016/s1097-2765(00)80143-4.

Bhalla, N., S. Biggins, and A.W. Murray. 2002. Mutation of YCS4, a Budding Yeast Condensin Subunit, Affects Mitotic and Nonmitotic Chromosome Behavior. *Mol Biol Cell*. 13:632–645. doi:10.1091/mbc.01-05-0264.

Bian, Q., E.C. Anderson, Q. Yang, and B.J. Meyer. 2020. Histone H3K9 methylation promotes formation of genome compartments in Caenorhabditis elegans via chromosome compaction and perinuclear anchoring. *Proc National Acad Sci*. 58:202002068. doi:10.1073/pnas.2002068117.

Bickmore, W.A. 2012. The Spatial Organization of the Human Genome. *Annu Rev Genom Hum G*. 14:67–84. doi:10.1146/annurev-genom-091212-153515.

Bicknell, A.A., and E.P. Ricci. 2017. When mRNA translation meets decay. *Biochem Soc T*. 45:339–351. doi:10.1042/bst20160243.

Blewitt, M.E., A.-V. Gendrel, Z. Pang, D.B. Sparrow, N. Whitelaw, J.M. Craig, A. Apedaile, D.J. Hilton, S.L. Dunwoodie, N. Brockdorff, G.F. Kay, and E. Whitelaw. 2008. SmcHD1, containing a structural-maintenance-of-chromosomes hinge domain, has a critical role in X inactivation. *Nat Genet*. 40:663–669. doi:10.1038/ng.142.

Boehning, M., C. Dugast-Darzacq, M. Rankovic, A.S. Hansen, T. Yu, H. Marie-Nelly, D.T. McSwiggen, G. Kokic, G.M. Dailey, P. Cramer, X. Darzacq, and M. Zweckstetter. 2018. RNA polymerase II clustering through carboxy-terminal domain phase separation. *Nat Struct Mol Biol*. 25:833–840. doi:10.1038/s41594-018-0112-y.

Boija, A., I.A. Klein, B.R. Sabari, A. Dall'Agnese, E.L. Coffey, A.V. Zamudio, C.H. Li, K. Shrinivas, J.C. Manteiga, N.M. Hannett, B.J. Abraham, L.K. Afeyan, Y.E. Guo, J.K. Rimel, C.B. Fant, J. Schuijers, T.I. Lee, D.J. Taatjes, and R.A. Young. 2018. Transcription Factors Activate Genes through the Phase-Separation Capacity of Their Activation Domains. *Cell*. 175:1842-1855.e16. doi:10.1016/j.cell.2018.10.042.

Bolková, J., and C. Lanctôt. 2016. Quantitative gene expression analysis in Caenorhabditis elegans using single molecule RNA FISH. *Methods (San Diego, Calif.)*. 98:42–49. doi:10.1016/j.ymeth.2015.11.008.

Borgmann, L.A.K.K., H. Hummel, M.H. Ulbrich, and P.L. Graumann. 2013. SMC condensation centers in Bacillus subtilis are dynamic structures. *Journal of bacteriology*. 195:2136–2145. doi:10.1128/jb.02097-12.

Borrie, M.S., J.S. Campor, H. Joshi, and M.R. Gartenberg. 2017. Binding, sliding, and function of cohesin during transcriptional activation. *Proceedings of the National Academy of Sciences*. 114:E1062–E1071. doi:10.1073/pnas.1617309114.

Bortle, K.V., M.H. Nichols, L. Li, C.-T. Ong, N. Takenaka, Z.S. Qin, and V.G. Corces. 2014. Insulator function and topological domain border strength scale with architectural protein occupancy. *Genome biology*. 15:R82-18. doi:10.1186/gb-2014-15-5-r82.

Bothma, J.P., H.G. Garcia, E. Esposito, G. Schlissel, T. Gregor, and M. Levine. 2014. Dynamic regulation of eve stripe 2 expression reveals transcriptional bursts in living Drosophila embryos. *Proceedings of the National Academy of Sciences of the United States of America*. 111:10598–10603. doi:10.1073/pnas.1410022111.

Boulin, T., J.F. Etchberger, and O. Hobert. 2006. Reporter gene fusions. *WormBook*. 1–23. doi:10.1895/wormbook.1.106.1.

Bouwman, B.A., and W. de Laat. 2015. Getting the genome in shape: the formation of loops, domains and compartments. *Genome Biol*. 16:154. doi:10.1186/s13059-015-0730-1.

Branco, M.R., and A. Pombo. 2006. Intermingling of Chromosome Territories in Interphase Suggests Role in Translocations and Transcription-Dependent Associations. *PLoS Biology*. 4:e138-9. doi:10.1371/journal.pbio.0040138.

Brandão, H.B., Z. Ren, X. Karaboja, L.A. Mirny, and X. Wang. 2020. DNA-loop extruding SMC complexes can traverse one another in vivo. *Biorxiv*. 2020.10.26.356329. doi:10.1101/2020.10.26.356329.

Branzei, D., J. Sollier, G. Liberi, X. Zhao, D. Maeda, M. Seki, T. Enomoto, K. Ohta, and M. Foiani. 2006. Ubc9- and Mms21-Mediated Sumoylation Counteracts Recombinogenic Events at Damaged Replication Forks. *Cell*. 127:509–522. doi:10.1016/j.cell.2006.08.050.

Breimann, L., A.K. Morao, J. Kim, D.S. Jimenez, N. Maryn, K. Bikkasani, M.J. Carrozza, S.E. Albritton, M. Kramer, L.A. Street, K. Cerimi, V.-F. Schumann, E. Bahry, S. Preibisch, A. Woehler, and S. Ercan. 2021. A noncatalytic activity of the H4K20 demethylase DPY-21 regulates condensin DC binding. *Biorxiv*. 2021.04.11.438056. doi:10.1101/2021.04.11.438056.

Breimann, L., F. Preusser, and S. Preibisch. 2019. Light-microscopy methods in C. elegans research. *Current Opinion in Systems Biology*. 13:82–92. doi:10.1016/j.coisb.2018.11.004.

Brejc, K., Q. Bian, S. Uzawa, B.S. Wheeler, E.C. Anderson, D.S. King, P.J. Kranzusch, C.G. Preston, and B.J. Meyer. 2017. Dynamic Control of X Chromosome Conformation and Repression by a Histone H4K20 Demethylase. *Cell*. 171:85-102.e23. doi:10.1016/j.cell.2017.07.041.

Briggs, K., and C.J. Fischer. 2014. All motors have to decide is what to do with the DNA that is given them. *Biomol Concepts*. 5:383–395. doi:10.1515/bmc-2014-0017.

Britton, R.A., D.C.-H. Lin, and A.D. Grossman. 1998. Characterization of a prokaryotic SMC protein involved in chromosome partitioning. *Gene Dev*. 12:1254–1259. doi:10.1101/gad.12.9.1254.

Brockdorff, N., A. Ashworth, G.F. Kay, P. Cooper, S. Smith, V.M. McCabe, D.P. Norris, G.D. Penny, D. Patel, and S. Rastan. 1991. Conservation of position and exclusive expression of mouse Xist from the inactive X chromosome. *Nature*. 351:329–331. doi:10.1038/351329a0.

Brockdorff, N., J.S. Bowness, and G. Wei. 2020. Progress toward understanding chromosome silencing by Xist RNA. *Gene Dev*. 34:733–744. doi:10.1101/gad.337196.120.

Broitman-Maduro, G., and M.F. Maduro. 2011. In situ Hybridization of Embryos with Antisense RNA Probes. Elsevier Inc. 253–270.

Brown, C.J., A. Ballabio, J.L. Rupert, R.G. Lafreniere, M. Grompe, R. Tonlorenzi, and H.F. Willard. 1991. A gene from the region of the human X inactivation centre is expressed exclusively from the inactive X chromosome. *Nature*. 349:38–44. doi:10.1038/349038a0.

Buckley, M.S., and J.T. Lis. 2014. Imaging RNA Polymerase II transcription sites in living cells. *Current opinion in genetics & development*. 25:126–130. doi:10.1016/j.gde.2014.01.002.

Bürmann, F., B.-G. Lee, T. Than, L. Sinn, F.J. O'Reilly, S. Yatskevich, J. Rappsilber, B. Hu, K. Nasmyth, and J. Löwe. 2019. A folded conformation of MukBEF and cohesin. *Nat Struct Mol Biol*. 26:227–236. doi:10.1038/s41594-019-0196-z.

Cacciatore, Á.S., and B.D. Rowland. 2019. Loop formation by SMC complexes: turning heads, bending elbows, and fixed anchors. *Current opinion in genetics & development*. 55:11–18. doi:10.1016/j.gde.2019.04.010.

Cai, L., C.K. Dalal, and M.B. Elowitz. 2008. Frequency-modulated nuclear localization bursts coordinate gene regulation. *Nature*. 455:485–490. doi:10.1038/nature07292.

Calvo, O., and J.L. Manley. 2003. Strange bedfellows: polyadenylation factors at the promoter. *Gene Dev*. 17:1321–1327. doi:10.1101/gad.1093603.

Cavalli, G., and E. Heard. 2019. Advances in epigenetics link genetics to the environment and disease. *Nature*. 571:489–499. doi:10.1038/s41586-019-1411-0.

Chalfie, M., Y. Tu, G. Euskirchen, W. Ward, and D. Prasher. 1994. Green fluorescent protein as a marker for gene expression. *Science*. 263:802–805. doi:10.1126/science.8303295.

Chan, K.-L., M.B. Roig, B. Hu, F. Beckouët, J. Metson, and K. Nasmyth. 2012. Cohesin's DNA Exit Gate Is Distinct from Its Entrance Gate and Is Regulated by Acetylation. *Cell*. 150:961–974. doi:10.1016/j.cell.2012.07.028.

Chan, R.C., A.F. Severson, and B.J. Meyer. 2004. Condensin restructures chromosomes in preparation for meiotic divisions. *J Cell Biology*. 167:613–625. doi:10.1083/jcb.200408061.

Chao, L.F.-I., M. Singh, J. Thompson, J.R. Yates, and K.A. Hagstrom. 2017. An SMC-like protein binds and regulates Caenorhabditis elegans condensins. *PLoS genetics*. 13:e1006614. doi:10.1371/journal.pgen.1006614.

Chao, W.C.H., Y. Murayama, S. Muñoz, A. Costa, F. Uhlmann, and M.R. Singleton. 2015. Structural Studies Reveal the Functional Modularity of the Scc2-Scc4 Cohesin Loader. *Cell Reports*. 12:719–725. doi:10.1016/j.celrep.2015.06.071.

Chapard, C., R. Jones, T. van Oepen, J.C. Scheinost, and K. Nasmyth. 2018. The topology of DNA entrapment by cohesin rings. *Biorxiv*. 495762. doi:10.1101/495762.

Charles, S., G. Aubry, H.-T. Chou, A.B. Paaby, and H. Lu. 2020. High-Temporal-Resolution smFISH Method for Gene Expression Studies in Caenorhabditis elegans Embryos. *Anal Chem*. doi:10.1021/acs.analchem.0c02966.

Charlesworth, B. 1996. The evolution of chromosomal sex determination and dosage compensation. *Curr Biol*. 6:149–162. doi:10.1016/s0960-9822(02)00448-7.

Chen, F.X., E.R. Smith, and A. Shilatifard. 2018. Born to run: control of transcription elongation by RNA polymerase II. *Nat Rev Mol Cell Bio*. 19:464–478. doi:10.1038/s41580-018-0010-5.

Chen, K.H., A.N. Boettiger, J.R. Moffitt, S. Wang, and X. Zhuang. 2015. Spatially resolved, highly multiplexed RNA profiling in single cells. *Science*. 348:aaa6090. doi:10.1126/science.aaa6090.

Chen, L.-F., Y.T. Lin, D.A. Gallegos, M.F. Hazlett, M. Gómez-Schiavon, M.G. Yang, B. Kalmeta, A.S. Zhou, L. Holtzman, C.A. Gersbach, J. Grandl, N.E. Buchler, and A.E. West. 2019. Enhancer Histone Acetylation Modulates Transcriptional Bursting Dynamics of Neuronal Activity-Inducible Genes. *Cell Reports*. 26:1174-1188.e5. doi:10.1016/j.celrep.2019.01.032.

Chen, R., T. Down, and J. Ahringer. 2013. The landscape of RNA polymerase II transcription initiation in C. elegans reveals a novel enhancer architecture. *Epigenet Chromatin*. 6:O21. doi:10.1186/1756-8935-6-s1-o21.

Cheung, A.C.M., and P. Cramer. 2011. Structural basis of RNA polymerase II backtracking, arrest and reactivation. *Nature*. 471:249–253. doi:10.1038/nature09785.

Cho, W.-K., J.-H. Spille, M. Hecht, C. Lee, C. Li, V. Grube, and I.I. Cisse. 2018. Mediator and RNA polymerase II clusters associate in transcription-dependent condensates. *Science*. 361:412–415. doi:10.1126/science.aar4199.

Chong, S., C. Dugast-Darzacq, Z. Liu, P. Dong, G.M. Dailey, C. Cattoglio, A. Heckert, S. Banala, L. Lavis, X. Darzacq, and R. Tjian. 2018. Imaging dynamic and selective low-complexity domain interactions that control gene transcription. *Science*. 361:eaar2555. doi:10.1126/science.aar2555.

Choppakatla, P., B. Dekker, E.E. Cutts, A. Vannini, J. Dekker, and H. Funabiki. 2020. Linker histone H1.8 inhibits chromatin-binding of condensins and DNA topoisomerase II to tune chromosome compaction and individualization. *Biorxiv*. 2020.12.20.423657. doi:10.1101/2020.12.20.423657.

Chu, D.S., H.E. Dawes, J.D. Lieb, R.C. Chan, A.F. Kuo, and B.J. Meyer. 2002. A molecular link between gene-specific and chromosome-wide transcriptional repression. *Genes & Development*. 16:796–805. doi:10.1101/gad.972702.

Chuang, P.-T., D.G. Albertson, and B.J. Meyer. 1994. DPY-27: A chromosome condensation protein homolog that regulates C. elegans dosage compensation through association with the X chromosome. *Cell*. 79:459–474. doi:10.1016/0092-8674(94)90255-0.

Chuang, P.-T., J.D. Lieb, and B.J. Meyer. 1996. Sex-Specific Assembly of a Dosage Compensation Complex on the Nematode X Chromosome. *Science*. 274:1736–1739. doi:10.1126/science.274.5293.1736.

Churchman, L.S., and J.S. Weissman. 2011. Nascent transcript sequencing visualizes transcription at nucleotide resolution. *Nature*. 469:368–373. doi:10.1038/nature09652.

Cieśla, M., E. Skowronek, and M. Boguta. 2018. Function of TFIIIC, RNA polymerase III initiation factor, in activation and repression of tRNA gene transcription. *Nucleic Acids Res*. 46:gky656-. doi:10.1093/nar/gky656.

Ciosk, R., M. Shirayama, T. Tanaka, A. Toth, A. Shevchenko, and K. Nasmyth. 2000. Cohesin's binding to chromosomes depends on a separate complex consisting of Scc2 and Scc4 proteins. *Molecular Cell*. 5:243–254. doi:10.1016/s1097-2765(00)80420-7.

Cisse, I.I., I. Izeddin, S.Z. Causse, L. Boudarene, A. Senecal, L. Muresan, C. Dugast-Darzacq, B. Hajj, M. Dahan, and X. Darzacq. 2013. Real-time dynamics of RNA polymerase II clustering in live human cells. *Science*. 341:664–667. doi:10.1126/science.1239053.

Clapier, C.R., J. Iwasa, B.R. Cairns, and C.L. Peterson. 2017. Mechanisms of action and regulation of ATP-dependent chromatin-remodelling complexes. *Nat Rev Mol Cell Bio*. 18:407–422. doi:10.1038/nrm.2017.26.

Coleman, R.A., Z. Liu, X. Darzacq, R. Tjian, R.H. Singer, and T. Lionnet. 2015. Imaging Transcription: Past, Present, and Future. *Cold Spring Harb Sym*. 80:1–8. doi:10.1101/sqb.2015.80.027201.

Colmenares, S.U., J.M. Swenson, S.A. Langley, C. Kennedy, S.V. Costes, and G.H. Karpen. 2017. Drosophila Histone Demethylase KDM4A Has Enzymatic and Non-enzymatic Roles in Controlling Heterochromatin Integrity. *Dev Cell*. 42:156-169.e5. doi:10.1016/j.devcel.2017.06.014.

Colón, W., J. Church, J. Sen, J. Thibeault, H. Trasatti, and K. Xia. 2017. Biological Roles of Protein Kinetic Stability. *Biochemistry-us*. 56:6179–6186. doi:10.1021/acs.biochem.7b00942.

Core, L., and K. Adelman. 2019. Promoter-proximal pausing of RNA polymerase II: a nexus of gene regulation. *Gene Dev*. 33:960–982. doi:10.1101/gad.325142.119.

Core, L.J., J.J. Waterfall, and J.T. Lis. 2008. Nascent RNA Sequencing Reveals Widespread Pausing and Divergent Initiation at Human Promoters. *Science*. 322:1845–1848. doi:10.1126/science.1162228.

Corless, S., and N. Gilbert. 2016. Effects of DNA supercoiling on chromatin architecture. *Biophysical Rev*. 8:245–258. doi:10.1007/s12551-016-0210-1.

Cramer, P. 2019. Organization and regulation of gene transcription. *Nature*. 1–10. doi:10.1038/s41586-019-1517-4.

Cramer, P., D.A. Bushnell, J. Fu, A.L. Gnatt, B. Maier-Davis, N.E. Thompson, R.R. Burgess, A.M. Edwards, P.R. David, and R.D. Kornberg. 2000. Architecture of RNA Polymerase II and Implications for the Transcription Mechanism. *Science*. 288:640–649. doi:10.1126/science.288.5466.640.

Crane, E., Q. Bian, R.P. McCord, B.R. Lajoie, B.S. Wheeler, E.J. Ralston, S. Uzawa, J. Dekker, and B.J. Meyer. 2015. Condensin-driven remodelling of X chromosome topology during dosage compensation. *Nature*. 523:240–244. doi:10.1038/nature14450.

Cremer, T., and C. Cremer. 2001. Chromosome territories, nuclear architecture and gene regulation in mammalian cells. *Nat Rev Genet*. 2:292–301. doi:10.1038/35066075.

Cremer, T., G. Kreth, H. Koester, R.H.A. Fink, R. Heintzmann, M. Cremer, I. Solovei, D. Zink, and C. Cremer. 2000. Chromosome Territories, Interchromatin Domain Compartment, and Nuclear Matrix: An Integrated View of the Functional Nuclear Architecture. *Crit Rev Eukar Gene*. 10:38. doi:10.1615/critreveukargeneexpr.v10.i2.60.

Csankovszki, G., K. Collette, K. Spahl, J. Carey, M. Snyder, E. Petty, U. Patel, T. Tabuchi, H. Liu, I. McLeod, J. Thompson, A. Sarkeshik, A. Sarkesik, J. Yates, B.J. Meyer, and K. Hagstrom. 2009a. Three Distinct Condensin Complexes Control C. elegans Chromosome Dynamics. *Curr Biol*. 19:9–19. doi:10.1016/j.cub.2008.12.006.

Csankovszki, G., P. McDonel, and B.J. Meyer. 2004. Recruitment and spreading of the C. elegans dosage compensation complex along X chromosomes. *Science*. 303:1182–1185. doi:10.1126/science.1092938.

Csankovszki, G., E.L. Petty, and K.S. Collette. 2009b. The worm solution: a chromosome-full of condensin helps gene expression go down. *Chromosome Res*. 17:621–635. doi:10.1007/s10577-009-9061-y.

Cubeñas-Potts, C., M.J. Rowley, X. Lyu, G. Li, E.P. Lei, and V.G. Corces. 2017. Different enhancer classes in Drosophila bind distinct architectural proteins and mediate unique chromatin interactions and 3D architecture. *Nucleic Acids Res*. 45:1714–1730. doi:10.1093/nar/gkw1114.

Cusanovich, D.A., A.J. Hill, D. Aghamirzaie, R.M. Daza, H.A. Pliner, J.B. Berletch, G.N. Filippova, X. Huang, L. Christiansen, W.S. DeWitt, C. Lee, S.G. Regalado, D.F. Read, F.J. Steemers, C.M. Disteche, C. Trapnell, and J. Shendure. 2018. A Single-Cell Atlas of In Vivo Mammalian Chromatin Accessibility. *Cell*. 174:1309-1324.e18. doi:10.1016/j.cell.2018.06.052.

Cuylen, S., and C.H. Haering. 2011. Deciphering condensin action during chromosome segregation. *Trends in cell biology*. 21:552–559. doi:10.1016/j.tcb.2011.06.003.

Cuylen, S., J. Metz, and C.H. Haering. 2011. Condensin structures chromosomal DNA through topological links. *Nature Publishing Group*. 18:894–901. doi:10.1038/nsmb.2087.

Dadiani, M., D. van Dijk, B. Segal, Y. Field, G. Ben-Artzi, T. Raveh-Sadka, M. Levo, I. Kaplow, A. Weinberger, and E. Segal. 2013. Two DNA-encoded strategies for increasing expression with opposing effects on promoter dynamics and transcriptional noise. *Genome Res*. 23:966–976. doi:10.1101/gr.149096.112.

Dahlsveen, I.K., G.D. Gilfillan, V.I. Shelest, R. Lamm, and P.B. Becker. 2006. Targeting Determinants of Dosage Compensation in Drosophila. *Plos Genet*. 2:e5. doi:10.1371/journal.pgen.0020005.

D'Ambrosio, C., C.K. Schmidt, Y. Katou, G. Kelly, T. Itoh, K. Shirahige, and F. Uhlmann. 2008. Identification of cis-acting sites for condensin loading onto budding yeast chromosomes. *Gene Dev*. 22:2215–2227. doi:10.1101/gad.1675708.

Daniels, B.R., T.M. Dobrowsky, E.M. Perkins, S.X. Sun, and D. Wirtz. 2010. MEX-5 enrichment in the C. elegans early embryo mediated by differential diffusion. *Development*. 137:2579–2585. doi:10.1242/dev.051326.

Dar, R.D., B.S. Razooky, A. Singh, T.V. Trimeloni, J.M. McCollum, C.D. Cox, M.L. Simpson, and L.S. Weinberger. 2012. Transcriptional burst frequency and burst size are equally modulated across the human genome. *Proc National Acad Sci*. 109:17454–17459. doi:10.1073/pnas.1213530109.

Darzacq, X., Y. Shav-Tal, V. de Turris, Y. Brody, S.M. Shenoy, R.D. Phair, and R.H. Singer. 2007. In vivo dynamics of RNA polymerase II transcription. *Nat Struct Mol Biol*. 14:796–806. doi:10.1038/nsmb1280.

Daugherty, A.C., R.W. Yeo, J.D. Buenrostro, W.J. Greenleaf, A. Kundaje, and A. Brunet. 2017. Chromatin accessibility dynamics reveal novel functional enhancers in C. elegans. *Genome Res*. 27:2096–2107. doi:10.1101/gr.226233.117.

Davey, N.E. 2019. The functional importance of structure in unstructured protein regions. *Curr Opin Struc Biol*. 56:155–163. doi:10.1016/j.sbi.2019.03.009.

Davidson, I.F., B. Bauer, D. Goetz, W. Tang, G. Wutz, and J.-M. Peters. 2019. DNA loop extrusion by human cohesin. *Science*. 366:1338–1345. doi:10.1126/science.aaz3418.

Davidson, I.F., D. Goetz, M.P. Zaczek, M.I. Molodtsov, P.J.H. in 't Veld, F. Weissmann, G. Litos, D.A. Cisneros, M. Ocampo-Hafalla, R. Ladurner, F. Uhlmann, A. Vaziri, and J. Peters. 2016. Rapid movement and transcriptional re-localization of human cohesin on DNA. *Embo J*. 35:2671–2685. doi:10.15252/embj.201695402.

Davis, T.L., and B.J. Meyer. 1997. SDC-3 coordinates the assembly of a dosage compensation complex on the nematode X chromosome. *Dev Camb Engl*. 124:1019–31.

Dawes, H.E., D.S. Berlin, D.M. Lapidus, C. Nusbaum, T.L. Davis, and B.J. Meyer. 1999. Dosage compensation proteins targeted to X chromosomes by a determinant of hermaphrodite fate. *Science*. 284:1800–1804. doi:10.1126/science.284.5421.1800.

Dekker, J., and L. Mirny. 2016. The 3D Genome as Moderator of Chromosomal Communication. *Cell*. 164:1110–1121. doi:10.1016/j.cell.2016.02.007.

Delaney, C.E., A.T. Chen, J.V. Graniel, K.J. Dumas, and P.J. Hu. 2017. A histone H4 lysine 20 methyltransferase couples environmental cues to sensory neuron control of developmental plasticity. *Development*. 144:dev.145722. doi:10.1242/dev.145722.

DeLong, L., J.D. Plenefisch, R.D. Klein, and B.J. Meyer. 1993. Feedback control of sex determination by dosage compensation revealed through Caenorhabditis elegans sdc-3 mutations. *Genetics*. 133:875–896. doi:10.1093/genetics/133.4.875.

de Wit, E., E.S.M. Vos, S.J.B. Holwerda, C. Valdes-Quezada, M.J.A.M. Verstegen, H. Teunissen, E. Splinter, P.J. Wijchers, P.H.L. Krijger, and W. de Laat. 2015. CTCF Binding Polarity Determines Chromatin Looping. *Mol Cell*. 60:676–684. doi:10.1016/j.molcel.2015.09.023.

Dey, S.S., J.E. Foley, P. Limsirichai, D.V. Schaffer, and A.P. Arkin. 2015. Orthogonal control of expression mean and variance by epigenetic features at different genomic loci. *Mol Syst Biol*. 11:806. doi:10.15252/msb.20145704.

Dickinson, D.J., and B. Goldstein. 2016. CRISPR-Based Methods for Caenorhabditis elegans Genome Engineering. *Genetics*. 202:885–901. doi:10.1534/genetics.115.182162.

Diebold-Durand, M.-L., H. Lee, L.B.R. Avila, H. Noh, H.-C. Shin, H. Im, F.P. Bock, F. Bürmann, A. Durand, A. Basfeld, S. Ham, J. Basquin, B.-H. Oh, and S. Gruber. 2017. Structure of Full-Length SMC and Rearrangements Required for Chromosome Organization. *Molecular Cell*. 67:334-347.e5. doi:10.1016/j.molcel.2017.06.010.

Dixon, J.R., I. Jung, S. Selvaraj, Y. Shen, J.E. Antosiewicz-Bourget, A.Y. Lee, Z. Ye, A. Kim, N. Rajagopal, W. Xie, Y. Diao, J. Liang, H. Zhao, V.V. Lobanenkov, J.R. Ecker, J.A. Thomson, and B. Ren. 2015. Chromatin architecture reorganization during stem cell differentiation. *Nature*. 518:331–336. doi:10.1038/nature14222.

Dixon, J.R., S. Selvaraj, F. Yue, A. Kim, Y. Li, Y. Shen, M. Hu, J.S. Liu, and B. Ren. 2012. Topological domains in mammalian genomes identified by analysis of chromatin interactions. *Nature*. 485:376–380. doi:10.1038/nature11082.

Dokshin, G.A., K.S. Ghanta, K.M. Piscopo, and C.C. Mello. 2018. Robust Genome Editing with Short Single-Stranded and Long, Partially Single-Stranded DNA Donors in Caenorhabditis elegans. *Genetics*. 210:781–787. doi:10.1534/genetics.118.301532.

Donovan, B.T., A. Huynh, D.A. Ball, H.P. Patel, M.G. Poirier, D.R. Larson, M.L. Ferguson, and T.L. Lenstra. 2019. Live-cell imaging reveals the interplay between transcription factors, nucleosomes, and bursting. *Embo J*. 38. doi:10.15252/embj.2018100809.

Dorsett, D. 2007. Roles of the sister chromatid cohesion apparatus in gene expression, development, and human syndromes. *Chromosoma*. 116:1–13. doi:10.1007/s00412-006-0072-6.

Dorsett, D., and M. Merkenschlager. 2013. Cohesin at active genes: a unifying theme for cohesin and gene expression from model organisms to humans. *Curr Opin Cell Biol*. 25:327–333. doi:10.1016/j.ceb.2013.02.003.

Dowen, J.M., S. Bilodeau, D.A. Orlando, M.R. Hübner, B.J. Abraham, D.L. Spector, and R.A. Young. 2013. Multiple Structural Maintenance of Chromosome Complexes at Transcriptional Regulatory Elements. *STEMCR*. 1:371–378. doi:10.1016/j.stemcr.2013.09.002.

Dumas, K.J., C.E. Delaney, S. Flibotte, D.G. Moerman, G. Csankovszki, and P.J. Hu. 2013. Unexpected Role for Dosage Compensation in the Control of Dauer Arrest, Insulin-Like Signaling, and FoxO Transcription Factor Activity in Caenorhabditis elegans. *Genetics*. 194:619–629. doi:10.1534/genetics.113.149948.

Dunlap, D., R. Yokoyama, H. Ling, H.-Y. Sun, K. McGill, S. Cugusi, and J.C. Lucchesi. 2012. Distinct contributions of MSL complex subunits to the transcriptional enhancement responsible for dosage compensation in Drosophila. *Nucleic Acids Res*. 40:11281–11291. doi:10.1093/nar/gks890.

Durand, N.C., M.S. Shamim, I. Machol, S.S.P. Rao, M.H. Huntley, E.S. Lander, and E.L. Aiden. 2016. Juicer Provides a One-Click System for Analyzing Loop-Resolution Hi-C Experiments. *Cell Syst*. 3:95–98. doi:10.1016/j.cels.2016.07.002.

Eaton, J.D., and S. West. 2020. Termination of Transcription by RNA Polymerase II: BOOM! *Trends Genet*. 36:664–675. doi:10.1016/j.tig.2020.05.008.

Edgar, L.G., N. Wolf, and W.B. Wood. 1994. Early transcription in Caenorhabditis elegans embryos. *Dev Camb Engl*. 120:443–51.

Eeftens, J.M., S. Bisht, J. Kerssemakers, M. Kschonsak, C.H. Haering, and C. Dekker. 2017. Real-time detection of condensin-driven DNA compaction reveals a multistep binding mechanism. *Embo J*. 36:3448–3457. doi:10.15252/embj.201797596.

Elbatsh, A.M.O., E. Kim, J.M. Eeftens, J.A. Raaijmakers, R.H. van der Weide, A. García-Nieto, S. Bravo, M. Ganji, J.U. de Bos, H. Teunissen, R.H. Medema, E. de Wit, C.H. Haering, C. Dekker, and B.D. Rowland. 2019. Distinct Roles for Condensin's Two ATPase Sites in Chromosome Condensation. *Molecular Cell*. 76:724-737.e5. doi:10.1016/j.molcel.2019.09.020.

Eldar, A., and M.B. Elowitz. 2010. Functional roles for noise in genetic circuits. *Nature*. 467:167–173. doi:10.1038/nature09326.

Elowitz, M.B., A.J. Levine, E.D. Siggia, and P.S. Swain. 2002. Stochastic gene expression in a single cell. *Science*. 297:1183–1186. doi:10.1126/science.1070919.

Ercan, S. 2015. Mechanisms of x chromosome dosage compensation. *Journal of Genomics*. 3:1–19. doi:10.7150/jgen.10404.

Ercan, S., L.L. Dick, and J.D. Lieb. 2009. The C. elegans Dosage Compensation Complex Propagates Dynamically and Independently of X Chromosome Sequence. *Current Biology*. 19:1777–1787. doi:10.1016/j.cub.2009.09.047.

Ercan, S., P.G. Giresi, C.M. Whittle, X. Zhang, R.D. Green, and J.D. Lieb. 2007. X chromosome repression by localization of the C. elegans dosage compensation machinery to sites of transcription initiation. *Nature Genetics*. 39:403–408. doi:10.1038/ng1983.

Ernst, J., P. Kheradpour, T.S. Mikkelsen, N. Shoresh, L.D. Ward, C.B. Epstein, X. Zhang, L. Wang, R. Issner, M. Coyne, M. Ku, T. Durham, M. Kellis, and B.E. Bernstein. 2011. Mapping and analysis of chromatin state dynamics in nine human cell types. *Nature*. 473:43–49. doi:10.1038/nature09906.

Fan, X., S.D. Henau, J. Feinstein, S.I. Miller, B. Han, C. Frøkjær-Jensen, and E.E. Griffin. 2019. SapTrap assembly of C. elegans MosSCI transgene vectors. *bioRxiv*. 7:e38198-38. doi:10.1101/805507.

Farcas, A.-M., P. Uluocak, W. Helmhart, and K. Nasmyth. 2011. Cohesin's Concatenation of Sister DNAs Maintains Their Intertwining. *Mol Cell*. 44:97–107. doi:10.1016/j.molcel.2011.07.034.

Femino, A.M., F.S. Fay, K. Fogarty, and R.H. Singer. 1998. Visualization of Single RNA Transcripts in Situ. *Science*. 280:585–590. doi:10.1126/science.280.5363.585.

Fierro, A.T. del, B. den Hamer, N. Jansz, K. Chen, T. Beck, H. Vanyai, N. Benetti, A.D. Gurzau, L. Daxinger, S. Xue, T.T.N. Ly, I. Wanigasuriya, K. Breslin, H. Oey, Y. Krom, D. van der Hoorn, L.F. Bouwman, M.E. Ritchie, B. Reversade, F. Prin, T. Mohun, S.M. van der Maarel, E. McGlinn,

J.M. Murphy, A. Keniry, J.C. de Greef, and M.E. Blewitt. 2021. SMCHD1 has separable roles in chromatin architecture and gene silencing that could be targeted in disease. doi:10.1101/2021.05.12.443934.

Fischler, M.A., and R.C. Bolles. 1987. Random Sample Consensus: A Paradigm for Model Fitting with Applications to Image Analysis and Automated Cartography. Morgan Kaufmann, San Francisco (CA). 726–740.

Foot, N., T. Henshall, and S. Kumar. 2017. Ubiquitination and the Regulation of Membrane Proteins. *Physiol Rev*. 97:253–281. doi:10.1152/physrev.00012.2016.

Fousteri, M.I., and A.R. Lehmann. 2000. A novel SMC protein complex in Schizosaccharomyces pombe contains the Rad18 DNA repair protein. *Embo J*. 19:1691–1702. doi:10.1093/emboj/19.7.1691.

Friedrich, D., L. Friedel, A. Finzel, A. Herrmann, S. Preibisch, and A. Loewer. 2019. Stochastic transcription in the p53-mediated response to DNA damage is modulated by burst frequency. *Molecular Systems Biology*. 15:e9068. doi:10.15252/msb.20199068.

Frietze, S., and P.J. Farnham. 2011. A Handbook of Transcription Factors. *Subcell Biochem*. 52:261–277. doi:10.1007/978-90-481-9069-0_12.

Frøkjær-Jensen, C., M.W. Davis, M. Ailion, and E.M. Jorgensen. 2012. Improved Mos1-mediated transgenesis in C. elegans. *Nature Publishing Group*. 9:117–118. doi:10.1038/nmeth.1865.

Frøkjær-Jensen, C., M.W. Davis, C.E. Hopkins, B.J. Newman, J.M. Thummel, S.-P. Olesen, M. Grunnet, and E.M. Jorgensen. 2008. Single-copy insertion of transgenes in Caenorhabditis elegans. *Nature Genetics*. 40:1375–1383. doi:10.1038/ng.248.

Fudenberg, G., N. Abdennur, M. Imakaev, A. Goloborodko, and L.A. Mirny. 2017. Emerging Evidence of Chromosome Folding by Loop Extrusion. *Cold Spring Harbor symposia on quantitative biology*. 82:45–55. doi:10.1101/sqb.2017.82.034710.

Fudenberg, G., M. Imakaev, C. Lu, A. Goloborodko, N. Abdennur, and L.A. Mirny. 2016. Formation of Chromosomal Domains by Loop Extrusion. *CellReports*. 15:2038–2049. doi:10.1016/j.celrep.2016.04.085.

Fukaya, T., B. Lim, and M. Levine. 2016. Enhancer Control of Transcriptional Bursting. *Cell*. 166:358–368. doi:10.1016/j.cell.2016.05.025.

Gabdank, I., S. Ramakrishnan, A.M. Villeneuve, and A.Z. Fire. 2016. A streamlined tethered chromosome conformation capture protocol. *Bmc Genomics*. 17:274. doi:10.1186/s12864-016-2596-3.

Galupa, R., and E. Heard. 2016. X-Chromosome Inactivation: A Crossroads Between Chromosome Architecture and Gene Regulation. *Annu Rev Genet*. 52:1–32. doi:10.1146/annurev-genet-120116-024611.

Ganji, M., I.A. Shaltiel, S. Bisht, E. Kim, A. Kalichava, C.H. Haering, and C. Dekker. 2018. Real-time imaging of DNA loop extrusion by condensin. *Science*. 360:102–105. doi:10.1126/science.aar7831.

Garcia, H.G., M. Tikhonov, A. Lin, and T. Gregor. 2013. Quantitative Imaging of Transcription in Living Drosophila Embryos Links Polymerase Activity to Patterning. *Curr Biol*. 23:2140–2145. doi:10.1016/j.cub.2013.08.054.

Gassler, J., H.B. Brandao, M. Imakaev, I.M. Flyamer, S. Ladstätter, W.A. Bickmore, J.-M. Peters, L.A. Mirny, and K. Tachibana. 2017. A mechanism of cohesin-dependent loop extrusion organizes zygotic genome architecture. *The EMBO Journal*. 36:3600–3618. doi:10.15252/embj.201798083.

Gause, M., Z. Misulovin, A. Bilyeu, and D. Dorsett. 2010. Dosage-Sensitive Regulation of Cohesin Chromosome Binding and Dynamics by Nipped-B, Pds5, and Wapl. *Molecular and Cellular Biology*. 30:4940–4951. doi:10.1128/mcb.00642-10.

Gdula, M.R., T.B. Nesterova, G. Pintacuda, J. Godwin, Y. Zhan, H. Ozadam, M. McClellan, D. Moralli, F. Krueger, C.M. Green, W. Reik, S. Kriaucionis, E. Heard, J. Dekker, and N. Brockdorff. 2019. The non-canonical SMC protein SmcHD1 antagonises TAD formation and compartmentalisation on the inactive X chromosome. *Nature Communications*. 10:30. doi:10.1038/s41467-018-07907-2.

Gergen, J.P. 1987. Dosage Compensation in Drosophila: Evidence That daughterless and Sex-lethal Control X Chromosome Activity at the Blastoderm Stage of Embryogenesis. *Genetics*. 117:477–85.

Gerlich, D., T. Hirota, B. Koch, J.-M. Peters, and J. Ellenberg. 2006a. Condensin I Stabilizes Chromosomes Mechanically through a Dynamic Interaction in Live Cells. *Current Biology*. 16:333–344. doi:10.1016/j.cub.2005.12.040.

Gerlich, D., B. Koch, F. Dupeux, J.-M. Peters, and J. Ellenberg. 2006b. Live-Cell Imaging Reveals a Stable Cohesin-Chromatin Interaction after but Not before DNA Replication. *Current Biology*. 16:1571–1578. doi:10.1016/j.cub.2006.06.068.

Gibcus, J.H., K. Samejima, A. Goloborodko, I. Samejima, N. Naumova, J. Nuebler, M.T. Kanemaki, L. Xie, J.R. Paulson, W.C. Earnshaw, L.A. Mirny, and J. Dekker. 2018. A pathway for mitotic chromosome formation. *Science*. 359:eaao6135-14. doi:10.1126/science.aao6135.

Giet, R., and D.M. Glover. 2001. Drosophila Aurora B Kinase Is Required for Histone H3 Phosphorylation and Condensin Recruitment during Chromosome Condensation and to Organize the Central Spindle during Cytokinesis. *J Cell Biology*. 152:669–682. doi:10.1083/jcb.152.4.669.

Ginno, P.A., L. Burger, J. Seebacher, V. Iesmantavicius, and D. Schübeler. 2018. Cell cycle-resolved chromatin proteomics reveals the extent of mitotic preservation of the genomic regulatory landscape. *Nature Communications*. 9:4048–12. doi:10.1038/s41467-018-06007-5.

Gladden, J.M., and B.J. Meyer. 2007. A ONECUT Homeodomain Protein Communicates X Chromosome Dose to Specify Caenorhabditis elegans Sexual Fate by Repressing a Sex Switch Gene. *Genetics*. 177:1621–1637. doi:10.1534/genetics.106.061812.

Gligoris, T.G., J.C. Scheinost, F. Bürmann, N. Petela, K.-L. Chan, P. Uluocak, F. Beckouët, S. Gruber, K. Nasmyth, and J. Löwe. 2014. Closing the cohesin ring: Structure and function of its Smc3-kleisin interface. *Science*. 346:963–967. doi:10.1126/science.1256917.

Glynn, E.F., P.C. Megee, H.-G. Yu, C. Mistrot, E. Unal, D.E. Koshland, J.L. DeRisi, and J.L. Gerton. 2004. Genome-Wide Mapping of the Cohesin Complex in the Yeast Saccharomyces cerevisiae. *Plos Biol*. 2:e259. doi:10.1371/journal.pbio.0020259.

Goehring, N.W., C. Hoege, S.W. Grill, and A.A. Hyman. 2011. PAR proteins diffuse freely across the anterior-posterior boundary in polarized C. elegans embryos. *The Journal of cell biology*. 193:583–594. doi:10.1083/jcb.201011094.

Golding, I., J. Paulsson, S.M. Zawilski, and E.C. Cox. 2005. Real-Time Kinetics of Gene Activity in Individual Bacteria. *Cell*. 123:1025–1036. doi:10.1016/j.cell.2005.09.031.

Golfier, S., T. Quail, H. Kimura, and J. Brugues. 2020. Cohesin and condensin extrude DNA loops in a cell cycle-dependent manner. *eLife*. 9. doi:10.7554/elife.53885.

Goloborodko, A., M.V. Imakaev, J.F. Marko, and L. Mirny. 2016a. Compaction and segregation of sister chromatids via active loop extrusion. *eLife*. 5. doi:10.7554/elife.14864.

Goloborodko, A., J.F. Marko, and L.A. Mirny. 2016b. Chromosome Compaction by Active Loop Extrusion. *Biophysical journal*. 110:2162–2168. doi:10.1016/j.bpj.2016.02.041.

Gómez-Marín, C., J.J. Tena, R.D. Acemel, M. López-Mayorga, S. Naranjo, E. de la Calle-Mustienes, I. Maeso, L. Beccari, I. Aneas, E. Vielmas, P. Bovolenta, M.A. Nobrega, J. Carvajal, and J.L. Gómez-Skarmeta. 2015. Evolutionary comparison reveals that diverging CTCF sites are signatures of ancestral topological associating domains borders. *Proc National Acad Sci*. 112:7542–7547. doi:10.1073/pnas.1505463112.

González-Aguilera, C., K. Ikegami, C. Ayuso, A. de Luis, M. Íñiguez, J. Cabello, J.D. Lieb, and P. Askjaer. 2014. Genome-wide analysis links emerin to neuromuscular junction activity in Caenorhabditis elegans. *Genome Biol*. 15:R21. doi:10.1186/gb-2014-15-2-r21.

Gorkin, D.U., I. Barozzi, Y. Zhao, Y. Zhang, H. Huang, A.Y. Lee, B. Li, J. Chiou, A. Wildberg, B. Ding, B. Zhang, M. Wang, J.S. Strattan, J.M. Davidson, Y. Qiu, V. Afzal, J.A. Akiyama, I. Plajzer-Frick, C.S. Novak, M. Kato, T.H. Garvin, Q.T. Pham, A.N. Harrington, B.J. Mannion, E.A. Lee, Y. Fukuda-Yuzawa, Y. He, S. Preissl, S. Chee, J.Y. Han, B.A. Williams, D. Trout, H. Amrhein, H. Yang, J.M. Cherry, W. Wang, K. Gaulton, J.R. Ecker, Y. Shen, D.E. Dickel, A. Visel, L.A. Pennacchio, and B. Ren. 2020. An atlas of dynamic chromatin landscapes in mouse fetal development. *Nature*. 583:744–751. doi:10.1038/s41586-020-2093-3.

Gottesfeld, J.M., and D.J. Forbes. 1997. Mitotic repression of the transcriptional machinery. *Trends Biochem Sci*. 22:197–202. doi:10.1016/s0968-0004(97)01045-1.

Grasser, F., M. Neusser, H. Fiegler, T. Thormeyer, M. Cremer, N.P. Carter, T. Cremer, and S. Muller. 2008. Replication-timing-correlated spatial chromatin arrangements in cancer and in primate interphase nuclei. *J Cell Sci*. 121:1876–1886. doi:10.1242/jcs.026989.

Green, L.C., P. Kalitsis, T.M. Chang, M. Cipetic, J.H. Kim, O. Marshall, L. Turnbull, C.B. Whitchurch, P. Vagnarelli, K. Samejima, W.C. Earnshaw, K.H.A. Choo, and D.F. Hudson. 2012. Contrasting roles of condensin I and condensin II in mitotic chromosome formation. *J Cell Sci*. 125:1591–1604. doi:10.1242/jcs.097790.

Green, R.A., A. Audhya, A. Pozniakovsky, A. Dammermann, H. Pemble, J. Monen, N. Portier, A. Hyman, A. Desai, and K. Oegema. 2008. Expression and imaging of fluorescent proteins in the C. elegans gonad and early embryo. *Caenorhabditis Elegans: Molecular Genetics and Development, Second Edition*. 85:179–218. doi:10.1016/s0091-679x(08)85009-1.

Grimm, J.B., B.P. English, J. Chen, J.P. Slaughter, Z. Zhang, A. Revyakin, R. Patel, J.J. Macklin, D. Normanno, R.H. Singer, T. Lionnet, and L.D. Lavis. 2015. A general method to improve fluorophores for live-cell and single-molecule microscopy. *Nature Methods*. 12:244–250. doi:10.1038/nmeth.3256.

Grimm, J.B., A.K. Muthusamy, Y. Liang, T.A. Brown, W.C. Lemon, R. Patel, R. Lu, J.J. Macklin, P.J. Keller, N. Ji, and L.D. Lavis. 2017. A general method to fine-tune fluorophores for live-cell and in vivo imaging. *Nature Methods*. 14:987–994. doi:10.1038/nmeth.4403.

Gruber, S., C.H. Haering, and K. Nasmyth. 2003. Chromosomal Cohesin Forms a Ring. *Cell*. 112:765–777. doi:10.1016/s0092-8674(03)00162-4.

Grünberg, S., L. Warfield, and S. Hahn. 2012. Architecture of the RNA polymerase II preinitiation complex and mechanism of ATP-dependent promoter opening. *Nat Struct Mol Biol*. 19:788–796. doi:10.1038/nsmb.2334.

Gu, F., Y. Lin, Z. Wang, X. Wu, Z. Ye, Y. Wang, and H. Lan. 2020. Biological roles of LSD1 beyond its demethylase activity. *Cell Mol Life Sci*. 77:3341–3350. doi:10.1007/s00018-020-03489-9.

Guacci, V., D. Koshland, and A. Strunnikov. 1997. A Direct Link between Sister Chromatid Cohesion and Chromosome Condensation Revealed through the Analysis of MCD1 in S. cerevisiae. *Cell*. 91:47–57. doi:10.1016/s0092-8674(01)80008-8.

Guizar-Sicairos, M., S.T. Thurman, and J.R. Fienup. 2008. Efficient subpixel image registration algorithms. *Opt Lett*. 33:156. doi:10.1364/ol.33.000156.

Gullerova, M., and N.J. Proudfoot. 2008. Cohesin Complex Promotes Transcriptional Termination between Convergent Genes in S. pombe. *Cell*. 132:983–995. doi:10.1016/j.cell.2008.02.040.

Guo, Y., Q. Xu, D. Canzio, J. Shou, J. Li, D.U. Gorkin, I. Jung, H. Wu, Y. Zhai, Y. Tang, Y. Lu, Y. Wu, Z. Jia, W. Li, M.Q. Zhang, B. Ren, A.R. Krainer, T. Maniatis, and Q. Wu. 2015. CRISPR Inversion of CTCF Sites Alters Genome Topology and Enhancer/Promoter Function. *Cell*. 162:900–910. doi:10.1016/j.cell.2015.07.038.

Guo, Y.E., J.C. Manteiga, J.E. Henninger, B.R. Sabari, A. Dall'Agnese, N.M. Hannett, J.-H. Spille, L.K. Afeyan, A.V. Zamudio, K. Shrinivas, B.J. Abraham, A. Boija, T.-M. Decker, J.K. Rimel, C.B. Fant, T.I. Lee, I.I. Cisse, P.A. Sharp, D.J. Taatjes, and R.A. Young. 2019. Pol II phosphorylation regulates a switch between transcriptional and splicing condensates. *Nature*. 572:543–548. doi:10.1038/s41586-019-1464-0.

Gutierrez-Escribano, P., S. Hormeño, J. Madariaga-Marcos, R. Solé-Soler, F.J. O'Reilly, K. Morris, C. Aicart-Ramos, R. Aramayo, A. Montoya, H. Kramer, J. Rappsilber, J. Torres-Rosell, F. Moreno-Herrero, and L. Aragon. 2020. Purified Smc5/6 Complex Exhibits DNA Substrate Recognition and Compaction. *Mol Cell*. 80:1039-1054.e6. doi:10.1016/j.molcel.2020.11.012.

Haarhuis, J.H.I., R.H. van der Weide, V.A. Blomen, J.O. Yáñez-Cuna, M. Amendola, M.S. van Ruiten, P.H.L. Krijger, H. Teunissen, R.H. Medema, B. van Steensel, T.R. Brummelkamp, E. de Wit, and B.D. Rowland. 2017. The Cohesin Release Factor WAPL Restricts Chromatin Loop Extension. *Cell*. 169:693-700.e14. doi:10.1016/j.cell.2017.04.013.

Haberle, V., and A. Stark. 2018. Eukaryotic core promoters and the functional basis of transcription initiation. *Nat Rev Mol Cell Bio*. 19:621–637. doi:10.1038/s41580-018-0028-8.

Hadjur, S., L.M. Williams, N.K. Ryan, B.S. Cobb, T. Sexton, P. Fraser, A.G. Fisher, and M. Merkenschlager. 2009. Cohesins form chromosomal cis-interactions at the developmentally regulated IFNG locus. *Nature*. 460:410–413. doi:10.1038/nature08079.

Haering, C.H., A.-M. Farcas, P. Arumugam, J. Metson, and K. Nasmyth. 2008. The cohesin ring concatenates sister DNA molecules. *Nature*. 454:297–301. doi:10.1038/nature07098.

Haering, C.H., J. Löwe, A. Hochwagen, and K. Nasmyth. 2002. Molecular Architecture of SMC Proteins and the Yeast Cohesin Complex. *Mol Cell*. 9:773–788. doi:10.1016/s1097-2765(02)00515-4.

Haeusler, R.A., M. Pratt-Hyatt, P.D. Good, T.A. Gipson, and D.R. Engelke. 2008. Clustering of yeast tRNA genes is mediated by specific association of condensin with tRNA gene transcription complexes. *Gene Dev*. 22:2204–2214. doi:10.1101/gad.1675908.

Hagstrom, K.A., V.F. Holmes, N.R. Cozzarelli, and B.J. Meyer. 2002. C. elegans condensin promotes mitotic chromosome architecture, centromere organization, and sister chromatid segregation during mitosis and meiosis. *Genes & Development*. 16:729–742. doi:10.1101/gad.968302.

Hahn, S. 1998. The Role of TAFs in RNA Polymerase II Transcription. *Cell*. 95:579–582. doi:10.1016/s0092-8674(00)81625-6.

Hallett, S.T., P. Schellenberger, L. Zhou, F. Beuron, E. Morris, J.M. Murray, and A.W. Oliver. 2021. Nse5/6 is a negative regulator of the ATPase activity of the Smc5/6 complex. *Nucleic Acids Res*. 49:gkab234-. doi:10.1093/nar/gkab234.

Halpern, K.B., and S. Itzkovitz. 2016. Single molecule approaches for quantifying transcription and degradation rates in intact mammalian tissues. *Methods*. 98:134–142. doi:10.1016/j.ymeth.2015.11.015.

Halpern, K.B., S. Tanami, S. Landen, M. Chapal, L. Szlak, A. Hutzler, A. Nizhberg, and S. Itzkovitz. 2015. Bursty Gene Expression in the Intact Mammalian Liver. *Molecular Cell*. 1–11. doi:10.1016/j.molcel.2015.01.027.

Hamada, F.N., P.J. Park, P.R. Gordadze, and M.I. Kuroda. 2005. Global regulation of X chromosomal genes by the MSL complex in Drosophila melanogaster. *Gene Dev*. 19:2289–2294. doi:10.1101/gad.1343705.

Hansen, A.S., C. Cattoglio, X. Darzacq, and R. Tjian. 2018. Recent evidence that TADs and chromatin loops are dynamic structures. *Nucleus*. 9:1–18. doi:10.1080/19491034.2017.1389365.

Hansen, A.S., I. Pustova, C. Cattoglio, R. Tjian, and X. Darzacq. 2016. CTCF and cohesin regulate chromatin loop stability with distinct dynamics. *Elife*. 6:e25776. doi:10.7554/elife.25776.

Hara, K., K. Kinoshita, T. Migita, K. Murakami, K. Shimizu, K. Takeuchi, T. Hirano, and H. Hashimoto. 2019. Structural basis of HEAT-kleisin interactions in the human condensin I subcomplex. *EMBO reports*. 20:3963–12. doi:10.15252/embr.201847183.

Harterink, M., D. hyun Kim, T.C. Middelkoop, T.D. Doan, A. van Oudenaarden, and H.C. Korswagen. 2011. Neuroblast migration along the anteroposterior axis of C. elegans is controlled by opposing gradients of Wnts and a secreted Frizzled-related protein. *Development*. 138:2915–2924. doi:10.1242/dev.064733.

Hartl, T.A., S.J. Sweeney, P.J. Knepler, and G. Bosco. 2008. Condensin II Resolves Chromosomal Associations to Enable Anaphase I Segregation in Drosophila Male Meiosis. *Plos Genet*. 4:e1000228. doi:10.1371/journal.pgen.1000228.

Hassler, M., I.A. Shaltiel, and C.H. Haering. 2018. Towards a Unified Model of SMC Complex Function. *Current biology : CB*. 28:R1266–R1281. doi:10.1016/j.cub.2018.08.034.

Hassler, M., I.A. Shaltiel, M. Kschonsak, B. Simon, F. Merkel, L. Thärichen, H.J. Bailey, J. Macošek, S. Bravo, J. Metz, J. Hennig, and C.H. Haering. 2019. Structural Basis of an Asymmetric Condensin ATPase Cycle. *Mol Cell*. 74:1175-1188.e9. doi:10.1016/j.molcel.2019.03.037.

Hauer, M.H., and S.M. Gasser. 2017. Chromatin and nucleosome dynamics in DNA damage and repair. *Gene Dev*. 31:2204–2221. doi:10.1101/gad.307702.117.

Hazbun, T.R., L. Malmström, S. Anderson, B.J. Graczyk, B. Fox, M. Riffle, B.A. Sundin, J.D. Aranda, W.H. McDonald, C.-H. Chiu, B.E. Snydsman, P. Bradley, E.G.D. Muller, S. Fields, D. Baker, J.R. Yates, and T.N. Davis. 2003. Assigning Function to Yeast Proteins by Integration of Technologies. *Mol Cell*. 12:1353–1365. doi:10.1016/s1097-2765(03)00476-3.

He, J., L. Shen, M. Wan, O. Taranova, H. Wu, and Y. Zhang. 2013. Kdm2b maintains murine embryonic stem cell status by recruiting PRC1 complex to CpG islands of developmental genes. *Nat Cell Biol*. 15:373–384. doi:10.1038/ncb2702.

Heger, P., B. Marin, and E. Schierenberg. 2009. Loss of the insulator protein CTCF during nematode evolution. *Bmc Mol Biol*. 10:84. doi:10.1186/1471-2199-10-84.

Heintzman, N.D., G.C. Hon, R.D. Hawkins, P. Kheradpour, A. Stark, L.F. Harp, Z. Ye, L.K. Lee, R.K. Stuart, C.W. Ching, K.A. Ching, J.E. Antosiewicz-Bourget, H. Liu, X. Zhang, R.D. Green, V.V. Lobanenkov, R. Stewart, J.A. Thomson, G.E. Crawford, M. Kellis, and B. Ren. 2009. Histone modifications at human enhancers reflect global cell-type-specific gene expression. *Nature*. 459:108–112. doi:10.1038/nature07829.

Hench, J., J. Henriksson, M. Lüppert, and T.R. Bürglin. 2009. Spatio-temporal reference model of Caenorhabditis elegans embryogenesis with cell contact maps. *Developmental Biology*. 333:1–13. doi:10.1016/j.ydbio.2009.06.014.

Hendy, O., J. Campbell, J.D. Weissman, D.R. Larson, and D.S. Singer. 2017. Differential context-specific impact of individual core promoter elements on transcriptional dynamics. *Mol Biol Cell*. 28:3360–3370. doi:10.1091/mbc.e17-06-0408.

Herzel, L., D.S.M. Ottoz, T. Alpert, and K.M. Neugebauer. 2017. Splicing and transcription touch base: co-transcriptional spliceosome assembly and function. *Nat Rev Mol Cell Bio*. 18:637–650. doi:10.1038/nrm.2017.63.

Hilfiker, A., D. Hilfiker-Kleiner, A. Pannuti, and J.C. Lucchesi. 1997. mof, a putative acetyl transferase gene related to the Tip60 and MOZ human genes and to the SAS genes of yeast, is required for dosage compensation in Drosophila. *Embo J*. 16:2054–2060. doi:10.1093/emboj/16.8.2054.

Hinshaw, S.M., V. Makrantoni, S.C. Harrison, and A.L. Marston. 2017. The Kinetochore Receptor for the Cohesin Loading Complex. *Cell*. 171:72-84.e13. doi:10.1016/j.cell.2017.08.017.

Hinshaw, S.M., V. Makrantoni, A. Kerr, A.L. Marston, and S.C. Harrison. 2015. Structural evidence for Scc4-dependent localization of cohesin loading. *Elife*. 4:e06057. doi:10.7554/elife.06057.

Hirano, M., and T. Hirano. 2004. Positive and negative regulation of SMC-DNA interactions by ATP and accessory proteins. *Embo Journal*. 23:2664–2673. doi:10.1038/sj.emboj.7600264.

Hirano, T. 2002. The ABCs of SMC proteins: two-armed ATPases for chromosome condensation, cohesion, and repair. *Genes & Development*. 16:399–414. doi:10.1101/gad.955102.

Hirano, T. 2006. At the heart of the chromosome: SMC proteins in action. *Nature Reviews Molecular Cell Biology*. 7:311–322. doi:10.1038/nrm1909.

Hirano, T. 2012. Condensins: universal organizers of chromosomes with diverse functions. *Genes & Development*. 26:1659–1678. doi:10.1101/gad.194746.112.

Hirano, T. 2016. Condensin-Based Chromosome Organization from Bacteria to Vertebrates. *Cell*. 164:847–857. doi:10.1016/j.cell.2016.01.033.

Hirano, T., R. Kobayashi, and M. Hirano. 1997. Condensins, Chromosome Condensation Protein Complexes Containing XCAP-C, XCAP-E and a Xenopus Homolog of the Drosophila Barren Protein. *Cell*. 89:511–521. doi:10.1016/s0092-8674(00)80233-0.

Hiratani, I., T. Ryba, M. Itoh, T. Yokochi, M. Schwaiger, C.-W. Chang, Y. Lyou, T.M. Townes, D. Schübeler, and D.M. Gilbert. 2008. Global Reorganization of Replication Domains During Embryonic Stem Cell Differentiation. *Plos Biol*. 6:e245. doi:10.1371/journal.pbio.0060245.

Hirota, T., D. Gerlich, B. Koch, J. Ellenberg, and J.-M. Peters. 2004. Distinct functions of condensin I and II in mitotic chromosome assembly. *J Cell Sci*. 117:6435–6445. doi:10.1242/jcs.01604.

Hnisz, D., K. Shrinivas, R.A. Young, A.K. Chakraborty, and P.A. Sharp. 2017. A Phase Separation Model for Transcriptional Control. *Cell*. 169:13–23. doi:10.1016/j.cell.2017.02.007.

Ho, J.W.K., Y.L. Jung, T. Liu, B.H. Alver, S. Lee, K. Ikegami, K.-A. Sohn, A. Minoda, M.Y. Tolstorukov, A. Appert, S.C.J. Parker, T. Gu, A. Kundaje, N.C. Riddle, E. Bishop, T.A. Egelhofer, S.S. Hu, A.A. Alekseyenko, A. Rechtsteiner, D. Asker, J.A. Belsky, S.K. Bowman, Q.B. Chen, R.A.-J. Chen, D.S. Day, Y. Dong, A.C. Dose, X. Duan, C.B. Epstein, S. Ercan, E.A. Feingold, F. Ferrari, J.M. Garrigues, N. Gehlenborg, P.J. Good, P. Haseley, D. He, M. Herrmann, M.M. Hoffman, T.E. Jeffers, P.V. Kharchenko, P. Kolasinska-Zwierz, C.V. Kotwaliwale, N. Kumar, S.A. Langley, E.N. Larschan, I. Latorre, M.W. Libbrecht, X. Lin, R. Park, M.J. Pazin, H.N. Pham, A. Plachetka, B. Qin, Y.B. Schwartz, N. Shoresh, P. Stempor, A. Vielle, C. Wang, C.M. Whittle, H. Xue, R.E. Kingston, J.H. Kim, B.E. Bernstein, A.F. Dernburg, V. Pirrotta, M.I. Kuroda, W.S. Noble, T.D. Tullius, M. Kellis, D.M. MacAlpine, S. Strome, S.C.R. Elgin, X.S. Liu, J.D. Lieb, J. Ahringer, G.H. Karpen, and P.J. Park. 2014. Comparative analysis of metazoan chromatin organization. *Nature*. 512:449–452. doi:10.1038/nature13415.

Hodgkin, J. 1983a. X chromosome dosage and gene expression in Caenorhabditis elegans: Two unusual dumpy genes. *Mol Gen Genetics Mgg*. 192:452–458. doi:10.1007/bf00392190.

Hodgkin, J. 1983b. Two types of sex determination in a nematode. *Nature*. 304:267–268. doi:10.1038/304267a0.

Hoencamp, C., O. Dudchenko, A.M.O. Elbatsh, S. Brahmachari, J.A. Raaijmakers, T. van Schaik, Á.S. Cacciatore, V.G. Contessoto, R.G.H.P. van Heesbeen, B. van den Broek, A.N. Mhaskar, H. Teunissen, B.G.S. Hilaire, D. Weisz, A.D. Omer, M. Pham, Z. Colaric, Z. Yang, S.S.P. Rao, N. Mitra, C. Lui, W. Yao, R. Khan, L.L. Moroz, A. Kohn, J.St. Leger, A. Mena, K. Holcroft, M.C. Gambetta, F. Lim, E. Farley, N. Stein, A. Haddad, D. Chauss, A.S. Mutlu, M.C. Wang, N.D. Young, E. Hildebrandt, H.H. Cheng, C.J. Knight, T.L.U. Burnham, K.A. Hovel, A.J. Beel, P.-J. Mattei, R.D. Kornberg, W.C. Warren, G. Cary, J.L. Gómez-Skarmeta, V. Hinman, K. Lindblad-Toh, F.D. Palma, K. Maeshima, A.S. Multani, S. Pathak, L. Nel-Themaat, R.R. Behringer, P. Kaur, R.H. Medema, B. van Steensel, E. de Wit, J.N. Onuchic, M.D. Pierro, E.L. Aiden, and B.D. Rowland. 2021. 3D genomics across the tree of life reveals condensin II as a determinant of architecture type. *Science*. 372:984–989. doi:10.1126/science.abe2218.

Holloway, D.M., and A.V. Spirov. 2017. Transcriptional bursting in Drosophila development: Stochastic dynamics of eve stripe 2 expression. *PLoS ONE*. 12:e0176228-24. doi:10.1371/journal.pone.0176228.

Hopfner, K.-P., A. Karcher, D.S. Shin, L. Craig, L.M. Arthur, J.P. Carney, and J.A. Tainer. 2000. Structural Biology of Rad50 ATPase ATP-Driven Conformational Control in DNA Double-Strand Break Repair and the ABC-ATPase Superfamily. *Cell*. 101:789–800. doi:10.1016/s0092-8674(00)80890-9.

Hoppe, C., J.R. Bowles, T.G. Minchington, C. Sutcliffe, P. Upadhyai, M. Rattray, and H.L. Ashe. 2020. Modulation of the Promoter Activation Rate Dictates the Transcriptional Response to Graded BMP Signaling Levels in the Drosophila Embryo. *Developmental Cell*. 1–23. doi:10.1016/j.devcel.2020.07.007.

Hornung, G., R. Bar-Ziv, D. Rosin, N. Tokuriki, D.S. Tawfik, M. Oren, and N. Barkai. 2012. Noise–mean relationship in mutated promoters. *Genome Res*. 22:2409–2417. doi:10.1101/gr.139378.112.

Hou, L., Y. Wang, Y. Liu, N. Zhang, I. Shamovsky, E. Nudler, B. Tian, and B.D. Dynlacht. 2019. Paf1C regulates RNA polymerase II progression by modulating elongation rate. *Proc National Acad Sci*. 116:14583–14592. doi:10.1073/pnas.1904324116.

Houlard, M., J. Godwin, J. Metson, J. Lee, T. Hirano, and K. Nasmyth. 2015. Condensin confers the longitudinal rigidity of chromosomes. *Nat Cell Biol*. 17:771–781. doi:10.1038/ncb3167.

Houston, S.I., K.J. McManus, M.M. Adams, J.K. Sims, P.B. Carpenter, M.J. Hendzel, and J.C. Rice. 2008. Catalytic Function of the PR-Set7 Histone H4 Lysine 20 Monomethyltransferase Is Essential for Mitotic Entry and Genomic Stability*. *J Biol Chem*. 283:19478–19488. doi:10.1074/jbc.m710579200.

Howe, F.S., H. Fischl, S.C. Murray, and J. Mellor. 2017. Is H3K4me3 instructive for transcription activation? *Bioessays*. 39:1–12. doi:10.1002/bies.201600095.

Hsieh, T.-H.S., C. Cattoglio, E. Slobodyanyuk, A.S. Hansen, O.J. Rando, R. Tjian, and X. Darzacq. 2020. Resolving the 3D Landscape of Transcription-Linked Mammalian Chromatin Folding. *Mol Cell*. 78:539-553.e8. doi:10.1016/j.molcel.2020.03.002.

Hsieh, T.-H.S., A. Weiner, B. Lajoie, J. Dekker, N. Friedman, and O.J. Rando. 2015. Mapping Nucleosome Resolution Chromosome Folding in Yeast by Micro-C. *Cell*. 162:108–119. doi:10.1016/j.cell.2015.05.048.

Hsu, D.R., P.T. Chuang, and B.J. Meyer. 1995. DPY-30, a nuclear protein essential early in embryogenesis for Caenorhabditis elegans dosage compensation. *Development*. 121:3323–3334. doi:10.1242/dev.121.10.3323.

Hsu, D.R., and B.J. Meyer. 1994. The dpy-30 gene encodes an essential component of the Caenorhabditis elegans dosage compensation machinery. *Genetics*. 137:999–1018. doi:10.1093/genetics/137.4.999.

Hu, B., T. Itoh, A. Mishra, Y. Katoh, K.-L. Chan, W. Upcher, C. Godlee, M.B. Roig, K. Shirahige, and K. Nasmyth. 2011. ATP hydrolysis is required for relocating cohesin from sites occupied by its Scc2/4 loading complex. *Current biology : CB*. 21:12–24. doi:10.1016/j.cub.2010.12.004.

Hudson, D.F., S. Ohta, T. Freisinger, F. Macisaac, L. Sennels, F. Alves, F. Lai, A. Kerr, J. Rappsilber, and W.C. Earnshaw. 2008. Molecular and genetic analysis of condensin function in vertebrate cells. *Molecular biology of the cell*. 19:3070–3079. doi:10.1091/mbc.e08-01-0057.

Ikegami, K., T.A. Egelhofer, S. Strome, and J.D. Lieb. 2010. Caenorhabditis elegans chromosome arms are anchored to the nuclear membrane via discontinuous association with LEM-2. *Genome Biol*. 11:R120. doi:10.1186/gb-2010-11-12-r120.

Ikegami, K., and J.D. Lieb. 2013. Integral Nuclear Pore Proteins Bind to Pol III-Transcribed Genes and Are Required for Pol III Transcript Processing in C. elegans. *Mol Cell*. 51:840–849. doi:10.1016/j.molcel.2013.08.001.

Ingolia, N.T., S. Ghaemmaghami, J.R.S. Newman, and J.S. Weissman. 2009. Genome-Wide Analysis in Vivo of Translation with Nucleotide Resolution Using Ribosome Profiling. *Science*. 324:218–223. doi:10.1126/science.1168978.

Iwasaki, O., A. Tanaka, H. Tanizawa, S.I.S. Grewal, and K. Noma. 2010. Centromeric Localization of Dispersed Pol III Genes in Fission Yeast. *Mol Biol Cell*. 21:254–265. doi:10.1091/mbc.e09-09-0790.

Janissen, R., M.M.A. Arens, N.N. Vtyurina, Z. Rivai, N.D. Sunday, B. Eslami-Mossallam, A.A. Gritsenko, L. Laan, D. de Ridder, I. Artsimovitch, N.H. Dekker, E.A. Abbondanzieri, and A.S. Meyer. 2018. Global DNA Compaction in Stationary-Phase Bacteria Does Not Affect Transcription. *Cell*. 174:1188-1199.e14. doi:10.1016/j.cell.2018.06.049.

Jans, J., J.M. Gladden, E.J. Ralston, C.S. Pickle, A.H. Michel, R.R. Pferdehirt, M.B. Eisen, and B.J. Meyer. 2009. A condensin-like dosage compensation complex acts at a distance to control expression throughout the genome. *Genes & Development*. 23:602–618. doi:10.1101/gad.1751109.

Jeppsson, K., K.K. Carlborg, R. Nakato, D.G. Berta, I. Lilienthal, T. Kanno, A. Lindqvist, M.C. Brink, N.P. Dantuma, Y. Katou, K. Shirahige, and C. Sjögren. 2014. The Chromosomal Association of the Smc5/6 Complex Depends on Cohesion and Predicts the Level of Sister Chromatid Entanglement. *Plos Genet*. 10:e1004680. doi:10.1371/journal.pgen.1004680.

Ji, N., and A. van Oudenaarden. 2012. Single molecule fluorescent in situ hybridization (smFISH) of C. elegans worms and embryos. *WormBook*. 1–16. doi:10.1895/wormbook.1.153.1.

Jimenez, D.S., J. Kim, B. Ragipani, B. Zhang, L.A. Street, M. Kramer, S.E. Albritton, L. Winterkorn, and S. Ercan. 2021. Condensin DC spreads linearly and bidirectionally from recruitment sites to create loop-anchored TADs in C. elegans. *Biorxiv*. 2021.03.23.436694. doi:10.1101/2021.03.23.436694.

Johnston, R.J., and C. Desplan. 2010. Stochastic Mechanisms of Cell Fate Specification that Yield Random or Robust Outcomes. *Annu Rev Cell Dev Bi*. 26:689–719. doi:10.1146/annurev-cellbio-100109-104113.

Jolma, A., Y. Yin, K.R. Nitta, K. Dave, A. Popov, M. Taipale, M. Enge, T. Kivioja, E. Morgunova, and J. Taipale. 2015. DNA-dependent formation of transcription factor pairs alters their binding specificity. *Nature*. 527:384–388. doi:10.1038/nature15518.

Jordán-Pla, A., S. Yu, J. Waldholm, T. Källman, A.-K.Ö. Farrants, and N. Visa. 2018. SWI/SNF regulates half of its targets without the need of ATP-driven nucleosome remodeling by Brahma. *Bmc Genomics*. 19:367. doi:10.1186/s12864-018-4746-2.

Jørgensen, S., G. Schotta, and C.S. Sørensen. 2013. Histone H4 Lysine 20 methylation: key player in epigenetic regulation of genomic integrity. *Nucleic Acids Res*. 41:2797–2806. doi:10.1093/nar/gkt012.

Julien, E., and W. Herr. 2004. A Switch in Mitotic Histone H4 Lysine 20 Methylation Status Is Linked to M Phase Defects upon Loss of HCF-1. *Mol Cell*. 14:713–725. doi:10.1016/j.molcel.2004.06.008.

Juven-Gershon, T., J.-Y. Hsu, J.W. Theisen, and J.T. Kadonaga. 2008. The RNA polymerase II core promoter — the gateway to transcription. *Curr Opin Cell Biol*. 20:253–259. doi:10.1016/j.ceb.2008.03.003.

Kaderi, B.E., S. Medler, S. Raghunayakula, and A. Ansari. 2009. Gene Looping Is Conferred by Activator-dependent Interaction of Transcription Initiation and Termination Machineries*. *J Biol Chem*. 284:25015–25025. doi:10.1074/jbc.m109.007948.

Kadoch, C., and G.R. Crabtree. 2015. Mammalian SWI/SNF chromatin remodeling complexes and cancer: Mechanistic insights gained from human genomics. *Sci Adv*. 1:e1500447. doi:10.1126/sciadv.1500447.

Kagey, M.H., J.J. Newman, S. Bilodeau, Y. Zhan, D.A. Orlando, N.L. van Berkum, C.C. Ebmeier, J. Goossens, P.B. Rahl, S.S. Levine, D.J. Taatjes, J. Dekker, and R.A. Young. 2010. Mediator and cohesin connect gene expression and chromatin architecture. *Nature*. 467:430–435. doi:10.1038/nature09380.

Kaitna, S., P. Pasierbek, M. Jantsch, J. Loidl, and M. Glotzer. 2002. The aurora B kinase AIR-2 regulates kinetochores during mitosis and is required for separation of homologous Chromosomes during meiosis. *Current Biology*. 12:798–812. doi:10.1016/s0960-9822(02)00820-5.

Kanno, T., D.G. Berta, and C. Sjögren. 2015. The Smc5/6 Complex Is an ATP-Dependent Intermolecular DNA Linker. *Cell Reports*. 12:1471–1482. doi:10.1016/j.celrep.2015.07.048.

Karachentsev, D., K. Sarma, D. Reinberg, and R. Steward. 2005. PR-Set7-dependent methylation of histone H4 Lys 20 functions in repression of gene expression and is essential for mitosis. *Gene Dev*. 19:431–435. doi:10.1101/gad.1263005.

Karlić, R., H.-R. Chung, J. Lasserre, K. Vlahoviček, and M. Vingron. 2010. Histone modification levels are predictive for gene expression. *Proc National Acad Sci*. 107:2926–2931. doi:10.1073/pnas.0909344107.

Kegel, A., H. Betts-Lindroos, T. Kanno, K. Jeppsson, L. Ström, Y. Katou, T. Itoh, K. Shirahige, and C. Sjögren. 2011. Chromosome length influences replication-induced topological stress. *Nature*. 471:392–396. doi:10.1038/nature09791.

Kelley, R.L., V.H. Meller, P.R. Gordadze, G. Roman, R.L. Davis, and M.I. Kuroda. 1999. Epigenetic Spreading of the Drosophila Dosage Compensation Complex from roX RNA Genes into Flanking Chromatin. *Cell*. 98:513–522. doi:10.1016/s0092-8674(00)81979-0.

Kempe, H., A. Schwabe, F. Crémazy, P.J. Verschure, and F.J. Bruggeman. 2015. The volumes and transcript counts of single cells reveal concentration homeostasis and capture biological noise. *Mol Biol Cell*. 26:797–804. doi:10.1091/mbc.e14-08-1296.

Ketel, C.S., E.F. Andersen, M.L. Vargas, J. Suh, S. Strome, and J.A. Simon. 2005. Subunit Contributions to Histone Methyltransferase Activities of Fly and Worm Polycomb Group Complexes. *Mol Cell Biol*. 25:6857–6868. doi:10.1128/mcb.25.16.6857-6868.2005.

Kim, D., G. Pertea, C. Trapnell, H. Pimentel, R. Kelley, and S.L. Salzberg. 2013. TopHat2: accurate alignment of transcriptomes in the presence of insertions, deletions and gene fusions. *Genome Biol*. 14:R36. doi:10.1186/gb-2013-14-4-r36.

Kim, E., J. Kerssemakers, I.A. Shaltiel, C.H. Haering, and C. Dekker. 2019a. DNA-loop extruding condensin complexes can traverse one another. *Nature*. 579:438–442. doi:10.1038/s41586-020-2067-5.

Kim, H.-S., V. Vanoosthuyse, J. Fillingham, A. Roguev, S. Watt, T. Kislinger, A. Treyer, L.R. Carpenter, C.S. Bennett, A. Emili, J.F. Greenblatt, K.G. Hardwick, N.J. Krogan, J. Bähler, and M.-C. Keogh. 2009. An acetylated form of histone H2A.Z regulates chromosome architecture in Schizosaccharomyces pombe. *Nat Struct Mol Biol*. 16:1286–1293. doi:10.1038/nsmb.1688.

Kim, J.H., T. Zhang, N.C. Wong, N. Davidson, J. Maksimovic, A. Oshlack, W.C. Earnshaw, P. Kalitsis, and D.F. Hudson. 2019b. Condensin I associates with structural and gene regulatory regions in vertebrate chromosomes. *Nat Commun*. 4:2537. doi:10.1038/ncomms3537.

Kim, K.-D. 2021. Potential roles of condensin in genome organization and beyond in fission yeast. *J Microbiol*. 1–11. doi:10.1007/s12275-021-1039-2.

Kim, K.H., W. Kim, T.P. Howard, F. Vazquez, A. Tsherniak, J.N. Wu, W. Wang, J.R. Haswell, L.D. Walensky, W.C. Hahn, S.H. Orkin, and C.W.M. Roberts. 2015. SWI/SNF-mutant cancers depend on catalytic and non-catalytic activity of EZH2. *Nat Med*. 21:1491–1496. doi:10.1038/nm.3968.

Kim, T.-K., R.H. Ebright, and D. Reinberg. 2000. Mechanism of ATP-Dependent Promoter Melting by Transcription Factor IIH. *Science*. 288:1418–1421. doi:10.1126/science.288.5470.1418.

Kim, Y., Z. Shi, H. Zhang, I.J. Finkelstein, and H. Yu. 2019c. Human cohesin compacts DNA by loop extrusion. *Science*. 366:1345-+. doi:10.1126/science.aaz4475.

Kimura, H., and P.R. Cook. 2001. Kinetics of Core Histones in Living Human CellsLittle Exchange of H3 and H4 and Some Rapid Exchange of H2b. *J Cell Biology*. 153:1341–1354. doi:10.1083/jcb.153.7.1341.

Kimura, K., and T. Hirano. 1997. ATP-Dependent Positive Supercoiling of DNA by 13S Condensin: A Biochemical Implication for Chromosome Condensation. *Cell*. 90:625–634. doi:10.1016/s0092-8674(00)80524-3.

Kimura, K., and T. Hirano. 2000. Dual roles of the 11S regulatory subcomplex in condensin functions. *Proc National Acad Sci*. 97:11972–11977. doi:10.1073/pnas.220326097.

Kinoshita, K., and T. Hirano. 2017. Dynamic organization of mitotic chromosomes. *Current Opinion in Cell Biology*. 46:46–53. doi:10.1016/j.ceb.2017.01.006.

Kinoshita, K., T.J. Kobayashi, and T. Hirano. 2015. Balancing acts of two HEAT subunits of condensin I support dynamic assembly of chromosome axes. *Developmental Cell*. 33:94–106. doi:10.1016/j.devcel.2015.01.034.

Kirkland, J.G., J.R. Raab, and R.T. Kamakaka. 2013. TFIIIC bound DNA elements in nuclear organization and insulation. *Biochimica Et Biophysica Acta Bba - Gene Regul Mech*. 1829:418–424. doi:10.1016/j.bbagrm.2012.09.006.

Kohlmaier, A., F. Savarese, M. Lachner, J. Martens, T. Jenuwein, and A. Wutz. 2004. A Chromosomal Memory Triggered by Xist Regulates Histone Methylation in X Inactivation. *Plos Biol*. 2:e171. doi:10.1371/journal.pbio.0020171.

Kong, M., E.E. Cutts, D. Pan, F. Beuron, T. Kaliyappan, C. Xue, E.P. Morris, A. Musacchio, A. Vannini, and E.C. Greene. 2020. Human Condensin I and II Drive Extensive ATP-Dependent

Compaction of Nucleosome-Bound DNA. *Mol Cell*. 79:99-114.e9. doi:10.1016/j.molcel.2020.04.026.

Kornberg, R.D. 1974. Chromatin Structure: A Repeating Unit of Histones and DNA. *Science*. 184:868–871. doi:10.1126/science.184.4139.868.

Kornberg, R.D. 2005. Mediator and the mechanism of transcriptional activation. *Trends Biochem Sci*. 30:235–239. doi:10.1016/j.tibs.2005.03.011.

Koyen, A.E., M.Z. Madden, D. Park, E.V. Minten, P. Kapoor-Vazirani, E. Werner, N.T. Pfister, R. Haji-Seyed-Javadi, H. Zhang, J. Xu, N. Deng, D.M. Duong, T.J. Pecen, Z. Frazier, Z.D. Nagel, J.-B. Lazaro, K.W. Mouw, N.T. Seyfried, C.S. Moreno, T.K. Owonikoko, X. Deng, and D.S. Yu. 2020. EZH2 has a non-catalytic and PRC2-independent role in stabilizing DDB2 to promote nucleotide excision repair. *Oncogene*. 39:4798–4813. doi:10.1038/s41388-020-1332-2.

Kramer, M., A.-L. Kranz, A. Su, L.H. Winterkorn, S.E. Albritton, and S. Ercan. 2015. Developmental Dynamics of X-Chromosome Dosage Compensation by the DCC and H4K20me1 in C. elegans. *PLoS genetics*. 11:e1005698. doi:10.1371/journal.pgen.1005698.

Kramer, M., P. Rao, and S. Ercan. 2016. Untangling the Contributions of Sex-Specific Gene Regulation and X-Chromosome Dosage to Sex-Biased Gene Expression in Caenorhabditis elegans. *Genetics*. 204:355–369. doi:10.1534/genetics.116.190298.

Kramer, M.A. 1991. Nonlinear principal component analysis using autoassociative neural networks. *Aiche J*. 37:233–243. doi:10.1002/aic.690370209.

Kranz, A.-L., C.-Y. Jiao, L.H. Winterkorn, S.E. Albritton, M. Kramer, and S. Ercan. 2013. Genome-wide analysis of condensin binding in Caenorhabditis elegans. *Genome biology*. 14:R112. doi:10.1186/gb-2013-14-10-r112.

Krassovsky, K., R.P. Ghosh, and B.J. Meyer. 2021. Genome-wide profiling reveals functional interplay of DNA sequence composition, transcriptional activity, and nucleosome positioning in driving DNA supercoiling and helix destabilization in C. elegans. *Genome Res*. doi:10.1101/gr.270082.120.

Krijger, P.H.L., and W. de Laat. 2016. Regulation of disease-associated gene expression in the 3D genome. *Nat Rev Mol Cell Bio*. 17:771–782. doi:10.1038/nrm.2016.138.

Kriz, A.J., D. Colognori, H. Sunwoo, B. Nabet, and J.T. Lee. 2021. Balancing cohesin eviction and retention prevents aberrant chromosomal interactions, Polycomb-mediated repression, and X-inactivation. *Mol Cell*. doi:10.1016/j.molcel.2021.02.031.

Kruesi, W.S., L.J. Core, C.T. Waters, J.T. Lis, and B.J. Meyer. 2013. Condensin controls recruitment of RNA polymerase II to achieve nematode X-chromosome dosage compensation. *eLife*. 2:e00808. doi:10.7554/elife.00808.

Kschonsak, M., F. Merkel, S. Bisht, J. Metz, V. Rybin, M. Hassler, and C.H. Haering. 2017. Structural Basis for a Safety-Belt Mechanism That Anchors Condensin to Chromosomes. *Cell*. 1–38. doi:10.1016/j.cell.2017.09.008.

Kubo, N., H. Ishii, X. Xiong, S. Bianco, F. Meitinger, R. Hu, J.D. Hocker, M. Conte, D. Gorkin, M. Yu, B. Li, J.R. Dixon, M. Hu, M. Nicodemi, H. Zhao, and B. Ren. 2021. Promoter-proximal CTCF binding promotes distal enhancer-dependent gene activation. *Nat Struct Mol Biol*. 28:152–161. doi:10.1038/s41594-020-00539-5.

Kueng, S., B. Hegemann, B.H. Peters, J.J. Lipp, A. Schleiffer, K. Mechtler, and J.-M. Peters. 2006. Wapl Controls the Dynamic Association of Cohesin with Chromatin. *Cell*. 127:955–967. doi:10.1016/j.cell.2006.09.040.

Kuroda, M.I., A. Hilfiker, and J.C. Lucchesi. 2016. Dosage Compensation in Drosophila—a Model for the Coordinate Regulation of Transcription. *Genetics*. 204:435–450. doi:10.1534/genetics.115.185108.

Kwok, R.S., Y.H. Li, A.J. Lei, I. Edery, and J.C. Chiu. 2015. The Catalytic and Non-catalytic Functions of the Brahma Chromatin-Remodeling Protein Collaborate to Fine-Tune Circadian Transcription in Drosophila. *Plos Genet*. 11:e1005307. doi:10.1371/journal.pgen.1005307.

Kwon, I., M. Kato, S. Xiang, L. Wu, P. Theodoropoulos, H. Mirzaei, T. Han, S. Xie, J.L. Corden, and S.L. McKnight. 2014. Phosphorylation-Regulated Binding of RNA Polymerase II to Fibrous Polymers of Low-Complexity Domains. *Cell*. 156:374. doi:10.1016/j.cell.2014.01.002.

Lakadamyali, M., and M.P. Cosma. 2020. Visualizing the genome in high resolution challenges our textbook understanding. *Nat Methods*. 17:371–379. doi:10.1038/s41592-020-0758-3.

Lam, A.J., F. St-Pierre, Y. Gong, J.D. Marshall, P.J. Cranfill, M.A. Baird, M.R. McKeown, J. Wiedenmann, M.W. Davidson, M.J. Schnitzer, R.Y. Tsien, and M.Z. Lin. 2012. Improving FRET dynamic range with bright green and red fluorescent proteins. *Nature Publishing Group*. 9:1005–1012. doi:10.1038/nmeth.2171.

Lambert, S.A., A. Jolma, L.F. Campitelli, P.K. Das, Y. Yin, M. Albu, X. Chen, J. Taipale, T.R. Hughes, and M.T. Weirauch. 2018. The Human Transcription Factors. *Cell*. 172:650–665. doi:10.1016/j.cell.2018.01.029.

Lammens, A., A. Schele, and K.-P. Hopfner. 2004. Structural biochemistry of ATP-driven dimerization and DNA-stimulated activation of SMC ATPases. *Current Biology*. 14:1778–1782. doi:10.1016/j.cub.2004.09.044.

Lammers, N.C., V. Galstyan, A. Reimer, S.A. Medin, C.H. Wiggins, and H.G. Garcia. 2020. Multimodal transcriptional control of pattern formation in embryonic development. *Proc National Acad Sci*. 117:836–847. doi:10.1073/pnas.1912500117.

Lancaster, L., H. Patel, G. Kelly, and F. Uhlmann. 2021. A role for condensin in mediating transcriptional adaptation to environmental stimuli. *Life Sci Alliance*. 4:e202000961. doi:10.26508/lsa.202000961.

Landick, R. 2006. The regulatory roles and mechanism of transcriptional pausing. *Biochem Soc T*. 34:1062–1066. doi:10.1042/bst0341062.

Langmead, B., and S.L. Salzberg. 2012. Fast gapped-read alignment with Bowtie 2. *Nat Methods*. 9:357–359. doi:10.1038/nmeth.1923.

Längst, G., and L. Manelyte. 2015. Chromatin Remodelers: From Function to Dysfunction. *Genes-basel*. 6:299–324. doi:10.3390/genes6020299.

Larschan, E., A.A. Alekseyenko, A.A. Gortchakov, S. Peng, B. Li, P. Yang, J.L. Workman, P.J. Park, and M.I. Kuroda. 2007. MSL Complex Is Attracted to Genes Marked by H3K36 Trimethylation Using a Sequence-Independent Mechanism. *Mol Cell*. 28:121–133. doi:10.1016/j.molcel.2007.08.011.

Larschan, E., E.P. Bishop, P.V. Kharchenko, L.J. Core, J.T. Lis, P.J. Park, and M.I. Kuroda. 2011. X chromosome dosage compensation via enhanced transcriptional elongation in Drosophila. *Nature*. 471:115–118. doi:10.1038/nature09757.

Larson, A.G., D. Elnatan, M.M. Keenen, M.J. Trnka, J.B. Johnston, A.L. Burlingame, D.A. Agard, S. Redding, and G.J. Narlikar. 2017. Liquid droplet formation by HP1α suggests a role for phase separation in heterochromatin. *Nature*. 547:236–240. doi:10.1038/nature22822.

Larson, D.R., C. Fritzsch, L. Sun, X. Meng, D.S. Lawrence, and R.H. Singer. 2013. Direct observation of frequency modulated transcription in single cells using light activation. *Elife*. 2:e00750. doi:10.7554/elife.00750.

Larsson, A.J.M., P. Johnsson, M. Hagemann-Jensen, L. Hartmanis, O.R. Faridani, B. Reinius, Å. Segerstolpe, C.M. Rivera, B. Ren, and R. Sandberg. 2018. Genomic encoding of transcriptional burst kinetics. *Nature*. 1–17. doi:10.1038/s41586-018-0836-1.

Lau, A.C., and G. Csankovszki. 2015. Balancing up and downregulation of the C. elegans X chromosomes. *Curr Opin Genet Dev*. 31:50–56. doi:10.1016/j.gde.2015.04.001.

Lau, A.C., K. Nabeshima, and G. Csankovszki. 2014. The C. elegans dosage compensation complex mediates interphase X chromosome compaction. *Epigenet Chromatin*. 7:31. doi:10.1186/1756-8935-7-31.

Lau, A.C., K.P. Zhu, E.A. Brouhard, M.B. Davis, and G. Csankovszki. 2016. An H4K16 histone acetyltransferase mediates decondensation of the X chromosome in C. elegans males. *Epigenet Chromatin*. 9:44. doi:10.1186/s13072-016-0097-x.

Lavoie, B.D., E. Hogan, and D. Koshland. 2004. In vivo requirements for rDNA chromosome condensation reveal two cell-cycle-regulated pathways for mitotic chromosome folding. *Gene Dev*. 18:76–87. doi:10.1101/gad.1150404.

Lawrence, M., S. Daujat, and R. Schneider. 2016. Lateral Thinking: How Histone Modifications Regulate Gene Expression. *Trends in Genetics*. 32:42–56. doi:10.1016/j.tig.2015.10.007.

Lazar-Stefanita, L., V.F. Scolari, G. Mercy, H. Muller, T.M. Guérin, A. Thierry, J. Mozziconacci, and R. Koszul. 2017. Cohesins and condensins orchestrate the 4D dynamics of yeast chromosomes during the cell cycle. *Embo J*. 36:2684–2697. doi:10.15252/embj.201797342.

Lee, B.-G., F. Merkel, M. Allegretti, M. Hassler, C. Cawood, L. x000E9 a Lecomte, F.J.O. x02019 Reilly, L.R. Sinn, P. Gutierrez-Escribano, M. Kschonsak, S. Bravo, T. Nakane, J. Rappsilber, L. Aragón, M. Beck, J.L. x000F6 we, and C.H. Haering. 2020. Cryo-EM structures of holo condensin reveal a subunit flip-flop mechanism. *Nature structural & molecular biology*. 1–26. doi:10.1038/s41594-020-0457-x.

Lee, C., H. Shin, and J. Kimble. 2019. Dynamics of Notch-Dependent Transcriptional Bursting in Its Native Context. *Dev Cell*. 50:426-435.e4. doi:10.1016/j.devcel.2019.07.001.

Lee, J.H., E.R. Daugharthy, J. Scheiman, R. Kalhor, J.L. Yang, T.C. Ferrante, R. Terry, S.S.F. Jeanty, C. Li, R. Amamoto, D.T. Peters, B.M. Turczyk, A.H. Marblestone, S.A. Inverso, A. Bernard, P. Mali, X. Rios, J. Aach, and G.M. Church. 2014. Highly Multiplexed Subcellular RNA Sequencing in Situ. *Science*. 343:1360–1363. doi:10.1126/science.1250212.

Lee, M.G., C. Wynder, N. Cooch, and R. Shiekhattar. 2005. An essential role for CoREST in nucleosomal histone 3 lysine 4 demethylation. *Nature*. 437:432–435. doi:10.1038/nature04021.

Lehmann, A.R., M. Walicka, D.J. Griffiths, J.M. Murray, F.Z. Watts, S. McCready, and A.M. Carr. 1995. The rad18 gene of Schizosaccharomyces pombe defines a new subgroup of the SMC superfamily involved in DNA repair. *Mol Cell Biol*. 15:7067–7080. doi:10.1128/mcb.15.12.7067.

Lengronne, A., Y. Katou, S. Mori, S. Yokobayashi, G.P. Kelly, T. Itoh, Y. Watanabe, K. Shirahige, and F. Uhlmann. 2004. Cohesin relocation from sites of chromosomal loading to places of convergent transcription. *Nature*. 430:573–578. doi:10.1038/nature02742.

Lenstra, T.L., J. Rodriguez, H. Chen, and D.R. Larson. 2015. Transcription Dynamics in Living Cells. *Annu Rev Biophys*. 45:1–23. doi:10.1146/annurev-biophys-062215-010838.

Leonard, J., N. Sen, R. Torres, T. Sutani, A. Jarmuz, K. Shirahige, and L. Aragón. 2015. Condensin Relocalization from Centromeres to Chromosome Arms Promotes Top2 Recruitment during Anaphase. *CellReports*. 13:2336–2344. doi:10.1016/j.celrep.2015.11.041.

Levine, M., C. Cattoglio, and R. Tjian. 2014. Looping Back to Leap Forward: Transcription Enters a New Era. *Cell*. 157:13–25. doi:10.1016/j.cell.2014.02.009.

Li, C., F. Cesbron, M. Oehler, M. Brunner, and T. Höfer. 2018a. Frequency Modulation of Transcriptional Bursting Enables Sensitive and Rapid Gene Regulation. *Cell Syst*. 6:409-423.e11. doi:10.1016/j.cels.2018.01.012.

Li, L., X. Lyu, C. Hou, N. Takenaka, H.Q. Nguyen, C.-T. Ong, C. Cubeñas-Potts, M. Hu, E.P. Lei, G. Bosco, Z.S. Qin, and V.G. Corces. 2015. Widespread Rearrangement of 3D Chromatin Organization Underlies Polycomb-Mediated Stress-Induced Silencing. *Mol Cell*. 58:216–231. doi:10.1016/j.molcel.2015.02.023.

Li, Y., K.W. Muir, M.W. Bowler, J. Metz, C.H. Haering, and D. Panne. 2018b. Structural basis for Scc3-dependent cohesin recruitment to chromatin. *Elife*. 7:e38356. doi:10.7554/elife.38356.

Lieb, J.D., M.R. Albrecht, P.-T. Chuang, and B.J. Meyer. 1998. MIX-1: An Essential Component of the C. elegans Mitotic Machinery Executes X Chromosome Dosage Compensation. *Cell*. 92:265–277. doi:10.1016/s0092-8674(00)80920-4.

Lieb, J.D., E.E. Capowski, P. Meneely, and B.J. Meyer. 1996. DPY-26, a Link Between Dosage Compensation and Meiotic Chromosome Segregation in the Nematode. *Science*. 274:1732–1736. doi:10.1126/science.274.5293.1732.

Lieberman-Aiden, E., N.L. van Berkum, L. Williams, M. Imakaev, T. Ragoczy, A. Telling, I. Amit, B.R. Lajoie, P.J. Sabo, M.O. Dorschner, R. Sandstrom, B. Bernstein, M.A. Bender, M. Groudine, A. Gnirke, J. Stamatoyannopoulos, L.A. Mirny, E.S. Lander, and J. Dekker. 2009. Comprehensive Mapping of Long-Range Interactions Reveals Folding Principles of the Human Genome. *Science*. 326:289–293. doi:10.1126/science.1181369.

Lin, Y.C., S. Jhunjhunwala, C. Benner, S. Heinz, E. Welinder, R. Mansson, M. Sigvardsson, J. Hagman, C.A. Espinoza, J. Dutkowski, T. Ideker, C.K. Glass, and C. Murre. 2010. A global network of transcription factors, involving E2A, EBF1 and Foxo1, that orchestrates B cell fate. *Nat Immunol*. 11:635–643. doi:10.1038/ni.1891.

Lionnet, T., K. Czaplinski, X. Darzacq, Y. Shav-Tal, A.L. Wells, J.A. Chao, H.Y. Park, V. de Turris, M. Lopez-Jones, and R.H. Singer. 2011. A transgenic mouse for in vivo detection of endogenous labeled mRNA. *Nat Methods*. 8:165–170. doi:10.1038/nmeth.1551.

Lipp, J.J., T. Hirota, I. Poser, and J.-M. Peters. 2007. Aurora B controls the association of condensin I but not condensin II with mitotic chromosomes. *J Cell Sci*. 120:1245–1255. doi:10.1242/jcs.03425.

Little, S.C., M. Tikhonov, and T. Gregor. 2013. Precise Developmental Gene Expression Arises from Globally Stochastic Transcriptional Activity. *Cell*. 154:789–800. doi:10.1016/j.cell.2013.07.025.

Liu, C.-H., A. Finke, M. Díaz, W. Rozhon, B. Poppenberger, T. Baubec, and A. Pecinka. 2015. Repair of DNA Damage Induced by the Cytidine Analog Zebularine Requires ATR and ATM in Arabidopsis. *Plant Cell*. 27:1788–1800. doi:10.1105/tpc.114.135467.

Liu, N.Q., M. Maresca, T. van den Brand, L. Braccioli, M.M.G.A. Schijns, H. Teunissen, B.G. Bruneau, E.P. Nora, and E. de Wit. 2021. WAPL maintains a cohesin loading cycle to preserve cell-type-specific distal gene regulation. *Nat Genet*. 53:100–109. doi:10.1038/s41588-020-00744-4.

Liu, T., A. Rechtsteiner, T.A. Egelhofer, A. Vielle, I. Latorre, M.-S. Cheung, S. Ercan, K. Ikegami, M. Jensen, P. Kolasinska-Zwierz, H. Rosenbaum, H. Shin, S. Taing, T. Takasaki, A.L. Iniguez, A. Desai, A.F. Dernburg, H. Kimura, J.D. Lieb, J. Ahringer, S. Strome, and X.S. Liu. 2011. Broad chromosomal domains of histone modification patterns in C. elegans. *Genome Research*. 21:227–236. doi:10.1101/gr.115519.110.

Liu, W., B. Tanasa, O.V. Tyurina, T.Y. Zhou, R. Gassmann, W.T. Liu, K.A. Ohgi, C. Benner, I. Garcia-Bassets, A.K. Aggarwal, A. Desai, P.C. Dorrestein, C.K. Glass, and M.G. Rosenfeld. 2010. PHF8 mediates histone H4 lysine 20 demethylation events involved in cell cycle progression. *Nature*. 1–8. doi:10.1038/nature09272.

Losada, A., M. Hirano, and T. Hirano. 1998. Identification of Xenopus SMC protein complexes required for sister chromatid cohesion. *Gene Dev*. 12:1986–1997. doi:10.1101/gad.12.13.1986.

Losick, R., and C. Desplan. 2008. Stochasticity and Cell Fate. *Science*. 320:65–68. doi:10.1126/science.1147888.

Love, M.I., W. Huber, and S. Anders. 2014. Moderated estimation of fold change and dispersion for RNA-seq data with DESeq2. *Genome Biol*. 15:550. doi:10.1186/s13059-014-0550-8.

Lu, F., B. Portz, and D.S. Gilmour. 2019. The C-Terminal Domain of RNA Polymerase II Is a Multivalent Targeting Sequence that Supports Drosophila Development with Only Consensus Heptads. *Mol Cell*. 73:1232-1242.e4. doi:10.1016/j.molcel.2019.01.008.

Lu, H., D. Yu, A.S. Hansen, S. Ganguly, R. Liu, A. Heckert, X. Darzacq, and Q. Zhou. 2018. Phase-separation mechanism for C-terminal hyperphosphorylation of RNA polymerase II. *Nature*. 558:318–323. doi:10.1038/s41586-018-0174-3.

Lu, Z., and Z. Lin. 2019. Pervasive and dynamic transcription initiation in Saccharomyces cerevisiae. *Genome Res*. 29:1198–1210. doi:10.1101/gr.245456.118.

Luo, Z., C. Lin, and A. Shilatifard. 2012. The super elongation complex (SEC) family in transcriptional control. *Nat Rev Mol Cell Bio*. 13:543–547. doi:10.1038/nrm3417.

Lupiáñez, D.G., K. Kraft, V. Heinrich, P. Krawitz, F. Brancati, E. Klopocki, D. Horn, H. Kayserili, J.M. Opitz, R. Laxova, F. Santos-Simarro, B. Gilbert-Dussardier, L. Wittler, M. Borschiwer, S.A. Haas, M. Osterwalder, M. Franke, B. Timmermann, J. Hecht, M. Spielmann, A. Visel, and S. Mundlos. 2015. Disruptions of Topological Chromatin Domains Cause Pathogenic Rewiring of Gene-Enhancer Interactions. *Cell*. 1–15. doi:10.1016/j.cell.2015.04.004.

Lupo, R., A. Breiling, M.E. Bianchi, and V. Orlando. 2001. Drosophila Chromosome Condensation Proteins Topoisomerase II and Barren Colocalize with Polycomb and Maintain Fab-7 PRE Silencing. *Mol Cell*. 7:127–136. doi:10.1016/s1097-2765(01)00161-7.

Luppino, J.M., D.S. Park, S.C. Nguyen, Y. Lan, Z. Xu, R. Yunker, and E.F. Joyce. 2020. Cohesin promotes stochastic domain intermingling to ensure proper regulation of boundary-proximal genes. *Nature Genetics*. 52:840–848. doi:10.1038/s41588-020-0647-9.

Lykke-Andersen, S., C.K. Mapendano, and T.H. Jensen. 2011. An ending is a new beginning: Transcription termination supports re-initiation. *Cell Cycle*. 10:863–865. doi:10.4161/cc.10.6.14931.

Lyon, M.F. 1961. Gene Action in the X-chromosome of the Mouse (Mus musculus L.). *Nature*. 190:372–373. doi:10.1038/190372a0.

Maamar, H., A. Raj, and D. Dubnau. 2007. Noise in Gene Expression Determines Cell Fate in *Bacillus subtilis*. *Science*. 317:526–529. doi:10.1126/science.1140818.

Maass, P.G., A.R. Barutcu, and J.L. Rinn. 2019. Interchromosomal interactions: A genomic love story of kissing chromosomes. *The Journal of cell biology*. 218:27–38. doi:10.1083/jcb.201806052.

Mahat, D.B., H. Kwak, G.T. Booth, I.H. Jonkers, C.G. Danko, R.K. Patel, C.T. Waters, K. Munson, L.J. Core, and J.T. Lis. 2016. Base-pair-resolution genome-wide mapping of active RNA polymerases using precision nuclear run-on (PRO-seq). *Nat Protoc*. 11:1455–1476. doi:10.1038/nprot.2016.086.

Makrantoni, V., and A.L. Marston. 2018. Cohesin and chromosome segregation. *Curr Biol*. 28:R688–R693. doi:10.1016/j.cub.2018.05.019.

Mapendano, C.K., S. Lykke-Andersen, J. Kjems, E. Bertrand, and T.H. Jensen. 2010. Crosstalk between mRNA 3′ End Processing and Transcription Initiation. *Mol Cell*. 40:410–422. doi:10.1016/j.molcel.2010.10.012.

Maria, S.R.S., V. Gangavarapu, R.E. Johnson, L. Prakash, and S. Prakash. 2007. Requirement of Nse1, a Subunit of the Smc5-Smc6 Complex, for Rad52-Dependent Postreplication Repair of UV-Damaged DNA in Saccharomyces cerevisiae ▿ . *Mol Cell Biol*. 27:8409–8418. doi:10.1128/mcb.01543-07.

Marras, S.A.E., Y. Bushkin, and S. Tyagi. 2019. High-fidelity amplified FISH for the detection and allelic discrimination of single mRNA molecules. *Proceedings of the National Academy of Sciences*. 37:201814463–6. doi:10.1073/pnas.1814463116.

Martens, K.J.A., A.N. Bader, S. Baas, B. Rieger, and J. Hohlbein. 2018. Phasor based single-molecule localization microscopy in 3D (pSMLM-3D): An algorithm for MHz localization rates using standard CPUs. *J Chem Phys*. 148:123311. doi:10.1063/1.5005899.

Martin, C.-A., J.E. Murray, P. Carroll, A. Leitch, K.J. Mackenzie, M. Halachev, A.E. Fetit, C. Keith, L.S. Bicknell, A. Fluteau, P. Gautier, E.A. Hall, S. Joss, G. Soares, J. Silva, M.B. Bober, A. Duker, C.A. Wise, A.J. Quigley, S.R. Phadke, T.D.D.D. Study, A.J. Wood, P. Vagnarelli, and A.P. Jackson. 2016. Mutations in genes encoding condensin complex proteins cause microcephaly through decatenation failure at mitosis. *Genes & Development*. 30:2158–2172. doi:10.1101/gad.286351.116.

Martínez-Balbás, M.A., A. Dey, S.K. Rabindran, K. Ozato, and C. Wu. 1995. Displacement of sequence-specific transcription factors from mitotic chromatin. *Cell*. 83:29–38. doi:10.1016/0092-8674(95)90231-7.

Maxwell, C.S., W.S. Kruesi, L.J. Core, N. Kurhanewicz, C.T. Waters, C.L. Lewarch, I. Antoshechkin, J.T. Lis, B.J. Meyer, and L.R. Baugh. 2014. Pol II Docking and Pausing at Growth and Stress Genes in C-elegans. *CellReports*. 6:455–466. doi:10.1016/j.celrep.2014.01.008.

Mazza, D., A. Abernathy, N. Golob, T. Morisaki, and J.G. McNally. 2012. A benchmark for chromatin binding measurements in live cells. *Nucleic Acids Res*. 40:e119–e119. doi:10.1093/nar/gks701.

McDonel, P., J. Jans, B.K. Peterson, and B.J. Meyer. 2006. Clustered DNA motifs mark X chromosomes for repression by a dosage compensation complex. *Nature*. 444:614–618. doi:10.1038/nature05338.

McStay, B. 2016. Nucleolar organizer regions: genomic 'dark matter' requiring illumination. *Gene Dev*. 30:1598–1610. doi:10.1101/gad.283838.116.

Megaridis, M.R., Y. Lu, E.N. Tevonian, K.M. Junger, J.M. Moy, K. Bohn-Wippert, and R.D. Dar. 2018. Fine-tuning of noise in gene expression with nucleosome remodeling. *APL Bioengineering*. 2:026106–13. doi:10.1063/1.5021183.

Meister, P., B.D. Towbin, B.L. Pike, A. Ponti, and S.M. Gasser. 2010. The spatial dynamics of tissue-specific promoters during C. elegans development. *Genes & Development*. 24:766–782. doi:10.1101/gad.559610.

Melby, T.E., C.N. Ciampaglio, G. Briscoe, and H.P. Erickson. 1998. The Symmetrical Structure of Structural Maintenance of Chromosomes (SMC) and MukB Proteins: Long, Antiparallel Coiled Coils, Folded at a Flexible Hinge. *J Cell Biology*. 142:1595–1604. doi:10.1083/jcb.142.6.1595.

Mello, C.C., J.M. KRAMER, D. Stinchcomb, and V. Ambros. 1991. Efficient Gene-Transfer in C-Elegans - Extrachromosomal Maintenance and Integration of Transforming Sequences. *Embo Journal*. 10:3959–3970. doi:10.1002/j.1460-2075.1991.tb04966.x.

Mengiste, T., E. Revenkova, N. Bechtold, and J. Paszkowski. 1999. An SMC-like protein is required for efficient homologous recombination in Arabidopsis. *Embo J*. 18:4505–4512. doi:10.1093/emboj/18.16.4505.

Menolfi, D., A. Delamarre, A. Lengronne, P. Pasero, and D. Branzei. 2015. Essential Roles of the Smc5/6 Complex in Replication through Natural Pausing Sites and Endogenous DNA Damage Tolerance. *Mol Cell*. 60:835–846. doi:10.1016/j.molcel.2015.10.023.

Meyer, B.J., and L.P. Casson. 1986. Caenorhabditis elegans compensates for the difference in X chromosome dosage between the sexes by regulating transcript levels. *Cell*. 47:871–881. doi:10.1016/0092-8674(86)90802-0.

Michaelis, C., R. Ciosk, and K. Nasmyth. 1997. Cohesins: Chromosomal Proteins that Prevent Premature Separation of Sister Chromatids. *Cell*. 91:35–45. doi:10.1016/s0092-8674(01)80007-6.

Miller, L.M., J.D. Plenefisch, L.P. Casson, and B.J. Meyer. 1988. xol-1: A gene that controls the male modes of both sex determination and X chromosome dosage compensation in C. elegans. *Cell*. 55:167–183. doi:10.1016/0092-8674(88)90019-0.

Miller, S.A., R.A. Policastro, S.S. Savant, S. Sriramkumar, N. Ding, X. Lu, H.P. Mohammad, S. Cao, J.H. Kalin, P.A. Cole, G.E. Zentner, and H.M. O'Hagan. 2020. Lysine-Specific Demethylase 1 Mediates AKT Activity and Promotes Epithelial-to-Mesenchymal Transition in PIK3CA-Mutant Colorectal Cancer. *Mol Cancer Res*. 18:264–277. doi:10.1158/1541-7786.mcr-19-0748.

Minnen, A., F. Bürmann, L. Wilhelm, A. Anchimiuk, M.-L. Diebold-Durand, and S. Gruber. 2016. Control of Smc Coiled Coil Architecture by the ATPase Heads Facilitates Targeting to Chromosomal ParB/parS and Release onto Flanking DNA. *Cell Reports*. 14:2003–2016. doi:10.1016/j.celrep.2016.01.066.

Mir, M., A. Reimer, J.E. Haines, X.-Y. Li, M. Stadler, H. Garcia, M.B. Eisen, and X. Darzacq. 2017. Dense Bicoid hubs accentuate binding along the morphogen gradient. *Gene Dev*. 31:1784–1794. doi:10.1101/gad.305078.117.

Miura, M., S. Dey, S. Ramanayake, A. Singh, D.S. Rueda, and C.R.M. Bangham. 2019. Kinetics of HTLV-1 reactivation from latency quantified by single-molecule RNA FISH and stochastic modelling. *PLOS Pathogens*. 15:e1008164-20. doi:10.1371/journal.ppat.1008164.

Mizuguchi, G., X. Shen, J. Landry, W.-H. Wu, S. Sen, and C. Wu. 2004. ATP-Driven Exchange of Histone H2AZ Variant Catalyzed by SWR1 Chromatin Remodeling Complex. *Science*. 303:343–348. doi:10.1126/science.1090701.

Mizuguchi, T., J. Barrowman, and S.I.S. Grewal. 2015. Chromosome domain architecture and dynamic organization of the fission yeast genome. *Febs Lett*. 589:2975–2986. doi:10.1016/j.febslet.2015.06.008.

Monneron, A., and W. Bernhard. 1969. Fine structural organization of the interphase nucleus in some mammalian cells. *J Ultra Mol Struct R*. 27:266–288. doi:10.1016/s0022-5320(69)80017-1.

Moore, B.T., J.M. Jordan, and L.R. Baugh. 2013. WormSizer: High-throughput Analysis of Nematode Size and Shape. *Plos One*. 8:e57142. doi:10.1371/journal.pone.0057142.

Moore, M.J., and N.J. Proudfoot. 2009. Pre-mRNA Processing Reaches Back toTranscription and Ahead to Translation. *Cell*. 136:688–700. doi:10.1016/j.cell.2009.02.001.

Moshkin, Y.M., L. Mohrmann, W.F.J. van Ijcken, and C.P. Verrijzer. 2006. Functional Differentiation of SWI/SNF Remodelers in Transcription and Cell Cycle Control ▿ †. *Mol Cell Biol*. 27:651–661. doi:10.1128/mcb.01257-06.

Mouridi, S.E., C. Lecroisey, P. Tardy, M. Mercier, A. Leclercq-Blondel, N. Zariohi, and T. Boulin. 2017. Reliable CRISPR/Cas9 Genome Engineering in Caenorhabditis elegansUsing a Single Efficient sgRNA and an Easily Recognizable Phenotype. *G3 (Bethesda, Md.)*. 7:1429–1437. doi:10.1534/g3.117.040824.

Mueller, F., A. Senecal, K. Tantale, H. Marie-Nelly, N. Ly, O. Collin, E. Basyuk, E. Bertrand, X. Darzacq, and C. Zimmer. 2013a. FISH-quant: automatic counting of transcripts in 3D FISH images. *Nature Methods*. 10:277–278. doi:10.1038/nmeth.2406.

Mueller, F., T.J. Stasevich, D. Mazza, and J.G. McNally. 2013b. Quantifying transcription factor kinetics: At work or at play? *Crit Rev Biochem Mol*. 48:492–514. doi:10.3109/10409238.2013.833891.

Muir, K.W., Y. Li, F. Weis, and D. Panne. 2020. The structure of the cohesin ATPase elucidates the mechanism of SMC–kleisin ring opening. *Nature structural & molecular biology*. 27:233–239. doi:10.1038/s41594-020-0379-7.

Munchel, S.E., R.K. Shultzaberger, N. Takizawa, and K. Weis. 2011. Dynamic profiling of mRNA turnover reveals gene-specific and system-wide regulation of mRNA decay. *Mol Biol Cell*. 22:2787–2795. doi:10.1091/mbc.e11-01-0028.

Munsky, B., G. Neuert, and A. van Oudenaarden. 2012. Using Gene Expression Noise to Understand Gene Regulation. *Science*. 336:183–187. doi:10.1126/science.1216379.

Murayama, Y., and F. Uhlmann. 2014. Biochemical reconstitution of topological DNA binding by the cohesin ring. *Nature*. 505:367–371. doi:10.1038/nature12867.

Murayama, Y., and F. Uhlmann. 2015. DNA Entry into and Exit out of the Cohesin Ring by an Interlocking Gate Mechanism. *Cell*. 163:1628–1640. doi:10.1016/j.cell.2015.11.030.

Nagano, T., Y. Lubling, T.J. Stevens, S. Schoenfelder, E. Yaffe, W. Dean, E.D. Laue, A. Tanay, and P. Fraser. 2013. Single-cell Hi-C reveals cell-to-cell variability in chromosome structure. *Nature*. 502:59–64. doi:10.1038/nature12593.

Narendra, V., M. Bulajić, J. Dekker, E.O. Mazzoni, and D. Reinberg. 2016. CTCF-mediated topological boundaries during development foster appropriate gene regulation. *Genes & Development*. 30:2657–2662. doi:10.1101/gad.288324.116.

Nasmyth, K. 2001. DISSEMINATING THE GENOME: Joining, Resolving, and Separating Sister Chromatids During Mitosis and Meiosis. *Annu Rev Genet*. 35:673–745. doi:10.1146/annurev.genet.35.102401.091334.

Nasmyth, K. 2011. Cohesin: a catenase with separate entry and exit gates? *Nat Cell Biol*. 13:1170–1177. doi:10.1038/ncb2349.

Nasmyth, K., and C.H. Haering. 2009. Cohesin: Its Roles and Mechanisms. *Genetics*. 43:525–558. doi:10.1146/annurev-genet-102108-134233.

Naumova, N., M. Imakaev, G. Fudenberg, Y. Zhan, B.R. Lajoie, L.A. Mirny, and J. Dekker. 2013. Organization of the Mitotic Chromosome. *Science*. 342:948–953. doi:10.1126/science.1236083.

Neuwald, A.F., and T. Hirano. 2000. HEAT Repeats Associated with Condensins, Cohesins, and Other Complexes Involved in Chromosome-Related Functions. *Genome Res*. 10:1445–1452. doi:10.1101/gr.147400.

Ni, J.Z., N. Kalinava, S.G. Mendoza, and S.G. Gu. 2018. The spatial and temporal dynamics of nuclear RNAi-targeted retrotransposon transcripts in Caenorhabditis elegans. *Development*. 145:dev.167346. doi:10.1242/dev.167346.

Nichols, M.H., and V.G. Corces. 2015. A CTCF Code for 3D Genome Architecture. *Cell*. 162:703–705. doi:10.1016/j.cell.2015.07.053.

Nicolas, D., B. Zoller, D.M. Suter, and F. Naef. 2018. Modulation of transcriptional burst frequency by histone acetylation. *Proceedings of the National Academy of Sciences of the United States of America*. 115:7153–7158. doi:10.1073/pnas.1722330115.

Nigon, V.M., and M.-A. Félix. 2017. History of research on C. elegans and other free-living nematodes as model organisms. *Wormbook*. 1–84. doi:10.1895/wormbook.1.181.1.

Niki, H., A. Jaffé, R. Imamura, T. Ogura, and S. Hiraga. 1991. The new gene mukB codes for a 177 kd protein with coiled-coil domains involved in chromosome partitioning of E. coli. *Embo J*. 10:183–93.

Nishide, K., and T. Hirano. 2014. Overlapping and Non-overlapping Functions of Condensins I and II in Neural Stem Cell Divisions. *PLoS genetics*. 10:e1004847-16. doi:10.1371/journal.pgen.1004847.

Nishimura, E.O., J.C. Zhang, A.D. Werts, B. Goldstein, and J.D. Lieb. 2015. Asymmetric Transcript Discovery by RNA-seq in C. elegans Blastomeres Identifies neg-1, a Gene Important for Anterior Morphogenesis. *Plos Genet*. 11:e1005117. doi:10.1371/journal.pgen.1005117.

Nishioka, K., J.C. Rice, K. Sarma, H. Erdjument-Bromage, J. Werner, Y. Wang, S. Chuikov, P. Valenzuela, P. Tempst, R. Steward, J.T. Lis, C.D. Allis, and D. Reinberg. 2002. PR-Set7 Is a Nucleosome-Specific Methyltransferase that Modifies Lysine 20 of Histone H4 and Is Associated with Silent Chromatin. *Mol Cell*. 9:1201–1213. doi:10.1016/s1097-2765(02)00548-8.

Nojima, T., T. Gomes, A.R.F. Grosso, H. Kimura, M.J. Dye, S. Dhir, M. Carmo-Fonseca, and N.J. Proudfoot. 2015. Mammalian NET-Seq Reveals Genome-wide Nascent Transcription Coupled to RNA Processing. *Cell*. 161:526–540. doi:10.1016/j.cell.2015.03.027.

Noma, K., H.P. Cam, R.J. Maraia, and S.I.S. Grewal. 2006. A Role for TFIIIC Transcription Factor Complex in Genome Organization. *Cell*. 125:859–872. doi:10.1016/j.cell.2006.04.028.

Nora, E.P., L. Caccianini, G. Fudenberg, K. So, V. Kameswaran, A. Nagle, A. Uebersohn, B. Hajj, A.L. Saux, A. Coulon, L.A. Mirny, K.S. Pollard, M. Dahan, and B.G. Bruneau. 2020. Molecular basis of CTCF binding polarity in genome folding. *Nat Commun*. 11:5612. doi:10.1038/s41467-020-19283-x.

Nora, E.P., A. Goloborodko, A.-L. Valton, J.H. Gibcus, A. Uebersohn, N. Abdennur, J. Dekker, L.A. Mirny, and B.G. Bruneau. 2016. Targeted Degradation of CTCF Decouples Local Insulation of Chromosome Domains from Genomic Compartmentalization. *Cell*. 169:930-944.e22. doi:10.1016/j.cell.2017.05.004.

Nora, E.P., B.R. Lajoie, E.G. Schulz, L. Giorgetti, I. Okamoto, N. Servant, T. Piolot, N.L. van Berkum, J. Meisig, J. Sedat, J. Gribnau, E. Barillot, N. Blüthgen, J. Dekker, and E. Heard. 2012. Spatial partitioning of the regulatory landscape of the X-inactivation centre. *Nature*. 485:381–385. doi:10.1038/nature11049.

Nuebler, J., G. Fudenberg, M. Imakaev, N. Abdennur, and L.A. Mirny. 2018. Chromatin organization by an interplay of loop extrusion and compartmental segregation. *Proc National Acad Sci*. 115:201717730. doi:10.1073/pnas.1717730115.

Nunez, R.V., L.B.R. Avila, and S. Gruber. 2019. Transient DNA Occupancy of the SMC Interarm Space in Prokaryotic Condensin. *Mol Cell*. 75:209-223.e6. doi:10.1016/j.molcel.2019.05.001.

Nusbaum, C., and B.J. Meyer. 1989. The Caenorhabditis-Elegans Gene Sdc-2 Controls Sex Determination and Dosage Compensation in Xx Animals. *Genetics*. 122:579–593.

Ocampo-Hafalla, M., S. Muñoz, C.P. Samora, and F. Uhlmann. 2016. Evidence for cohesin sliding along budding yeast chromosomes. *Open Biology*. 6:150178–14. doi:10.1098/rsob.150178.

Ohno, S., and T.S. Hauschka. 1960. Allocycly of the X-chromosome in tumors and normal tissues. *Cancer Res*. 20:541–5.

Olins, A.L., and D.E. Olins. 1974. Spheroid Chromatin Units (ν Bodies). *Science*. 183:330–332. doi:10.1126/science.183.4122.330.

Oliveira, R.A., S. Heidmann, and C.E. Sunkel. 2007. Condensin I binds chromatin early in prophase and displays a highly dynamic association with Drosophila mitotic chromosomes. *Chromosoma*. 116:259–274. doi:10.1007/s00412-007-0097-5.

Ono, T., Y. Fang, D.L. Spector, and T. Hirano. 2004. Spatial and Temporal Regulation of Condensins I and II in Mitotic Chromosome Assembly in Human Cells. *Mol Biol Cell*. 15:3296–3308. doi:10.1091/mbc.e04-03-0242.

Ono, T., A. Losada, M. Hirano, M.P. Myers, A.F. Neuwald, and T. Hirano. 2003. Differential Contributions of Condensin I and Condensin II to Mitotic Chromosome Architecture in Vertebrate Cells. *Cell*. 115:109–121. doi:10.1016/s0092-8674(03)00724-4.

Oromendia, A.B., and A. Amon. 2014. Aneuploidy: implications for protein homeostasis and disease. *Dis Model Mech*. 7:15–20. doi:10.1242/dmm.013391.

Ozbudak, E.M., M. Thattai, I. Kurtser, A.D. Grossman, and A. van Oudenaarden. 2002. Regulation of noise in the expression of a single gene. *Nat Genet*. 31:69–73. doi:10.1038/ng869.

Padovan-Merhar, O., G.P. Nair, A.G. Biaesch, A. Mayer, S. Scarfone, S.W. Foley, A.R. Wu, L.S. Churchman, A. Singh, and A. Raj. 2015. Single Mammalian Cells Compensate for Differences in Cellular Volume and DNA Copy Number through Independent Global Transcriptional Mechanisms. *Molecular Cell*. 58:339–352. doi:10.1016/j.molcel.2015.03.005.

Paix, A., A. Folkmann, D. Rasoloson, and G. Seydoux. 2015. High Efficiency, Homology-Directed Genome Editing in Caenorhabditis elegans Using CRISPR-Cas9 Ribonucleoprotein Complexes. *Genetics*. 201:47–54. doi:10.1534/genetics.115.179382.

Palecek, J.J., and S. Gruber. 2015. Kite Proteins: a Superfamily of SMC/Kleisin Partners Conserved Across Bacteria, Archaea, and Eukaryotes. *Structure*. 23:2183–2190. doi:10.1016/j.str.2015.10.004.

Papantonis, A., and P.R. Cook. 2013. Transcription Factories: Genome Organization and Gene Regulation. *Chem Rev*. 113:8683–8705. doi:10.1021/cr300513p.

Parada, L.A., J.J.R. and T. Misteli, and T. Misteli. 2003. An uncertainty principle in chromosome positioning. *Trends Cell Biol*. 13:393–396. doi:10.1016/s0962-8924(03)00149-1.

Parelho, V., S. Hadjur, M. Spivakov, M. Leleu, S. Sauer, H.C. Gregson, A. Jarmuz, C. Canzonetta, Z. Webster, T. Nesterova, B.S. Cobb, K. Yokomori, N. Dillon, L. Aragon, A.G. Fisher, and M. Merkenschlager. 2008. Cohesins Functionally Associate with CTCF on Mammalian Chromosome Arms. *Cell*. 132:422–433. doi:10.1016/j.cell.2008.01.011.

Parker, D.M., L.P. Winkenbach, S. Boyson, M.N. Saxton, C. Daidone, Z.A. Al-Mazaydeh, M.T. Nishimura, F. Mueller, and E.O. Nishimura. 2020. mRNA localization is linked to translation regulation in the Caenorhabditis elegans germ lineage. *Development*. 147:dev186817. doi:10.1242/dev.186817.

Parthasarathy, R. 2012. Rapid, accurate particle tracking by calculation of radial symmetry centers. *Nature Methods*. 9:724–726. doi:10.1038/nmeth.2071.

Parvin, J.D., and P.A. Sharp. 1993. DNA topology and a minimal set of basal factors for transcription by RNA polymerase II. *Cell*. 73:533–540. doi:10.1016/0092-8674(93)90140-l.

Paul, M.R., A. Hochwagen, and S. Ercan. 2018a. Condensin action and compaction. *Curr Genet*. 65:407–415. doi:10.1007/s00294-018-0899-4.

Paul, M.R., T.E. Markowitz, A. Hochwagen, and S. Ercan. 2018b. Condensin Depletion Causes Genome Decompaction Without Altering the Level of Global Gene Expression in Saccharomyces cerevisiae. *Genetics*. 210:genetics.301217.2018. doi:10.1534/genetics.118.301217.

Paulson, J.R., and U.K. Laemmli. 1977. The structure of histone-depleted metaphase chromosomes. *Cell*. 12:817–828. doi:10.1016/0092-8674(77)90280-x.

Peccoud, J., and B. Ycart. 1995. Markovian Modeling of Gene-Product Synthesis. *Theor Popul Biol*. 48:222–234. doi:10.1006/tpbi.1995.1027.

Petela, N.J., T.G. Gligoris, J. Metson, B.-G. Lee, M. Voulgaris, B. Hu, S. Kikuchi, C. Chapard, W. Chen, E. Rajendra, M. Srinivisan, H. Yu, J. Löwe, and K.A. Nasmyth. 2018. Scc2 Is a Potent Activator of Cohesin's ATPase that Promotes Loading by Binding Scc1 without Pds5. *Mol Cell*. 70:1134-1148.e7. doi:10.1016/j.molcel.2018.05.022.

Petty, E.L., K.S. Collette, A.J. Cohen, M.J. Snyder, and G. Csankovszki. 2009. Restricting Dosage Compensation Complex Binding to the X Chromosomes by H2A.Z/HTZ-1. *Plos Genet*. 5:e1000699. doi:10.1371/journal.pgen.1000699.

Pferdehirt, R.R., W.S. Kruesi, and B.J. Meyer. 2011. An MLL/COMPASS subunit functions in the C. elegans dosage compensation complex to target X chromosomes for transcriptional regulation of gene expression. *Genes & Development*. 25:499–515. doi:10.1101/gad.2016011.

Pferdehirt, R.R., and B.J. Meyer. 2013. SUMOylation is essential for sex-specific assembly and function of the Caenorhabditis elegans dosage compensation complex on X chromosomes. *Proceedings of the National Academy of Sciences of the United States of America*. 110:E3810-9. doi:10.1073/pnas.1315793110.

Piazza, I., A. Rutkowska, A. Ori, M. Walczak, J. Metz, V. Pelechano, M. Beck, and C.H. Haering. 2014. Association of condensin with chromosomes depends on DNA binding by its HEAT-repeat subunits. *Nature Publishing Group*. 1–12. doi:10.1038/nsmb.2831.

Piccoli, G.D., J. Torres-Rosell, and L. Aragón. 2009. The unnamed complex: what do we know about Smc5-Smc6? *Chromosome Res*. 17:251–263. doi:10.1007/s10577-008-9016-8.

Pizarro, L., and L. Norambuena. 2014. Regulation of protein trafficking: Posttranslational mechanisms and the unexplored transcriptional control. *Plant Sci*. 225:24–33. doi:10.1016/j.plantsci.2014.05.004.

Plenefisch, J.D., L. DeLong, and B.J. Meyer. 1989a. Genes that implement the hermaphrodite mode of dosage compensation in Caenorhabditis elegans. *Genetics*. 121:57–76.

Plenefisch, J.D., L. DeLong, and B.J. Meyer. 1989b. Genes that implement the hermaphrodite mode of dosage compensation in Caenorhabditis elegans. *Genetics*. 121:57–76.

Pomiankowski, A., R. Nöthiger, and A. Wilkins. 2004. The Evolution of the Drosophila Sex-Determination Pathway. *Genetics*. 166:1761–1773. doi:10.1534/genetics.166.4.1761.

Pope, B.D., T. Ryba, V. Dileep, F. Yue, W. Wu, O. Denas, D.L. Vera, Y. Wang, R.S. Hansen, T.K. Canfield, R.E. Thurman, Y. Cheng, G. Gülsoy, J.H. Dennis, M.P. Snyder, J.A. Stamatoyannopoulos, J. Taylor, R.C. Hardison, T. Kahveci, B. Ren, and D.M. Gilbert. 2014.

Topologically associating domains are stable units of replication-timing regulation. *Nature*. 515:402–405. doi:10.1038/nature13986.

Potts, P.R., M.H. Porteus, and H. Yu. 2006. Human SMC5/6 complex promotes sister chromatid homologous recombination by recruiting the SMC1/3 cohesin complex to double-strand breaks. *Embo J*. 25:3377–3388. doi:10.1038/sj.emboj.7601218.

Praitis, V., E. Casey, D. Collar, and J. Austin. 2001. Creation of low-copy integrated transgenic lines in Caenorhabditis elegans. *Genetics*. 157:1217–1226.

Ptashne, M. 1988. How eukaryotic transcriptional activators work. *Nature*. 335:683–689. doi:10.1038/335683a0.

Raab, J.R., and R.T. Kamakaka. 2010. Insulators and promoters: closer than we think. *Nat Rev Genet*. 11:439–446. doi:10.1038/nrg2765.

Racko, D., F. Benedetti, J. Dorier, and A. Stasiak. 2017. Transcription-induced supercoiling as the driving force of chromatin loop extrusion during formation of TADs in interphase chromosomes. *Nucleic Acids Res*. 46:gkx1123-. doi:10.1093/nar/gkx1123.

Raj, A., P. van den Bogaard, S.A. Rifkin, A. van Oudenaarden, and S. Tyagi. 2008. Imaging individual mRNA molecules using multiple singly labeled probes. *Nature Publishing Group*. 5:877–879. doi:10.1038/nmeth.1253.

Raj, A., and A. van Oudenaarden. 2008. Nature, Nurture, or Chance: Stochastic Gene Expression and Its Consequences. *Cell*. 135:216–226. doi:10.1016/j.cell.2008.09.050.

Raj, A., C.S. Peskin, D. Tranchina, D.Y. Vargas, and S. Tyagi. 2006. Stochastic mRNA Synthesis in Mammalian Cells. *PLoS Biology*. 4:e309. doi:10.1371/journal.pbio.0040309.

Raj, A., S.A. Rifkin, E. Andersen, and A. van Oudenaarden. 2010. Variability in gene expression underlies incomplete penetrance. *Nature*. 463:913–918. doi:10.1038/nature08781.

Ramírez, F., V. Bhardwaj, L. Arrigoni, K.C. Lam, B.A. Grüning, J. Villaveces, B. Habermann, A. Akhtar, and T. Manke. 2018. High-resolution TADs reveal DNA sequences underlying genome organization in flies. *Nat Commun*. 9:189. doi:10.1038/s41467-017-02525-w.

Ramírez, F., D.P. Ryan, B. Grüning, V. Bhardwaj, F. Kilpert, A.S. Richter, S. Heyne, F. Dündar, and T. Manke. 2016. deepTools2: a next generation web server for deep-sequencing data analysis. *Nucleic Acids Res*. 44:W160–W165. doi:10.1093/nar/gkw257.

Ramirez-Gonzalez, R.H., R. Bonnal, M. Caccamo, and D. MacLean. 2012. Bio-samtools: Ruby bindings for SAMtools, a library for accessing BAM files containing high-throughput sequence alignments. *Source Code Biology Medicine*. 7:6. doi:10.1186/1751-0473-7-6.

Ranjan, A., V.Q. Nguyen, S. Liu, J. Wisniewski, J.M. Kim, X. Tang, G. Mizuguchi, E. Elalaoui, T.J. Nickels, V. Jou, B.P. English, Q. Zheng, E. Luk, L.D. Lavis, T. Lionnet, and C. Wu. 2020. Live-cell single particle imaging reveals the role of RNA polymerase II in histone H2A.Z eviction. *Elife*. 9:e55667. doi:10.7554/elife.55667.

Rao, S.S.P., S.-C. Huang, B.G.S. Hilaire, J.M. Engreitz, E.M. Perez, K.-R. Kieffer-Kwon, A.L. Sanborn, S.E. Johnstone, G.D. Bascom, I.D. Bochkov, X. Huang, M.S. Shamim, J. Shin, D. Turner, Z. Ye, A.D. Omer, J.T. Robinson, T. Schlick, B.E. Bernstein, R. Casellas, E.S. Lander, and

E.L. Aiden. 2017. Cohesin Loss Eliminates All Loop Domains. *Cell*. 171:305-320.e24. doi:10.1016/j.cell.2017.09.026.

Rao, S.S.P., M.H. Huntley, N.C. Durand, E.K. Stamenova, I.D. Bochkov, J.T. Robinson, A.L. Sanborn, I. Machol, A.D. Omer, E.S. Lander, and E.L. Aiden. 2014. A 3D Map of the Human Genome at Kilobase Resolution Reveals Principles of Chromatin Looping. *Cell*. 159:1665–1680. doi:10.1016/j.cell.2014.11.021.

Rawlings, J.S., M. Gatzka, P.G. Thomas, and J.N. Ihle. 2010. Chromatin condensation via the condensin II complex is required for peripheral T-cell quiescence. *The EMBO Journal*. 30:263–276. doi:10.1038/emboj.2010.314.

Rea, S.L., D. Wu, J.R. Cypser, J.W. Vaupel, and T.E. Johnson. 2005. A stress-sensitive reporter predicts longevity in isogenic populations of Caenorhabditis elegans. *Nat Genet*. 37:894–898. doi:10.1038/ng1608.

Redemann, S., S. Schloissnig, S. Ernst, A. Pozniakowsky, S. Ayloo, A.A. Hyman, and H. Bringmann. 2011. Codon adaptation-based control of protein expression in C. elegans. *Nature Publishing Group*. 8:250–252. doi:10.1038/nmeth.1565.

Reinke, V., M. Krause, and P. Okkema. 2013. Transcriptional regulation of gene expression in C. elegans. *WormBook*. 1–34. doi:10.1895/wormbook.1.45.2.

Rhodes, J., D. Mazza, K. Nasmyth, and S. Uphoff. 2017a. Scc2/Nipbl hops between chromosomal cohesin rings after loading. *eLife*. 6:11202. doi:10.7554/elife.30000.

Rhodes, J.D.P., J.H.I. Haarhuis, J.B. Grimm, B.D. Rowland, L.D. Lavis, and K.A. Nasmyth. 2017b. Cohesin Can Remain Associated with Chromosomes during DNA Replication. *CellReports*. 20:2749–2755. doi:10.1016/j.celrep.2017.08.092.

Richard, P., and J.L. Manley. 2009. Transcription termination by nuclear RNA polymerases. *Gene Dev*. 23:1247–1269. doi:10.1101/gad.1792809.

Rickels, R., L. Wang, M. Iwanaszko, P.A. Ozark, M.A. Morgan, A. Piunti, N. Khalatyan, S.H.A. Soliman, E.J. Rendleman, J.N. Savas, E.R. Smith, and A. Shilatifard. 2020. A small UTX stabilization domain of Trr is conserved within mammalian MLL3-4/COMPASS and is sufficient to rescue loss of viability in null animals. *Gene Dev*. 34:1493–1502. doi:10.1101/gad.339762.120.

Robellet, X., Y. Thattikota, F. Wang, T.-L. Wee, M. Pascariu, S. Shankar, É. Bonneil, C.M. Brown, and D. D'Amours. 2015. A high-sensitivity phospho-switch triggered by Cdk1 governs chromosome morphogenesis during cell division. *Gene Dev*. 29:426–439. doi:10.1101/gad.253294.114.

Robert, V., and J.-L. Bessereau. 2007. Targeted engineering of the Caenorhabditis elegans genome following Mos1-triggered chromosomal breaks. *Embo Journal*. 26:170–183. doi:10.1038/sj.emboj.7601463.

Rodríguez-Carballo, E., L. Lopez-Delisle, N. Yakushiji-Kaminatsui, A. Ullate-Agote, and D. Duboule. 2019. Impact of genome architecture on the functional activation and repression of Hox regulatory landscapes. *Bmc Biol*. 17:55. doi:10.1186/s12915-019-0677-x.

Rodríguez-Carballo, E., L. Lopez-Delisle, Y. Zhan, P.J. Fabre, L. Beccari, I. El-Idrissi, T.H.N. Huynh, H. Ozadam, J. Dekker, and D. Duboule. 2017. The HoxD cluster is a dynamic and resilient TAD boundary controlling the segregation of antagonistic regulatory landscapes. *Gene Dev*. 31:2264–2281. doi:10.1101/gad.307769.117.

Roeder, R.G., and W.J. Rutter. 1969. Multiple Forms of DNA-dependent RNA Polymerase in Eukaryotic Organisms. *Nature*. 224:234–237. doi:10.1038/224234a0.

Rohner, S., V. Kalck, X. Wang, K. Ikegami, J.D. Lieb, S.M. Gasser, and P. Meister. 2013. Promoter- and RNA polymerase II–dependent hsp-16 gene association with nuclear pores in Caenorhabditis elegans. *J Cell Biol*. 200:589–604. doi:10.1083/jcb.201207024.

Rosin, L.F., S.C. Nguyen, and E.F. Joyce. 2018. Condensin II drives large-scale folding and spatial partitioning of interphase chromosomes in Drosophila nuclei. *PLoS genetics*. 14:e1007393. doi:10.1371/journal.pgen.1007393.

Rosonina, E., and B.J. Blencowe. 2004. Analysis of the requirement for RNA polymerase II CTD heptapeptide repeats in pre-mRNA splicing and 3′-end cleavage. *Rna*. 10:581–589. doi:10.1261/rna.5207204.

Rougvie, A.E., and J.T. Lis. 1988. The RNA polymerase II molecule at the 5′ end of the uninduced hsp70 gene of D. melanogaster is transcriptionally engaged. *Cell*. 54:795–804. doi:10.1016/s0092-8674(88)91087-2.

Rowley, M.J., A. Poulet, M.H. Nichols, B.J. Bixler, A.L. Sanborn, E.A. Brouhard, K. Hermetz, H. Linsenbaum, G. Csankovszki, E.L. Aiden, and V.G. Corces. 2020. Analysis of Hi-C data using SIP effectively identifies loops in organisms from C. elegans to mammals. *Genome Res*. 30:447–458. doi:10.1101/gr.257832.119.

Rubin, A.J., B.C. Barajas, M. Furlan-Magaril, V. Lopez-Pajares, M.R. Mumbach, I. Howard, D.S. Kim, L.D. Boxer, J. Cairns, M. Spivakov, S.W. Wingett, M. Shi, Z. Zhao, W.J. Greenleaf, A. Kundaje, M. Snyder, H.Y. Chang, P. Fraser, and P.A. Khavari. 2017. Lineage-specific dynamic and pre-established enhancer–promoter contacts cooperate in terminal differentiation. *Nat Genet*. 49:1522–1528. doi:10.1038/ng.3935.

Ruiten, M.S. van, and B.D. Rowland. 2018. SMC Complexes: Universal DNA Looping Machines with Distinct Regulators. *Trends in Genetics*. 1–11. doi:10.1016/j.tig.2018.03.003.

Rullan, M., D. Benzinger, G.W. Schmidt, A. Milias-Argeitis, and M. Khammash. 2018. An Optogenetic Platform for Real-Time, Single-Cell Interrogation of Stochastic Transcriptional Regulation. *Mol Cell*. 70:745-756.e6. doi:10.1016/j.molcel.2018.04.012.

Ryba, T., I. Hiratani, J. Lu, M. Itoh, M. Kulik, J. Zhang, T.C. Schulz, A.J. Robins, S. Dalton, and D.M. Gilbert. 2010. Evolutionarily conserved replication timing profiles predict long-range chromatin interactions and distinguish closely related cell types. *Genome Res*. 20:761–770. doi:10.1101/gr.099655.109.

Ryu, J.-K., C. Bouchoux, H.W. Liu, E. Kim, M. Minamino, R. de Groot, A.J. Katan, A. Bonato, D. Marenduzzo, D. Michieletto, F. Uhlmann, and C. Dekker. 2021. Bridging-induced phase separation induced by cohesin SMC protein complexes. *Sci Adv*. 7:eabe5905. doi:10.1126/sciadv.abe5905.

Sabari, B.R., A. Dall'Agnese, A. Boija, I.A. Klein, E.L. Coffey, K. Shrinivas, B.J. Abraham, N.M. Hannett, A.V. Zamudio, J.C. Manteiga, C.H. Li, Y.E. Guo, D.S. Day, J. Schuijers, E. Vasile, S. Malik, D. Hnisz, T.I. Lee, I.I. Cisse, R.G. Roeder, P.A. Sharp, A.K. Chakraborty, and R.A. Young. 2018. Coactivator condensation at super-enhancers links phase separation and gene control. *Science*. 361:eaar3958-13. doi:10.1126/science.aar3958.

Sainsbury, S., C. Bernecky, and P. Cramer. 2015. Structural basis of transcription initiation by RNA polymerase II. *Nature Reviews Molecular Cell Biology*. 16:129–143. doi:10.1038/nrm3952.

Saitoh, N., I.G. Goldberg, E.R. Wood, and W.C. Earnshaw. 1994. ScII: an abundant chromosome scaffold protein is a member of a family of putative ATPases with an unusual predicted tertiary structure. *J Cell Biology*. 127:303–318. doi:10.1083/jcb.127.2.303.

Samata, M., and A. Akhtar. 2018. Dosage Compensation of the X Chromosome: A Complex Epigenetic Assignment Involving Chromatin Regulators and Long Noncoding RNAs. *Annu Rev Biochem*. 87:1–28. doi:10.1146/annurev-biochem-062917-011816.

Sanborn, A.L., S.S.P. Rao, S.-C. Huang, N.C. Durand, M.H. Huntley, A.I. Jewett, I.D. Bochkov, D. Chinnappan, A. Cutkosky, J. Li, K.P. Geeting, A. Gnirke, A. Melnikov, D. McKenna, E.K. Stamenova, E.S. Lander, and E.L. Aiden. 2015. Chromatin extrusion explains key features of loop and domain formation in wild-type and engineered genomes. *Proc National Acad Sci*. 112:E6456–E6465. doi:10.1073/pnas.1518552112.

Sarge, K.D., and O.-K. Park-Sarge. 2005. Gene bookmarking: keeping the pages open. *Trends Biochem Sci*. 30:605–610. doi:10.1016/j.tibs.2005.09.004.

Saunders, A., L.J. Core, and J.T. Lis. 2006. Breaking barriers to transcription elongation. *Nat Rev Mol Cell Bio*. 7:557–567. doi:10.1038/nrm1981.

Schauer, T., Y. Ghavi-Helm, T. Sexton, C. Albig, C. Regnard, G. Cavalli, E.E. Furlong, and P.B. Becker. 2017. Chromosome topology guides the Drosophila Dosage Compensation Complex for target gene activation. *EMBO reports*. e201744292-15. doi:10.15252/embr.201744292.

Schilbach, S., M. Hantsche, D. Tegunov, C. Dienemann, C. Wigge, H. Urlaub, and P. Cramer. 2017. Structures of transcription pre-initiation complex with TFIIH and Mediator. *Nature*. 551:204–209. doi:10.1038/nature24282.

Schindelin, J., I. Arganda-Carreras, E. Frise, V. Kaynig, M. Longair, T. Pietzsch, S. Preibisch, C. Rueden, S. Saalfeld, B. Schmid, J.-Y. Tinevez, D.J. White, V. Hartenstein, K. Eliceiri, P. Tomancak, and A. Cardona. 2012. Fiji: an open-source platform for biological-image analysis. *Nature Methods*. 9:676–682. doi:10.1038/nmeth.2019.

Schleiffer, A., S. Kaitna, S. Maurer-Stroh, M. Glotzer, K. Nasmyth, and F. Eisenhaber. 2003. Kleisins: A Superfamily of Bacterial and Eukaryotic SMC Protein Partners. *Mol Cell*. 11:571–575. doi:10.1016/s1097-2765(03)00108-4.

Schmidt, U., M. Weigert, C. Broaddus, and G. Myers. 2018. Cell Detection with Star-convex Polygons. *Arxiv*. doi:10.1007/978-3-030-00934-2_30.

Schmitz, M.L., J.M.G. Higgins, and M. Seibert. 2020. Priming chromatin for segregation: functional roles of mitotic histone modifications. *Cell Cycle*. 19:625–641. doi:10.1080/15384101.2020.1719585.

Schotta, G., M. Lachner, K. Sarma, A. Ebert, R. Sengupta, G. Reuter, D. Reinberg, and T. Jenuwein. 2004. A silencing pathway to induce H3-K9 and H4-K20 trimethylation at constitutive heterochromatin. *Gene Dev*. 18:1251–1262. doi:10.1101/gad.300704.

Schwalb, B., M. Michel, B. Zacher, K. Frühauf, C. Demel, A. Tresch, J. Gagneur, and P. Cramer. 2016. TT-seq maps the human transient transcriptome. *Science*. 352:1225–1228. doi:10.1126/science.aad9841.

Schwarzer, W., N. Abdennur, A. Goloborodko, A. Pekowska, G. Fudenberg, Y. Loe-Mie, N.A. Fonseca, W. Huber, C.H. Haering, L. Mirny, and F. Spitz. 2017. Two independent modes of

chromatin organization revealed by cohesin removal. *Nature Publishing Group*. 551:51–56. doi:10.1038/nature24281.

Segil, N., M. Guermah, A. Hoffmann, R.G. Roeder, and N. Heintz. 1996. Mitotic regulation of TFIID: inhibition of activator-dependent transcription and changes in subcellular localization. *Gene Dev*. 10:2389–2400. doi:10.1101/gad.10.19.2389.

Seidel, H.S., M. Ailion, J. Li, A. van Oudenaarden, M.V. Rockman, and L. Kruglyak. 2011. A Novel Sperm-Delivered Toxin Causes Late-Stage Embryo Lethality and Transmission Ratio Distortion in C. elegans. *Plos Biol*. 9:e1001115. doi:10.1371/journal.pbio.1001115.

Seitan, V.C., A.J. Faure, Y. Zhan, R.P. McCord, B.R. Lajoie, E. Ing-Simmons, B. Lenhard, L. Giorgetti, E. Heard, A.G. Fisher, P. Flicek, J. Dekker, and M. Merkenschlager. 2013. Cohesin-based chromatin interactions enable regulated gene expression within preexisting architectural compartments. *Genome Res*. 23:2066–2077. doi:10.1101/gr.161620.113.

Senecal, A., B. Munsky, F. Proux, N. Ly, F.E. Braye, C. Zimmer, F. Mueller, and X. Darzacq. 2014. Transcription Factors Modulate c-Fos Transcriptional Bursts. *CellReports*. 8:75–83. doi:10.1016/j.celrep.2014.05.053.

Sentenac, A. 2008. Eukaryotic RNA Polymerase. *Critical Rev Biochem*. 18:31–90. doi:10.3109/10409238509082539.

Serrano, D., G. Cordero, R. Kawamura, A. Sverzhinsky, M. Sarker, S. Roy, C. Malo, J.M. Pascal, J.F. Marko, and D. D'Amours. 2020. The Smc5/6 Core Complex Is a Structure-Specific DNA Binding and Compacting Machine. *Mol Cell*. 80:1025-1038.e5. doi:10.1016/j.molcel.2020.11.011.

Sexton, T., E. Yaffe, E. Kenigsberg, F. Bantignies, B. Leblanc, M. Hoichman, H. Parrinello, A. Tanay, and G. Cavalli. 2012. Three-Dimensional Folding and Functional Organization Principles of the Drosophila Genome. *Cell*. 148:458–472. doi:10.1016/j.cell.2012.01.010.

Seydoux, G., and M.A. Dunn. 1997. Transcriptionally repressed germ cells lack a subpopulation of phosphorylated RNA polymerase II in early embryos of Caenorhabditis elegans and Drosophila melanogaster. *Dev Camb Engl*. 124:2191–201.

Seydoux, G., and A. Fire. 1994. Soma-germline asymmetry in the distributions of embryonic RNAs in Caenorhabditis elegans. *Dev Camb Engl*. 120:2823–34.

Shaffer, S.M., M.-T. Wu, M.J. Levesque, and A. Raj. 2013. Turbo FISH: A Method for Rapid Single Molecule RNA FISH. *PLoS ONE*. doi:10.1371/journal.pone.0075120.g001.

Shandilya, J., and S.G.E. Roberts. 2012. The transcription cycle in eukaryotes: From productive initiation to RNA polymerase II recycling. *Biochimica Et Biophysica Acta Bba - Gene Regul Mech*. 1819:391–400. doi:10.1016/j.bbagrm.2012.01.010.

Sharma, R., D. Jost, J. Kind, G. Gómez-Saldivar, B. van Steensel, P. Askjaer, C. Vaillant, and P. Meister. 2014. Differential spatial and structural organization of the X chromosome underlies dosage compensation in C. elegans. *Gene Dev*. 28:2591–2596. doi:10.1101/gad.248864.114.

Sharma, R., and P. Meister. 2015. Linking dosage compensation and X chromosome nuclear organization in C. elegans. *Nucleus*. 6:266–272. doi:10.1080/19491034.2015.1059546.

Shilatifard, A., W.S. Lane, K.W. Jackson, R.C. Conaway, and J.W. Conaway. 1996. An RNA Polymerase II Elongation Factor Encoded by the Human ELL Gene. *Science*. 271:1873–1876. doi:10.1126/science.271.5257.1873.

Sieburth, L.E., and J.N. Vincent. 2018. Beyond transcription factors: roles of mRNA decay in regulating gene expression in plants. *F1000research*. 7:F1000 Faculty Rev-1940. doi:10.12688/f1000research.16203.1.

Singh, A., and M. Soltani. 2013. Quantifying Intrinsic and Extrinsic Variability in Stochastic Gene Expression Models. *Plos One*. 8:e84301. doi:10.1371/journal.pone.0084301.

Singh, J., and R.A. Padgett. 2009. Rates of in situ transcription and splicing in large human genes. *Nat Struct Mol Biol*. 16:1128–1133. doi:10.1038/nsmb.1666.

Skinner, S.O., H. Xu, S. Nagarkar-Jaiswal, P.R. Freire, T.P. Zwaka, and I. Golding. 2016. Single-cell analysis of transcription kinetics across the cell cycle. *eLife*. 5:e59928-3. doi:10.7554/elife.12175.

Snider, C.E., A.D. Stephens, J.G. Kirkland, O. Hamdani, R.T. Kamakaka, and K. Bloom. 2014. Dyskerin, tRNA genes, and condensin tether pericentric chromatin to the spindle axis in mitosis. *J Cell Biol*. 207:189–199. doi:10.1083/jcb.201405028.

Snyder, M.J., A.C. Lau, E.A. Brouhard, M.B. Davis, J. Jiang, M.H. Sifuentes, and G. Csankovszki. 2016. Anchoring of Heterochromatin to the Nuclear Lamina Reinforces Dosage Compensation-Mediated Gene Repression. *Plos Genet*. 12:e1006341. doi:10.1371/journal.pgen.1006341.

Sofueva, S., E. Yaffe, W. Chan, D. Georgopoulou, M.V. Rudan, H. Mira-Bontenbal, S.M. Pollard, G.P. Schroth, A. Tanay, and S. Hadjur. 2013. Cohesin-mediated interactions organize chromosomal domain architecture. *Embo J*. 32:3119–3129. doi:10.1038/emboj.2013.237.

Soppa, J., K. Kobayashi, M. Noirot-Gros, D. Oesterhelt, S.D. Ehrlich, E. Dervyn, N. Ogasawara, and S. Moriya. 2002. Discovery of two novel families of proteins that are proposed to interact with prokaryotic SMC proteins, and characterization of the Bacillus subtilis family members ScpA and ScpB. *Mol Microbiol*. 45:59–71. doi:10.1046/j.1365-2958.2002.03012.x.

Soufi, A., M.F. Garcia, A. Jaroszewicz, N. Osman, M. Pellegrini, and K.S. Zaret. 2015. Pioneer Transcription Factors Target Partial DNA Motifs on Nucleosomes to Initiate Reprogramming. *Cell*. 161:555–568. doi:10.1016/j.cell.2015.03.017.

Ståhl, P.L., F. Salmén, S. Vickovic, A. Lundmark, J.F. Navarro, J. Magnusson, S. Giacomello, M. Asp, J.O. Westholm, M. Huss, A. Mollbrink, S. Linnarsson, S. Codeluppi, Å. Borg, F. Pontén, P.I. Costea, P. Sahlén, J. Mulder, O. Bergmann, J. Lundeberg, and J. Frisén. 2016. Visualization and analysis of gene expression in tissue sections by spatial transcriptomics. *Science*. 353:78–82. doi:10.1126/science.aaf2403.

Stasevich, T.J., Y. Hayashi-Takanaka, Y. Sato, K. Maehara, Y. Ohkawa, K. Sakata-Sogawa, M. Tokunaga, T. Nagase, N. Nozaki, J.G. McNally, and H. Kimura. 2014. Regulation of RNA polymerase II activation by histone acetylation in single living cells. *Nature*. 516:272–275. doi:10.1038/nature13714.

Stec, N., K. Doerfel, K. Hills-Muckey, V.M. Ettorre, S. Ercan, W. Keil, and C.M. Hammell. 2021. An Epigenetic Priming Mechanism Mediated by Nutrient Sensing Regulates Transcriptional Output during C. elegans Development. *Curr Biol*. 31:809-826.e6. doi:10.1016/j.cub.2020.11.060.

Steensel, B. van, and E.E.M. Furlong. 2019. The role of transcription in shaping the spatial organization of the genome. *Nat Rev Mol Cell Bio*. 20:327–337. doi:10.1038/s41580-019-0114-6.

Stigler, J., G.Ö. Çamdere, D.E. Koshland, and E.C. Greene. 2016. Single-Molecule Imaging Reveals a Collapsed Conformational State for DNA-Bound Cohesin. *Cell Reports*. 15:988–998. doi:10.1016/j.celrep.2016.04.003.

St-Pierre, J., M. Douziech, F. Bazile, M. Pascariu, É. Bonneil, V. Sauvé, H. Ratsima, and D. D'Amours. 2009. Polo Kinase Regulates Mitotic Chromosome Condensation by Hyperactivation of Condensin DNA Supercoiling Activity. *Mol Cell*. 34:416–426. doi:10.1016/j.molcel.2009.04.013.

Stracy, M., and A.N. Kapanidis. 2017. Single-molecule and super-resolution imaging of transcription in living bacteria. *Methods (San Diego, Calif.)*. 1–12. doi:10.1016/j.ymeth.2017.04.001.

Strahl, B.D., and C.D. Allis. 2000. The language of covalent histone modifications. *Nature*. 403:41–45. doi:10.1038/47412.

Straub, T., and P.B. Becker. 2007. Dosage compensation: the beginning and end of generalization. *Nat Rev Genet*. 8:47–57. doi:10.1038/nrg2013.

Straub, T., A. Zabel, G.D. Gilfillan, C. Feller, and P.B. Becker. 2013. Different chromatin interfaces of the Drosophila dosage compensation complex revealed by high-shear ChIP-seq. *Genome Res*. 23:473–485. doi:10.1101/gr.146407.112.

Street, L.A., A.K. Morao, L.H. Winterkorn, C.-Y. Jiao, S.E. Albritton, M. Sadic, M. Kramer, and S. Ercan. 2019. Binding of an X-Specific Condensin Correlates with a Reduction in Active Histone Modifications at Gene Regulatory Elements. *Biorxiv*. 212:729–742. doi:10.1534/genetics.119.302254.

Strick, T.R., T. Kawaguchi, and T. Hirano. 2004. Real-Time Detection of Single-Molecule DNA Compaction by Condensin I. *Curr Biol*. 14:874–880. doi:10.1016/j.cub.2004.04.038.

Ström, L., H.B. Lindroos, K. Shirahige, and C. Sjögren. 2004. Postreplicative Recruitment of Cohesin to Double-Strand Breaks Is Required for DNA Repair. *Mol Cell*. 16:1003–1015. doi:10.1016/j.molcel.2004.11.026.

Strunnikov, A.V., V.L. Larionov, and D. Koshland. 1993. SMC1: an essential yeast gene encoding a putative head-rod-tail protein is required for nuclear division and defines a new ubiquitous protein family. *J Cell Biology*. 123:1635–1648. doi:10.1083/jcb.123.6.1635.

Sulston, J.E., and H.R. Horvitz. 1977. Post-embryonic cell lineages of the nematode, Caenorhabditis elegans. *Developmental Biology*. 56:110–156. doi:10.1016/0012-1606(77)90158-0.

Sulston, J.E., E. Schierenberg, J.G. White, and J.N. Thomson. 1983. The embryonic cell lineage of the nematode Caenorhabditis elegans. *Developmental Biology*. 100:64–119. doi:10.1016/0012-1606(83)90201-4.

Sural, T.H., S. Peng, B. Li, J.L. Workman, P.J. Park, and M.I. Kuroda. 2008. The MSL3 chromodomain directs a key targeting step for dosage compensation of the Drosophila melanogaster X chromosome. *Nat Struct Mol Biol*. 15:1318–1325. doi:10.1038/nsmb.1520.

Sutani, T., T. Yuasa, T. Tomonaga, N. Dohmae, K. Takio, and M. Yanagida. 1999. Fission yeast condensin complex: essential roles of non-SMC subunits for condensation and Cdc2 phosphorylation of Cut3/SMC4. *Gene Dev*. 13:2271–2283. doi:10.1101/gad.13.17.2271.

Suter, D.M., N. Molina, D. Gatfield, K. Schneider, U. Schibler, and F. Naef. 2011. Mammalian genes are transcribed with widely different bursting kinetics. *Science*. 332:472–474. doi:10.1126/science.1198817.

Swain, P.S., M.B. Elowitz, and E.D. Siggia. 2002. Intrinsic and extrinsic contributions to stochasticity in gene expression. *Proc National Acad Sci*. 99:12795–12800. doi:10.1073/pnas.162041399.

Swanson, C.I., N.C. Evans, and S. Barolo. 2010. Structural Rules and Complex Regulatory Circuitry Constrain Expression of a Notch- and EGFR-Regulated Eye Enhancer. *Dev Cell*. 18:359–370. doi:10.1016/j.devcel.2009.12.026.

Swygert, S.G., S. Kim, X. Wu, T. Fu, T.-H. Hsieh, O.J. Rando, R.N. Eisenman, J. Shendure, J.N. McKnight, and T. Tsukiyama. 2019. Condensin-Dependent Chromatin Compaction Represses Transcription Globally during Quiescence. *Molecular Cell*. 73:533-546.e4. doi:10.1016/j.molcel.2018.11.020.

Tada, K., H. Susumu, T. Sakuno, and Y. Watanabe. 2011. Condensin association with histone H2A shapes mitotic chromosomes. *Nature*. 1–10. doi:10.1038/nature10179.

Takahashi, K., and S. Yamanaka. 2016. A decade of transcription factor-mediated reprogramming to pluripotency. *Nat Rev Mol Cell Bio*. 17:183–193. doi:10.1038/nrm.2016.8.

Takemoto, A., A. Murayama, M. Katano, T. Urano, K. Furukawa, S. Yokoyama, J. Yanagisawa, F. Hanaoka, and K. Kimura. 2007. Analysis of the role of Aurora B on the chromosomal targeting of condensin I. *Nucleic Acids Res*. 35:2403–2412. doi:10.1093/nar/gkm157.

Takizawa, T., K.J. Meaburn, and T. Misteli. 2008. The Meaning of Gene Positioning. *Cell*. 135:9–13. doi:10.1016/j.cell.2008.09.026.

Talbert, P.B., and S. Henikoff. 2017. Histone variants on the move: substrates for chromatin dynamics. *Nat Rev Mol Cell Bio*. 18:115–126. doi:10.1038/nrm.2016.148.

Tanaka, A., H. Tanizawa, S. Sriswasdi, O. Iwasaki, A.G. Chatterjee, D.W. Speicher, H.L. Levin, E. Noguchi, and K. Noma. 2012. Epigenetic Regulation of Condensin-Mediated Genome Organization during the Cell Cycle and upon DNA Damage through Histone H3 Lysine 56 Acetylation. *Mol Cell*. 48:532–546. doi:10.1016/j.molcel.2012.09.011.

Tantale, K., F. Mueller, A. Kozulic-Pirher, A. Lesne, J.-M. Victor, M.-C. Robert, S. Capozi, R. Chouaib, V. Bäcker, J. Mateos-Langerak, X. Darzacq, C. Zimmer, E. Basyuk, and E. Bertrand. 2016. A single-molecule view of transcription reveals convoys of RNA polymerases and multi-scale bursting. *Nat Commun*. 7:12248. doi:10.1038/ncomms12248.

Tavakoli, S., Y. Liu, J.L. Potts, and S.H. Rouhanifard. 2020. Click chemistry-based amplification and detection of endogenous RNA and DNA molecules in situ using clampFISH probes. 641. 1st ed. Elsevier Inc.

Taylor, E.M., A.C. Copsey, J.J.R. Hudson, S. Vidot, and A.R. Lehmann. 2007. Identification of the Proteins, Including MAGEG1, That Make Up the Human SMC5-6 Protein Complex ▿ . *Mol Cell Biol*. 28:1197–1206. doi:10.1128/mcb.00767-07.

Tedeschi, A., G. Wutz, S. Huet, M. Jaritz, A. Wuensche, E. Schirghuber, I.F. Davidson, W. Tang, D.A. Cisneros, V. Bhaskara, T. Nishiyama, A. Vaziri, A. Wutz, J. Ellenberg, and J.-M. Peters. 2013. Wapl is an essential regulator of chromatin structure and chromosome segregation. *Nature*. 501:564–568. doi:10.1038/nature12471.

Terakawa, T., S. Bisht, J.M. Eeftens, C. Dekker, C.H. Haering, and E.C. Greene. 2017. The condensin complex is a mechanochemical motor that translocates along DNA. *Science*. 358:672–676. doi:10.1126/science.aan6516.

Teves, S.S., and S. Henikoff. 2014. Transcription-generated torsional stress destabilizes nucleosomes. *Nat Struct Mol Biol*. 21:88–94. doi:10.1038/nsmb.2723.

Thadani, R., J. Kamenz, S. Heeger, S. Muñoz, and F. Uhlmann. 2018. Cell-Cycle Regulation of Dynamic Chromosome Association of the Condensin Complex. *Cell Reports*. 23:2308–2317. doi:10.1016/j.celrep.2018.04.082.

Thiecke, M.J., G. Wutz, M. Muhar, W. Tang, S. Bevan, V. Malysheva, R. Stocsits, T. Neumann, J. Zuber, P. Fraser, S. Schoenfelder, J.-M. Peters, and M. Spivakov. 2020. Cohesin-Dependent and -Independent Mechanisms Mediate Chromosomal Contacts between Promoters and Enhancers. *Cell Reports*. 32:107929. doi:10.1016/j.celrep.2020.107929.

Thomas, M.C., and C.-M. Chiang. 2008. The General Transcription Machinery and General Cofactors. *Crit Rev Biochem Mol*. 41:105–178. doi:10.1080/10409230600648736.

Thompson, R.E., D.R. Larson, and W.W. Webb. 2002. Precise Nanometer Localization Analysis for Individual Fluorescent Probes. *Biophys J*. 82:2775–2783. doi:10.1016/s0006-3495(02)75618-x.

Tinetti, G., A. Vidal-Madjar, M.-C. Liang, J.-P. Beaulieu, Y. Yung, S. Carey, R.J. Barber, J. Tennyson, I. Ribas, N. Allard, G.E. Ballester, D.K. Sing, and F. Selsis. 2007. Structural basis for substrate loading in bacterial RNA polymerase. *Nature*. 448:163–168. doi:10.1038/nature05931.

Tittel-Elmer, M., A. Lengronne, M.B. Davidson, J. Bacal, P. François, M. Hohl, J.H.J. Petrini, P. Pasero, and J.A. Cobb. 2012. Cohesin Association to Replication Sites Depends on Rad50 and Promotes Fork Restart. *Mol Cell*. 48:98–108. doi:10.1016/j.molcel.2012.07.004.

Tolhuis, B., R.-J. Palstra, E. Splinter, F. Grosveld, and W. de Laat. 2002. Looping and Interaction between Hypersensitive Sites in the Active β-globin Locus. *Mol Cell*. 10:1453–1465. doi:10.1016/s1097-2765(02)00781-5.

Tome, J.M., N.D. Tippens, and J.T. Lis. 2018. Single-molecule nascent RNA sequencing identifies regulatory domain architecture at promoters and enhancers. *Nat Genet*. 50:1533–1541. doi:10.1038/s41588-018-0234-5.

Towbin, B.D., C. González-Aguilera, R. Sack, D. Gaidatzis, V. Kalck, P. Meister, P. Askjaer, and S.M. Gasser. 2012. Step-wise methylation of histone H3K9 positions heterochromatin at the nuclear periphery. *Cell*. 150:934–947. doi:10.1016/j.cell.2012.06.051.

Trcek, T., M. Grosch, A. York, H. Shroff, T. Lionnet, and R. Lehmann. 2015. Drosophila germ granules are structured and contain homotypic mRNA clusters. *Nat Commun*. 6:7962. doi:10.1038/ncomms8962.

Trent, C., B. Purnell, S. Gavinski, J. Hageman, C. Chamblin, and W.B. Wood. 1991. Sex-specific transcriptional regulation of the C. elegans sex-determining gene her-1. *Mech Develop*. 34:43–55. doi:10.1016/0925-4773(91)90090-s.

Tsanov, N., A. Samacoits, R. Chouaib, A.-M. Traboulsi, T. Gostan, C. Weber, C. Zimmer, K. Zibara, T. Walter, M. Peter, E. Bertrand, and F. Mueller. 2016. smiFISH and FISH-quant – a flexible single RNA detection approach with super-resolution capability. *Nucleic Acids Research*. 44:e165–e165. doi:10.1093/nar/gkw784.

Tunnacliffe, E., and J.R. Chubb. 2020. What Is a Transcriptional Burst? *Trends in Genetics*. 36:288–297. doi:10.1016/j.tig.2020.01.003.

Uhlmann, F. 2016. SMC complexes: from DNA to chromosomes. *Nature Reviews Molecular Cell Biology*. doi:10.1038/nrm.2016.30.

Uhlmann, F., D. Wernic, M.-A. Poupart, E.V. Koonin, and K. Nasmyth. 2000. Cleavage of Cohesin by the CD Clan Protease Separin Triggers Anaphase in Yeast. *Cell*. 103:375–386. doi:10.1016/s0092-8674(00)00130-6.

Ünal, E., A. Arbel-Eden, U. Sattler, R. Shroff, M. Lichten, J.E. Haber, and D. Koshland. 2004. DNA Damage Response Pathway Uses Histone Modification to Assemble a Double-Strand Break-Specific Cohesin Domain. *Mol Cell*. 16:991–1002. doi:10.1016/j.molcel.2004.11.027.

Urban, E.A., and R.J. Johnston. 2018. Buffering and Amplifying Transcriptional Noise During Cell Fate Specification. *Frontiers Genetics*. 9:591. doi:10.3389/fgene.2018.00591.

Varshavsky, A. 2012. The Ubiquitin System, an Immense Realm. *Biochemistry-us*. 81:167–176. doi:10.1146/annurev-biochem-051910-094049.

Vastenhouw, N.L., Y. Zhang, I.G. Woods, F. Imam, A. Regev, X.S. Liu, J. Rinn, and A.F. Schier. 2010. Chromatin signature of embryonic pluripotency is established during genome activation. *Nature*. 464:922–926. doi:10.1038/nature08866.

Vermeulen, M., H.C. Eberl, F. Matarese, H. Marks, S. Denissov, F. Butter, K.K. Lee, J.V. Olsen, A.A. Hyman, H.G. Stunnenberg, and M. Mann. 2010. Quantitative Interaction Proteomics and Genome-wide Profiling of Epigenetic Histone Marks and Their Readers. *Cell*. 142:967–980. doi:10.1016/j.cell.2010.08.020.

Vermeulen, M., K.W. Mulder, S. Denissov, W.W.M.P. Pijnappel, F.M.A. van Schaik, R.A. Varier, M.P.A. Baltissen, H.G. Stunnenberg, M. Mann, and H.Th.M. Timmers. 2007. Selective Anchoring of TFIID to Nucleosomes by Trimethylation of Histone H3 Lysine 4. *Cell*. 131:58–69. doi:10.1016/j.cell.2007.08.016.

Vian, L., A. Pekowska, S.S.P. Rao, K.-R. Kieffer-Kwon, S. Jung, L. Baranello, S.-C. Huang, L.E. Khattabi, M. Dose, N. Pruett, A.L. Sanborn, A. Canela, Y. Maman, A. Oksanen, W. Resch, X. Li, B. Lee, A.L. Kovalchuk, Z. Tang, S. Nelson, M.D. Pierro, R.R. Cheng, I. Machol, B.G.S. Hilaire, N.C. Durand, M.S. Shamim, E.K. Stamenova, J.N. Onuchic, Y. Ruan, A. Nussenzweig, D. Levens, E.L. Aiden, and R. Casellas. 2018. The Energetics and Physiological Impact of Cohesin Extrusion. *Cell*. 173:1165-1178.e20. doi:10.1016/j.cell.2018.03.072.

Vielle, A., J. Lang, Y. Dong, S. Ercan, C. Kotwaliwale, A. Rechtsteiner, A. Appert, Q.B. Chen, A. Dose, T. Egelhofer, H. Kimura, P. Stempor, A. Dernburg, J.D. Lieb, S. Strome, and J. Ahringer. 2012. H4K20me1 contributes to downregulation of X-linked genes for C. elegans dosage compensation. *PLoS genetics*. 8:e1002933. doi:10.1371/journal.pgen.1002933.

Vietri Rudan, M., C. Barrington, S. Henderson, C. Ernst, D.T. Odom, A. Tanay, and S. Hadjur. 2015. Comparative Hi-C Reveals that CTCF Underlies Evolution of Chromosomal Domain Architecture. *Cell Reports*. 10:1297–1309. doi:10.1016/j.celrep.2015.02.004.

Villa, R., T. Schauer, P. Smialowski, T. Straub, and P.B. Becker. 2016. PionX sites mark the X chromosome for dosage compensation. *Nature*. 537:244–248. doi:10.1038/nature19338.

Villeneuve, A.M., and B.J. Meyer. 1987. sdc-1: A link between sex determination and dosage compensation in C. elegans. *Cell*. 48:25–37. doi:10.1016/0092-8674(87)90352-7.

Vos, S.M., L. Farnung, M. Boehning, C. Wigge, A. Linden, H. Urlaub, and P. Cramer. 2018. Structure of activated transcription complex Pol II–DSIF–PAF–SPT6. *Nature*. 560:607–612. doi:10.1038/s41586-018-0440-4.

Wada, Y., Y. Ohta, M. Xu, S. Tsutsumi, T. Minami, K. Inoue, D. Komura, J. Kitakami, N. Oshida, A. Papantonis, A. Izumi, M. Kobayashi, H. Meguro, Y. Kanki, I. Mimura, K. Yamamoto, C. Mataki, T. Hamakubo, K. Shirahige, H. Aburatani, H. Kimura, T. Kodama, P.R. Cook, and S. Ihara. 2009. A wave of nascent transcription on activated human genes. *Proc National Acad Sci*. 106:18357–18361. doi:10.1073/pnas.0902573106.

Walters, M.C., S. Fiering, J. Eidemiller, W. Magis, M. Groudine, and D.I. Martin. 1995. Enhancers increase the probability but not the level of gene expression. *Proc National Acad Sci*. 92:7125–7129. doi:10.1073/pnas.92.15.7125.

Walther, N., M.J. Hossain, A.Z. Politi, B. Koch, M. Kueblbeck, Ø. Ødegård-Fougner, M. Lampe, and J. Ellenberg. 2018. A quantitative map of human Condensins provides new insights into mitotic chromosome architecture. *J Cell Biology*. 217:2309–2328. doi:10.1083/jcb.201801048.

Wan, Y., D.G. Anastasakis, J. Rodriguez, M. Palangat, P. Gudla, G. Zaki, M. Tandon, G. Pegoraro, C.C. Chow, M. Hafner, and D.R. Larson. 2021. Dynamic imaging of nascent RNA reveals general principles of transcription dynamics and stochastic splice site selection. *Cell*. doi:10.1016/j.cell.2021.04.012.

Wang, B.-D., D. Eyre, M. Basrai, M. Lichten, and A. Strunnikov. 2005. Condensin Binding at Distinct and Specific Chromosomal Sites in the Saccharomyces cerevisiae Genome†. *Mol Cell Biol*. 25:7216–7225. doi:10.1128/mcb.25.16.7216-7225.2005.

Wang, C., C. Liu, D. Roqueiro, D. Grimm, R. Schwab, C. Becker, C. Lanz, and D. Weigel. 2015. Genome-wide analysis of local chromatin packing in Arabidopsis thaliana. *Genome Res*. 25:246–256. doi:10.1101/gr.170332.113.

Wang, D., D.A. Bushnell, K.D. Westover, C.D. Kaplan, and R.D. Kornberg. 2006. Structural Basis of Transcription: Role of the Trigger Loop in Substrate Specificity and Catalysis. *Cell*. 127:941–954. doi:10.1016/j.cell.2006.11.023.

Wang, D., A. Mansisidor, G. Prabhakar, and A. Hochwagen. 2016a. Condensin and Hmo1 Mediate a Starvation-Induced Transcriptional Position Effect within the Ribosomal DNA Array. *Cell Reports*. 14:1010–1017. doi:10.1016/j.celrep.2016.01.005.

Wang, F., J. Flanagan, N. Su, L.-C. Wang, S. Bui, A. Nielson, X. Wu, H.-T. Vo, X.-J. Ma, and Y. Luo. 2012. RNAscope A Novel in Situ RNA Analysis Platform for Formalin-Fixed, Paraffin-Embedded Tissues. *J Mol Diagnostics*. 14:22–29. doi:10.1016/j.jmoldx.2011.08.002.

Wang, S.-P., Z. Tang, C.-W. Chen, M. Shimada, R.P. Koche, L.-H. Wang, T. Nakadai, A. Chramiec, A.V. Krivtsov, S.A. Armstrong, and R.G. Roeder. 2017. A UTX-MLL4-p300 Transcriptional Regulatory Network Coordinately Shapes Active Enhancer Landscapes for Eliciting Transcription. *Mol Cell*. 67:308-321.e6. doi:10.1016/j.molcel.2017.06.028.

Wang, W., M. Carey, and J. Gralla. 1992. Polymerase II promoter activation: closed complex formation and ATP-driven start site opening. *Science*. 255:450–453. doi:10.1126/science.1310361.

Wang, X., W.E. Allen, M.A. Wright, E.L. Sylwestrak, N. Samusik, S. Vesuna, K. Evans, C. Liu, C. Ramakrishnan, J. Liu, G.P. Nolan, F.-A. Bava, and K. Deisseroth. 2018. Three-dimensional intact-tissue sequencing of single-cell transcriptional states. *Science*. 361:eaat5691. doi:10.1126/science.aat5691.

Wang, Z., B.J. Ramsey, D. Wang, K. Wong, H. Li, E. Wang, and Z. Bao. 2016b. An Observation-Driven Agent-Based Modeling and Analysis Framework for C. elegans Embryogenesis. *PLoS ONE*. 11:e0166551-16. doi:10.1371/journal.pone.0166551.

Weber, C.M., and S. Henikoff. 2014. Histone variants: dynamic punctuation in transcription. *Gene Dev*. 28:672–682. doi:10.1101/gad.238873.114.

Webster, C.M., L. Wu, D. Douglas, and A.A. Soukas. 2013. A non-canonical role for the C. elegans dosage compensation complex in growth and metabolic regulation downstream of TOR complex 2. *Development*. 140:3601–3612. doi:10.1242/dev.094292.

Weinberger, L., Y. Voichek, I. Tirosh, G. Hornung, I. Amit, and N. Barkai. 2012. Expression Noise and Acetylation Profiles Distinguish HDAC Functions. *Mol Cell*. 47:193–202. doi:10.1016/j.molcel.2012.05.008.

Weirauch, M.T., and T.R. Hughes. 2011. A Handbook of Transcription Factors. *Subcell Biochem*. 52:25–73. doi:10.1007/978-90-481-9069-0_3.

Wells, J.N., T.G. Gligoris, K.A. Nasmyth, and J.A. Marsh. 2017. Evolution of condensin and cohesin complexes driven by replacement of Kite by Hawk proteins. *Current biology : CB*. 27:R17–R18. doi:10.1016/j.cub.2016.11.050.

Wells, M.B., M.J. Snyder, L.M. Custer, and G. Csankovszki. 2012. Caenorhabditis elegans Dosage Compensation Regulates Histone H4 Chromatin State on X Chromosomes. *Mol Cell Biol*. 32:1710–1719. doi:10.1128/mcb.06546-11.

Wendt, K.S., K. Yoshida, T. Itoh, M. Bando, B. Koch, E. Schirghuber, S. Tsutsumi, G. Nagae, K. Ishihara, T. Mishiro, K. Yahata, F. Imamoto, H. Aburatani, M. Nakao, N. Imamoto, K. Maeshima, K. Shirahige, and J.-M. Peters. 2008. Cohesin mediates transcriptional insulation by CCCTC-binding factor. *Nature*. 451:796–801. doi:10.1038/nature06634.

Wheeler, B.S., E. Anderson, C. Frøkjær-Jensen, Q. Bian, E. Jorgensen, and B.J. Meyer. 2016. Chromosome-wide mechanisms to decouple gene expression from gene dose during sex-chromosome evolution. *Elife*. 5:e17365. doi:10.7554/elife.17365.

Whittle, C.M., K.N. McClinic, S. Ercan, X. Zhang, R.D. Green, W.G. Kelly, and J.D. Lieb. 2008. The Genomic Distribution and Function of Histone Variant HTZ-1 during C. elegans Embryogenesis. *Plos Genet*. 4:e1000187. doi:10.1371/journal.pgen.1000187.

Wilhelm, L., F. Buermann, A. Minnen, H.-C. Shin, C.P. Toseland, B.-H. Oh, and S. Gruber. 2015. SMC condensin entraps chromosomal DNA by an ATP hydrolysis dependent loading mechanism in Bacillus subtilis. *eLife*. 4. doi:10.7554/elife.06659.

Wolff, J., V. Bhardwaj, S. Nothjunge, G. Richard, G. Renschler, R. Gilsbach, T. Manke, R. Backofen, F. Ramírez, and B.A. Grüning. 2018. Galaxy HiCExplorer: a web server for reproducible Hi-C data analysis, quality control and visualization. *Nucleic Acids Res*. 46:gky504-. doi:10.1093/nar/gky504.

Wolff, J., L. Rabbani, R. Gilsbach, G. Richard, T. Manke, R. Backofen, and B.A. Grüning. 2020. Galaxy HiCExplorer 3: a web server for reproducible Hi-C, capture Hi-C and single-cell Hi-C data analysis, quality control and visualization. *Nucleic Acids Res*. 48:W177–W184. doi:10.1093/nar/gkaa220.

Wood, A.J., A.F. Severson, and B.J. Meyer. 2010. Condensin and cohesin complexity: the expanding repertoire of functions. *Nature Publishing Group*. 11:391–404. doi:10.1038/nrg2794.

Woodcock, C.L.F., J.P. Safer, and J.E. Stanchfield. 1976. Structural repeating units in chromatin I. Evidence for their general occurrence. *Exp Cell Res*. 97:101–110. doi:10.1016/0014-4827(76)90659-5.

Woodward, J., G.C. Taylor, D.C. Soares, S. Boyle, D. Sie, D. Read, K. Chathoth, M. Vukovic, N. Tarrats, D. Jamieson, K.J. Campbell, K. Blyth, J.C. Acosta, B. Ylstra, M.J. Arends, K.R. Kranc, A.P. Jackson, W.A. Bickmore, and A.J. Wood. 2016. Condensin II mutation causes T-cell lymphoma through tissue-specific genome instability. *Genes & Development*. 30:2173–2186. doi:10.1101/gad.284562.116.

Wu, C., M. Simonetti, C. Rossell, M. Mignardi, R. Mirzazadeh, L. Annaratone, C. Marchiò, A. Sapino, M. Bienko, N. Crosetto, and M. Nilsson. 2018. RollFISH achieves robust quantification of single- molecule RNA biomarkers in paraffin-embedded tumor tissue samples. *Communications Biology*. 1–8. doi:10.1038/s42003-018-0218-0.

Wu, S., K. Li, Y. Li, T. Zhao, T. Li, Y.-F. Yang, and W. Qian. 2017. Independent regulation of gene expression level and noise by histone modifications. *Plos Comput Biol*. 13:e1005585. doi:10.1371/journal.pcbi.1005585.

Wu, S., W. Wang, X. Kong, L.M. Congdon, K. Yokomori, M.W. Kirschner, and J.C. Rice. 2010. Dynamic regulation of the PR-Set7 histone methyltransferase is required for normal cell cycle progression. *Gene Dev*. 24:2531–2542. doi:10.1101/gad.1984210.

Wu, Y., B. Han, T.J. Gauvin, J. Smith, A. Singh, and E.E. Griffin. 2019. Single-molecule dynamics of the P granule scaffold MEG-3 in the Caenorhabditis elegans zygote. *Molecular biology of the cell*. 30:333–345. doi:10.1091/mbc.e18-06-0402.

Wutz, G., C. Várnai, K. Nagasaka, D.A. Cisneros, R.R. Stocsits, W. Tang, S. Schoenfelder, G. Jessberger, M. Muhar, M.J. Hossain, N. Walther, B. Koch, M. Kueblbeck, J. Ellenberg, J. Zuber, P. Fraser, and J.-M. Peters. 2017. Topologically associating domains and chromatin loops depend on cohesin and are regulated by CTCF, WAPL, and PDS5 proteins. *The EMBO Journal*. 36:3573–3599. doi:10.15252/embj.201798004.

Xing, H., N.L. Vanderford, and K.D. Sarge. 2008. The TBP–PP2A mitotic complex bookmarks genes by preventing condensin action. *Nat Cell Biol*. 10:1318–1323. doi:10.1038/ncb1790.

Xing, H., D.C. Wilkerson, C.N. Mayhew, E.J. Lubert, H.S. Skaggs, M.L. Goodson, Y. Hong, O.-K. Park-Sarge, and K.D. Sarge. 2005. Mechanism of hsp70i Gene Bookmarking. *Science*. 307:421–423. doi:10.1126/science.1106478.

Yamaguchi, Y., H. Shibata, and H. Handa. 2013. Transcription elongation factors DSIF and NELF: Promoter-proximal pausing and beyond. *Biochimica Et Biophysica Acta Bba - Gene Regul Mech*. 1829:98–104. doi:10.1016/j.bbagrm.2012.11.007.

Yeong, F.M., H. Hombauer, K.S. Wendt, T. Hirota, I. Mudrak, K. Mechtler, T. Loregger, A. Marchler-Bauer, K. Tanaka, J.-M. Peters, and E. Ogris. 2003. Identification of a Subunit of a Novel Kleisin-β/SMC Complex as a Potential Substrate of Protein Phosphatase 2A. *Curr Biol*. 13:2058–2064. doi:10.1016/j.cub.2003.10.032.

Yokoyama, Y., H. Zhu, R. Zhang, and K. Noma. 2015. A novel role for the condensin II complex in cellular senescence. *Cell Cycle*. 14:2160–2170. doi:10.1080/15384101.2015.1049778.

Yonker, S.A., and B.J. Meyer. 2003. Recruitment of C. elegans dosage compensation proteins for gene-specific versus chromosome-wide repression. *Development*. 130:6519–6532. doi:10.1242/dev.00886.

Yoshimura, S.H., and T. Hirano. 2016. HEAT repeats - versatile arrays of amphiphilic helices working in crowded environments? *Journal of cell science*. 129:3963–3970. doi:10.1242/jcs.185710.

Yu, M., and B. Ren. 2016. The Three-Dimensional Organization of Mammalian Genomes. *Annu Rev Cell Dev Bi*. 33:1–25. doi:10.1146/annurev-cellbio-100616-060531.

Yudkovsky, N., J.A. Ranish, and S. Hahn. 2000. A transcription reinitiation intermediate that is stabilized by activator. *Nature*. 408:225–229. doi:10.1038/35041603.

Yuen, K.C., and J.L. Gerton. 2018. Taking cohesin and condensin in context. *PLoS genetics*. 14:e1007118. doi:10.1371/journal.pgen.1007118.

Yuen, K.C., B.D. Slaughter, and J.L. Gerton. 2017. Condensin II is anchored by TFIIIC and H3K4me3 in the mammalian genome and supports the expression of active dense gene clusters. *Science Advances*. 3:e1700191. doi:10.1126/sciadv.1700191.

Zhao, H., B.K. Bhowmik, Z.M. Petrushenko, and V.V. Rybenkov. 2020. Alternating Dynamics of oriC, SMC, and MksBEF in Segregation of Pseudomonas aeruginosa Chromosome. *mSphere*. 5. doi:10.1128/msphere.00238-20.

Zhao, Y., Y. Hou, Y. Xu, Y. Luan, H. Zhou, X. Qi, M. Hu, D. Wang, Z. Wang, Y. Fu, J. Li, S. Zhang, J. Chen, J. Han, X. Li, and S. Zhao. 2021. A compendium and comparative epigenomics analysis of cis-regulatory elements in the pig genome. *Nat Commun*. 12:2217. doi:10.1038/s41467-021-22448-x.

Zuin, J., J.R. Dixon, M.I.J.A. van der Reijden, Z. Ye, P. Kolovos, R.W.W. Brouwer, M.P.C. van de Corput, H.J.G. van de Werken, T.A. Knoch, W.F.J. van IJcken, F.G. Grosveld, B. Ren, and K.S. Wendt. 2014. Cohesin and CTCF differentially affect chromatin architecture and gene expression in human cells. *Proc National Acad Sci*. 111:996–1001. doi:10.1073/pnas.1317788111.

APPENDIX

smFISH probe-sets

Table 11 DPY-23 exonic probes

acgaacaatccaccaatcat	caacttttccggcaacatga
cacttctccttttgtgattgt	ggcattccactcaaatagga
tcgtctcgatagattctcga	tcgttgatgccaaatttgca
tgacgttgactcggaaggcg	cgactttccttcgatggtaa
cgaacttgctgtcgggcatg	ttgtttggatcatcacttcc
aagtacgagccatgttggtg	acagtcatcaatggccactg
ccacgcttcacatggaagaa	gcttcacgcattggtggaat
tgacgtgtcaccgcacaaat	tgctccgtctcaaatttcgt
aaaaccatggcagcgttgac	cgtccggtgggataaaagaa
tcggcgaagcgtttcaagaa	cagttggatatccttagtgg
tccaaagtaagactgcatgg	ccaatgggatcacacggaat
agttgttcttcacattctcc	cttccatcttgttacgagac
gagaatctcgtcgagcaact	gcttgaagttagacttgacg
tattctgggggtatccaaag	agcttttgagcaagaaggga
aaagttttcagcacaccagg	tggggttggaatgcgaactt
atttgtgactgctcctcttt	gttgaacgccggatgtattt
aatttggccagtcacttgag	gcttttcccttcatgcaaat
tttcggcggtacttaatacc	ttccacacaatggcattctc
aataacatccaggaagagct	aatttggctttccttcattc
gattcatgagcaagttgaca	agagaagatcgatttccgca
tccagatggagcaaacggaa	tccatttcttcttctcaacg
caccttcaagtagcgaactt	ctcaaagttcatgctgaccg
aatagttcagttttggctca	tagcatctggtttcatacag
ccatttgatgacgtcatgat	ccgatcttccaatgtaacga

Table 12 DPY-23 intronic probes

gaacatttccaaacatgcca	cttctgcccaattttcttag
cgcaccacttttttcttttaa	ttgtacagctcaaagtgtgt
catttctttatttccctgtt	ttctctgattgcagtttctt
aacagcgcggcaaacatttt	tagttaatgttctactgcca
gtgaacaaacagtctcggca	tatccctttttcggcaataat
tgtacaccatcgcatttttc	ccttttagtaaatatccca
gatttcttcttgtttgggtc	aaatttgttatttcaagccc
agtgtgtccctaatactttt	gttttcctttagttacaggt
ttgatactcctccttgaaca	tgtttcactgttacggacga
gcattttgtttttgggcaac	acaattccaccaatttttga
gcgtgacgctttttttcatat	attcaaactttgtctcctgt
gtgtacaggtgggcagaata	ccacaaatcttgatctcgtg
ttgaacctgaaagcgtgagc	gaaattcaggggatcaagcc
gggttcgtgaataaagagcg	ctcttggttaactattgtgt
ccgtgcacacaaaacacagt	cacttttttgattgtgagctc
tggttatctagatttttgct	ttaaggaagctgttggtccc
ctatgtattctcctgagaca	tgccaatttgcgacagattg
agtatgcacgtcgttattgt	acatttgcttagcagtcaga
tcccggaaactcagactaac	tgcagcacagttttgcatat
caataaagtatcagtttccc	cttcagtcaaggtttggaaa
atgagagccatgattggtaa	atgctccaaaagctttagta
atgctcagtcagtgtatgag	gcctgtgagaacttttttcat
tctgccgcttcgttttaatc	ggttcaattattgaggtgga
attcttgcccaaaatggagc	
ctcccacttttctcgttttc	

Table 13 C16H3-3a exonic probes

aagtgggcgagggagagaaa	gcaatttgggcacttcatta
gtttttcagggaattctggt	actttcggaagctcaaaggc
aattcaaatttgggcgccac	aggattcgcaggaggaattc
atcaaaatttcgaggcccttt	tcaagcgtttttctcgtttc
gttatccgagaggtttgatc	gtccctgaaattcgtgattt
attggttcagagttaagcca	cttataatcccctgttttga
agtaccgcaagtagacgtag	ttccctttcgacaaatggac
ttattgacgacgaggcttcg	ttgtcttctaacccaaatcc
atcaggattaacgagaggcc	ttctcacatctcagttgtga
ctgttaagcggtcgatctag	cgggaaaatttgcgtcctta
tatgtaggaagttggcaggg	tttcataacctgtcacagca
gagcaagtttacgtagcagg	actcactatttggtaccgac
aatcacgacgcagactacgt	ctacctacaatgtccttagt
ttgccgtttttcaactaacc	ttcgctttccactcaaacat
tttactccctctagatgtta	aaggaggccctatatagtta
caagccgaacagttgtcatt	ccttgaaagtgttttggacc
agacctacgtaggagtgatg	aaacccccgatttttttttg
cgcgagtctacgtaagagtg	acttttctctttccgttttt
agtctatgaaggactagcgc	ctctatctctctgtcatacg
ttttccggtgtatcaacttc	gaaatggtcagtggttctct
ttcaaggtatctcgtgttct	tggatgatttgtggttacca
acttttccgttatctatcgt	gactccatgagtcttgtgaa
taggagtacaagtcgactcc	ctccctatctattcatctat
ggctgttatcaagtccaatt	
ccacatcgcagaaagagcaa	

Table 14 C16H3.3a intronic probes

aagtgggcgagggagagaaa	ctccctatctattcatctat
gtttttcagggaattctggt	acttttctctttccgttttt
aattcaaatttgggcgccac	ctctatctctctgtcatacg
atcaaaatttcgaggccctt	gaaatggtcagtggttctct
gttatccgagaggtttgatc	gcaatttgggcacttcatta
attggttcagagttaagcca	actttcggaagctcaaaggc
agtaccgcaagtagacgtag	aggattcgcaggaggaattc
ttattgacgacgaggcttcg	tcaagcgtttttctcgtttc
atcaggattaacgagaggcc	gtccctgaaattcgtgattt
ctgttaagcggtcgatctag	cttataatcccctgttttga
tatgtaggaagttggcaggg	ttccctttcgacaaatggac
gagcaagtttacgtagcagg	ttgtcttctaacccaaatcc
aatcacgacgcagactacgt	ttctcacatctcagttgtga
ttgccgtttttcaactaacc	cgggaaaatttgcgtcctta
tttactccctctagatgtta	tttcataacctgtcacagca
caagccgaacagttgtcatt	actcactatttggtaccgac
agacctacgtaggagtgatg	ctacctacaatgtccttagt
cgcgagtctacgtaagagtg	ttcgctttccactcaaacat
agtctatgaaggactagcgc	aaggaggccctatatagtta
ttttccggtgtatcaacttc	ccttgaaagtgttttggacc
ttcaaggtatctcgtgttct	aaacccccgatttttttttg
acttttccgttatctatcgt	
taggagtacaagtcgactcc	
ggctgttatcaagtccaatt	
ccacatcgcagaaagagcaa	
tggatgatttgtggttacca	
gactccatgagtcttgtgaa	

Table 15 RAB-6.2 exonic probes

taccaaagtccgacattttt	attaagctccttggcctttc
agcttgaatttcttcaacgg	ggcagaagtctcgatgaaca
actttgttccccgaggaaca	tgcttcacattgtagccggc
tgattagggaggtttttccg	tccggcgatacgacggaaaa
aaggagtcgtacatgaagcg	ccttgatgattcctggtagg
tggtggcctggtaggtgttg	tttggtggctccactgggtc
ttactcaggaagtcgattcc	gattgggtccatcgtgacca
ttcggtcctccaagtacatg	cggtgacaatttgacgctga
tcccaaagttgaagacgaac	tagcaccagcacgatccctc
gaaacgttcctgtccagcgg	ttgctcaggaatacaaagag
tgtaggatgggatgagtgag	atcacaacctttttttgaca
acagcaactgtagaatcacg	aattatgcgttgagattgga
gttggtgatgtcataaacca	ggggcggaggatgctttaaa
ggaagtttgatggaaagagt	tcttcatgacaaaaccatta
tacggacgtcgtcaatccac	tttaaggggataattaata
attacatcacttccacgctc	aaaacttactggcgatagcg
cttgttgccgaccaacatga	ttttggggaattttaagata
gcctcttatcggaaagatcg	acacagaaaaaatcgataat
tctccttcgtcggtggtgac	agaagccattcagagttcat
ccatcgcataagttaataga	
caaagaaaattacacatgtt	
ataataataatttattatg	

Table 16 RAB-6.2 intronic probes

ctacggtagaatttcaatca	ttaaatgcatattccgccgt
tttagaaacttgagaattca	taaaacttcagcctggagct
cgcaaaaactgatttcttac	tcatactgaaagttatgccg
cggattttgaaatcatttct	aggttttaagctagccaaga
catcagaaaaacttcttcca	ctccaaacaatatctttaga
tgtgaagctttacagcatga	ttcagttaaagctatttcct
aaatttctcccagaggatcc	gatccaatttatgttaacgt
actatatacactactatagt	gaagctagttcaagttagtg
accaatatagttattatagt	taaacttgaggtaggtccag
tgccagtgactattgtagta	gcgtaggctctgattataaa
gctagaagcttttcgcatta	atagagagcttgggcttgaa
tgttttttgagcttctcttc	tgtgtttaaggatgagctgg
tctaacttttctatcaatat	gcttatgtagtaggttcaac
aaataatggtttccttttgg	ttatgggagattcagcttat
tagttcaaaatcaagattaa	attttgctcaggaaaaatca
agagtttttttcattgcccac	tttttagcctaatgtaacgt
tgaagctttttttgtcgttac	ctaattctgtttagaatgcg
ctgcaaaaaagttggggtta	cgcaaggtaagtttagcttg
tagcggaaactctcattcga	agatcagctcgaaacaggcc
ccactacacaatttaattga	atagttcagctaagaccacg
tatgtaagtcttatgtcagt	ggttaacaggtttcagaaaa
aaaaggtttttaaaacttac	tacacattgagtttattagt
aaatcatggctttttgaagt	caaattaatagacctggagc

Table 17 NRR-1 exonic probes

ccacgtcgtctcaagtagac	gctcatcttgattttcttcg
agtttccttagtgagcacac	ctgaagacggtgtggagtgg
ttggtgttgcgcgagaatat	tgtgagctggtcgatgattt
caaagcacacgtcgtcttcg	gaattatgcagcgtcgcaac
gaactgtagggggaagacga	aaagtaggcaaggggacgtc
aacacgtgcattggtggttc	actttaaggtcagtggtctc
cagtgtaccgttcatactat	cgtattggtcagactcacgt
agatggctttgcagttgatc	ccgggaagagctctttgaaa
gttcatcgttgcgagttgac	ccacatacgaatgtcgttca
agatggctttgcagttgatc	agatgcgcatctcgcgaatg
cgttgcgagttgaccattgg	aaacatcgaacgtctttgcc
ggctgatccattcatataca	tcaaaaaggttgagcctctg
cgttggtgtgggaaacggag	caaagtttcttgtacccacc
atttttgatcattgcccatc	aaaacttcaatcccccaaca
agccattcgcttataagacg	ccgacagcataatttttggg
caaggtccgagcaaactgcg	caacttcagatttgcctagc
cactccgtagtgatatccag	tgttctagaattttctggga
gttcgtcggaagaaggtttt	ctccagcgctgatatttaat
tgaaggtttgctcactgact	ccactttaggaagctaatga
caatttccattatattggca	ctttttttcagggatattca
gacggcatgcacatcgaatg	acgagtgtcactgcaaaact
ataggcatttgttgaagcgg	ataagcggacaaccaattct
cgatctcgatcattctggat	ttgagcagttttggttttga
ttttatagcacacggcttgt	
cgctacgaaaatggttccac	

Table 18 NHR-1 intronic probes

attttccaactttccgagta	ctccgtaggatgtcatcaaa
ccactgggaaagagcatgat	atctttaatttgcaatcccc
acgctagttcacctaaatgc	gctctaattatcacgcttct
aactgacaacactgtctcct	attttcccgccggaaaaata
gtaaagcttcaaggttcggg	accagagatcaacttcacgt
atattgttgggggttaagc	aatccgcggcttaactcaaa
tgggggtcgagtgtaaaagt	gcctttcaaaagggtgtttt
gcaaagaacacgattgtccc	cagctagcaaaaccgactga
gaggaaacggatagcggagt	gctagattgttatgctctca
cctcctaagcattatcacat	tagttccttttcagtcttga
gtcactgagtgaggactaga	acgtcagcgtttttaagca
tgagttcattgtttgcttgt	gagcatagtttgttgtcagt
gcaagcaaaccagagaacca	gcaaaaagtcctgcttctga
aaggtgaacttggcatgtgt	tccattctattaaactccca
acttttactattggccgaga	gctgtcaagttattttggca
ttttctccccttattcaaag	ctccaaacattttacagcgc
gcgattttctacttgatcgc	tggttcctagtgttttcaat
tatgtgctctcgaaagcgtg	tcatttgccgacagttctaa
ccatctttctaaattgcctc	ttggggtaaatgtgtttcgc
aatcttggtacccttatgtt	ccccatattaggttacaatg
ggaacaccatctagttcttt	tttctctttttcgagcgtg
acggctactagttaagtacc	atgtctcgagtttgtttgga
ttattaccttcctcaaaccg	aatgggtgactgggaacgtg
accggacaatttgcgatttc	
atattcaggagctcttcact	

Table 19 W04G3.5 exonic probes

gagcttgcatcagctctttc	gattcttcctcgtctttttg
gagtttccggtaagaagcac	ttgacgtccatcttcaagac
cattttcgccaactcaggat	gaagtgacatttggtggtgg
gcgaatctcaagtctctctg	ctcctgagctgggagaaaat
ttgtaaacagtcgcttctcc	acaactgtaagtggtggctt
gtttgatgtcaacggaggtt	cataattgcaatccgtccac
tgaagacgtgttttccacga	tgagcgtcgtcaatgatgtc
cgttgttcacgttctttgac	ttcagcggcggcaacaaacg
atgagaacaagcagctccat	aatcttgtatgcaccacgag
catcgatgtcttgcaagcat	agaaccccatgagtggcaat
ggcatgatgactgtgattgt	gaagtgcaggagcatcagac
cattgtttgctgtatgggag	tcggtgattggagaagcttc
gattgacgaacgacggagca	cgtgtggaacagtgttggta
catctcggcaacaagtttca	gtgacaacgcattttctgga
tgagactaaacgactggcac	agacgtccacagtcttgatc
tctccttcttgtacaaatcc	gcgaattgcctcacaaatca
ctgggcacgaaaagaatcct	ccatcgactcgttgtgaaag
cggtgaagcacgaagattgt	gtgacgtcacggaacagttg
ttggtcttgatgtgttggag	gtgaactgagagcaatgaga
gcattcttgtaatccggaat	tagacggactcaagaagcgt
cggcgacttggcaacgatga	gttgggggaaaagtggtcta
aagaagtggccttgttcatg	gttggcacaggaaatgtatt
tccgtgaataacagccacac	ttcatcatgggaatcaatca
gtttagtttccgacttttc	atgcactgagacctattctg

Table 20 W04G3.5 intronic probes

cttaatgcaacacaaaattt	agcttatttctcactttctc
tgtcaatataattttagatt	gtgaatgagaaagaaattga
caagaacatttgcaactcac	atcatgtgtttgtgtataat
aagattgcaatttagtttcc	atgtctgttaactcgcccaa
aaatctttttacacactaac	atatatcaagagaaaaactc
agttctagtaatgtgtaaaa	caacattcaccacaagtaga
aactagaactgagtactgcc	aagtgagtcgtcgtttcaga
ttcgcactaaaactgaaact	agaagtttcgaaaacagggt
aaaactgtcgatgacacatt	atggagccggatagagagaa
ttttcgaaaatttgcctatg	gggagtcgacaaaacttata
atacataaacaaattctccc	gacaaacgagacaaaaatga
agatcgaaaaaaaaactata	tgtgtgatgttcttaagtga
gcaagcggcttaaaaatttg	aaactcaacatgaagtgtgt
actatgaaaacctttttgtt	ctggaaattcaacaggatat
ctgaaaataaaaacacttta	gctttaaatgtatcgcataa
gacttgttggaattatctta	agcttgttaaaacagaatta
aattgtccgatatatttcca	ctccaactttgttcaattaa
ttagtttcaaaaattcaaat	tttctctcagtacaaagcaa
tatgagggtacttaaaggaa	ggtggtgtcaatggagtcaa
ctgcaaagtgatgattgagt	tatttgaaattaaattccgt
tcttttaaatttataactca	atgatacatttcttatacta
agcctgtttctaccataaat	atttttgttaactctgtgac
gaatatttgaattattgttc	gtgcgtcaactgaattttca

Table 21 WDR-5.2 exonic probes

tgctcttcatcttgagaagc	gtgttccagaagggttgaaa
ggtttccgcaccaactattg	tcgaatgatccagaggcaat
actggaagagatggctgact	acaccagatgcgaatagttt
gctataataggacgcattgg	aaatcgtgtttccattgcgt
taagaccatagctggggatg	gaactaaccggatcctcgtg
ccaaattgtggaattcccat	tccgtcgcggttaaaacaca
cgaagcttgagctggcagac	taggatcccgaggctagata
gcgttgaagaaagcataggc	cccaaattcgaactattcca
gtgcagagctataacttggt	acacaagtgccggtagtcga
acttgggttcggcattggag	ctcttcgtcgatcaacgttt
agtttgtaggtaggccaaag	tgacatgtgtgattggagga
gtgcgcatttggaatttcag	gtatatattttccgtttggt
tgatccctgagatcgacttt	gtattgttgaggtttgaggc
taccgtccgtctggagaaaa	tttggtagtcccacagtttg
atactacaatccgcagatcc	tactctttgagcactctcag
tacacaaaatccatcctcca	gtatttggaattttcgtgcc
ccaagccgatgacccataag	taaccgaaaaattcgcggcc
gctccatgagaactcattga	gctgacaatccatttacctc
gcacgagacaatgagtttcg	acactttgtgatcttccgag
ctttgactagtttgtcatcg	cttgtctgaaggttccagat
cgaccactgctgacatcaaa	gccatctaatgtctgaagga
ccctttcaaagtcttgacac	gacaatcggtgcacatgaca
cagcagaacacgtagtttgt	gcggcagaagcaattatgtt
ttatgactgggatcgccaga	ttgatccgcatatctggctc

AMA-1 exonic probes: design ready catalog number: VSMF-6001-5

Table 22 AMA-1 intronic probes

gggttaaaatcgggggtttc	tattctttggcaatttccgg
tcctggattttaggcctaaa	ccccactcaaagtacaattt
attttcgaccgactttggag	ttgggggtcatttttcgaac
tttgacaactttccactgga	atttgcgaagtttttcctgg
attagctcattctcagcttt	ctcgaaacgtgtacctttttt
atgggcaaaatccggcaatt	gatgattttagtggcggttt
ttacgatttttccagtctca	atggcaaatagctgtgcgat
cttatcggccaaaaagtgca	gacttttctgggtgcaaact
ctgttctaacgggatttgca	tttattcccaacgcaactga
tcgggcttaaaaccacttttt	acaggcttttgaacattcca
attccaattcttaagcgcat	gtctcaacagttggagtttt
gtcttgaatggttttccatg	gccgaattttcaccctaaaa
ttcctaaaccgcaattgtga	tttcgcacaatttcagccaa
ttttgagtcattttctggcg	gtacttttcgagttttcctt
tcacacaaaatcacgccagc	gcccaaatagacagatttca
ttttcctcaagttttggtcg	ttttcgaacgttttctcgcg
aggtggtttccagggaaaat	gatagattcccccagaaatg
tccatcacaattttccagtt	gttgccaacttatcacattt
ttcctcgatcaaatttcgga	cttcggtgatttttgctact
tcccatcaaaaatccagtca	gcgcctaatttctggagaat
tagcattttgagcgacactc	actgttacatttttcgcagt
ttttcaagtatccaggctta	agttttcctccgaatattct
aacataggccaattttcgca	atttccgcaacattttcaca
ctctccaatttttttagggt	gtccgtaactttgctttttg

Table 23 PHA-4 exonic probes

gaatacgtcggcagatagtc	aaacatattcccacagtgct
gttggtagtttaacgtagta	tacggaggtagcatccattc
gcagcagtctggtactgata	cttgaccttgaatctcttct
gttgtagttcagaagtccat	aattgttgggagttggcatt
cagtggcatactggctgtag	ccatttttggaatgtgttgt
tagttcgatccgagctgatt	gttggatcctcttctttgat
catgaaattggctgggctga	tgatgatgtggtcgtgatgg
aagaggtgaaattcctcctc	gggatcagagaataagcacc
cggtggtgccagtggtaaaa	cttgatctccttctttgtag
cattgcttcttccgatgacc	catcttgcacagctttcagc
agcaaccgtcgagcttgatc	aagattggcagcagctgcag
ccagaataagacctatcggc	gttcccgatgggtcaattag
tcctgaatcgtgagttcttg	actgtgattaacagccgacg
cttttccgtgacagtttcaa	tagtgtgccaacacttgaga
cataagttccatgtcttctg	attgagtgtcatctgtgctt
gagtatggaggtttcgattg	ggtaaggagacgcgtattga
gacttttgaattgccatagt	tgtggcaaaatccgaactgt
tcagacaatgtcaattgtct	aattctgggattgtgggaga
atccatgatccaattgtaga	gtgttgtagagtgtgttgtt
attgttctgatagtaaggga	gtcaattcctggataactgc
ttgagttttgccatctttgt	attctggtatactccgttgg
cattgaaggagagggagtgg	ggttggtggagctgtaaaga
ctggcaacctttacaaagca	
tgaagagtccagaaggatcc	

Table 24 PHA-4 intronic probes

tttatttttgacaccctacc	actcattttgtgcttgggaa
gccatatggtttttattct	tatagagagcgccactcaag
tacgccagacggttatacaa	atcgggacaaaacgtgtcca
cagtgcatttacctactcaa	ctgcagaaaaggtagtcctt
aatgttgagccgtattggac	ttgggcgcacggtataataa
cactttgctacttttagct	acagcttcacgcatcaatgg
tctattttcttctggacacc	tctccggtaatttctcattt
tcttcttttggtaggaggac	atcttttcactaacgcgcac
atatttggcttcttgggcaa	cgtttccggaaaacatccat
ttttggttgtgtgtgtgttt	tcactggctagattttatct
attgtaatctccacgtggtg	gggggtcaacaaaacatcgt
ttcaactgactcatggctga	accagactccaatttttact
ccatttcggatttttacctt	tcttactattatgaccgagt
tatcgcttagccacagtaac	gccgctaaaatttttgcagg
agaggtgaaggagaggctag	tttttgcagcgcagagtgat
aaaggtaagtagaacgcccc	tgaaacatttttttcgggcct
gaacctgagccttggaaatt	cggctccttaaagaccaata
caaataagtcccgtttgacc	ttagaggcccgtaaaattgc
acgtggagctagacatggaa	ttgctatcagtgcatttttt
ttagaaaattcggaagcccc	gaggagcactttgaactgga
aagtttgctttgaggtctgg	ccttctaaataagccccaaa
gtgagaacagggtcaaactt	ggtgcattttgcatactttc
catgcattgtcttaaccgta	gcaacgggccatgttaatta
gagctttcagagtgaagagt	actaggctttctatcgactt

Table 25 MDH-1 exonic probes

cggtgaccaaaacgcgaagt	agagtgatttccccagatga
ggatgacgatcgagtaaccg	tgacatctgggaattgagtt
tttccgaatacagttccgtc	ttcttgttaacggtagcgtg
aacgagctccactggttgtt	gtaagcgtcggtctcagttc
agcattgtgggacgtcgaga	tgaaggaaagcgttgtctcc
acaactccttcgagaatgtt	tggacagtggcgatgaatgg
agcacaatcctggagctcaa	cttctcaatgatgactcctc
caacgctgaaaagggttgga	acattgcagacgagagcttt
gacttttcatcagtgacagc	tggatgtgatcacaagcggc
gtagtcgataccggtgaagg	cttggttccgaaatgccagt
gcatggctccgaccaagaaa	cagccatggagacgaattgc
agcaagaagatctttgcgct	ccgtatgaaccatcggatgg
tccttgtgacttgaagatct	gaaaatgagtccttgtggga
cttggcatactcagcaagag	cctcgatggtaactgggaat
ctgggtttccaacaacgata	agaccttgaacaatcttcca
acttggcagcaatgaatgca	ccttggcaaaatcgtcgaag
agttcttggctgggatcttt	ttggtggtagcagcgatctt
tccaatctggtcatggcaga	ctttagagcatcatctctct
ttgagcaagagcacggttat	ttagatgttggcatcatcgc
ttgttccggttttaagggcg	aagtttaagggagcggttgg
acgttcttgacatttccgat	aaacgacaagacggcctact

Table 26 DPY-27 exonic probes

tgtcagcatatggtctatca	aagccaattccgattctaca
ccaggatcattgtcaagttc	attccgctagtatcagtatc
cctcctgaattgatcaatgc	cgagttgcttcttcaagact
ttcacgatttattgtgcggg	gccattcagtgtgcaataac
tctttttgcgatgcatcttt	tctcttcttgctttaactgc
tcatatcaattccagcacgt	acggtcacttctctatagtt
tcattagtgcaatcgcttca	acttgacgtttcagatctgc
caagcattccttcttcattc	attgctcaatttgctgcttg
attgtgaacttttgtgctcc	aaacattcggtccattttcc
caaagacttttaggtgtccc	ctgctcaattgagtccttat
ttgtttcagcataacggcac	taattgcagtttgtcgtgca
ctttgcctcaagcatgatat	ctctccaacttccaattgag
ccagctcagtgacaatacta	gtttgcaattgcgcattgat
cttcgattgccaatcgattc	tgacaaatttgccaggtgga
agagattctcgcattctctg	ccagcttgcaaatcttgtta
attcgagttgcatgttttgc	gaagcgacacaatcatcgca
cgattgcagaagctcatctg	ccttcagcttatcgctaaac
tgtttgcaatgtccctttaa	tgaatctcgccattctcaac
gctttgtcaaacttcagctt	agtagtacccaagaatgcga
gaagcccggaaataatccag	atcggtagattttccttctt
ctagtttgcacaacgtggta	catcgatttcatccatcacg
agaccaaagtccgagagttt	caggctgacattgttcaagt
ttcatcttcctcttcaactt	tcggatccaccataatgtta
acgacaattggtggtggaga	ctgagcccattactcaaatc

Abbreviations

ATP	Adenosine triphosphate
Chr	chromosome
Condensin DC	Condensin complex associated with X chromosome dosage compensation in C. elegans. Contains DPY-27 SMC protein.
DCC	dosage compensation complex
FRAP	Fluorescence recovery after photobleaching
NEBD	Nuclear envelope breakdown
rex	Recruitment element on the X
DSB	double-strand break
HAWK	HEAT repeat proteins associated with kleisins
KITEs	kleisin interacting tandem winged-helix elements
Hi-C	Chromosome conformation capture method (all-vs-all)
WAPL	Wings apart-like subunit
NIPBL	Cohesin loader nipped-B-like protein
CTCF	CCCTC-binding factor
HEAT	Huntingtin, elongation factor 3, protein phosphatase 2A

kite	kleisin interacting tandem winged-helix elements
rDNA	ribosomal DNA
smFISH	Single-molecule RNA fluorescence in situ hybridization
SMC	structural maintenance of chromosome
SNP	single nucleotide polymorphism
TAD	topologically associating domain

Prefixes and units

G	giga (10^9)	bp	base pair(s)	h	hour(s)
M	mega (10^6)	kb	kilobases	min	minute(s)
k	kilo (10^3)	Da	Dalton	sec	second(s)
m	milli (10^{-3})	°C	degrees Celsius	l	liter
µ	micro (10^{-6})	A	Ampère	g	gram
n	nano (10^{-9})	V	Volt		
p	pico (10^{-12})	M	molar		

Index of Figures

Index of Tables

Erklärung

Hiermit erkläre ich, die Dissertation selbstständig und nur unter Verwendung der angegebenen Hilfen und Hilfsmittel angefertigt zu haben. Ich habe mich anderwärts nicht um einen Doktorgrad beworben und besitze keinen entsprechenden Doktorgrad. Ich erkläre, dass ich die Dissertation oder Teile davon nicht bereits bei einer anderen wissenschaftlichen Einrichtung eingereicht habe und dass sie dort weder angenommen noch abgelehnt wurde. Ich erkläre die Kenntnisnahme der dem Verfahren zugrunde liegenden Promotionsordnung der Lebenswissenschaftlichen Fakultät der Humboldt-Universität zu Berlin vom 5. März 2015. Weiterhin erkläre ich, dass keine Zusammenarbeit mit gewerblichen Promotionsberaterinnen/ Promotionsberatern stattgefunden hat und dass die Grundsätze der Humboldt-Universität zu Berlin zur Sicherung guter wissenschaftlicher Praxis eingehalten wurden.

Declaration

I hereby declare that I completed the doctoral thesis independently based on the stated resources and aids. I have not applied for a doctoral degree elsewhere and do not have a corresponding doctoral degree. I have not submitted the doctoral thesis, or parts of it, to another academic institution and the thesis has not been accepted or rejected. I declare that I have acknowledged the Doctoral Degree Regulations which underlie the procedure of the Faculty of Life Sciences of Humboldt-Universität zu Berlin, as amended on 5th March 2015. Furthermore, I declare that no collaboration with commercial doctoral degree supervisors took place, and that the principles of Humboldt-Universität zu Berlin for ensuring good academic practice were abided by.

Berlin,

……..……..

Laura Breimann